# Engineered novel multifunctional hybrid nanofiber reinforcement for improving the flexural strength and fracture of cementitious composites for sustainable concrete

By

Hasan Shams Aldeen Hasan Mohammed

Thesis submitted for the degree of Doctor of Philosophy at
Lancaster University

Submitted

June, 2019

# Acknowledgments

Undertaking this PhD has been a truly life-changing experience for me, and it would not have been possible to do without the support and guidance that I received from many people.

I would like to express my gratitude first and foremost to my two supervisors, Professor Mohamed Saafi and Professor Jianqiao Ye, for their guidance, support and highly appreciated assistance that they have provided at all stages of this PhD research. Their patience, knowledge and technical abilities have allowed me to learn tremendously and enhance several skills during this project. Their encouragement and detailed feedback are also greatly appreciated.

I am grateful to the academic staff at Lancaster University Engineering Department. Special appreciation goes to Mark Salisbury, and the other technicians at the Engineering Department for their technical support with experimental works carried out during this research.

A very special thank you to my dad, Dr. Shams aldeed Hasan as well as my uncles, Mohamed Hasan and Hunain Mahmood for their support and encouragements.

I would like to say a heartfelt thank you to my brother Husien for helping me enormously and thank my wife Zahraa Younus for her love and support since we get married.

Finally, I gratefully acknowledge the funding received towards my PhD from the Higher Committee of Education in Iraq (HCED).

# List of Publications

Hasan, H., Huang, B., Saafi, M., Sun, J., Chi, Y., Whale, E., Hepworth, D., Ye, J. 2019. Novel engineered high performance sugar beetroot 2D nanoplatelet-cementitious composites. Construction and Building materials, 202, 546-562.

Hasan Hasan, Mohamed Saafi, and Jianquio Ye. Engineered multifunctional nanofiber reinforcement for improving the flexural strength and fracture of cementitious composites, Cement and Concrete Research (under preparation)

Hasan Hasan and Mohamed Saafi, (2018) Engineered nano cementitious composites for Sustainable concrete structures. NANOSTRUC 2018 (The 4th International Conference on Structural Nano Composites, HTW Berlin University of Applied Sciences, Germany, May 2018.

Hasan Hasan, Mohamed Saafi, and Jianquio Ye. Engineered Nano Cementitious Composites for Sustainable Concrete Structures. Faculty of Science and Technology, Lancaster University, Departmental Postgraduate Research Conference,July 2016.

Hasan Hasan, Mohamed Saafi, and Jianquio Ye. Engineered Nano Cementitious Composites for Sustainable Concrete Structures. Faculty of Science and Technology, Lancaster University, Departmental Postgraduate Research Conference,July 2017.

Hasan Hasan, Mohamed Saafi, and Jianquio Ye. Engineered Nano Cementitious Composites for Sustainable Concrete Structures. Faculty of Science and Technology, Lancaster University, Departmental Postgraduate Research Conference,July 2018.

# ABSTRACT

The carbonaceous nanomaterials (Multi wall carbon nanotubes (MWCNT), functionalised MWCNT and Carbon nanofibers (CNFs)) have outstanding properties (mechanical, electrical, etc., which can make them effectual nonoreinforcements for enhancing the properties of cementitious composites. unfortunately, these nanomaterials have a high tendency to agglomerate due to their strong Van der Waals self-attraction and hydrophobic surfaces. To date, ensuring a uniform dispersion in water and in the cementitious composite is the main challenge that hinders their effective use as a nano reinforcing agent.

To address the issue of agglomeration of carbonaceous nanomaterials in cementitious composites, for the first time, a green process was developed to synthesise highly dispersible multifunctional hybrid nanoparticles using bio-derived nanoplatelets (BNPs) and MWCNT. Multifunctional hybrid nanoparticles BNP/MWCNT suspensions were analysed using Optical microscopy, Ultraviolet–visible spectroscopy (Uv-vis), Scanning Election microscopy (SEM), elemental analysis (energy dispersive X-ray diffraction (EDX) and thermal characterization (TG-DTG).

In this work, extensive experimental studies have been conducted to investigate the hydration mechanism and microstructure characteristics of cementitious composites with BNP. The SEM, EDX, TG-DTG, Transmission Electron Microscopy (TEM), and X-ray diffraction (XRD) were used in this investigation. The mechanical properties of the resulting composites were characterised through compressive, flexural strength. More specially, the effect of BNP on fracture properties of cementitious composites has been investigated. The work has also focused on evaluating the effect of BNP/MWCNT on the

hydration mechanism, microstructure characteristics and mechanical properties (compressive, flexural strength). As well as, the experiments were performed to examine the effects of BNP/MWNCT on fracture properties of cementitious composites. The obtained results on dispersion showed that, BNP, can be used to disperse MWCNT in aqueous solution and well dispersed MWCNT in aqueous solution were achieved.

Addition of BNP resulted in cementitious composites to improve flexural strength, fracture properties and the microstructure of cementitious composites. The addition of multifunctional hybrid BNP/MWCNT to cementitious composites resulted in a significant improvement in the performance of cementitious composites and this gain could be attributed to uniform distribution of MWCNT, effective reinforcement effects, crack bridging and chemical bonding between BNP/MWCNT and cement hydrated products.

# List of Figures

# List of tables

# Nomenclature

| | |
|---|---|
| a CNC | adsorbed cellulose nanocrystals |
| AFM | atomic force microscopy |
| AFm | alumina, ferric oxide, mono-sulfate" or ($Al_2O_3$ – $Fe_2O_3$ – mono) |
| Aft | alumina, ferric oxide, tri-sulfate" or ($Al_2O_3$ – $Fe_2O_3$ – tri). |
| BNP | bio nano-platelets |
| BNP/MWCNT | hybrid bio nano-platelets/multi wall carbon nanotubes |
| $CaSO_4$ | calcium sulfate |
| $C_3A$ | tricalcium aluminate ($3\ CaO \cdot Al_2O_3$) |
| $C_4AF$ | tetracalcium Aluminoferrite ($4\ CaO\ Al_2O_3Fe_2O_3$) |
| $3CaO.Al_2O_3.3CaSO_4.32H_2O$ | ettringite |
| $3(3CaO.Al_2O_3.CaSO_4.12H_2O)$ | monosulfate |
| $4CaO.Al_2O_3.13H_2O$ | hydrated calcium aluminate |
| $CaSO_4.2H_2O$ | CH ($Ca(OH)_2$) calcium hydroxide |
| CNC | cellulose nanocrystals |
| CNFs | carbon nanofibres |
| CNTs | carbon nanotubes |
| CNT-OPC | ordinary portland cement with carbon nanotubes |
| $CO_2$ | carbon dioxide |
| COOH | carboxyl group |
| C-S-H | calcium silicate hydrate |
| $C_2S$ | dicalcium silicate (Belite) ($2\ CaO \cdot SiO_2$) |
| $C_3S$ | tricalcium silicate (Alite) ($3\ CaO \cdot SiO_2$) |

| | |
|---|---|
| DOH | degree of hydration |
| EDX | energy dispersive X-ray diffraction |
| fCNC | free cellulose nanocrystals |
| FE-SEM | field emission scanning electron microscopy |
| FTIR | fourier-transform infrared spectroscopy |
| G | graphene |
| GO | graphene oxide |
| H | hydrogen |
| HCL | hydrochloric acid |
| $HNO_3$ | nitric acid |
| $H_2SO_4$ | sulfuric acid |
| MS | mass spectroscopy |
| MWCNT | multi wall carbon nanotubes |
| NFC | nano fibrillated cellulose |
| NS | nano-silica |
| OH | hydroxy group |
| OPC | ordinary portland cement |
| SEM | scanning electron microscope |
| SDS | sodium dodecyl sulfate |
| $SO_3H$ | sulfonyl group |
| SWCNT | single-walled carbon nanotubes |
| w/c | water to cement weight ratio |
| WRA | water reducing agents |
| TEM | transmission electron microscopy |

| | |
|---|---|
| TGA | thermo gravimetric analysis |
| TG-DTG | thermal characterization |
| Uv-Vis | spectroscopic ulraviolet visbile Spectroscopic |
| XRD | x-ray diffraction |

# Variables

| | |
|---|---|
| $\delta_{\circ}$ | the displacement at final failure of the beam |
| $P(\delta)$ | the load-displacement curve of froce verus CMOD |
| ABS | absorbance of UV-vis spectroscopy |
| $a$ | the depth of the slot |
| Al | aliminum |
| CI | crystallinity index |
| b | width of beam in (mm) |
| C | carbon |
| ºC | celsius |
| Ca | calcium |
| $CaCO_3$ | calcium carbonate |
| CMOD | crack mouth opening displacement |
| E | ettringite |
| E | modulus of elasticity (GPa) |
| g | gram |
| $g$ | accelaration due to gravity |
| $G_f$ | fracture energy of the composite |
| hrs | hours |

| | |
|---|---|
| $I_{am}$ | intensity of the amorphous cellulose between the planes (200) and (110) |
| K | potassium |
| $K_{IC}$ | fracture toughness of the composite |
| L | length of beam in (mm) |
| $\mathrm{m} = m_1 + m_2$ | $m_1$ is the mass of the beam between the supports, and $m_2$ is the mass of the part of the loading fixture not attached to the machine that follows the beam during failure. |
| ml | milliliter |
| Mg | magnesium |
| nm | nano-meter |
| O | oxygen |
| P | portlandite ($Ca(OH)_2$) |
| $P_{max}$ | the peal load |
| $S$ | the span of the beam |
| Si | silicon |
| SP | superpactizer |
| $t$ | the width of the specimen |
| w | watt |
| $w_{\circ}$ | the area under the load-displacement curve |

# Table of contents

## 1. Chapter One: Introduction....……………………...………..29

## 2. Chapter Two: Literature Review…………....………………36

# 3. Chapter Three: 3 Manufacturing and properties of sugar beetroot-based BNP……………………………………………….94

# 4. Chapter Four: Nanoengineered cementitious composites using bio-based 2D nanoplatelets……………………………..107

# 5. Chapter Five: Engineering of multifunctional hybrid BNP/MWCNT nanoparticles…………………………………140

# 6. Chapter Six: Cementitious composites reinforced by multifunctional hybrid BNP/MWCNT nanoparticles……….202

# Chapter one

## 1 Introduction

### 1.1 Problem Statement

The construction sector in the UK faces serious challenges as the EU attempts to meet its $CO_2$ emissions reduction by 2050. A key issue is curbing the overall demand for ordinary Portland cement (OPC). OPC production is one of the main contributors to $CO_2$ emissions, counting for about 5-7% of the total global $CO_2$ emissions (Zhang et al., 2014; Benhelal et al., 2013). Because there are no other alternative cementitious materials on the horizon that can replace OPC, the production of OPC is forecast to double in the next 30 years to meet the rising global demand for new civil infrastructure due to the growth in population. This will result in more $CO_2$ emissions.

Two popular research directions that have emerged recently relating to the reduction of embodied $CO_2$ of concrete: “do more with less” and “built to last” strategies. The “do more with less” strategy involves increasing the formation or enhancing the nanoscale properties of calcium silicate hydrate (CSH) phase, the main building block that controls the overall performance of concrete. By increasing the performance of concrete, it may be possible to design concrete members with smaller size which in return reduces the volume of concrete thereby reducing the demand on OPC. The first approach to this, deals with controlling and amplifying the CSH growth using reactive nanomaterials, whereas the second approach involves strengthening the CSH products with carbonaceous nanomaterials such as carbon nanotubes (CNTs), carbon nanofibers (CNFs), graphene and graphene oxide (GO) (Cao et al., 2015; Lv et al., 2013; Lv et al., 2014a; Lv et al., 2014b). The “built to last” strategy consists of continuously monitoring the “true state of health” of concrete, adapting the self-sensing approach using CNTs, CNFs and graphene fillers such as conductive fillers to measure and monitor the electrical properties of concrete structures. The “Big Health Data” obtained from the monitoring, enables owners to extend the service life of concrete structures safely and economically. This can help lower the $CO_2$ footprint by reducing the amount of materials required for major repairs or replacement (Kang et al., 2006; Han et al., 2009). Unfortunately, the potential application of CNTs, CNFs and graphene in concrete is currently held back by one major issue: These nanomaterials are not dispersible in water and tend to agglomerate, leading to a nonhomogeneous microstructure thereby providing moderate performance enhancement of cementitious materials. The agglomerates also act as stress concentration points in the matrix which result in cracks and a significant reduction in the mechanical properties (Njuguna et al., 2015; Muhammad Maqbool Sadiq et al., 2017; Onuaguluchi et al., 2014; Metaxa et al., 2012a; Yu et al., 2007; Zhou et al., 2017). As such, there is a need for new approaches for future high-performance cementitious materials that exhibit paradigm-shifting properties to build infrastructure with lower cement content and enable built infrastructure to inherently perform multiple functions such as self-health monitoring.

Therefore, the objective of this work is to engineer novel multifunctional nanomaterials to address obstacles that are currently inhibiting the widespread application of CNTs in cementitious composites. Specifically, this research provides a new green synthesis of hybrid multifunctional nanoparticles to significantly enhance the mechanical properties and fracture resistance of cementitious composites.

## 1.2 Research Concept and Novelty

To address the issue of agglomeration of carbonaceous nanomaterials in cementitious composites, for the first time a green process was developed to synthesize highly dispersible multifunctional hybrid nanoparticles using bio-derived nanoplatelets (BNP) and multiwall carbon nanotubes (MWCNT). Figure 1.1 shows the concept of the proposed multifunctional hybrid nanoparticles. The BNP sheets were synthesized from sugar beetroot waste and contain hydrophilic and hydrophobic functional groups (figure 1.1c) thus enabling them to self-assemble with MWCNT to create hybrid BNP/MWCNT nanoparticles. As shown in fig. 1a, the MWCNT are attached to the BNP sheets through the hydrogen bonding mechanism resulting from the BNP hydrophobic sites and the MWCNT hydrophobic planes fig. 1.1d). Once in the cement paste, the hybrid BNP/MWCNT nanoparticles are uniformly dispersed due to the electrostatic repulsion forces between the BNP sheets generated by the large number of charged hydroxyl functional and $CH_2OH$ groups on their surface.

When they are present in the cement matrix, the hybrid BNP/MWCNT nanoparticles perform multiple functions: 1) Owing to their functional groups (figure 1.1(c)), the BNP adhere to the surface of the cement particles and use their somewhat porous structure to act as both water reservoirs and short-circuit diffusion functions to provide or transport water to the un-hydrated cement cores, thus fueling the formation of CSH. 2) The hydroxyl functional groups (fig. 1.1c) on the surface of BNP prevent the agglomeration of the cement particles, thereby creating the so-called steric stabilization effect for improved workability and hydration of cement particles. 3) The adsorbed BNP remain in the high density CSH, creating new intercalated CSH/BNP/MWCNT nanocomposites (fig. 1.1e) with increased strength and toughness, and denser microstructure and 4) the MWCNT form uniformly distributed conductive networks in the cement matrix resulting in an improved electrical property which can be used to monitor the structural integrity of concrete structures.

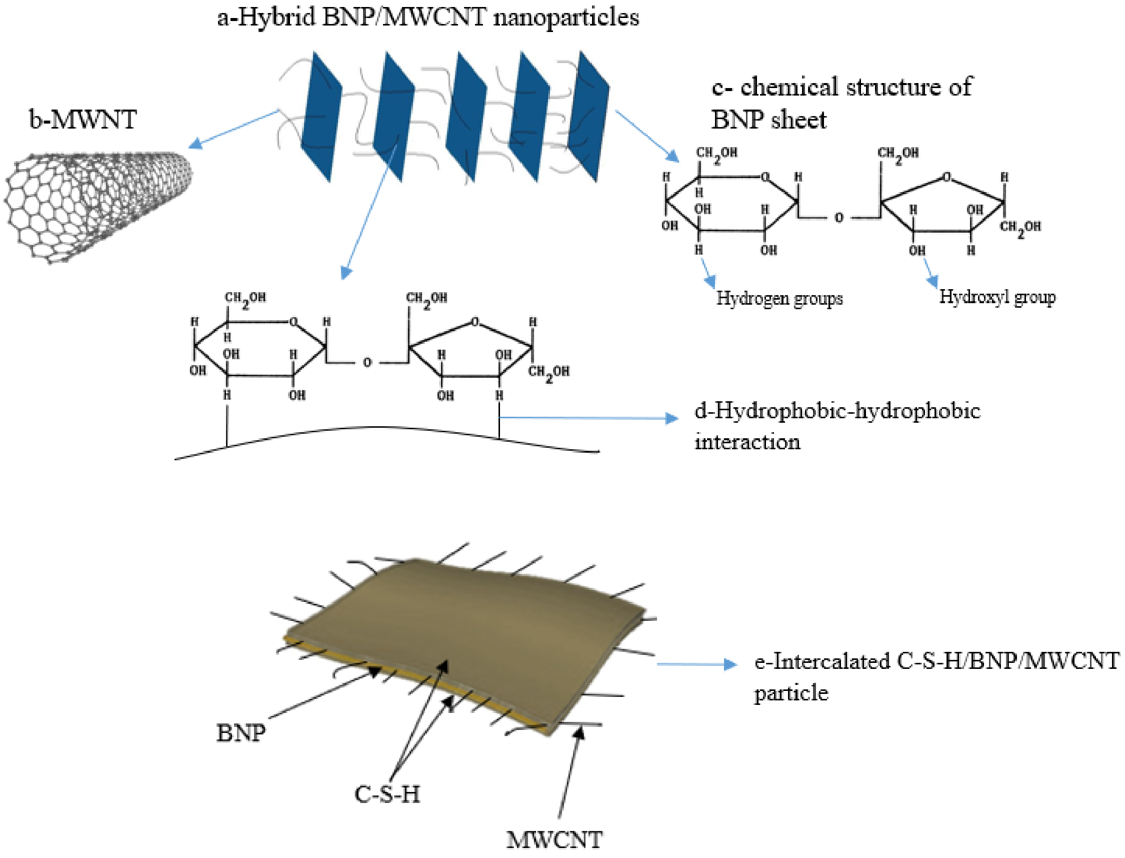

**Figure 1.1:** Proposed hybrid BNP/MWCNT nanoparticles

## 1.3. Aim

The aim of this research is to engineer new hybrid multifunctional nanoparticles for application in cementitious composites. The proposed hybrid multifunctional nanoparticles address the roadblock to using CNTs in cement-based materials to enhance their performance and functionality.

## 1.4 Objectives

1. To develop novel multifunctional hybrid BNP/MWCNT nanoparticles for large-scale applications in cement-based materials.
2. To investigate the colloidal properties and stability of the hybrid BNP/MWCNT nanoparticles in aqueous solutions.
3. To elucidate the effect of BNP on the hydration, chemical composition, morphology and microstructure of cementitious composites and understand their interaction with cement hydration phases.
4. To determine the influence of BNP on the mechanical and fracture properties of cementitious composites.
5. To quantify the effect of the hybrid BNP/MWCNT particles on the hydration, chemical composition, morphology and microstructure of cementitious composites and uncover their interaction with the cement hydration phases.
6. To determine the influence of the hybrid BNP/MWCNT particles on the mechanical and fracture properties of cementitious composites.
7. To establish the strengthening mechanisms in the cementitious composites as a result of the addition of BNP/MWCNT particles.

## 1.5 Thesis Structure

This thesis is comprised of seven chapters. Chapter 1 introduces background, research novelty, aim and the objectives of this research. A brief description of the proposed multifunctional hybrid BNP/MWCNT particles is also included to set the scene for this research.

Chapter 2 covers the literature review including the most relevant and up-to-date research activities in the area of cementitious composites reinforced with nanomaterials. This will consist of an overview of MWCNT, GO, graphene, and cellulose nanocrystals (CNC), and reactive nanoparticles such as nano silica, their properties and usage in cement-based materials will also be discussed.

Chapter 3 introduces the BNP sheets and their manufacturing process. Chapter 3 also investigates the properties of BNP, and their colloidal properties and stability in aqueous solution using optical microscopy and Uv-Vis Spectroscopic microscopy.

Chapter 4 examines the influence of BNP on the hydration, morphology, microstructure characteristics and mechanical properties of cement pastes. Analytical tools such as X-ray diffraction (XRD) and Energy-dispersive X-ray spectroscopy (EDS) were employed to identify the hydration phases and their chemical composition of the cement pastes. The effect of BNP on the degree of hydration (DOH) of the cement paste was also examined using Thermo Gravimetric Analysis (TGA). In addition, Scanning Electron Microscopy (SEM) and Transmission Electron Microscope (TEM) were used to analyze the morphology and microstructure of the hardened cement paste and examine the interaction between the BNP sheets and the cement matrix. In addition, the distribution of the BNP sheets within the cement matrix was evaluated and the effect of the BNP sheets on the mechanical properties and fracture resistance of the hardened cement pastes were determined.

Chapter 5 investigates the colloidal properties and stability of the multifunctional hybrid BNP/MWCNT nanoparticles using optical microscopy and Uv-Vis Spectroscopic microscopy. Chapter 5 also studies the interaction between BNP and MWCNT using TGA, SEM and EDS. The colloidal properties of the hybrid BNP/MWCNT are compared with those of hybrid GO/MWCNT and Cellulose crystal /MWCNT.

Chapter 6 examines the performance, the hydration, the morphology and microstructure of cementitious composites reinforced by different BNP/MWCNT concentrations. Chapter 6 studies the hydration mechanism of cementitious composites using XRD, EDS and TGA analysis. Chapter 6 also investigates the morphology and microstructure of cementitious composites and the interaction between hybrid BNP/MWCNT and cement matrix using SEM analysis. Furthermore, the mechanical properties of cementitious composites reinforced by hybrid BNP/MWCNT were evaluated.

Chapter 6 also studies the fracture characteristics of the cementitious composites containing the hybrid BNP/MWCNT. The effect of the hybrid multifunctional nanoparticles on cementitious fracture energy and fracture toughness were determined and the toughening mechanisms of BNP/MWCNT were uncovered.

Finally, chapter seven contains the conclusions and reflective evaluation of the whole study and proposes topics for future research.

# Chapter Two

## 2 Literature Review

### 2.1 Introduction

This chapter provides the necessary background knowledge to understand the properties of nanomaterials used in cementitious composites including MWCNT, graphene (G), graphene oxides (GO) and cellulose nanocrystals (CNC). In addition, the effect of these nanomaterials on the properties of the cementitious composites is discussed in detail. This chapter also discusses some of the commonly used approaches to disperse MWCNT in aqueous solution and their mixing with cementitious composites.

### 2.2 Nano reinforcing materials for cementitious composites

#### 2.2.1 MWCNT

MWCNT can be defined as one-dimensional growth of materials to form nanotubes. They have attracted worldwide interest in recent years due to their high tensile strength, ultra-high Young's modulus, high aspect ratio, ultra-light weight, chemical and thermal stability, inherent electrical, corrosion resistivity and transport properties. As a result, MWCNT are deemed to have great potential applications in composite materials. MWCNT are commonly produced by a thermal chemical vapor deposition process and their hollow structures are tubular shaped, described as ultrathin filaments of carbon formed by layering carbon atoms bonded in a hexagonal pattern, as shown in figure 2.1.

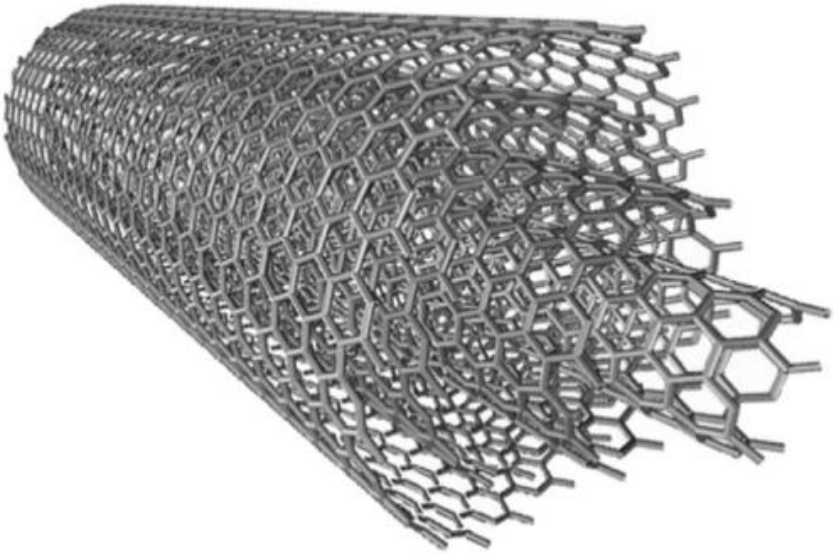

**Figure 2.1:** Structure of MWCNT formed by four rolled sheets of graphene (Zannotti et al., 2016)

Since their discovery (Iijima, 1991) many researchers have studied their usage in various applications such as hydrogen storage, field emission device, ultracapacitor, electronic scanning probe, sensor, biomedical material, coatings, batteries and filters (Ling et al., 2013; Scheibe et al., 2010; White et al., 2016; Shtein et al., 2013).

MWCNT display extraordinary physical properties such as its great strength of 100 times that of steel, whilst only one sixth of its density (Wong, Sheehan et al. 1997), making it the strongest material known and Young's modulus from 500-1000GPa (Krishman, Dujardin et al. 1998; Popov, vanDoren et al. 2000). Research on MWCNT-reinforced composites has been performed in a variety of areas including nano-composites, nanotube-metal composites and ceramic matrix composites due to their extraordinary mechanical properties such as high tensile strength and ultra-high Young’s modulus (Yu et al., 2000; Peyvandi et al., 2014).

SEM image of bundles of MWCNT, with a diameter between 1-100 nm and a length of several microns is shown in Figure 2.2.

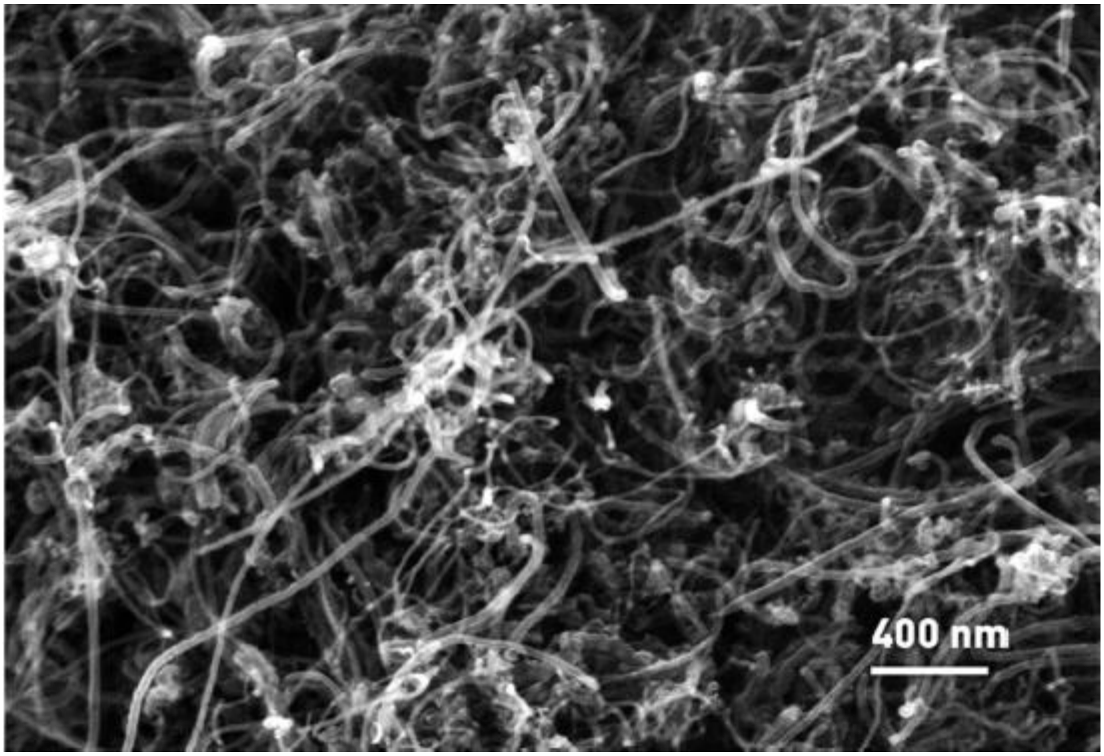

**Figure** 2.2: SEM micrograph of a bundle of MWCNT (Dassios et al., 2015)

### 2.2.2 Graphene (G)

G is a recent structure of carbon in two-dimensional (2D) form which has attracted both experimental and theoretical scientists. The basic form of graphene is a Single-layer, which is a planar sp2-bonded six-membered-ring sheet of carbon, wherein it is the basic building block for MWCNT. Single layer graphene is a single layer of carbon atoms arranged in a hexagonal lattice, which has a large surface area of approximately 2630 m2g-1, high young's modulus around 1 TPa and its morphology consists of carbon atoms bonded together with pia bonds with one carbon atom thickness (Zhu et al., 2010). Moreover, G has properties such as high thermal conductivity, mechanical stiffness, fracture strength, and exceptional electrical mobility due to its extraordinary carrier transport behaviour. The structure of G with its single layer of bonded carbon atoms forming a honeycomb crystal lattice is shown in figure 2.3. In addition, a Transmission Electron Microscope (TEM) image of a single layer of G shows that, GO has plate shape with 2D dimensions of several microns and a thickness of several nanometres which is illustrated in figures 2.4 and 2.5. In addition, G is a very expensive material which limits its application and there are problems relating to its agglomeration due to van der forces.

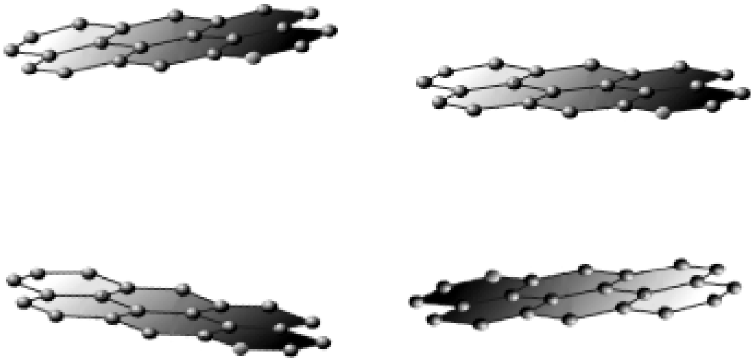

**Figure 2.3:** G structure (Blomquist, 2016)

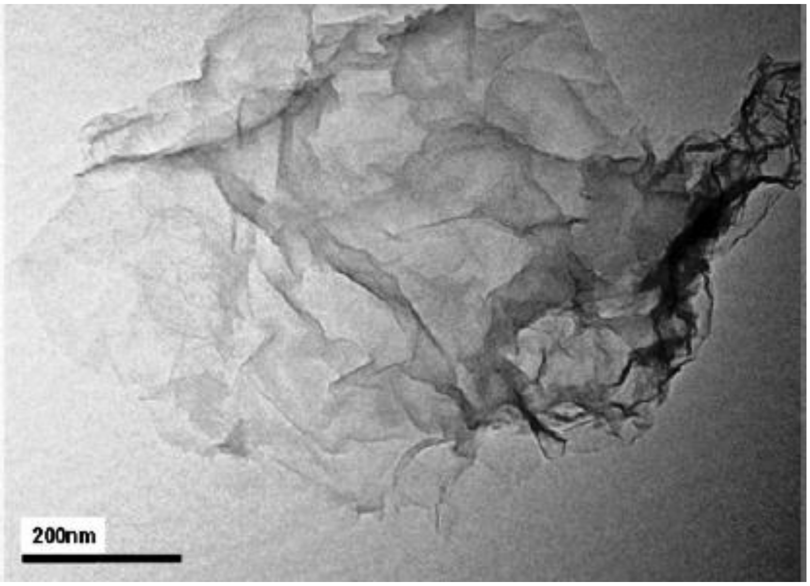

**Figure 2.4:** TEM Image of Single Layer G (Pu et al., 2011)

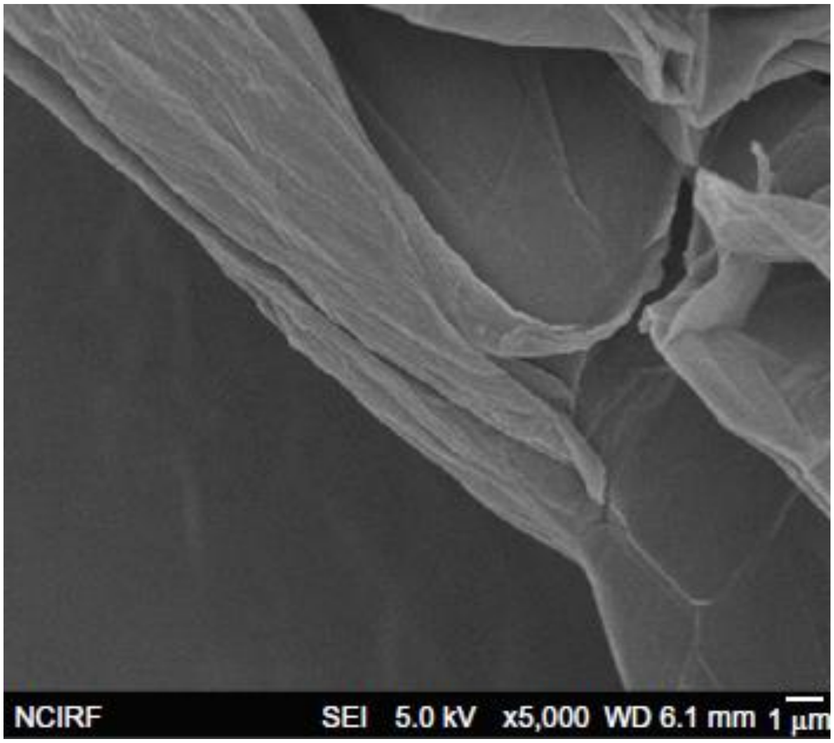

**Figure 2.5:** SEM Image of Single Layer G (Gurunathan et al., 2013)

### 2.2.3 GO

GO is produced by the oxidization of graphene. It has powerful properties such as high surface area and ultrahigh strength and is a highly promising material. It can be used with cementitious material, polymer and ceramic to produce composite materials (Li et al., 2015). Figure 2.6 shows the chemical structure of GO, which consists of a single layer of bonded carbon atoms forming a honeycomb crystal lattice. This lattice is covered with several chemical groups such as carboxyl (-COOH) and hydroxyl groups (-OH) anchored at the edges of nanosheets, making the GO surface chemically more reactive with cement particles and dispersible in aqueous solutions. Moreover, nano-sheets of GO, which consist of hydrophilic oxygenated graphene sheets, are shown in figure 2.7. Figure 2.8 shows the process of manufacturing GO from chemical oxidation of G and the sonication process of Graphite oxide to produce GO.

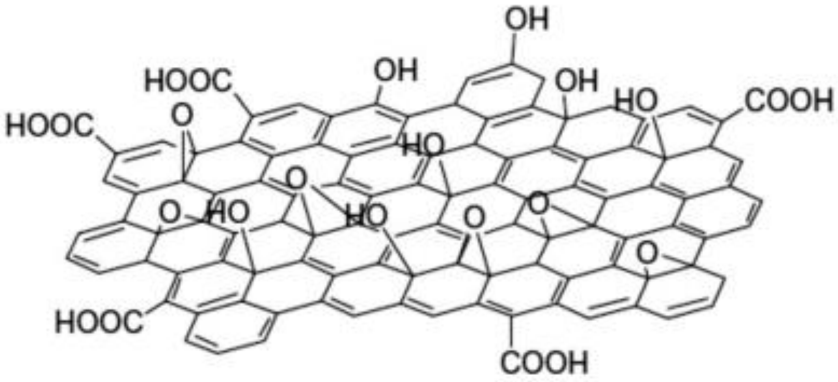

**Figure 2.6:** Chemical structure of GO (Nasrollahzadeh et al., 2015)

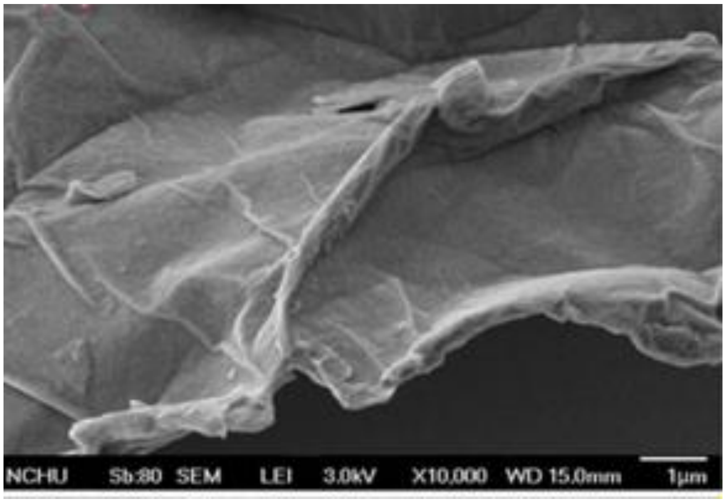

**Figure 2.7:** SEM Image of GO (Brahmayya et al., 2017)

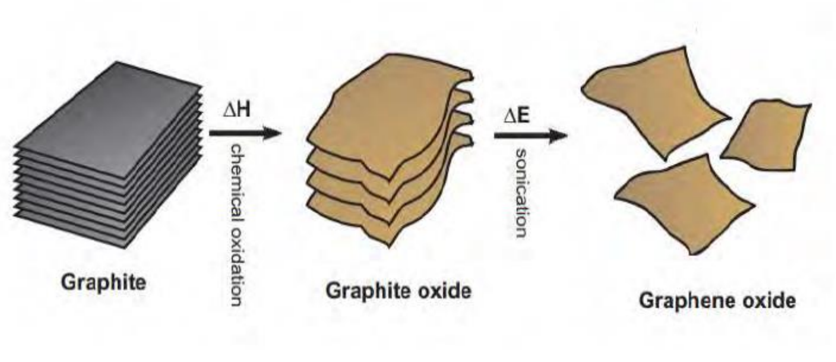

**Figure 2.8:** Schematic manufacturing of GO (Hantel, 2013)

### 2.2.4 CNC

One of the most important bio materials is CNC, which has attracted great interest in the nanocomposite field since it has unique properties such as nanoscale dimensions, high surface area, unique morphology, low density, and high mechanical properties. Moreover, it is a green material which is renewable and biodegradable and can be effortlessly modified. In addition, CNC have a shape of needle-like cellulose particles with a diameter between 10-100 nm and a length typically between 0.05-0.5 microns, thus CNC have different aspect ratios. CNC are extracted from wood and plant material; however their length and diameter depend on the source material and the hydrolysis conditions. The production of CNC from this extracted wood and plant material has a highly crystalline nature thereby resulting in the desired physical and mechanical properties described above. The most well-developed technique to produce CNC is Acid hydrolysis. Figure 2.9 shows a TEM image of CNC that are needle-like cellulose particles with a diameter between 10-100 nm and a length typically between 300-500 nm. Figure 2.10 illustrates the chemical structure of CNC which shows functional groups (-OH) which make CNC dispersible in aqueous solution.

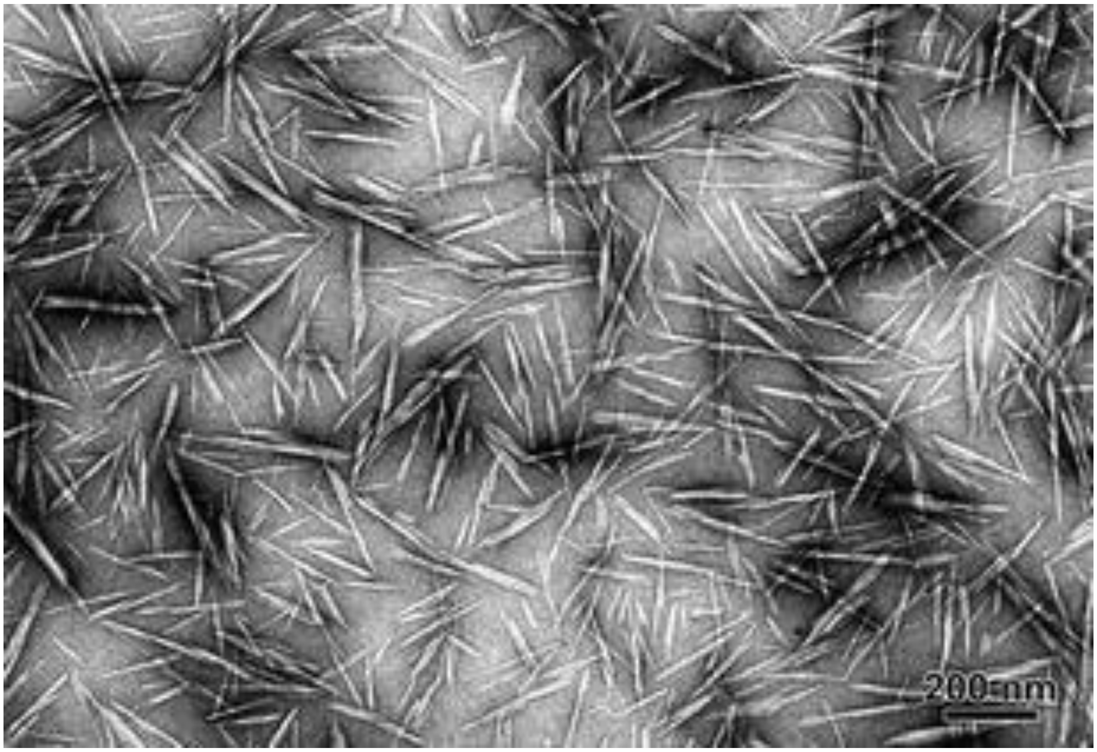

**Figure 2.9:** TEM image of CNC (Habibi et al., 2008)

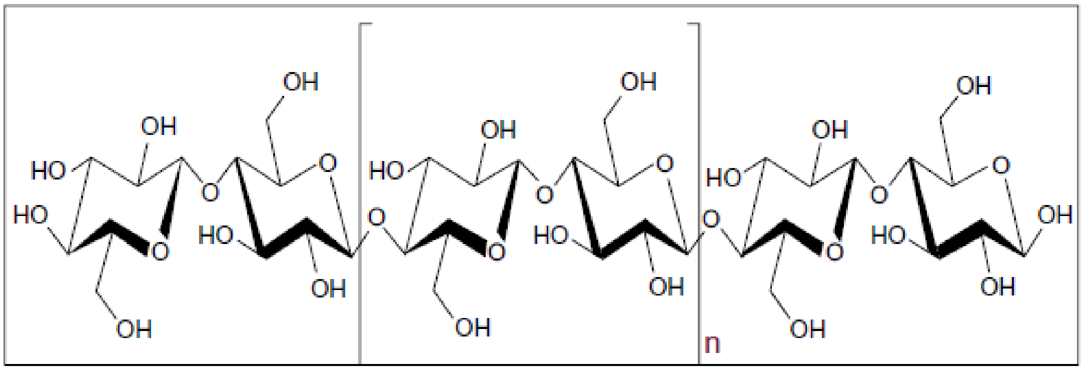

**Figure 2.10:** The chemical structure of CNC (George and Sabapathi, 2015)

### 2.2.5 Nano-Silica (NS)

NS has a very fine particle size (about several to one hundred nanometers) and an extremely high pozzolanic reactivity. The Nano sized particle size feature of NS would be favorable for its penetration into the pores of cement (Hou et al., 2014). The NS shown below in

Figures 2.11 and 2.12 show a density of approximately 1.3 g/ml and an approximate surface area of 220 m2/g (Du et al., 2015).

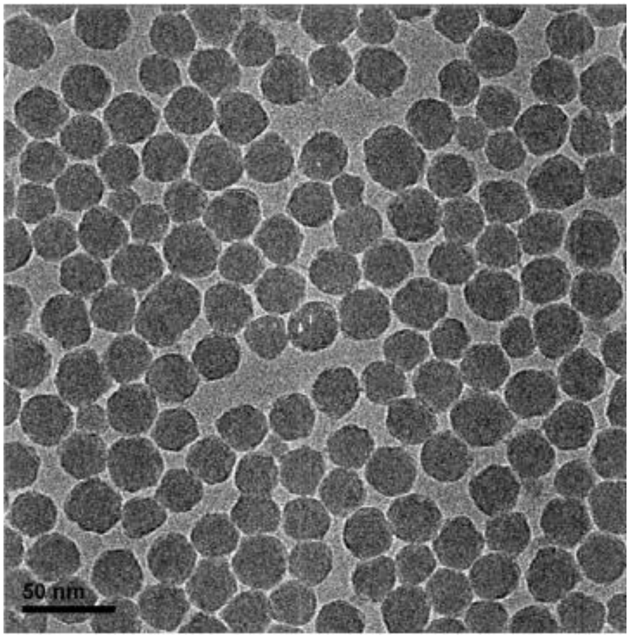

**Figure 2.11:** Transmission electron micrograph of NS (Du et al., 2015)

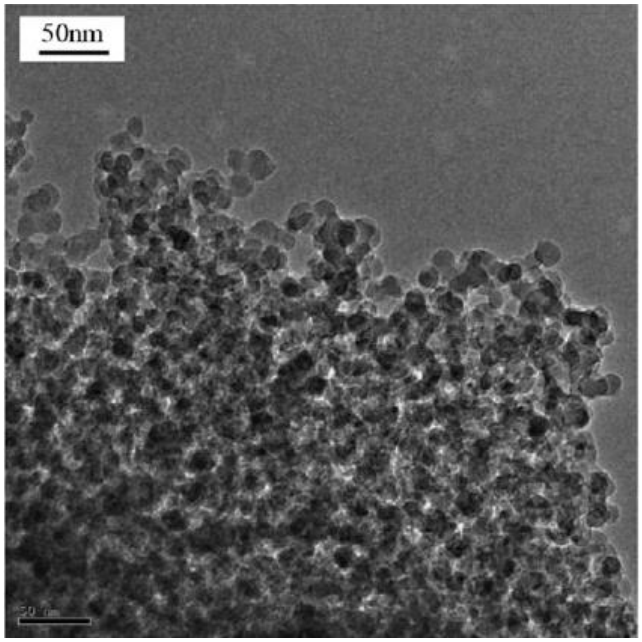

**Figure 2.12:** Transmission electron micrograph of NS (Kong et al., 2015)

## 2.3.0 Dispersion of MWCNT

Although MWCNT have unique properties that make them attractive materials to employ in the many applications previously mentioned in Section 2.2.1; they have issues relating to the presence of attractive forces (Van der Waals), which causes particles agglomeration (Ling et al., 2013; Scheibe et al., 2010; White et al., 2016; Shtein et al., 2013). These agglomerative particles have difficulty dispersing uniformly into matrices, and these particles become weak areas in the overall structure. Hence, there is a need to deagglomerate and distribute these particles within matrices. The mechanism of dispersion could be described as a splitting up the parts of agglomerates into small fragments under high stress or exfoliating the parts of agglomerates into small fragments under a comparatively lower stress. The dispersion of MWCNT depends on many factors such as length of MWCNT, diameter, intensity, volume fraction, matrix viscosity and attractive forces. Different chemical and physical methods have been used to disperse MWCNT in aqueous solution, polymer materials and cementitious materials (Parveen et al., 2013). A comprehensive review of the literature in the field of MWCNT dispersion is presented in the following sections.

### 2.3.1 Methods of dispersion of MWCNT

#### 2.3.1.1 Dispersion of MWCNT via functionalization with acids

Functionalization of MWCNT can be defined as a modification of their surfaces by adding carbonyl group (CO) and hydroxyl group (OH). This functionalization permits dispersion of MWCNT in water and organic solvents (Hung et al., 2008). Hung and others (2008) investigated the reaction of thin MWCNT with a mixture of concentrated $HNO_3$ and $H_2SO_4$. A mixture of 86.4% $HNO_3$ and 98% of $H_2SO_4$ (1:3) volume proportion was used for carboxylation of purified thin MWCNT (200 ml of mixture/g MWCNT). At a temperature of 80 ± 3 ºC, the mixture was treated for 3-4 hrs with constant stirring and refluxing, in addition to the evolution of a light brown gas. This process was followed by cooling and centrifuging the mixture. Distilled water was then used for washing the sample four times followed by washing with 5% HCl. Finally, the sample was dried under pressure and weighed. Figure 2.13 shows the process of functionalization of thin MWCNT, as described above, and figure 2.14 illustrates the TEM images of thin MWCNT prepared, also described above. There are some bundles of MWCNT and single nanotubes of MWCNT. It was observed that a stable aqueous solution with a solubility of 3.13 g/l was formed from carboxylated thin MWCNT.

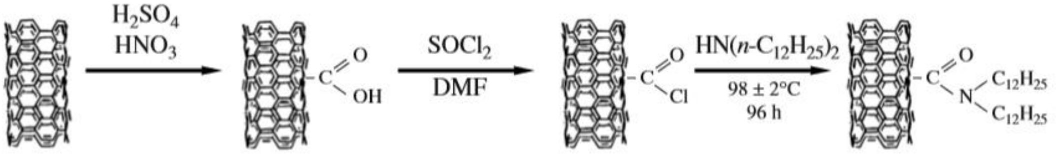

**Figure 2.13:** Schematic of the functionalization process of MWCNT (Hung et al., 2008)

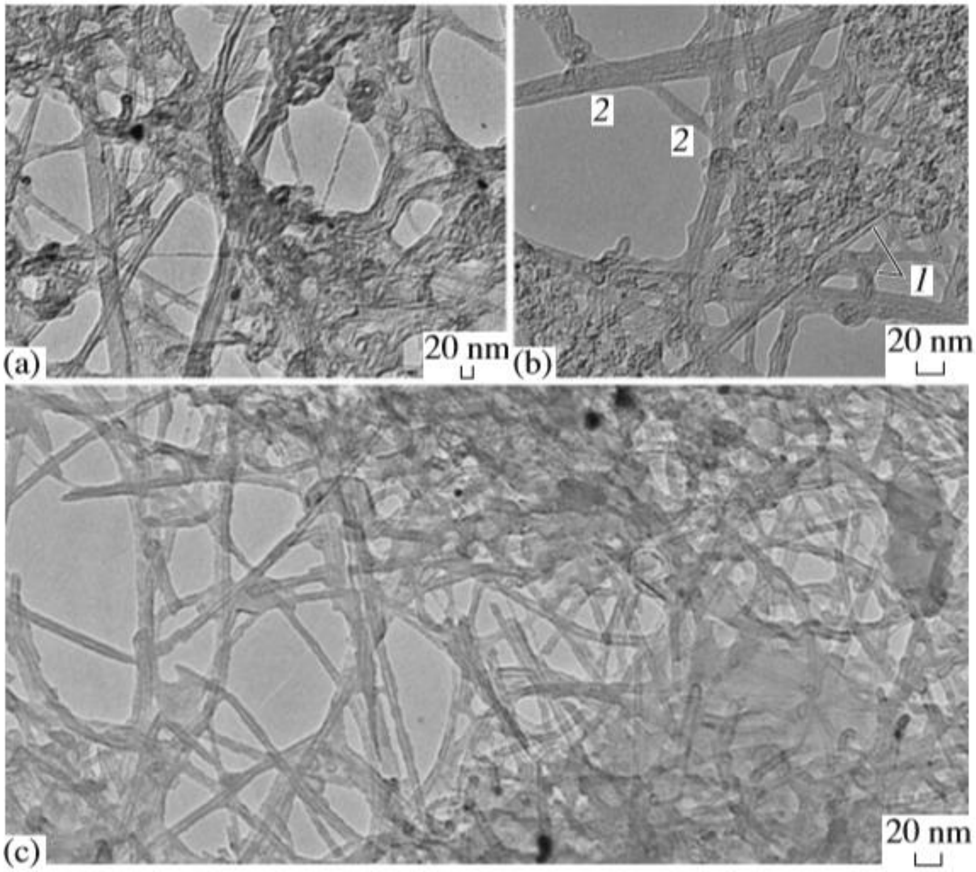

**Figure 2.14:** TEM images of (a) as-prepared, (b) carboxylated and (c) amidated then MWCNT; (1) bundles, (2) single nanotubes (Hung et al., 2008)

Peng et al. (2003) studied the effects of acid functionalization on the performance of single-walled carbon nanotubes (SWCNT). The acid functionalization was completed via reactions of SWCNT with succinic or glutaric at 80-90ºC. It was concluded that acid functionalization led to increased solubility of SWCNT.

In summary: as described above this functionalization treatment permits dispersion of MWCNT in water however, this method has also some disadvantages such as, excessive damage to the surfaces of MWCNT (i.e., damage to MWCNT structure may occur due to extreme use of acids and chemicals at high concentrations in the chemical functionalization techniques). Furthermore, this method negatively affects the performance of cementitious composites due to excessive formation of ettringite due to existence of sulphate ions (i.e. if the sulphuric acid was used in functionalization treatment, some sulphate ions probably were left over from washing off the sulphuric acid, which would lead to create sulphate functional group, and these could lead to excessive ettringite. This negatively impacts upon the mechanical performance of the cementitious composites (Abu Al-Rub et al., 2012).

### 2.3.1.2 Dispersion via noncovalent bonding methods

Noncovalent bonding methods include dispersing MWCNT with the use of chemicals to sustain long term uniform dispersion in aqueous solution and a variety of other liquid solutions. These methods used chemical materials to disperse MWCNT without causing excessive damage to their surfaces as well as maintaining the original properties of MWCNT. An example of a chemical used in this way is GO, which uniformly distributes in aqueous solution due to having OH groups on their surfaces. The GO solution is mixed with MWCNT followed by ultransonic mixing to separate the bundles. An ultrasonic mixer causes separation through the creation of acoustic energy throughout a liquid medium via a high frequency driver. In 2015, Lu et al. published a paper in which they described the effects of the addition of GO/MWCNT to cementitious composites. Interestingly, the dispersion of MWCNT in the GO solution was examined by UV-Vis spectroscopy and optical microscopy, and extensive results carried out showed that, this method produced acceptable dispersion of MWCNT in aqueous solution. This may have happened due to repulsion forces (i.e. a force under the influence of which objects tend to move away from each other through having the same magnetic polarity or electric charge) that were created between the surfaces of MWCNT due to the high electrostatic repulsion of GO. Figure 2.15(a) shows the agglomeration of MWCNT due to van der forces, figure 2.15(b) shows the dispersion of GO due to high repulsion forces as described above, and figure 2.15(c) shows the functionalized MWCNT in GO solution; there is a clear dispersion of MWCNT in this case. Figure 2.16(a) shows typical optical microscope images for MWCNT in aqueous solution. There is a clear agglomeration of MWCNT in this image as well as figure 2.16(b), which shows distributed MWCNT/GO in aqueous solution. In addition, a major problem with this experiment was that GO is too expensive and cannot be used on an industrial scale.

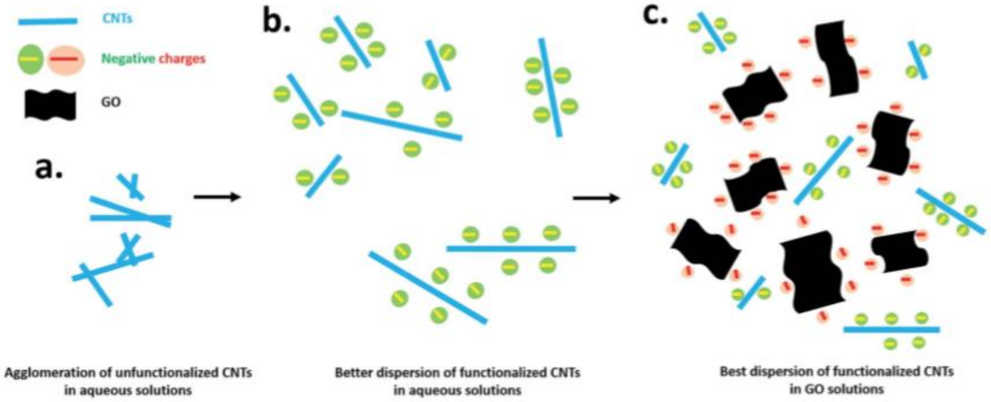

**Figure 2.15:** Scheme showing the dispersion of (a) unfunctionalized MWCNT and (b) functionalized MWCNT in the aqueous solution and (c) functionalized MWCNT in the GO solution (Lu et al., 2015)

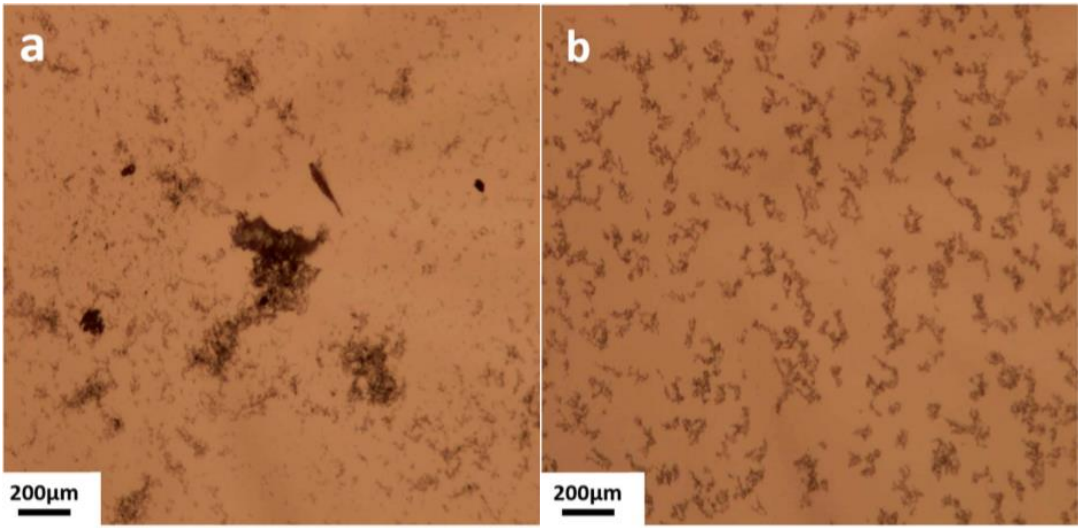

**Figure 2.16:** Typical optical microscope image of (a) MWCNT/aqueous and (b)MWCNT/GO solutions (Lu et al., 2015)

Xiaoyu et al., 2013 produced a humidity sensor from GO/MWCNT composites. The results obtained from SEM's images of GO/MWCNT showed that the MWCNT align between the GO sheets. Although there is an acceptable dispersion obtained through this method GO is too expensive and consequently there is a limitation to apply this method of dispersion for use on an industrial scale. Oliver et al. 2012, studied the dispersion of SWCNT by CNC. The results of this investigation showed that, highly stable dispersions of SWCNT by CNC solution was obtained. The experiments, which used atomic force microscopy (AFM) and TEM, produced good results showing formation of hybrid particles. These hybrid particles consist from CNC accumulated on a SWCNT parallel to the axis of nanotubes by a self-assembly process (layer by layer deposition). The reason for that might be the interaction between CNC and SWCNT as a consequence of CNC specific crystalline (200) phases and (200) (hydrophobic phases) and SWCNT hydrophobic carbon structure which expel water molecules and stabilize the SWNTs suspension. Furthermore, CNC have long range electrostatic repulsion forces between them that may also have positive effects on stabilizing SWCNT /CNC. In addition, Trigueiro et al. 2014 produced film through the layer by layer process of MWCNT, chitosan and CNC. Using SEM investigation, they concluded that the MWCNT were well dispersed by CNC through the same mechanism described by Oliver et al. (2012). It should be noted that these two studies require further research into their mechanisms and potential applications.

In summary: as discussed above, the using non covalent method to disperse MWCNT has many advantages such as it disperses MWCNT without causing excessive damage to their surfaces as well as maintaining the original properties of MWCNT. However, as discussed above, this method has some limitations such as, GO is expensive material and cannot be used in industrial scale as well as CNC are short fibers thereby their advantages will be limited. Furthermore, using CNC in high concentration is problematic due to difficulties to achieve uniform dispersion thus it requires to use more energy or chemicals to overcome these difficulties.

#### 2.3.1.3 Dispersion of MWCNT using surfactants

To disperse MWCNT without causing excessive damage to their surface, surfactants have been commonly used. The basis for this technique involves combining MWCNT with surfactants into aqueous solution after which ultrasonic mixing is used to separate the MWCNT bundles. Many researchers have studied the use of surfactants to disperse MWCNT in cementitious materials using a range of different types and concentrations. Jang et al. (2015) investigated mechanical properties of cement paste reinforced by MWCNT and dispersion. They used ADVA Cast 575 (Grace Corporation) as the surfactant and studied its effects on cement paste properties. This surfactant was a polycarboxylate-based water-reducing admixture and was added at 0, 0.1, and 0.5 percentage by weight of cement. Dispersion of MWCNT was controlled through both surfactants use and ultra-sonication. MWCNT percentage raged from zero to 0.5% by the mass of cement. Ultra-sonication energy was 22 KHz and pulse mode has been used, cycles of 15 seconds on and 15 seconds off. Then, to prevent evaporation, the sample was put in an ice bath throughout the sonication process. It was found that MWCNT in distilled water without surfactant tended to agglomerate and settle immediately, indicating their instability in distilled water. On the other hand, the presence of surfactant with MWCNT led to enhanced dispersion. It was observed that surfactant had a positive effect on dispersion of MWCNT in cement matrices. According to this research, the compressive and tensile strength of MWCNT/cement composites with surfactant increased for percentage of MWCNT between 0-0.25%. The compressive strength increased by 20%, and the tensile strength also increased by 40% for 0.25% of MWCNT with added surfactant.

Metaxa et al. (2012) investigated the effect of highly dispersed MWCNT-based materials. Surfactant (SFC) was used and the proportions of surfactant to MWCNT were 0, 1.5, 4.0, 5.0, 6.25, and 8.0; the cement paste had a w/c=0.5 reinforced with 0.08 wt. percentage MWCNT. Furthermore, a 500w cup-horn high-intensity ultrasonic processor was used for sonication with constant energy, a cylindrical trip and temperature controller. The temperature controller was used to prevent the overheating of suspensions.

According to results, individual MWCNT were only noticed on the failure surface for the samples which had surfactant with a proportion of surfactant to MWCNT between 4- 6.25. A higher average load was increased at all ages for the samples with a surfactant to MWCNT ratio of 4.0 and a less average load was noticed for samples with a surfactant to MWCNT ratio lower or higher than 4.0. The authors suggested that a lower amount of surfactant meant lower molecules were absorbed to the carbon surface leading to decreased protection from agglomeration. On the other hand, the higher amount of surfactant could lead to bridging flocculation between the surfactant molecules. However, an increased amount of surfactant could cause a decrease of the electrostatic repulsion forces between the MWCNT.

Sobolkina and others (2012) studied the effect of dispersion for two types of carbon nanotubes (CNTs) on the mechanical properties of the cement matrix. Two types of surfactant were used; the first was an anionic sodium dodecyl sulfate (SDS, mw-288.38 g/mol) and the second type was a nonionic polyoxyethylene (23) laurylether (denoted below as Brij 35, MW = 1198g/mol). The proportions of CNT to surfactant were 1:0, 1:1 and 1:2. Furthermore, the minimum proportions were 1:0.24 for CNTs with SDS and 1:0.02 for Brij 35. For sonication purposes, cup-horn high-intensity ultrasonic homogenizer with a cylindrical tip was used at an amplitude of 70% of the maximum. Sonication periods were 30, 150, 210 min. A sonication period of less than 30 minutes was unacceptable due to the poor quality of dispersion. Furthermore, evaporation of the water during sonication was controlled by covering and cooling the glass container.

UV-VIS Spectroscopy was used to study the relationship between CNTs, surfactant concentration and sonication time. It was found that better dispersion was achieved with CNT/surfactant ratio equal to 1:1 – 1:1.5 and a sonication time of 120 min.

Abu Al-Rub et al (2012) investigated the effects of adding surface-treated and untreated carbon nanofibers (CNF) to nanocomposite cement. A solution of sulphuric acid

($H_2SO_4$) and Nitric acid ($HNO_3$) was used to functionalize surface treated nanofilaments and an ultrasonic mixer was used for dispersal. Two concentrations of untreated and treated CNF and CNT were used, the first was 0.1% by weight of cement and the second concentration was 0.2% by weight of cement. A commercial superplasticizer, ADVA cast 575 (Grace Coporation) was used as a surfactant in a ratio of 0.005 surfactant/cement. This amount of surfactant was found to be insufficient as there were some difficulties in putting the solution into the moulds. However, delayed hydration could have occurred if amounts of surfactant were increased. Cement paste showed better mechanical properties with untreated nanofilaments and this may have been due to better dispersion through surfactant action and sonication. In addition, treated nanofilaments produced weaker mechanical properties. This could be explained by the presence of the excessive formation of ettringite due to the presence of sulphates.

Surfactant effects on dispersion of MWCNT in aqueous solution were investigated by Yu et al. (2007). Different amounts of MWCNT were added in aqueous surfactant solution with different concentrations of the surfactant sodium dodecyl sulphate (SDS;90%). The results of this study showed that surfactant molecules were absorbed on surfaces of MWCNT preventing agglomeration but the greatest concentration of MWCNT found to be well dispersed in aqueous surfactant solution was 1.4-wt%.

In summary: as described above, this method has many advantages such as it enables MWCNT to disperse in aqueous solution and cementitious composites without causing excessive damage to their surfaces as well as maintaining the original properties of MWCNT. However, as discussed above, this method has many disadvantages such as, low amount of surfactant could cause poor dispersion of MWCNT in aqueous solution and cementitious composites (i.e. agglomeration of MWCNT in cementitious composites induces stress concentration limiting the strength of cementitious composites and leading to a nonhomogeneous microstructure thereby providing moderate performance enhancement of cementitious materials). Furthermore, low amount of surfactant could lead to lack of workability (i.e. difficulties in putting fresh mixes into moulds). In the other hand, high amount of surfactants could delay hydration process of cementitious composites as well as it could lead to bridging flocculation between the surfactant molecules and could cause a decrease of the electrostatic repulsion forces between the MWCNT.

#### 2.3.1.4 Dispersion via physical technique (ultrasonication)

Dispersion of MWCNT using physical methods such as ultrasonication has been widely researched. Different amounts of energy and time durations have been used for instance, (Dassios et al., 2015)) investigated the effects of sonication parameters such as sonication time and intensity on homogeneous surfactant-assisted dispersion of MWCNT in aqueous solution. In this study a range of different sonication times and intensities were used. In addition, liquid mode laser diffraction and SEM were used to study the dispersion of MWCNT in surfactant aqueous solution and the effects of sonication parameters on the tube aspect ratio. The results of Dassios's study showed that an energy density rate 7.7 J min-1Ml-1 is applicable for a duration of 90 min to achieve well dispersed MWCNT and without significant change to the tube length (thereby indicating minimal damage to MWCNT structure) with the same experimental conditions specific to this study. However, according to previous research, we can conclude that ultra-sonication alone was not sufficient to achieve well-dispersed MWCNT. Figure 2.17 illustrates the mechanism to make cavitation bubbles which create shear forces to disperse MWCNT by physical forces by ultrasonication method.

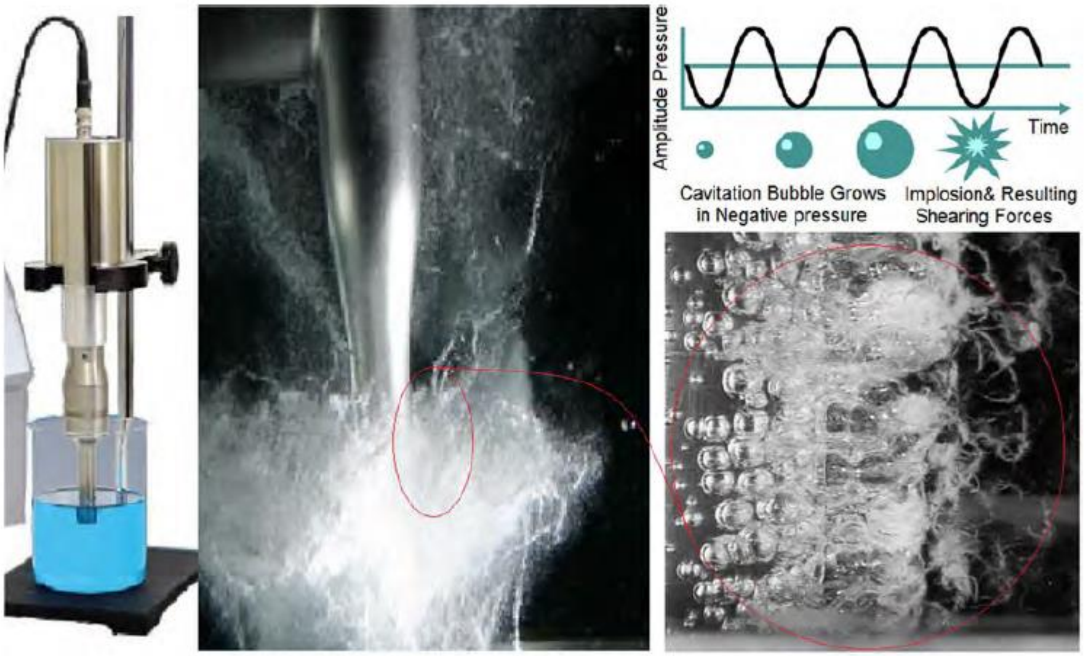

**Figure 2.17:** Shear forces created by cavitation bubbles are created in time of ultrasonication (Alhelfi and Sunden, 2016)

In summary, as described above, ultrasonication method is commonly used to separate the bundles of MWCNT to individual tubes and it could be used with other method to help dispersion process. However, as discussed above, this method has many disadvantages like it could cause significant change in length of MWCNT due to shear forces during sonication. Furthermore, MWCNT tend to settle down immediately, indicating their instability when ultrasonication was used only.

## 2.4.0 Cementitious materials reinforced with nanomaterials

### 2.4.1 Carbon Nanotubes reinforced cementitious composites

CNTs are employed extensively in many fields of nanocomposite materials due to their original mechanical, thermal, chemical, and electrical properties. In cementitious nanocomposites, under the conditions of uniform dispersion of CNTs and good bonding between CNTs and the hydrated cement matrix, the addition of CNTs to cementitious composites materials could result in excellent mechanical properties through effective crack bridging.

Earlier attempts have been made to add CNTs in cementitious matrices at amounts ranging from 0.5 to 2% (by the weight of cement). The major challenge associated with the incorporation of CNTs in cement-based matrices is poor dispersion. Poor dispersion of CNTs leads to a formation of many defect sites in nanocomposites and limits the efficiency of the CNTs in the cement matrix. From previous studies, CNTs can also have an effect on the early hydration process producing higher hydration rates.

Abu Al-Rub, (2012) studied the mechanical properties of nanocomposite cement incorporating surface-treated and untreated CNTs and CNFs. Different dosages of CNTs and CNFs were added to a cement paste with/without chemical treatment. 0.1% and 0.2% of both CNTs and CNFs were put into the cement paste by the weight of cement. Furthermore, CNTs and CNFs were also added in a solution of sulfuric acid ($H_2SO_4$) and nitric acid ($HNO_3$) for surface treatment. An ultrasonic mixer was used for dispersing CNTs and CNFs by producing air bubbles. The Young’s modulus, flexural, ductility and modulus of toughness of cement paste were recorded at 7, 14 and 28 days. SEM was used to investigate the microstructure of cement paste. Experimental results showed that the chemical treatment demeaned nanomaterial mechanical properties. In contrast, untreated CNTs and CNFs contributed to an enhancement of mechanical properties. Average ductility increased by 73%, the flexural strength increased by 60%, the average Young’s modulus increased by 25% and the average modulus of toughness increased by 170%. Figure 2.18 shows SEM image of untreated MWCNT embedded in cement paste and work was undertaken by the MWCNT to bridge cracking and to decrease crack propagation at nano level.

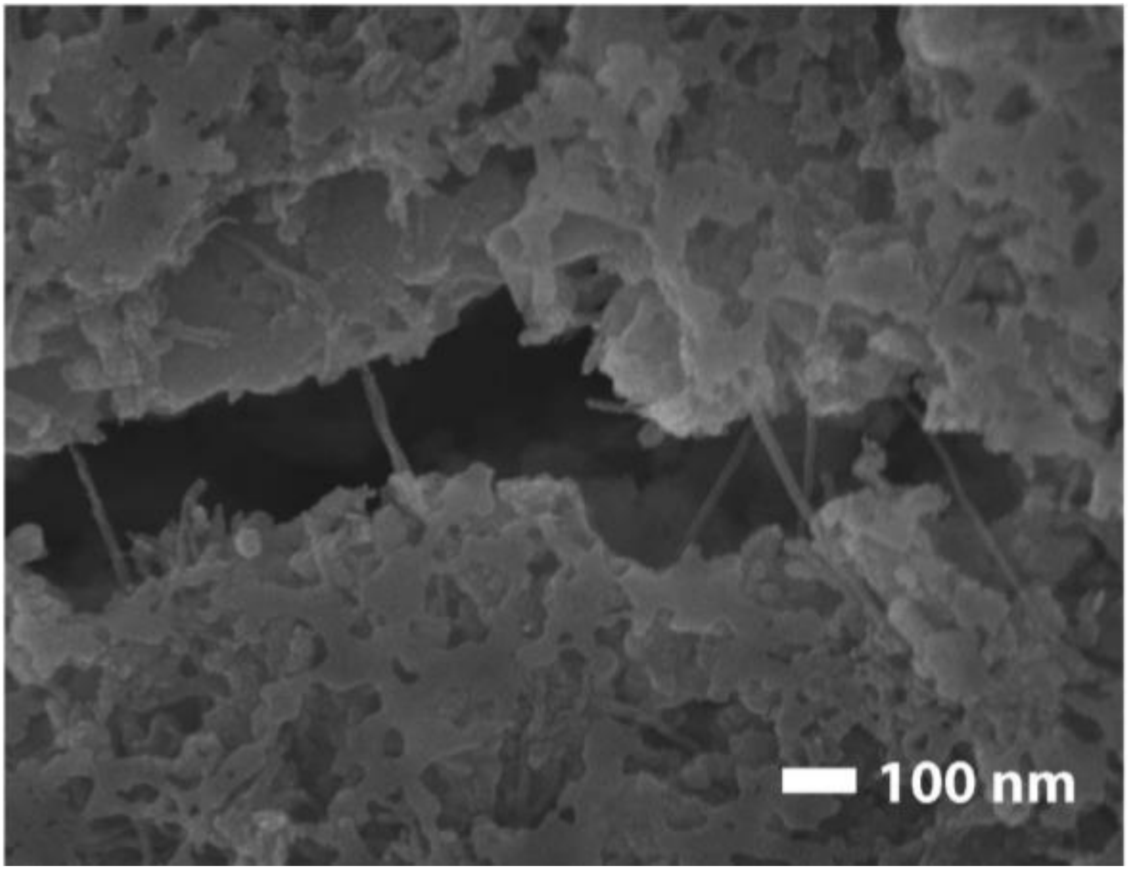

**Figure 2.18:** SEM image of untreated MWCNT embedded in cement paste bridging a nano-sized crack

The observed improvements in the mechanical properties of cement could have been gained due to the existence of interfacial bonds between the Nano filaments and cement, however these improvements were not seen for surface-treated CNFs. It could be concluded that the chemical treatment has negative effects on the mechanical properties, and these may have been caused by excessive formation of ettringite due to the existence of sulphates. Although there is a clear increase in flexural strength, ductility and Young's modulus, there is a limitation in crack bridging of microcracks and there is agglomeration of CNTs in cement, which induces stress concentrations limiting the strength of the cement pastes. Many studies have examined the relationship between MWCNT and cementitious composites. In 2015, LU et al. published a paper in which they described the effects of addition GO/MWCNT composites to cement paste. The dispersion of MWCNT in the GO solution were examined via UV- vis spectroscopy and optical microscopy and MWCNT were found to be better dispersed in the GO solution than in aqueous solution alone. This may have happened due to the higher electrostatic repulsion produced by the GO. In addition, it was also shown that the addition of GO/MWCNT composites to cement paste improved compressive strength and flexural strength of cement paste by 21.13% and 24.21% respectively. However, the addition of only MWCNT to cementitious composites improved compressive strength and flexural strength of cement paste by 6.40% and 10.14% respectively; and the addition of only GO to cement paste improved compressive strength and flexural strength of cement paste by 11.05% and 16.20% respectively.

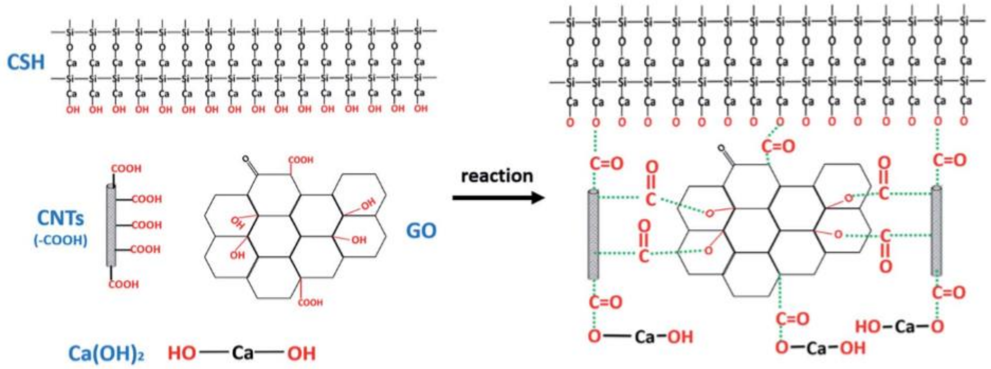

**Figure 2.19:** Mechanism of GO/MWCNT/cement paste composite with enhanced mechanical properties (Lu et al., 2015)

Clearly there was a synergistic effect resulting in improvements in both compressive strength and flexural strength. This improvement of cement paste by addition GO/MWCNT composites is most likely due to tow effects. First, the better dispersion of CNTs thereby more CNTs contribute to the mechanical improvement of cement paste. Second, the two phases of hydration products C-S-H and $Ca(OH)_2$ are likely connected as shown in figure 2.19 with GO and CNTs together. GO sheets interlock with cement hydration products and at same time bridge CNTs by chemical bonding thus the mechanical properties of the GO/CNTs/cement paste are significantly enhanced. Although there is clearly an increase in both flexural strength and compressive strength; there are limitations with crack bridging of microcracks due to the short CNTs do not have the length to bridge the cracks with a large width, agglomerations of MWCNT in cement (which induce stress concentrations limiting the strength of the cement pastes) and further GO is an expensive material to use as surfactant agent, and hence not suitable for large scale industrial use.

The effect of ultra-sonication on dispersion and mechanical properties of MWCNT cement mortar was studied by S. Alrekabi, (2015). The results of this investigation show that for modest sonication intensity there is a requirement for longer duration of sonication, which could lead to a decline in the aspect ratio of MWCNT by fracturing the tubes. In case of higher sonication intensity there is rapid sonication of MWCNT. Furthermore, a significant increase of the individual dispersed tubes in water were shown with intensive sonication with surfactant. A decline in the aspect ratio was noticed whilst observing individual tubes but also that this could cause loses in reinforcement effects due to limitations in length to bridge microcracks.

Collins et al., (2012) discussed the dispersion, workability, and strength of CNT-OPC paste mixtures with and without several generically different dispersant/ surfactants as admixtures. These admixtures were air entrained, styrene butadiene rubber, polycarboxylates, calcium naphthalene sulfonate, and lignosulfonate formulations. The results of their investigations showed that for CNT in aqueous solution only there are CNT agglomerations in aqueous solution, despite mechanical agitation by magnetic stirring and ultra-sonication which was used for dispersion. Furthermore, CNTs were dispersed in aqueous solutions by air entrained but it can be observed that sedimentation happened within days of mixing.

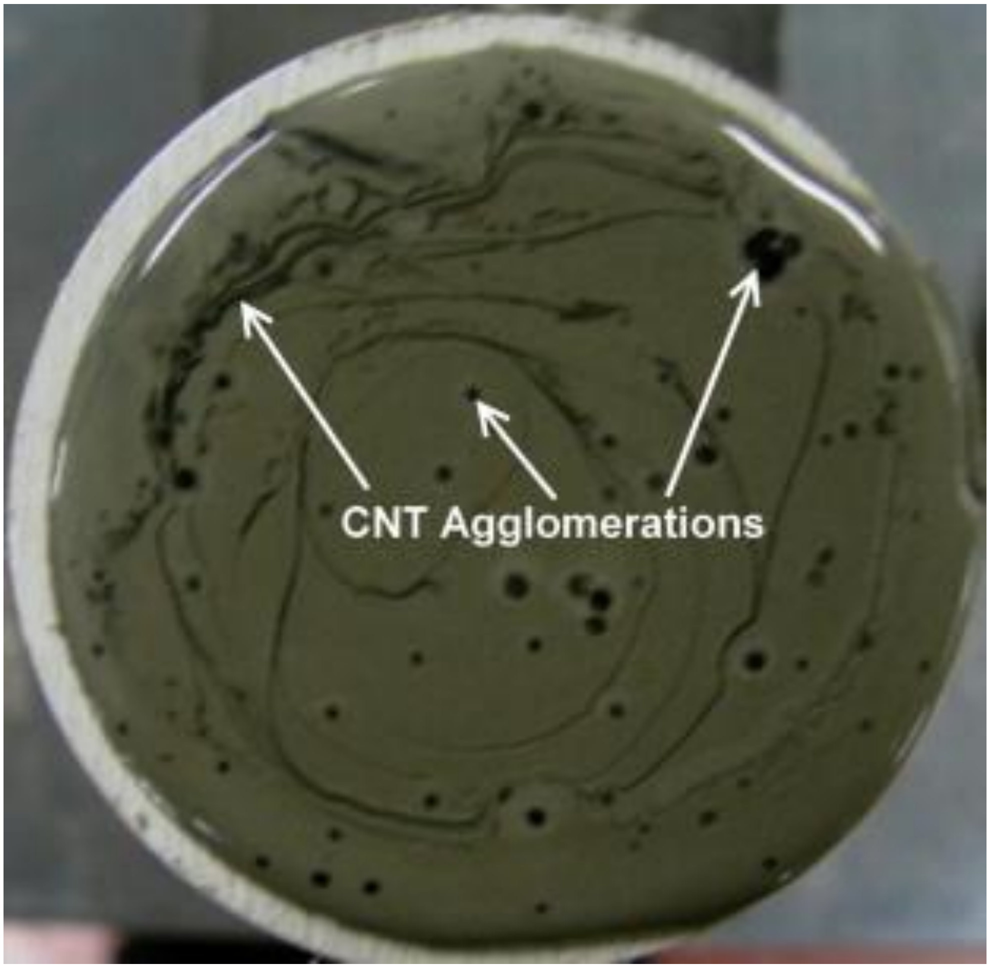

**Figure 2.20:** CNT Agglomerations in fresh cement paste (Collins et al., 2012)

In addition, proper dispersion of CNT in aqueous solutions was achieved after ultrasonication with polycarboxylate and lignosulfonate admixtures. A little visible sedimentation was observed even 9 days following mixing that gives an indication of proper dispersion of CNT in aqueous solution. Furthermore, despite proper dispersion of CNT in aqueous solution with the lignosulfonate admixture, the addition of CNT to OPC paste mixtures decreases strength and consistency that could be caused by the existence of agglomerates of CNT as shown in figure 2.20 and figure 2.21, and that lead to a decline in compressive strength. Although the compressive strength of CNT-OPC paste enhanced with an addition of polycarboxylate to the mixture, there was a clear reduction in workability.

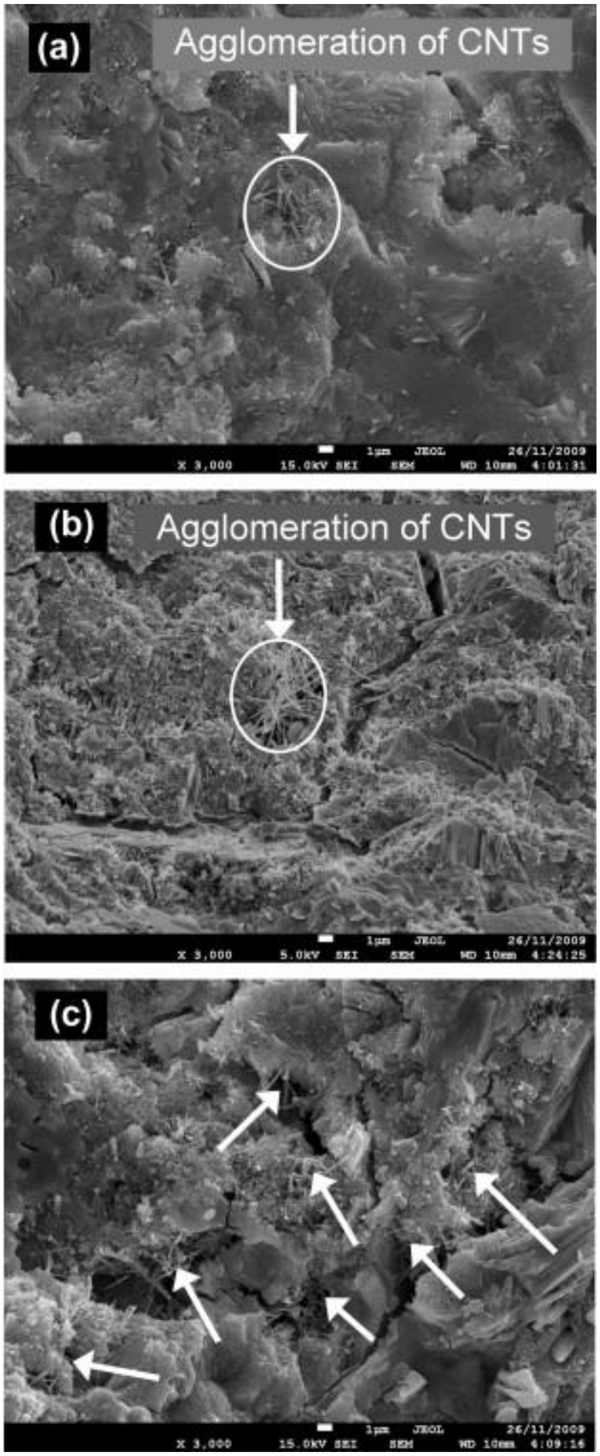

**Figure 2.21:** Typical SEM images of Agglomerations of CNTs in cement pastes (Collins et al., 2012)

Sobolkina et al. (2012) studied a dispersion of CNT and the mechanical properties of cement matrices. Sonication with anionic and non-ionic surfactants in varying concentrations was used in this study. UV-VIS spectroscopy was used for determining the relationship between the quality of CNT dispersion, the sonication time and surfactant concentration. The visual observations by SEM revealed that most nitrogen-doped CNT were observed as individual broken CNT. In addition, the destruction of CNT caused by sonication was not identified after the treatment of a mixture of single-, double- and multi-walled CNT.

Furthermore, the improvement of cement pastes by dispersed CNT lead to an increase in the compressive strength by 40%. In contrast, no significant enhancement was seen for quasi-static loading. The investigation at microscopic level showed that the bridging of the C-S-H phases changed depending on types of CNT. Lastly, the CNT addition has positive effects on mechanical properties of hardened cement paste. According to the results of the study, a better result could be obtained when the ratio of CNT-surfactant was 1:1 - 1:1.5 and sonication time about 120 min.

A discontinuous network or individual fibres were seen by microscopic examination in cement paste with CNT. This shape of distribution happened as the CNT have insufficient length caused by shear forces during sonication and by misalignment attributable to twisting and curling. Hence, CNT did not have the ability to bind neighbouring C-S-H clusters and to bridge the voids between them. The lack of improvement in the tensile strength of the cement matrix may therefore be explained by CNT not possessing enough ability to bind and bridge the voids. Finally, although CNT exhibited proper dispersion in an aqueous solution, there was destruction of CNT (broken and short CNT was observed) and the dispersion was not fully achieved in the cement matrix. This causes the loss of reinforcement benefit and the lack of ability to bridge cracks in the cement matrix.

Musso et al. (Musso, Tulliani et al. 2009) studied the effect of the addition of three types of MWCNT (as-grown, annealed and functionalized) to cement mortar (0.4:1:1.5) on its flexural and compressive properties. Thermogravimetric analysis (TGA) was used to evaluate the phase composition of composites, an X-ray diffractometer (XRD) was operated to analyse mass spectroscopy (MS), and SEM techniques were employed to investigate microstructure and the mineralogy. The observations from the flexure test results seem to indicate that the addition of carboxyl functionalized MWCNT led to a 40% decrease in the strength of the cement mortar and the addition of pristine MWCNT led to a 34% increase in flexural strength. The flexural strength of cement-based materials increased by about 9% with annealed MWCNT. Compressive strength test results showed comparable trends with compressive strength resulting in a sharp drop with carboxyl-functionalized MWCNT. Although there is a clear increase in flexural strength with the addition of pristine MWCNT and a slight increase again with the addition of annealed MWCNT, there is a limitation in bridging microcracks and agglomeration of MWCNT is evident in cement especially, which induces stress concentrations limiting the strength of the cement pastes.

Xu et al. (2015) compared the microstructure and flexural and compressive strength of unreinforced Portland cement paste versus Portland cement paste reinforced with MWCNT. The test included MWCNT of 0.0% to 0.2% by weight of cement. The use of an additional 0.1-wt% MWCNT improved the results of the mechanical properties of the cement paste, increasing the compressive strengths at 7-day and 28-day intervals by 22% and 15% respectively. The flexural strength of cement pastes appeared to improve when reinforced with MWCNT. The microstructure, obtained by SEM analysis, can be seen in the visual observations below. Figure 2.22(b) shows a good dispersion of MWCNT in an aqueous solution with individual MWCNT forming after dispersion, while figure 2.22(a) shows bundles and large agglomerations of MWCNT before dispersion.

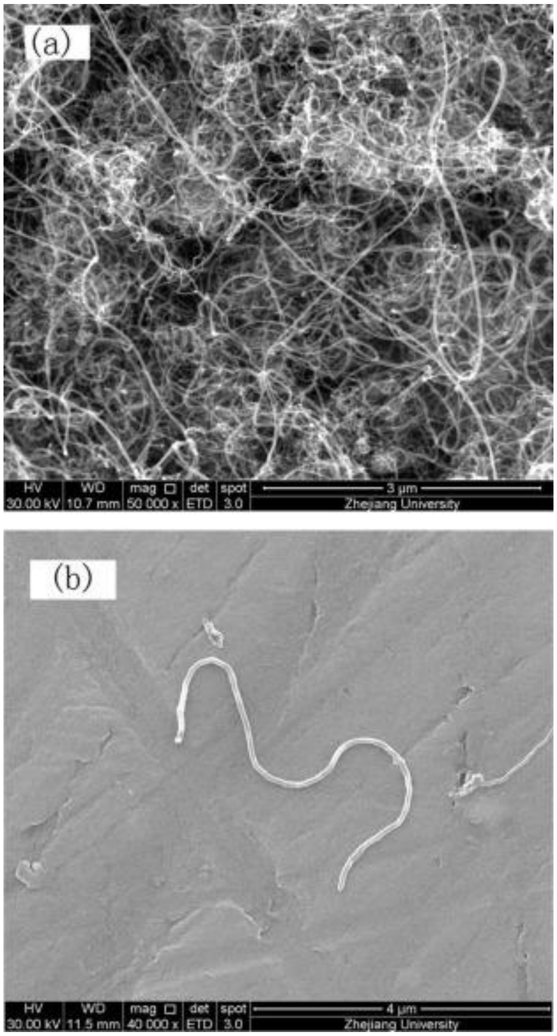

**Figure 2.22:** SEM of MWCNT: (a) before dispersion (b) after dispersion (Xu et al., 2015)

In addition, debonding, crack bridging and mesh filling can also be observed from SEM as shown in figure 2.23. In figure 2.23(a) the corresponding MWCNT was oriented along the same direction and had the same size, thereby it is presumably a slip of a MWCNT and debonding occurred. It can be observed in figure 2.23(b) that MWCNT work on crack bridging and in figure 2.23(c) a MWCNT was between cement hydration products.

In order to measure pore distribution in the MWCNT-reinforced cement pastes, pressured-mercury testing was used. The findings showed that the pore size distribution tend to gel pores, which have a positive influence on mechanical strength. Interestingly, the addition of MWCNT to cement paste did not lead to high increase of mechanical properties of cement paste but it led to a slight improvement.

Li et al. (2005) compared the mechanical properties of unreinforced cement paste versus reinforced cement paste with modified MWCNT by using a $H_2SO_4$ and $HNO_3$ mixture solution. From the test results, the treated MWCNT effectively improved the mechanical properties of cement paste and the failure strain of cement. In order to determine the porosity and pore size distribution of the composites, Mercury intrusion porosimetry was employed and it can be observed that the porosity decreased with the addition of MWCNT. Fourier-transform infrared spectroscopy was used to characterize the phase composition. The results showed that MWCNT and the hydrations of cement have interfacial interactions between each other. A high bonding strength between the reinforcement and cement matrix will be produced by these interfacial interactions. SEM was used in order to analyse the mineralogy and microstructure of cement paste. The visual observation of the microstructure obtained through SEM analysis revealed evidence of crack bridging across cracks by MWCNT, which explains the load transfer in case of tension. Although there is a clear increase in flexural and compressive strength with the addition of treated MWCNT, the chemical treatment is a sophisticated process which involves many chemical materials.

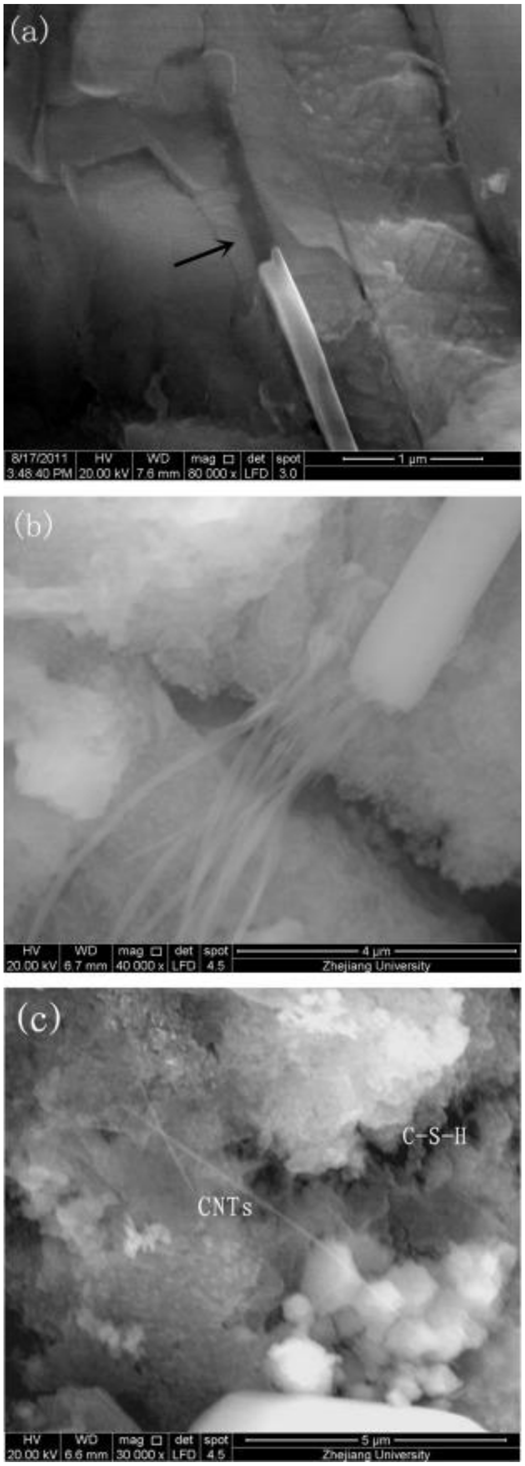

**Figure 2.23:** SEM image of (a) debonding, (b) crack bridging, and (c) a single CNT in hydration products (Xu et al., 2015)

Al-Rub et al. (2012) compared the flexural strength of unreinforced cement paste versus the flexural strength of cementitious nanocomposites reinforced by different concentrations of long MWCNT (high length/diameter aspect ratios of 1250–3750) and short MWCNT (aspect ratio of about 157) in cement paste. Mechanical properties of the cement/MWCNT composites were evaluated at intervals of 7, 14, and 28 days by flexural bending tests. The results of flexural strength for short 0.2-wt% MWCNT and long 0.1-wt% MWCNT can be compared with the results of the plain cement sample at 28 days. It found that there was increase by 269% and 65% respectively, which shows that the addition of short 0.1-wt% MWCNT and short 0.2-wt% MWCNT led to an increase in ductility at 28 days by 86% and 81% respectively. It seems that there is little to distinguish between the mechanical performance of nanocomposites with a low concentration of long MWCNT and the mechanical performance of nanocomposites with a higher concentration of short MWCNT. The visual observation of the microstructure obtained by SEM analysis revealed evidence of micro-crack bridging. There had been breakage and withdrawal of MWCNT across the micro-cracks as shown in figure 2.24. The results show a clear increase in flexural strength and ductility with the addition of short 0.2-wt% MWCNT and long 0.1-wt% MWCNT, however, there is variability in the results. Although all samples are cast from the same mix and cured under the same conditions with a uniform distribution of MWCNT in aqueous solution, all these processes do not guarantee a uniform distribution of the MWCNT in the composite. This has led to a non-uniform distribution of stress in the composite beam and will cause variability in the flexural strength from one sample to another sample of the same composite.

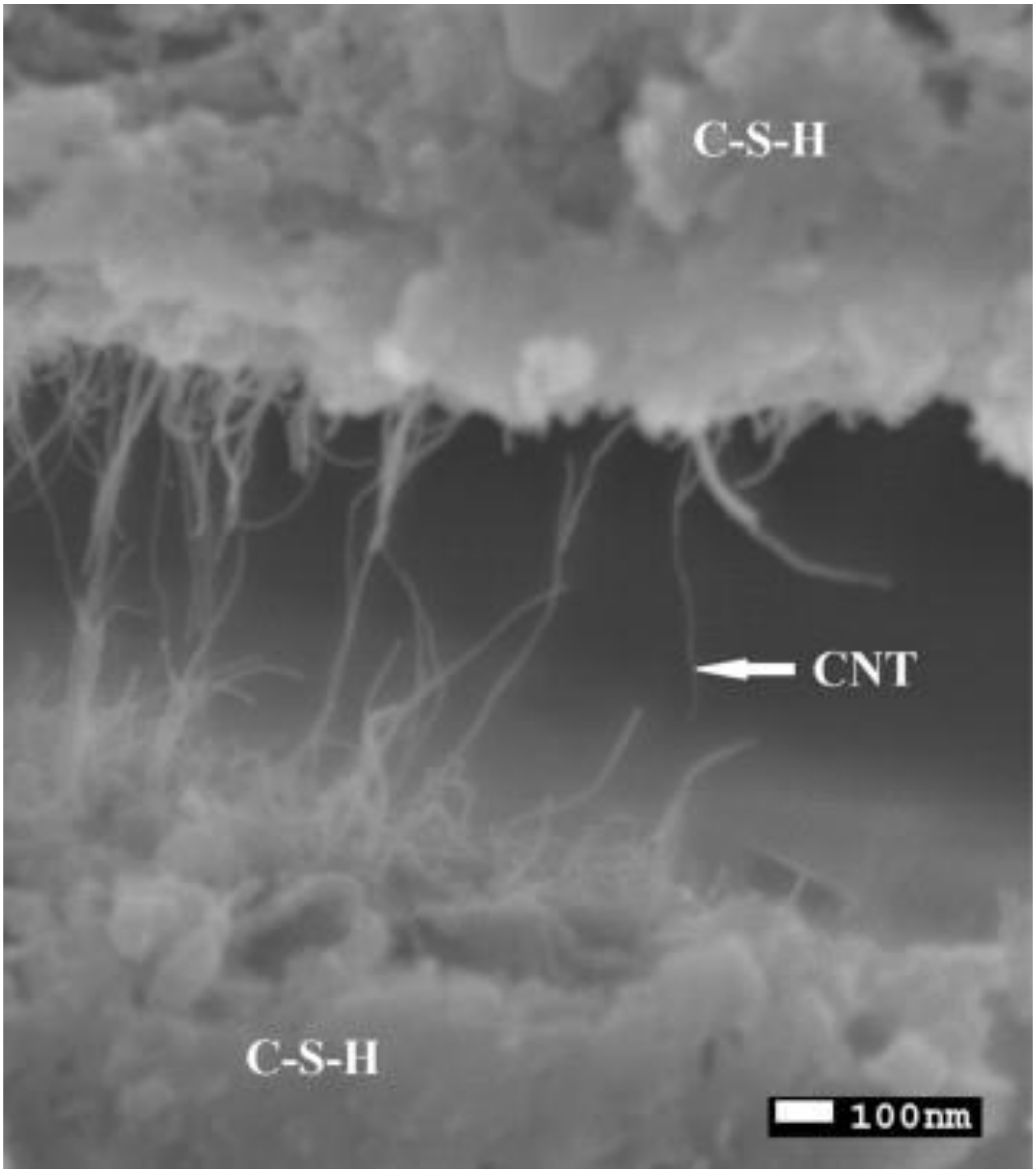

**Figure 2.24:** SEM image showing the micro-cracking bridging and breakage of the MWCNT within the cement paste composite (Abu Al-Rub et al., 2012)

The non-uniform distribution of MWCNT in the composite could be caused by the assembly of cement grains once added to the aqueous solution. These grains would hydrate and work as a filter preventing MWCNT to pass among the grains leading to a large area with few MWCNT and other areas with large agglomerations of MWCNT as shown in figure 2.25. More details were discussed in the paper of (Tyson et al., 2011).

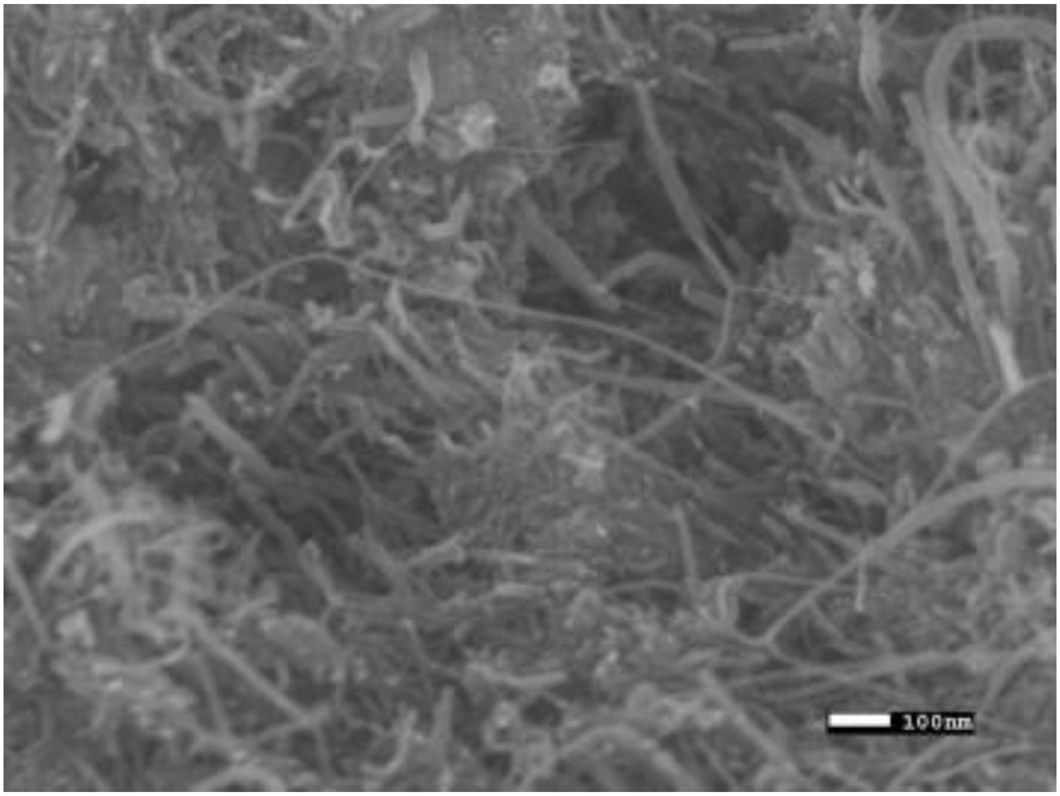

**Figure 2.25:** SEM image of MWCNT agglomerations within a small area of cement paste (Abu Al-Rub et al., 2012)

Jang et al. (2016) investigated mechanical properties of cement paste reinforced by MWCNT and the dispersion of MWCNT. A surfactant was used and the effect of surfactant on cement paste properties was studied. ADVA Cast 575 was used. This surfactant was a polycarboxylate-based water reducing admixture. A surfactant was added by percentage of the weight of the cement (0, 0.1, and 0.5).

Surfactant and ultra-sonication were used to control dispersion of the MWCNT. MWCNT percentage ranged from 0 to 0.5% by the mass of cement. Ultra-sonication energy was 22 KHz and pulse mode was used, cycles of 15 seconds on and 15 seconds off. Then, to prevent evaporation, the sample was put in an ice bath throughout the sonication process.

It was found that MWCNT in distilled water without surfactant tended to agglomerate and settle immediately, which indicates that MWCNT were unstable in distilled water. On the other hand, the presence of surfactant with MWCNT led to enhanced dispersion. It was observed that surfactant has a positive effect on dispersion of MWCNT in cement matrices. The compressive and tensile strength of MWCNT/cement composites with surfactant increased the percentage of MWCNT by between 0-0.25%. For the sample of 0.25% of MWCNT with a surfactant, the compressive strength increased by 20% and the tensile strength increased by 40%. The study of mechanical properties of cement paste reinforced by MWCNT is considered the most important but it is clear that further research relating to the dispersion of MWCNT is necessary.

Konsta-Gdoutos et al. (2010) studied the effect of highly dispersed MWCNT on cement-based materials. SFC as a surfactant was used and the proportion of surfactant to MWCNT was 0, 1.5, 4.0, 5.0, 6.25, and 8.0. These quantities of surfactant were added to cement paste (w/c=0.5) reinforced with 0.08 wt. percentage MWCNT. Furthermore, a 500w cup-horn high-intensity ultrasonic processor was used for sonication with constant energy, a cylindrical trip and temperature control. The temperature control was used to prevent the suspensions from overheating. It has been observed that only individual MWCNT were noticed on the failure surface for the samples which have surfactant with a proportion of surfactant to MWCNT between 4- 6.25 as shown in figure 2.26. A higher average load strength was increased at all ages for the samples with a surfactant to MWCNT ratio of 4.0 and a less average load strength was noticed for samples with a surfactant to MWCNT ratio lower or higher than 4.0.

The results showed that a lower amount of surfactant means less molecules are absorbed to the carbon surface nanotubes and this could lead to lower protection from agglomeration. On the other hand, the higher amount of surfactant could lead to bridging flocculation between the surfactant molecules, although a huge amount of surfactant causes a decrease of the electrostatic repulsion forces between the MWCNT.

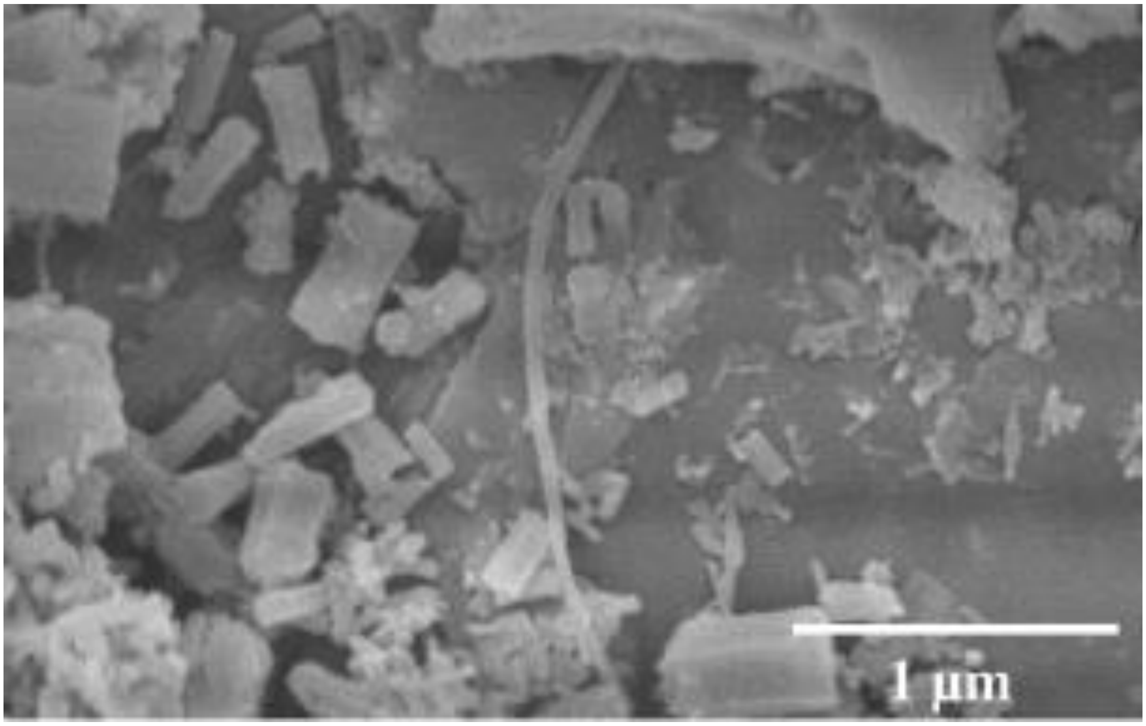

**Figure 2.26:** Dispersion of MWCNT in cementitious composite at 6.25 surfactant/MWCNT (Konsta-Gdoutos et al., 2010)

In Summary: as discussed above, using MWCNT in cementitious composites has advantages such as, the MWCNT reinforced nanocomposites exhibit higher flexural strength, ductility and young’s modulus when compared to plain cement samples. However, as discussed above, this method has many disadvantages such as agglomerations of MWCNT which induces stress concentrations limiting the strength of cementitious composites and leading to a nonhomogeneous microstructure thereby providing moderate performance enhancement of cementitious materials. Furthermore, there are limitations in crack bridging, some treatments could change the length of MWCNT thereby broken MWCNT and discontinuous network of MWCNT are resulted, hence MWCNT do not have the ability to bridge neighbouring C-S-H clusters and bridge the voids between them.

### 2.4.2 Graphene Oxides (GO) reinforced cementitious composites

Recently an investigation was performed by (Lv et al., 2013) regarding the effects of GO nanosheets on mechanical properties and the microstructure of hardened cement paste. Testing mechanical strength and SEM provide a convenient way for detecting shape changes of cement hydration crystals and mechanical strength. Oxidization and ultrasonic dispersion were employed to prepare GO. Figure 2.27 revealed that flower-like crystals formed due to regulation caused by GO nanosheets and figure 2.28 illustrates the schematic diagram of the regulation mechanism of cement hydration crystals with the presence of GO nanosheets, which work as a template to regulate cement hydration crystals. Many oxygen functional groups, including -OH, -COOH and -$SO_3H$, are on the surface of GO (figure 2.28(a)). These functional groups react with $C_2S$, $C_3S$ and $C_3A$ and the hydration products formed at the growth points are shown in figure 2.28(b). At these growth points on the GO surface, the hydration reaction continues to take place (figure 2.28(c)). The surface characteristics of GO control the growth points and growth pattern of the hydration products, thus GO has a template like effect and thereby could produce many neighbouring rod-like hydration crystals from a thick column-like shape and flower shaped crystals (figure 2.28(e)). These column products which grow on the GO surface in one direction due to limited space produce great stress around them, saving the column shape. These column products contain C-S-H, $Ca(OH)_2$ and rod-like Aft and AFm. When the growth of the column-shaped crystals take place in a pore, crack or loose structure they form the flower-like crystals due to available space around them which enables them to grow in this shape (figure 2.28(f)). These flower-like crystals disperse in pores and cracks and work as fillers thus minimizing crack propagation and remarkably increasing the tensile/flexural strength of cement composites.

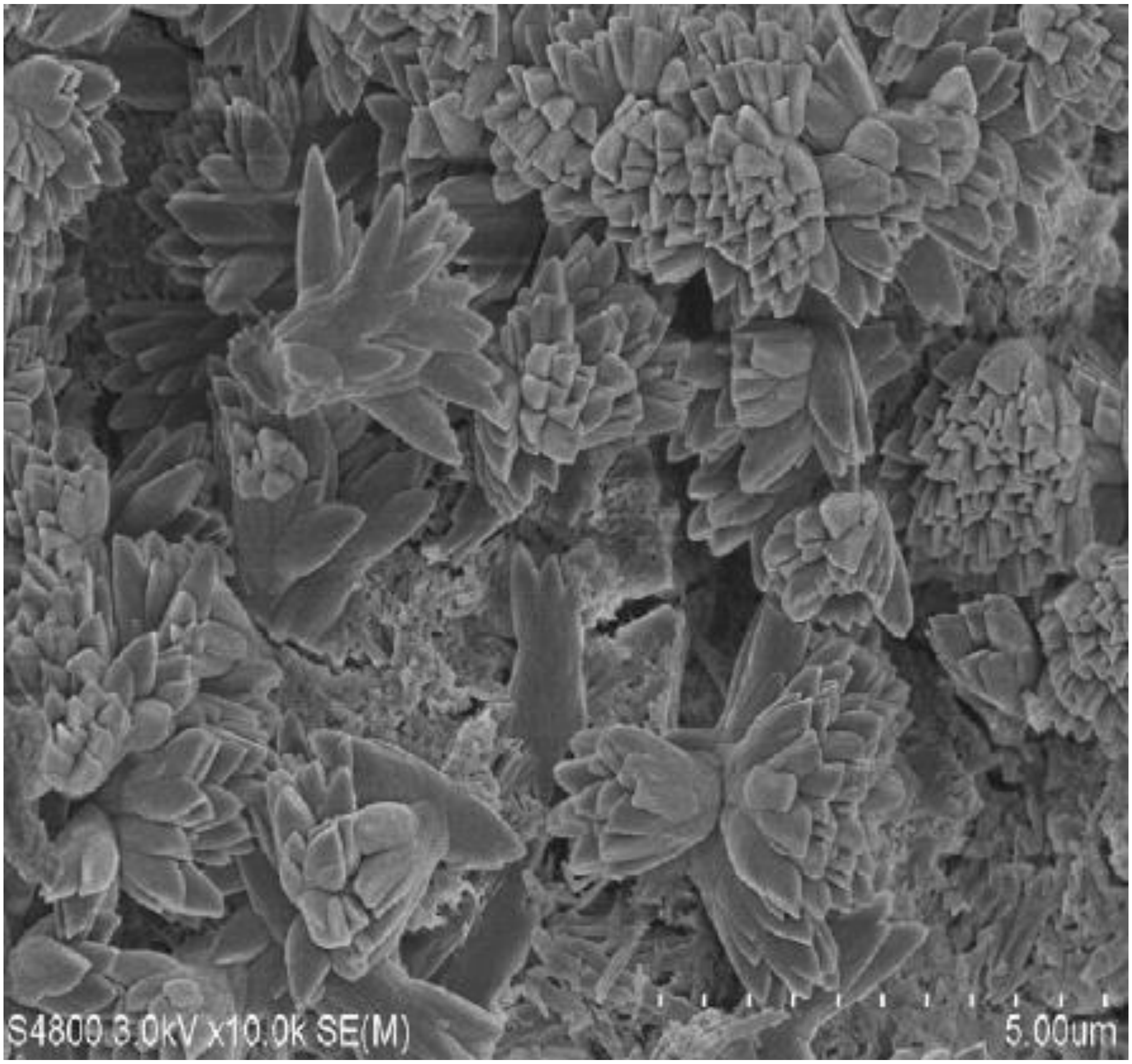

**Figure 2.27:** SEM image of cement hydration crystals (Lv et al., 2013)

From the results, there is a clear increase in the tensile/flexural strength of cement composite, however, there is a limitation for the use of GO in construction materials since there are health issues, complex processes for production and GO is an expensive material, which prevent its use on an industrial scale.

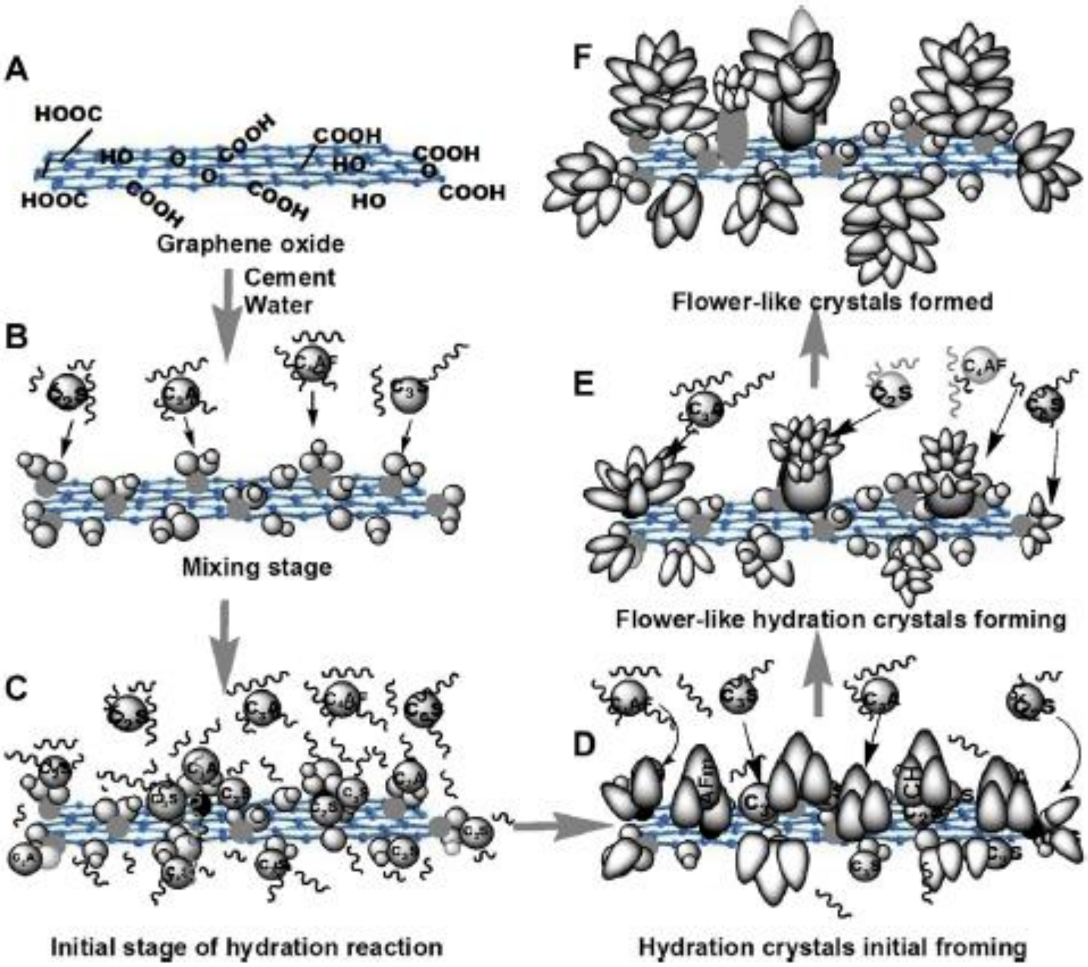

**Figure 2.28:** Schematic diagram of regulation of GO on cement hydration crystals (Lv et al., 2013)

Lv et al., (2014a) investigated the influences of GO nanosheets with different sizes and dosages on the mechanical strength of cementitious composites, cement hydration and crystal shapes. The visual observation of the microstructure obtained by SEM analysis revealed that at low GO dosage (<0.03%) flower-like crystals are more prominent and at high dosage (>0.03%) polyhedral or lamellar crystals are more prominent. The mechanical properties of cement paste increased significantly with smaller GO nanosheets. Based on SEM images, the addition of GO nanosheets to cement paste can promote the production of rod like crystals and assembly of flower-like crystals at low dosage and polyhedral and lamellar crystals at high dosage. Figure 2.29 reveals the formation of flower-like crystals due to regulation caused by GO nanosheets at low dosage. Figure 2.30 shows the formation of polyhedral and lamellar crystals due to regulation caused by GO nanosheets at high dosage.

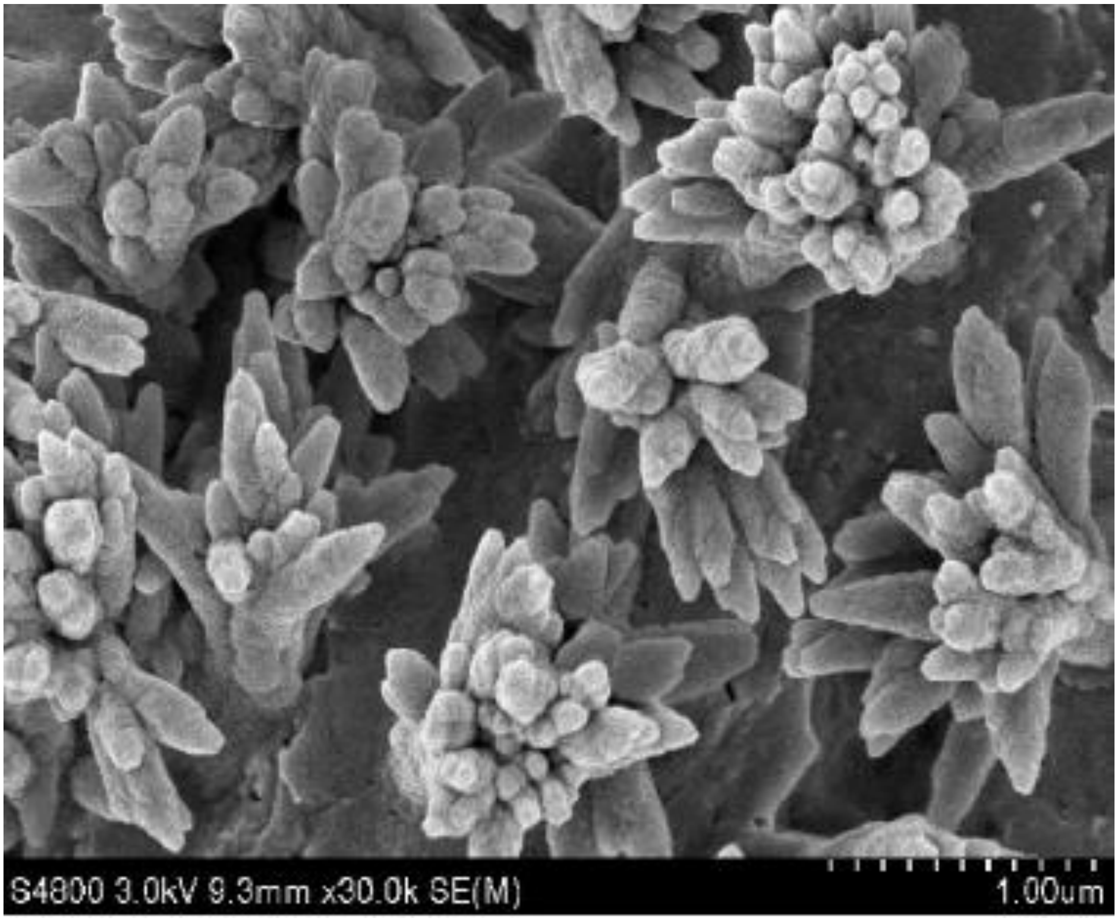

**Figure 2.29:** SEM image of cement hydration crystals (Lv et al., 2014a)

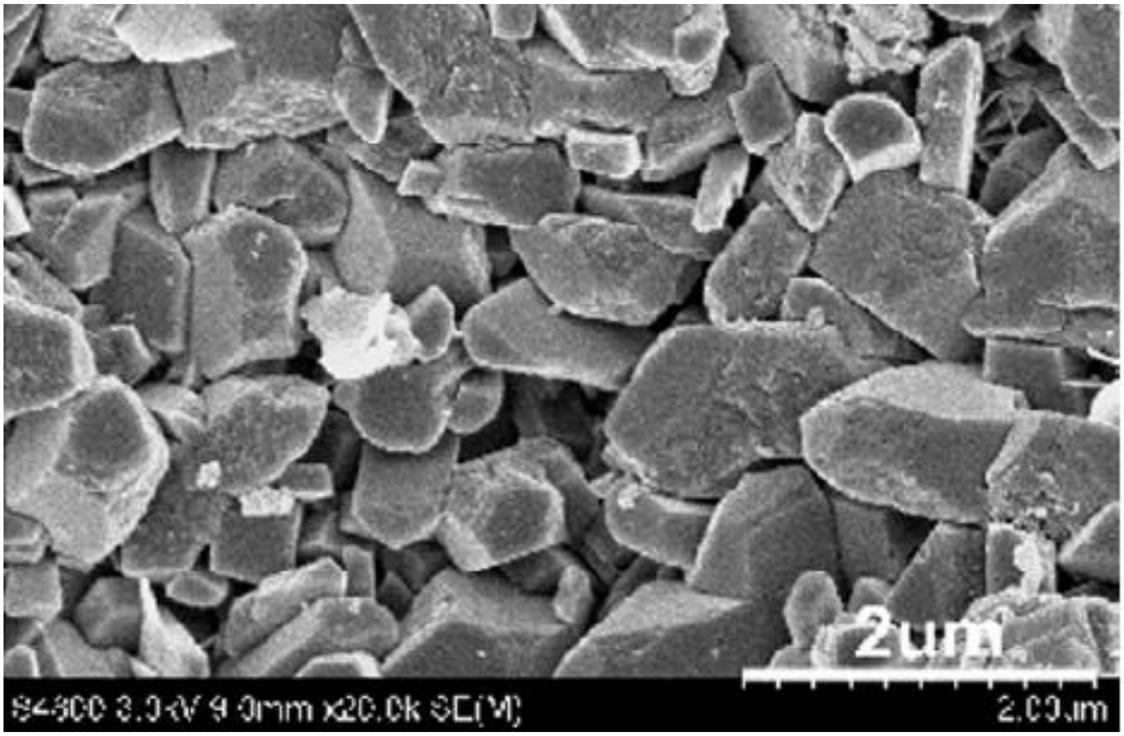

**Figure 2.30:** SEM image of cement hydration crystals (Lv et al., 2014a)

It is important to highlight that the formation of flower-like crystals in holes and cracks in cement paste, filling these and developing multipoint network connections, has great impact on the flexural strength, porosity, pore diameter, and based on SEM images dense and cross-linked structures are observed at all the crystal types. The reduction of porosity, pore diameter and dense structure help to enhance the mechanical properties of the cementitious composites. Finally, the results of this research show that the formation and properties of cement hydration crystals and the mechanical strength of cement paste are greatly affected positively by the addition of GO nanosheets. From the results, there is a clear increase in the tensile/flexural strength of cement composite, however, GO is a very expensive material and difficult to use in construction material due to health issues and sophisticated processes to produce GO.

Lv et al., (2014b) investigated the effects of GO nanosheets on the mechanical strength of cementitious composites and cement hydration crystal shapes. The oxidation of graphite was employed following sonication exfoliation to prepare GO nanosheets. The investigations on the GO nanosheets by FTIR and AFM (figure 2.31) showed that the GO nanosheets have a thickness of about 6 nm and the GO surface is covered with oxygenated groups (–OH, –O–, –COOH and $–SO_3H$). In addition, many oxygen functional groups, including -OH, -COOH and $-SO_3H$, are on the surface of GO (figure 2.32(a)). These functional groups react with $C_2S$, $C_3S$ and $C_3A$ and the hydration products formed at the growth points are shown in figure 2.32(b). At these growth points on the GO surface, the hydration reaction continues to take place (figure 2.32(c)). The characteristics of GO control the growth points and growth pattern of the hydration products, thus GO works like a template. GO could therefore produce many neighbouring rod-like hydration crystals from a thick column-like shape, flower-shaped crystals and polyhedron-shape (figure 2.32(d)). These column-like products on the GO surface grow in one direction due to compact space. The compact space creates a great stress around them, keeping the column shape. These column products contain C-S-H, $Ca(OH)_2$ and rod-like of AFt, AFm (figure 2.32(e)). When the column-shaped crystals grow in a pore, crack or loose structure, they form the flower like crystals due to available space around them (figure 2.32(f)). These flower-like crystals disperse in pores and cracks and work as fillers thus minimizing crack propagation.

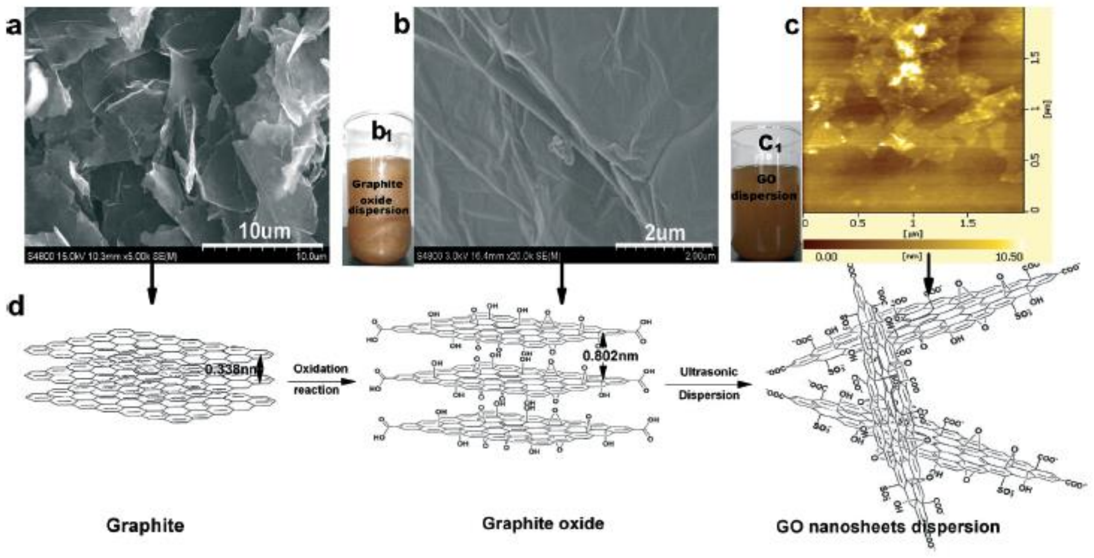

**Figure 2.31:** (a) SEM image of graphite, (b1) photograph of the graphite oxide dispersion, (b) SEM image of the graphite oxide membrane, (c1) photograph of the GO nanosheet dispersion, (c) AFM image of the GO nanosheets, (d) proposed mechanism for the formation of the GO nanosheets (Lv et al., 2014b)

From the results, there is a clear increase the tensile/flexural strength of cement composite. These mechanical properties are markedly increased with the addition of GO nanosheets due to regulation of the C-S-H and Ca(OH)2 which are controlled by GO.

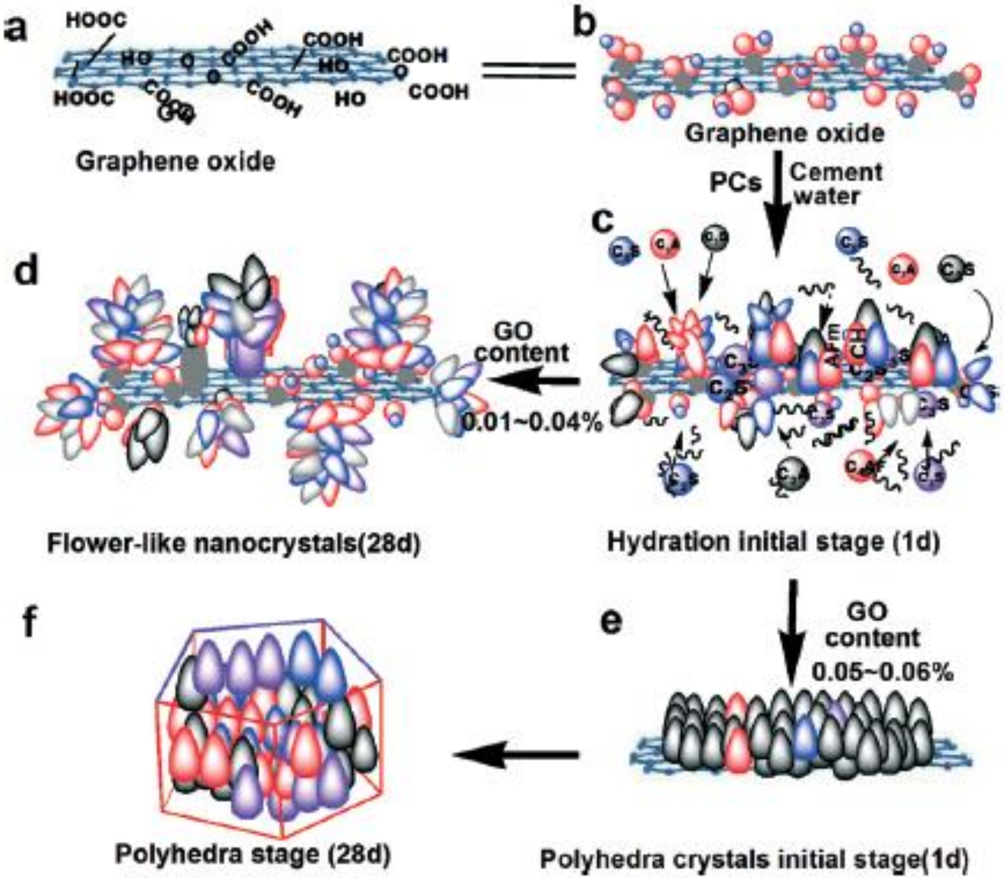

**Figure 2.32:** Schematic diagram of the regulatory mechanism of GO nanosheets on cement hydration crystals(Lv et al., 2014b)

Horszczaruk et al., (2015) compared the properties of plain cement paste versus reinforced cement paste with 3-wt.% of GO. At an early stage, the mechanical response of the GO-reinforced cement was investigated. Infrared, Raman and XRD techniques were employed to investigate the kinetics of the hydration process. In order to investigate the morphology of the nanocomposite, SEM was used. The results of this study show that cement nanocomposite with 3-wt% GO exhibited enhanced Young's modulus. In addition, the kinetics of the hydration process are not strongly affected by GO addition. Furthermore, based on SEM images of hardened cement pastes containing GO, it is found that the morphology of the reinforced sample is almost the same as the reference. From the results, there is a clear enhancement of Young's modulus of cement composite due to a uniform distribution of GO flakes in the cement matrix. However, there are limitations in the use of GO in construction materials since there are health issues, complex production processes and it is an expensive material, preventing its use on an industrial scale.

Babak et al., (2014) presented a paper on the effect of GO on the mechanical properties of cement composites. In order to improve the dispersion of GO flakes in the cement, a polycarboxylate superplasticizer was used. The experimental work includes measuring the mechanical properties of plain cement paste and GO-cement nanocomposites containing 0.1–2-wt.% GO and 0.5-wt.%. The results showed that the addition of 1.5% GO per mass of cement resulted in increased tensile strength of 48% in cement composite. In order to observe the fracture surface of samples containing 1.5-wt.% GO, ultra-high-resolution field emission scanning electron microscopy (FE-SEM) was used. The observation of fracture surface obtained by FE-SEM revealed that the homogeneous distribution of the GO flakes in the matrix was observed. In addition, effective bonding between the GO surfaces and the surrounding cement matrix was observed. Moreover, XRD diffraction data showed that the addition of GO additives improve the formation of C-S-H gel in cement composite. From the results, there is a clear enhancement of the tensile strength of cement composite due to homogeneous distribution of the GO flakes in the matrix, improving the formation of C-S-H gel in cement composite and homogeneous distribution of the GO flakes in the matrix.

In Summary: as described above, addition GO to cementitious composites has many advantages such as, the tensile/flexural strength of cementitious composites increases and the microstructure of cementitious composites is positively modified (i.e. GO has a template like effect and thereby could produce many neighbouring rod-like hydration crystals from a thick column-like shape and flower-like crystals. These flower-like crystals disperse in pores and cracks and work as fillers thereby minimizing crack propagation and enhancing the tensile/flexural strength of cement composites). However, as discussed above, there many limitations such as, the GO is expensive material, which prevent its use in industrial scale and its production process is sophisticated.

### 2.4.3 Cellulose nanocrystals reinforced cementitious composites

Cao et al., (2015) studied the effects of the addition of CNC to cementitious composites. Seven percentages of CNC ranging from 0% to 1.5% by the volume of cement were added to cementitious composites. An increase of approximately 30% was noticed for flexural strength for cementitious composite with a 0.2% volume of CNC with respect to cement. The rate of hydration of cementitious composite increased with the use of CNC, which was observed through isothermal calorimetry (IC) and thermogravimetric analysis (TAG). In addition, this increased hydration could be explained by two mechanisms. The first mechanism is steric stabilization which disperses cement particles similarly to that of many water reducing agents (WRA). The second mechanism is short circuit diffusion. It seems that this mechanism increases hydration rate by increasing the transportation of water from outside the hydration products to the dehydrated cement cores. Figure 2.33 shows a comparison between BSE-images of plain cementitious composite and 1.5% CNC cementitious composite, one interesting feature observed by 1.5% CNC cementitious composite was that a ring formed around the dehydrated cement grains. The adhering of CNC onto cement particles led to the steric stabilization effect. As a result, a continuation of the hydration process took place as shown in figure 2.34, illustrating how CNC may increase the hydration of the cement grain that have CNC on their surfaces due to steric stabilization effect. The results show a clear increase of flexural strength of cement composite having 0.2% volume of CNC with respect to cement. However, CNC are short fibres thereby significantly limiting their ability both to work as crack bridging and to improve the degree of hydration, as they could only transfer water to limited distances. Furthermore, CNC are one dimensional fibre thus they can only work in one dimension, compared with GO’s two-dimensional function. Lastly, the addition of CNC in high percentages is problematic in that there could be a lack of uniform dispersion thereby requiring the use of more energy or chemicals to disperse them.

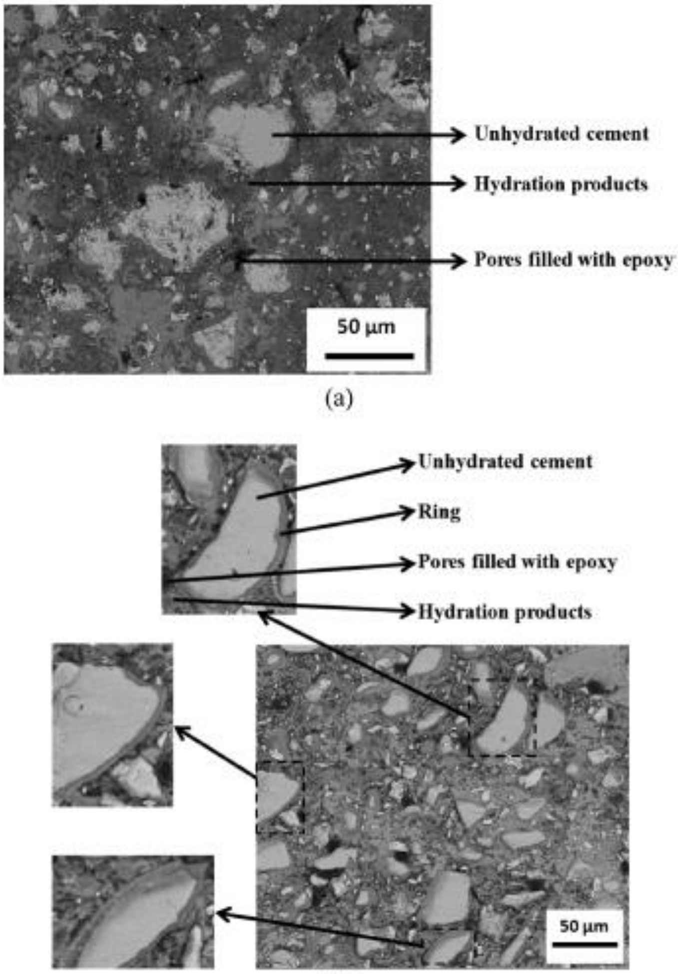

(a)

(b)

**Figure 2.33:** BSE-SEM images of (a) reference and (b) 1.5% mixture at the age of 7 days. The 1.5% CNC mixture shows ring features surrounding the unhydrated cement cores (Cao et al., 2015).

In 2016 Cao et al. published a paper in which they described the influence of CNC on the microstructure of the cement paste. They have used a novel centrifugation method to measure the concentrations of the adsorbed cellulose nanocrystals (a CNC) on the cement surface and the free cellulose nanocrystals (fCNC) which are mobile in water. The results showed that there is an increase in the degree of hydration and there is reduction in porosity.

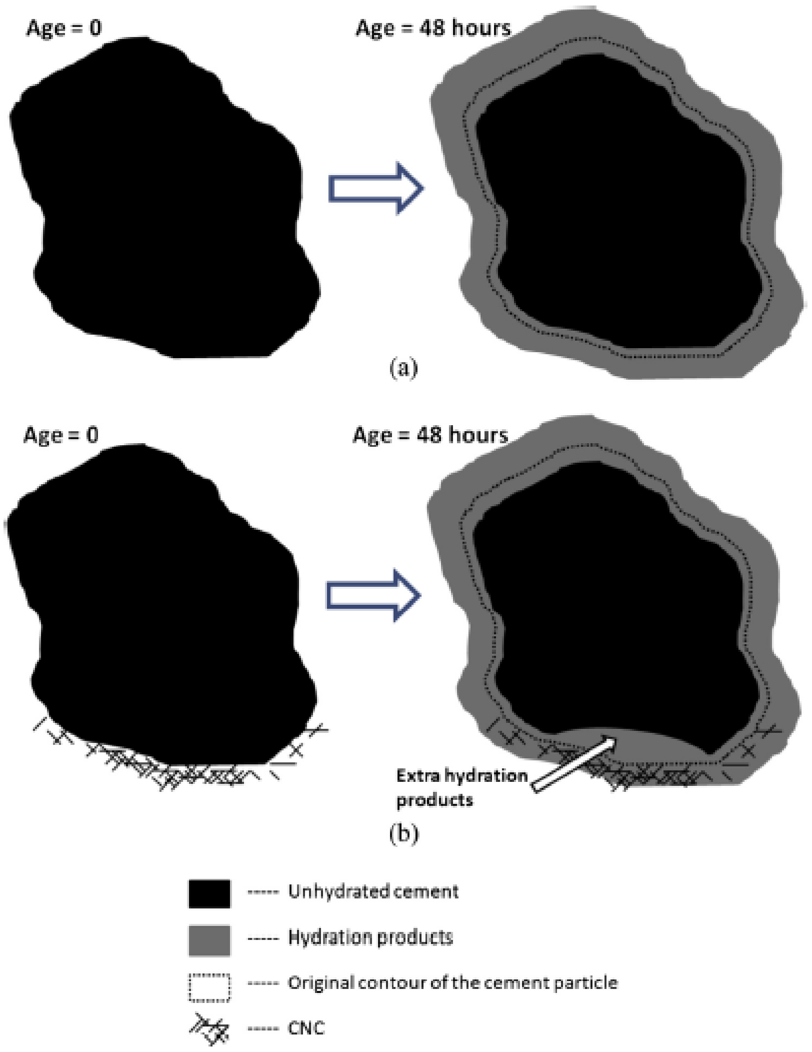

**Figure 2.34:** A schematic illustration of the proposed hydration products forming around the cement grain from the age of 0-48 h in the (a) plain cement and (b) cement with CNC on a portion of the cement particle showing short circuit diffusion (Cao et al., 2015).

In addition, the nanoindentation results showed that there is an improvement of reduced modulus of high-density C-S-H. The reason for the improvements might be the high elastic modulus of CNC, which range from 110 to 220 Gpa, which is higher than that of the interfacial region (high density C-S-H) that have elastic modulus about 40-110 Gpa. For this reason, the elastic modulus of high-density C-S-H can be increased by CNC and another possible reason for this improvement is that CNC additions could cause a modification to the C-S-H (e.g. its structure or chemistry etc). Despite, the success demonstrated with this method, it suffers limitations, for instance, the ability to crack bridging and the enhancement of the degree of hydration are limited because the CNC are short fibres. In addition, CNC work in one dimension only due to CNC are one dimensional fibre thus their effects are limited to one dimension.

Mònica Ardanuy et al. (2012) examined the addition of Nano fibrillated cellulose (NFC) in the cement mortar composites. The experiments were performed to examine the effects of the extent of fibrillation of the fibres and the reinforcement final size on the mechanical performance of cement composites. Two types of fibres were used in this research, the first type was conventional pulps obtained by subjecting sisal fibres to a soft mechanical treatment. The second type was NFC pulps obtained by the application of a high intensity refining process. These fibres were dispersed in cement mortars and the samples were cured for 28 days. Flexural tests were used to test the mechanical performance of the different composites. flexural properties had improved with the addition of NFC to cement mortar. From the results, there is a clear increase of flexural strength of cement composite having NFC with respect to the cement composite having conventional pulps. However, the cement composite with NFC showed brittle behaviour due to the NFC contributing low capability to bridge incipient cracks bridging. This was because of their small size. Additionally, NFC has a high aspect ratio which produces an enhancement of fibre-matrix interaction, resulting in an excessively strong fibre-matrix bonding which although includes a more effective stress transfer from the matrix to the NFC, consequently also an embrittlement of the composite. In addition, an optimisation of the refining time is required to obtain long NFC fibres to improve the ductility while retaining the flexural properties of cement composite.

Mejdoub et al. (2017) studied the effect of adding NFC to Portland cement pastes. The porosity, thermal properties, compressive strength and degree of cement hydration of cement paste were investigated. The amount of NFC as a partial replacement ranged from 0.0% to 0.5% by weight of cement. NFC was made from eucalyptus pulp by using a high-pressure homogenization method. The results revealed that, the compressive strength had increased by more than 50% with 0.3-wt.% of NFC. Furthermore, porosity was decreased with NFC addition and the greatest result was achieved with 0.3-wt.% of NFC. Additionally, the degree of hydration had increased with NFC content and this was confirmed by using X-ray diffraction and Fourier Transform Infrared Spectroscopy. It seems reasonable to think that the NFC encourage the hydration of cement by producing more $Ca(OH)_2$ and C-S-H gel. From the results, there is a clear increase in the compressive strength of cement composite, however, it is difficult to define the performance of cement paste based on the results shown here. It seems that the increase of compressive strength was very high and did not match the increase of hydration and the changes of microstructure of cement pastes, hence the results are not consistent or reliable. Additionally, the NFC contributed low capability to bridge incipient cracks bridging because of their small size.

In Summary: as discussed above, addition CNC to cementitious composites has many advantages such as, a clear increase of flexural strength of cementitious composite having CNC and a clear increase of hydration rate of cementitious composite having CNC. However as discussed above, CNC are short fibres thereby their short length significantly limiting their ability to work as crack bridging and to improve the hydration process, since they could only transfer water to limited distance. Furthermore, CNC are one dimensional fibers thus they can only work in one dimensional direction compared with GO who has two dimensional. Lastly, the addition CNC in high concentration is problematic in that there could be a lack of uniform dispersion thereby requiring the uses of more energy or more chemicals to disperse them.

### 2.4.4 Nano silica (NS) with cementitious composites materials

Among all the nanomaterials, NS is the most widely used material for improving the performance of cement and concrete because of its pozzolanic reactivity and the pore-filling effect. The formation of C–S–H from calcium hydroxide by pozzolanic reaction was much quicker when NS was added to cement paste than that of plain cement paste with other pozzolanic materials (Beneficial Role of Nanosilica in Cement Based Materials--a Review, 2013; Singh et al., 2013). It is assumed that the NS can react with fillers, pozzolan and seeds much more effectively due to its much finer particle size and much greater pozzolanic reactivity than silica fume. Due to these fine particles, large surface area and high $SiO_2$ content, nano silica is a very reactive pozzolanic. Due to its pozzolanic reactivity and ultrafine particle size, it was reported that NS improved the compressive strength of cement-based materials significantly and made the microstructure denser as well. Due to its extremely fine size, in the range of 10-500 nm which is similar to the size of CNTs, NS could be intermixed with agglomerated CNTs and mechanically separate CNTs into dispersed fibers during the mixing process. However, the largest disadvantage of NS is their tendency to agglomerate in cementitious composites and the loss of high surface area of NS is most likely due to grain growth which could take place when NS used directly in a bulk composite. When fine particles are added to cementitious materials, they have a strong tendency to form settlements or agglomerations when it contacts water. Thus, there is a need to increase the repulsive forces between adjacent colloidal particles by adding proper chemical admixtures or by adding extra water to disperse the solid particles in aqueous solution (Elkady et al., 2013)

In Summary: as described above, NS improved the compressive strength of cement-based materials significantly and made the microstructure denser as well as NS could be intermixed with agglomerated CNTs and mechanically separate CNTs into dispersed fibers during the mixing process. However as discussed above, the major drawback of using NS is their tendency to agglomerate in cementitious composites. This is probably due to, in part, to grain growth when NS used directly in a bulk composite.

## 2.5 Hydration Mechanism of cement

Hydration of cement is a complex sequence of interactions occurring between water and chemical phases of the cement, tricalcium silicate ($3CaO\cdot SiO_2$ or "$C_3S$"), dicalcium silicate ($2CaO\cdot SiO_2$ or "$C_2S$"), tricalcium aluminate ($3CaO\cdot Al2O_3$ or "$C_3A$") and tetracalcium alumino ferrite ($4CaO\cdot Al_2O_3.Fe_2O_3$ or "$C_4AF$"), which are hydraulic and consequently interact with water, thus a range of hydrated phases are formed as a result of these interactions. $Ca(OH)_2$ and C-S-H are produced predominantly as hydrated cement products. C-S-H gel and $Ca(OH)_2$ are two major products from the reaction of C3S and C2S with water. C-S-H gel is the main cementing compound during the curing process. It has a layer structure and contains both free water and chemically bound water. $Ca(OH)_2$ nucleates and grows within free capillary pore spaces. It takes up about 20–25 vol% of the cement paste. Hydration reaction equilibrium as well as nucleation and growth of hydrated cement products may be rearranged by the presence of foreign substances (Xiuxuan et al., 2016). The reaction of $C_3A$ and calcium sulfate ($CaSO_4.2H_2O$) produced Ettringite ($3CaO.Al_2O_3.3CaSO_4.32H_2O$) and hydrated calcium sulfoaluminate. With curing time, the Ettringite is replaced with monosulfate $3(3CaO.Al_2O_3.CaSO_4.12H_2O)$. In addition, with curing time and if there is $C_3A$ unhydrated with presence $Ca(OH)_2$, both will react with water and hydrated calcium aluminate ($4CaO.Al_2O_3.13H_2O$) will be formed. Finally, $C_4AF$ reacts with water and $Ca(OH)_2$ at a low hydration rate resulting in $C_4FH_{13}$ as well as hydrated calcium aluminate. The equations 1-6 show these reactions (John et al., 1998).

$$2(3CaO.SiO_2) + 6H_2O \longrightarrow 3CaO.2SiO_2.3H_2O + 3Ca(OH)_2 \text{ …………………….. (1)}$$

$C_3S$ C-S-H gel CH rod- and needle-like

$$2(2CaO.SiO_2) + 4H_2O \longrightarrow 3CaO.2SiO_2.3H_2O + Ca(OH)_2 \text{ …………………….....(2)}$$

$C_2S$ C-S-H gel CH rod- and needle-like

$$3CaO.Al_2O_3 + 3(CaSO_4.2H_2O) + 26H_2O \longrightarrow 3CaO.Al_2O_3.3CaSO_4.32H_2O\text{…….(3)}$$

$C_3A$ calcium sulfate AFt rod-like

Then

$$2(3CaO.Al_2O_3) + 3CaO.Al_2O_3.3CaSO_4.32H_2O + 4H_2O \longrightarrow 3(3CaO.Al_2O_3.CaSO_4.12H_2O)\text{..(4)}$$

$C_3A$ AFt rod-like monosulfate

Then

$$3CaO.Al_2O_3 + Ca(OH)_2 + 12H_2O \longrightarrow 4CaO.Al_2O_3.13H_2O\text{……………………..……..(5)}$$

$C_3A$ CH rod- and needle-like hydrated calcium aluminate

$$4CaO.Al_2O_3.Fe_2O_3 + 4Ca(OH)_2 + 22H_2O \longrightarrow 4CaO.Al_2O_3.13H_2O + 4CaO.Fe_2O_3.13H_2O\text{…..(6)}$$

$C_4AF$ CH rod- and needle-like hydrated calcium aluminate

## 2.6 Conclusions of current nanomaterials in cementitious materials

In this chapter, the literature review of different nanomaterials and their applications in cementitious composites have been discussed. This includes MWCNT, G, GO, CNC, and NS. The use of MWCNT, G and GO may be valuable for reinforcing cement hydration at the nano-scale, bridging nano and micro cracks to prevent initial crack propagation and refining the pore structure to densify the cement matrix. However, their benefit extends beyond this to create a self-sensing and self-healing approach, due to MWCNT, GO and G being conductive fillers, and they could easily be used to measure and monitor the electrical properties of concrete structures. The use of CNC in cementitious composites enhances the rate of hydration of this material and this increase in hydration could be explained by two mechanisms. The first mechanism is steric stabilization which disperses cement particles similarly to that of many water reducing agents (WRA). The second mechanism is short circuit diffusion. It seems that this mechanism increases the hydration rate by increasing the transportation of water from outside of the hydration products to the dehydrated cement cores. NS has a positive impact on compressive strength of cementitious composites due to its pozzolanic reactivity, very fine particle size and large surface area.

Despite extensive research efforts over the last decade on cementitious composites modified with nanomaterials, several roadblocks to the widespread application of these nanomaterials in the construction industry still remain. One of the major problems is their agglomeration of nanomaterials in the cement paste, which results in defects that hinder their benefits to cementitious materials. Compared to G and GO, MWCNT are relatively inexpensive and could be very effective reinforcing materials if their agglomeration in cementitious materials is reduced. In this research, the characteristics of BNP will be studied, and the performance of cementitious composites modified with BNP will be investigated. In addition, the development and evaluation of the proposed hybrid BNP/MWCNT nanoparticles will be studied and the performance of cementitious composites modified with hybrid BNP/MWCNT will be investigated.

# Chapter three

# 3 Manufacturing and properties of sugar beetroot-based BNP

## 3.1 Introduction

This chapter provides information about BNP and its production process. Chapter 3 investigates the characteristics of BNP and its microstructure using XRD, FTIR, TGA/DTA, UV-vis spectroscopy and SEM/EDX. The colloidal properties and stability of BNP in aqueous solution were also studied.

## 3.2 Sugar beetroot as a sustainable reinforcing nanomaterial for cementitious composite

It is widely known that the British sugar beet chain supports up to 9500 jobs in the UK, with 3500 partners producing and directly employing a skilled work force of 1400. The British sugar company supply around eight million tonnes of sugar beet a year and their advanced manufacturing plants can produce 1.4 million tonnes of sugar a year. Currently, British sugar focuses on improving efficiency and reducing waste, and their policies have led to the development of a range of co-products. Electricity, for example, has been generated to a city the size of Peterborough and has produced up to 70 million litres of Bioethanol annually. Our industrial partner Cellucomp Company, which is a Scottish company, has developed a material made from sugar beet waste. According to Cellucomp's Chief Executive, Christian Kemp-Griffin, when we get down to very, very small sized nanomaterials they can have incredible strength properties, which enables them to strengthen other products when added to them.

Furthermore, Cellucomp used carrot as a raw material to produce bio nanomaterial because of its availability in shops, but then moved to sugar beet due to sheer volume of extracted waste in factories from sugar production. Approximately 20% of sugar is derived from sugar beet root globally. Although wood is used by other nano cellulose manufacturers, sugar beet is preferable due to its quick growth and easy methods for break down, and most of the plant is wasted in factories so its use in this way has a positive environmental impact. It also takes less energy to produce this material than it would to make nanocellulose from something else like trees.

## 3.3 Production of BNP

As shown in figure 3.1, the sugar beet pulp waste recovered from existing industrial processes was first diluted with water to form a mixture having a concentration of between 0.1% to 1% solids content by weight then treated with 0.5 M sodium hydroxide (NaOH), raising and maintaining the pH of the solution at pH 14 and to extract hemicellulose and the majority of pectin from the cellulose of the cells within the mixture. The resulting mixture was then heated to 90℃ for five hours and homogenised periodically during the heating period for a total of one hour with a mixer blade rotating at a rate of 11 m/s. A further period of homogenisation for five minutes occurs at the end of the heating period, with a mixer blade rotating at a rate of 30 m/s. Homogenisation process separates the cells along the line of the middle lamella and breaks the separated cells into BNP with about 50 um in width, 50 um in length and 40 nm in thickness. Subsequently a dispersant Span 20 (Span is a registered trade mark of Croda International PLC, Goole UK) is added to the mixture. These coats the surface of the Bio Nano platelets and prevents the cellulose platelets aggregating, allowing them to be more readily re-dispersed in aqueous media.

The resultant mixture is then filtered to remove the dissolved materials to a solid content of less than 8% by weight. A small volume of this composition is placed between two absorbent sheets covering the interior surface of the two spaced apart metal plates. The absorbent sheets are able to remove water from the material by a wicking action as the material is compressed.

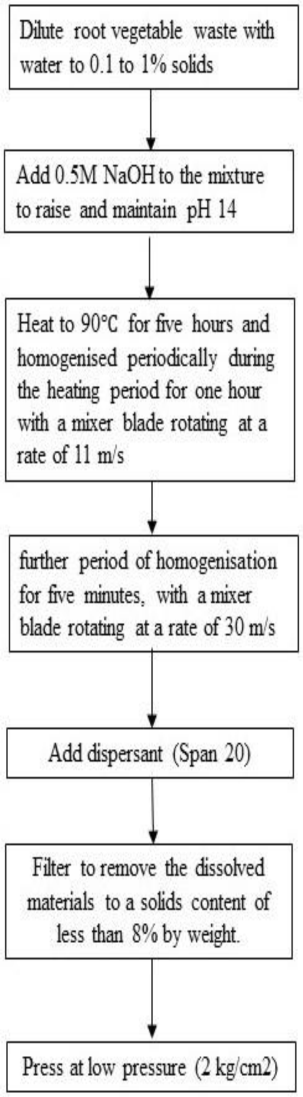

**Figure 3.1:** Flow diagram of the method of producing a composition of the BNP (USA Patent No: 9834664).

The upper metal plate then exerts a low pressure onto the top surface of the material. The material is allowed to expand laterally between the absorbent sheets as the pressure is applied to form a thin sheet of material approximately 2mm or less thick. As the composition is compressed (at 2 kg/cm$^2$) to reduce water content thus, water is wicked out by the absorbent sheets, thereby reducing the water content of the composition. The resulting sheets of material are then cut into suitable sized small pieces whilst ensuring that the material is not compressed, sheared or rolled during cutting otherwise the porosity of the platelet along with their flat shape can be compromised. Compositions made using the above method typically comprise up to 25 to 35% solids of cellulose platelets by weight with sheet shape having about 50 um in width, 50 um in length and 40 nm in thickness (USA Patent No: 9834664).

## 3.4 Experimental programme

Optical microscopy and ultraviolet-visible spectrophotometer were employed to examine the dispersion properties and stability of BNP at sonication times of 30, 50 and 100 min. Scanning electron microscopy with energy dispersive X-ray spectroscopy (SEM/EDX) and X-ray diffraction (XRD) were used to determine the chemical composition, morphology and microstructure of BNP. An Agilent Technologies Exoscan 4100 Fourier-transform mid-infrared spectrometer (FTIR) with diffuse sample interface was used to analyze the BNP. The instrumental conditions for the spectral collection were 128 scans at a resolution of 8 cm$^{-1}$. The spectral changes both in terms of size and position were used to identify the functional groups on the BNP sheets. Thermogravimetric analysis (TGA) was carried out to study the thermal stability of BNP under temperatures between 25 and 1100°C at a rate of 10 ˚C/min in nitrogen (N2).

# 3.5 Experimental results and discussion

## 3.5.1 Properties of BNP

### 3.5.1.1 Characterization of BNP

The chemical components of BNP obtained from the EDX elemental analysis are given in Table 1. As indicated in this table, the BNP are mostly containing carbon, oxygen and hydrogen. The main chemical components are carbon 47.61% and oxygen 46.91%. The BNP contains some sodium and chloride impurities as a result of their chemical treatments. The XRD pattern of BNP is shown in figure 3.2 As can be seen, the BNP exhibited two main peaks at $2\theta = 15$ and 22 which are constitute the structure of cellulose. The XRD pattern suggests that the BPN structure can be divided into two regions. The narrow peak at $2\theta = 15$ represents the crystalline region of BNP with a surface (110) plane. This surface (110) plane is hydrophilic in nature due to the exposure to a large number of hydroxyl (OH) groups, thus good dispersion in aqueous solutions (Meng et al, 2014). The somewhat broad peak at $2\theta = 22.5$ with surface (200) plane indicates the existence of both crystalline and amorphous regions of BNP. The amorphous region w is associated with the amorphous lignin and hemicellulose components of BNP and the crystalline region is highly hydrophobic because of the existence of C-H moieties (Meng et al, 2014). The crystallinity index (CI) of BNP was calculated using the following equations (Meng et al, 2014):

$$\mathrm{CI}\ (\%) = 100 \text{ x } \frac{I_{002} - I_{am}}{I_{002}} \qquad (1)$$

Where $I_{002}$ is the intensity of the XRD peak at $2\theta = 22.5$ and plane (200), and $I_{am}$ is the intensity of the amorphous cellulose between the planes (200) and (110) at $2\theta = 18$, the average *CI* was calculated to be about 64% which is indicative of high tensile strength and stiffness of the BNP sheets (Meng et al, 2014) . As a result, the proposed BNP are a good candidate for reinforcing composite materials. Figure 3.3 shows the FTIR spectrum of BNP. The absorption band between 3600 cm$^{-1}$and 3000 cm$^{-1}$ is due to the vibration of hydrogen-bonded hydroxyl groups in the structure of BNP which indicates the hydrophilic nature in BNP. The prominent peak at 2900 cm$^{-1}$ is due to the stretching vibration of saturated C-H in cellulose. The prominent peak at 1030 cm$^{-1}$ is related to the bending vibration of the absorbed water molecules. The two peaks at 1371 cm$^{-1}$ and 1443 cm$^{-1}$ are due to asymmetric and symmetric bending vibrations in the BNP.

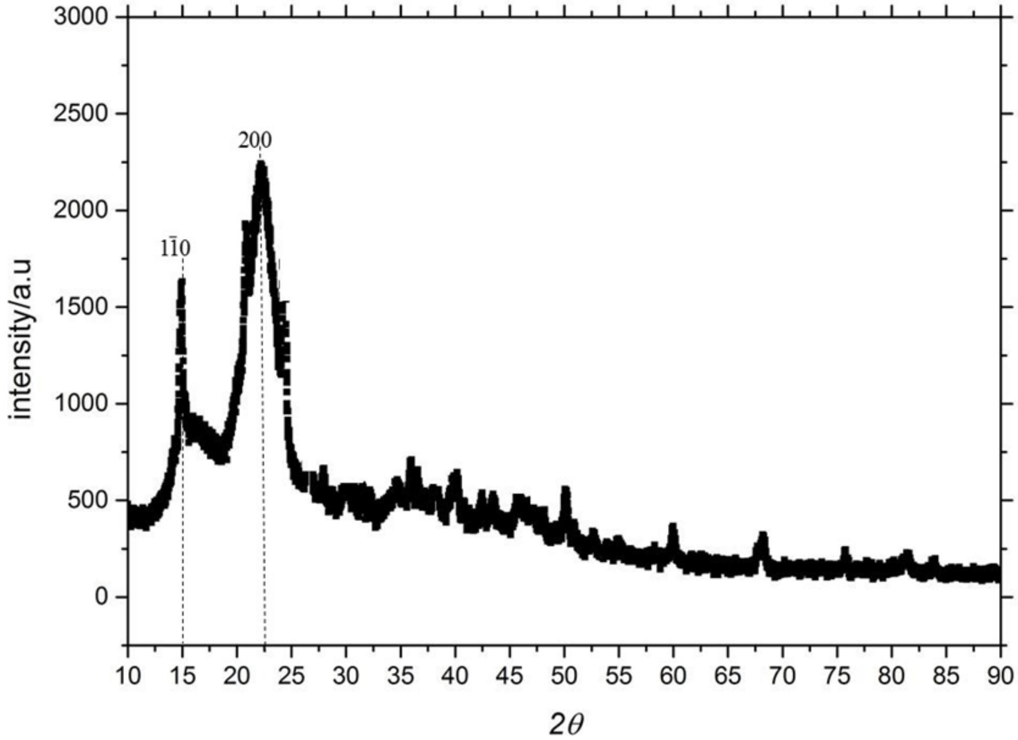

**Figure 3.2:** XRD spectrum of BNP sheets showing crystalline region at 2θ = 15 and amorphous/crystalline regions at 2θ = 22.5.

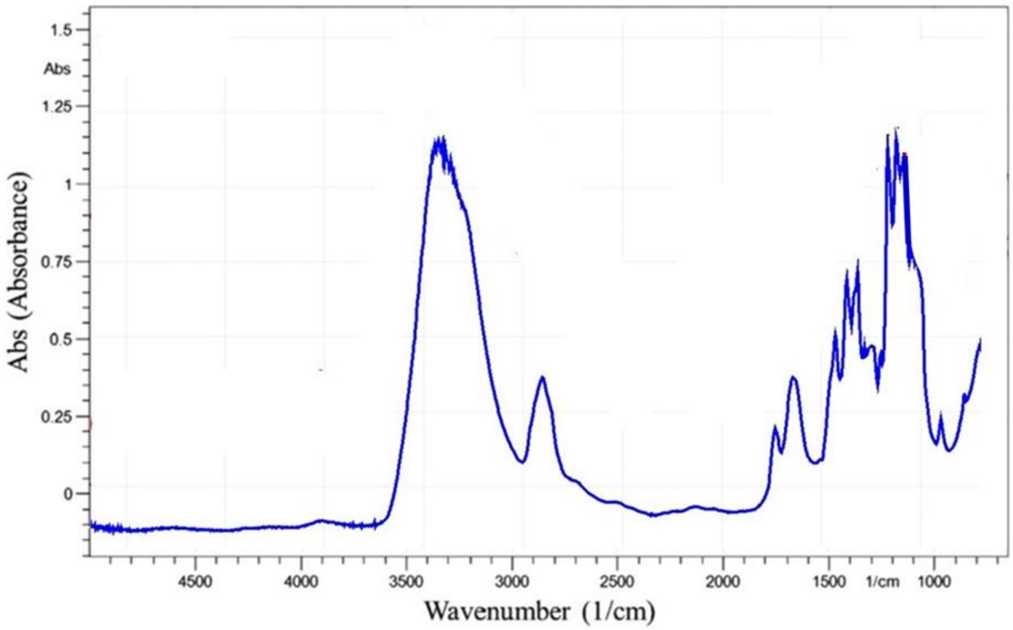

**Figure 3.3:** Diffusion FTIR spectra of BNP

The TGA/DTA results shown in figure 3.4 illustrate the thermal stability of BNP. As can be seen from this figure, the BNP exhibit a small mass loss when heated from 25 to 200°C due to the evaporation of water content. A significant mass loss is observed between 200 and 700°C as a consequence of elimination of hydroxyl groups and decomposition of the carbon chains (Meng et al, 2014). The mass loss remains constant at temperatures between 700 and 1100°C. The DTA spectrum shows a sharp peak at a temperature of about 260°C due to the dehydration of BNP and a broad peak at about 500°C due to the decomposition of BNP (Meng et al, 2014). Overall, the BNP exhibit a good thermal stability in the temperature range of 25 to 100°C, which is the range in which cementitious composites are typically operating.

Figure 3.5(a) shows a typical micrograph of BNP which indicates that the BNP material has wrinkled texture resulting from the treatment of the sugar beet root. The texture of BNP typically consists of crumpled and stacked thin sheets. As shown in fig. 3.5(b), like graphene oxide (GO), clearly there is a highly textured morphology in the form of roughness and ribs enabling the BNP sheets to morph around complex shapes and interact mechanically, thus significantly enhancing the mechanical properties of the cementitious composites (Saafi et al, 2013). It can be seen from fig. 3.5(b), that the BNP sheets are composed of randomly oriented. In addition, nanofibers of BNP, residue of Xylem cells surrounded with stacked thin sheets were seen in this figure.

**Table 3.1:** Chemical composition of BNP

| Chemical components | C | O | Ca | Al | Cl | Mg | Si | Na |
|---|---|---|---|---|---|---|---|---|
| Content (%) | 47.61 | 46.91 | 1.86 | 1.81 | 0.67 | 0.57 | 0.40 | 0.17 |

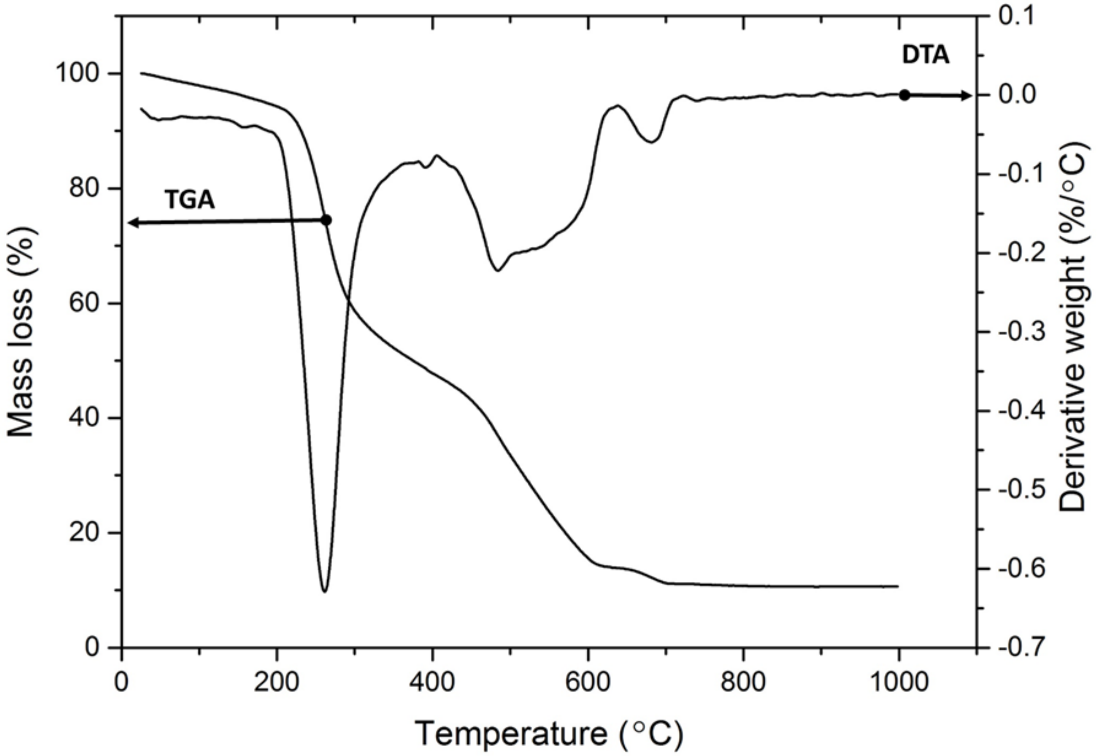

**Figure 3.4:** TGA curve and DTA curve for BNP

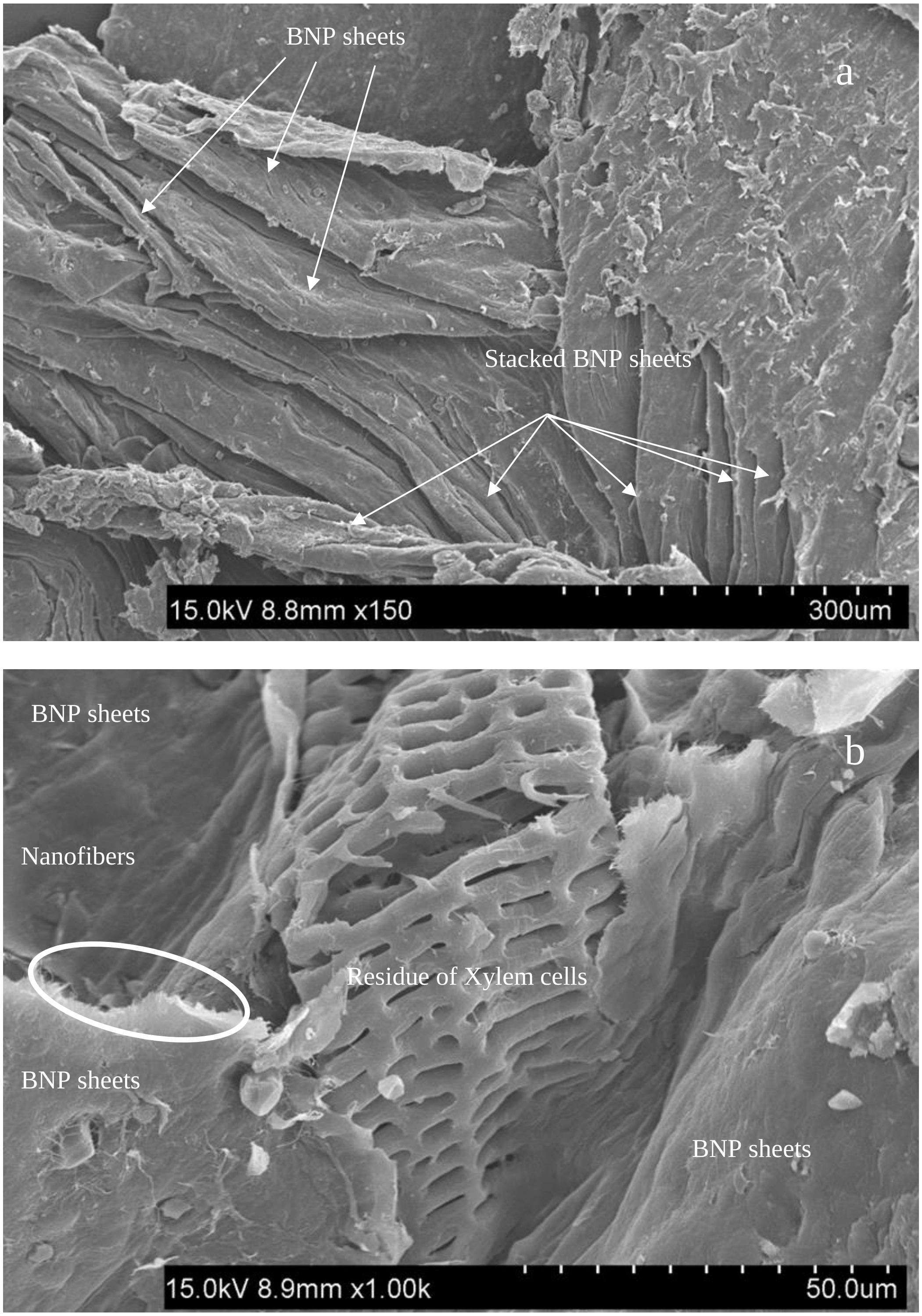

**Figure 3.5:** SEM images of BNP (a) SEM image showing the morphology of BNP sheets (b) close up view of crumpled BNP sheets.

### 3.5.1.2 Colloidal properties and stability of BNP aqueous solutions

The colloidal properties and stability of BNP aqueous suspensions were determined in terms of state of aggregation and microscale dispersion of BNP in an aqueous solution. Figure 3.6(b) depicts a typical optical microscope image of the prepared BNP aqueous suspensions shown in figure 3.6(a). As can be seem, the BNP seem to be uniformly dispersed without agglomeration and the optical image 3.6(b) illustrates BNP and residue of Xylem cells which have bigger size than BNP size. Figure 3.7 shows the UV-vis spectroscopy spectra of a BNP aqueous solution as a function of sonication time. As shown, the absorbance of the BNP exhibits a maximum between 300 and 320 nm at all sonication times. As the sonication time increases, the areas under the spectrum lines representing the absorbance increase as well, resulting in highly dispersed BNP sheets in water.

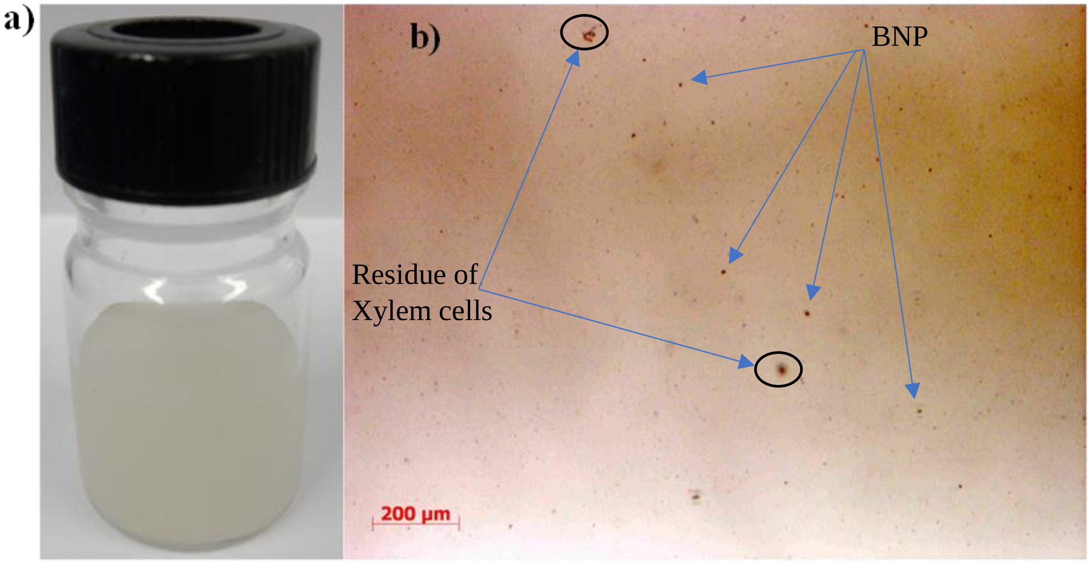

**Figure 3.6:** (a) BNP aqueous solution (2g/L) after 30 min of sonication (b) optical image of the BNP aqueous solution.

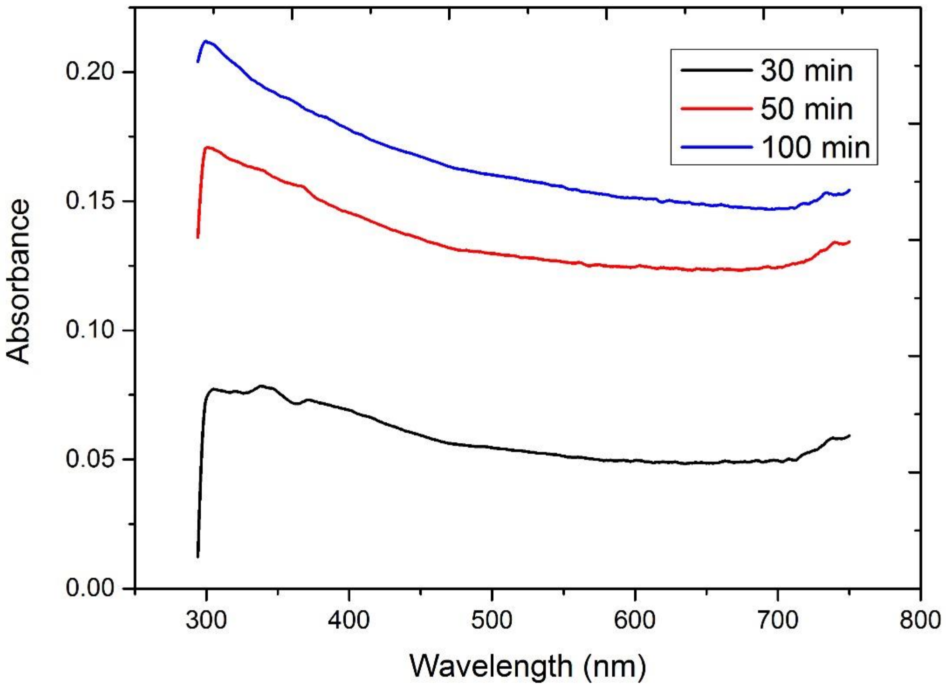

**Figure 3.7:** UV-vis spectroscopy results of BNP aqueous solutions at different sonication times

Figure 3.8 shows a schematic representation of the chemical structure of a cellulose fragment employed within the biocomposite material. The cellulose platelets are composed of at least 1.5 available hydrogen per glucose residue, consequently it is possible for the cellulose platelets to functionalise the glucose residue. Additionally, hydroxyl groups (OH groups) are present and can lead to the possibility of proton transfer, or functionalisation of the glucose residue (Hepworth et al., 2015).

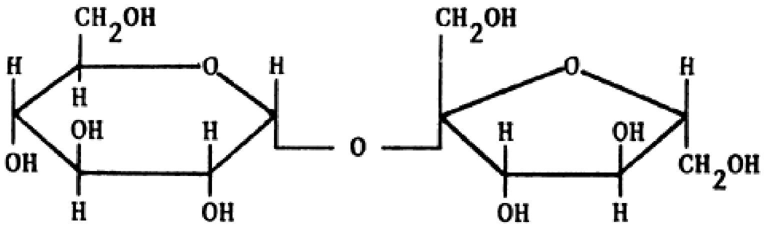

**Figure 3.8:** Chemical structure of cellulose fragment

BNP are more dispersible in aqueous solution because they have high numbers of hydroxyl groups (-OH groups) which enable cellulose platelets to be more highly hydrated. And they are better than microfibrillar cellulose that usually forms a gel or other solid at relatively low proportion by weight of solids, wherein the cellulose platelets have been found not to form a gel even at high concentrations (Hepworth et al., 2015).

## 3.6 Conclusions

Experimental tests have been carried out to investigate the properties of BNP. The experimental programme has been described and the results obtained from experimental tests have been presented, discussed and analysed. The manufacturing process for the production of BNP had been summarised. The chemical components of BNP obtained from the EDX elemental analysis showed that the BNP are mostly carbon, oxygen and hydrogen. The XRD patterns suggest that the BNP structure can be divided into two regions: the crystalline region and amorphous region. The (CI) of BNP was 64% which is indicative of high tensile strength and stiffness of the BNP. As a result, the proposed BNP are a good candidate for reinforcing composite materials. The FTIR spectrum of BNP showed that there are two main types of absorption. The first absorption is due to hydrogen bonded hydroxyl groups in the structure of BNP which indicates the hydrophilic nature of the BNP and the second absorption is due to stretching vibrations of saturated C-H in cellulose.

The TGA/DTA results showed that the BNP display a good thermal stability in temperature range of 25 to 100℃, which is the typical range which cementitious composites use. The SEM results showed that the texture of BNP typically consists of crumpled and stacked thin sheets like GO. Clearly there is a high textured morphology in the form of roughness and ribs enabling the BNP sheets to morph around complex shapes and interact mechanically, thus significantly enhancing the mechanical properties of the cementitious composites. The colloidal properties of BNP aqueous solution showed that BNP have a high stability and uniformity distribution without agglomeration due to the hydrophilic nature of BNP, owing to a large number of hydroxyl (OH) groups. According to above results and discussions, BNP is a good candidate for cementitious composites because of its excellent properties that enable BNP to disperse uniformly within aqueous solution without agglomeration. In addition, its thermal stability and high textured morphology allow it to morph around complex shapes and interact mechanically. Finally, in the next chapter the effect of the addition of BNP to cementitious composites will be examined.

# Chapter four

# 4 Nanoengineered cementitious composites using bio-based 2D nanoplatelets

## 4.1 Introduction

In this chapter, the performance of cementitious composites modified with bio waste-derived 2D cellulose nanoplatelets (BNP) has been investigated. The BNP particles were produced from sugar beet waste that resemble 2D graphene oxide platelets in terms of high surface area, excellent mechanical properties, good dispersibility in aqueous solutions, hydroxyl groups (OH groups) and crack bridging and arrest mechanisms. The effect of different BNP concentrations on the hydration, microstructure and flexural strength and of cementitious composites was elucidated and the results are reported herein.

## 4.2 Experimental Program

### 4.2.1 Preparation of BNP/cement paste composites

Ordinary Portland cement (OPC) type CEM I 52.5N was used to prepare the cementitious composites with a water-to-cement ratio of 0.35. It is worth mentioning that the internal water of BNP paste was considered in calculation of water. A commercially available superplasticizer (Glenium 51) was used at a concentration of 1-wt% to enhance the workability of the cement pastes. The cement paste composites were modified with BNP at loadings of 0.20, 0.40 and 0.6-wt%. The BNP were first added to the required water and superplasticizer, followed by mild sonication for 30 min using a probe sonicator. The resulting suspension was then blended with the cement and mixed for 7 min. For each BNP loading, twelve prisms (40mm×40mm×160mm) were prepared. The prisms were de-moulded after 24 hrs then left to cure in water at a temperature of 21°C for 7, 14 and 28 days.

### 4.2.2 Characterization of hydration and microstructure BNP/cement composites

Cementitious samples with BNP loadings of 0.0, 0.2, 0.4 and 0.6 wt% were collected from the fractured flexural prisms at 7, 14 and 28 days to characterize the effect of BNP on the degree of hydration and microstructure of the composites. Thermogravimetric analysis (TGA) was carried out to elucidate the effect of BNP on the hydration mechanism of the cementitious composites and estimate their degree of hydration (DOH) and the content of $Ca(OH)_2$. In this experiment, the samples were heated from 25 to 1100 ˚C at a rate of 10 ˚C/min under nitrogen (N2). In addition, TGA measurements were performed on BNP and cement particles for correction purposes (Cao et al, 2014). X-ray diffraction (XRD) analysis was also carried out to further investigate the DOH and determine the crystallinity of the cementitious composites. Scanning electron microscopy coupled with energy dispersive X-ray spectroscopy (SEM/EDX) was employed to carry out elemental analysis on the chemical composition of the cementitious composites and investigate the microstructure characteristics such as distribution of BNP and their crack bridging mechanism. Transition electron microscopy (TEM) analysis was also conducted on the hardened cement pastes to study the alteration processes associated with the addition of BNP.

### 4.2.3 Mechanical characterization of BNP/cement composites

For each BNP loading, twelve beams (40mm×40mm×160mm) were prepared and subjected to a four-point bending test, according to ASTM C78 to determine their flexural strength as shown in figures 4.1 and 4.2. The four-point bending tests were carried out under displacement control with a rate of 0.1 mm/min. During testing, load and deflection at the centre were recorded continuously. Furthermore, twelve cubes (50mm×50mm×50mm) were prepared and subjected to a compressive loading with a compressive stress rate of 0.5 MPa\min to determine their compressive strength, following to ASTM C109/C 109M. The compressive strength and flexural strength were calculated according to these equations (C 78), (C 109/C 109M).

$fm = P/A$…………………………………………………………………………...(1)

$R = Pl/bh^2$……………...……………………………………………………...…….(2)

Where

$fm$: compressive strength (MPa); P: total maximum load (N); A: area of loaded surface (mm$^2$); R: Flexural strength (MPa); b and h are width and height of the specimen (mm); L is the length of support distance (mm).

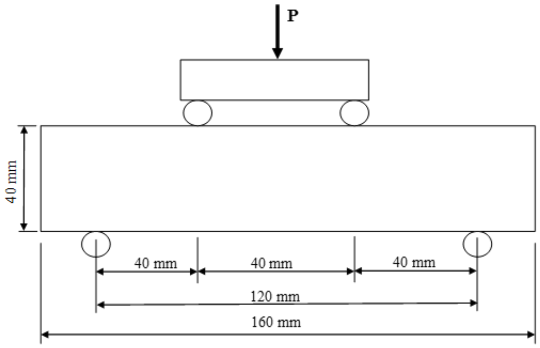

**Figure 4.1:** Experimental test setups, flexural strength test setup

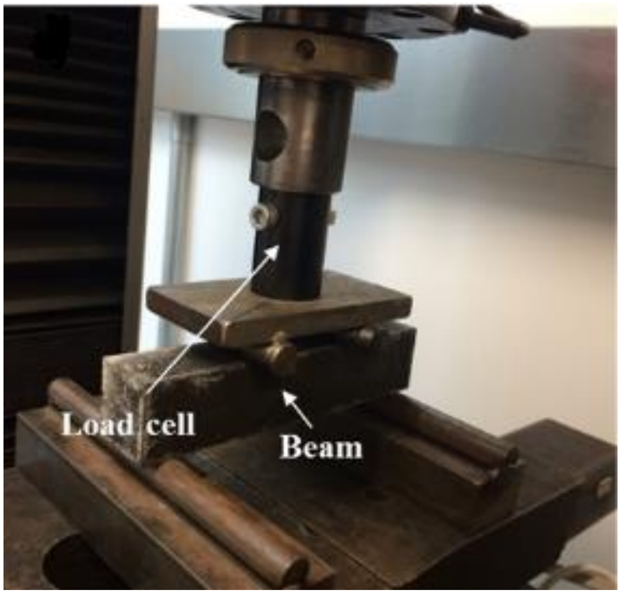

**Figure 4.2:** Test setup, flexural strength test setup.

## 4.3 Results and discussion

### 4.3.1 Influence of BNP on the degree of hydration of cementitious composites: TGA/DTA results

The thermogravimetric analysis (TGA) results in terms of weight loss and derivative of the weight loss (DTA) are presented in figure 4.3 for the cement paste composites containing 0.00-wt% BNP, 0.20-wt% BNP, 0.40-wt% BNP and 0.60-wt% BNP. In this figure, the percentage of the weight loss gradually decreases as the temperature increases and the inflections in the DTA represent the decomposition of specific phases of the cement paste composites. The TGA/DTA provides insight into the chemical reaction mechanisms in cementitious materials during heating (Cao et al, 2016). It was observed that calcium-silicate-hydrate (C-S-H) and carboaluminate phases lose their bound water in the temperature range 180-300°C, the dehydroxylation of calcium hydroxide $Ca(OH)_2$) takes place in the temperature range 430-480°C and the decarbonation of calcium carbonate

($CaCO_3$) occurs in the temperature range 600–780°C (Cao et al, 2016). From figure 4.3, it can be observed that the mass loss of the cement paste composites decreases with increasing BNP concentration. This is due to the increase of the high-density C-S-H content and the creation of new intercalated BNP/C-S-H nanocomposites with higher density. This is consistent with Rehman et al. 2018 findings where they have shown that the decrease in the mass loss of GO reinforced cementitious composites is attributed to both the bonding of C–S–H with the GO sheets and the increase of the C–S–H content. In this case, the GO sheets tend to increase the amount of C-S-H product, thereby filling the pores in the matrix thus less amount of water is available for evaporation (Rehman et al, 2018).

The degree of hydration (DOH) is directly correlated to the amount of Ca(OH)2 which can be calculated with the method introduced by Wang et al. (2018) and Musa (2014) In this method, the mass loss of Ca(OH)2 at different ages was measured and found between 400-500°C and the Ca(OH)2 content was assessed from the TGA curve and calculated according to the equation below:

$$CH = [\frac{4.11dW480}{W120}](100)\text{……………………………………………………………}(1)$$

Where

$CH$= Calcium hydroxide (mass %)

$dW480$ = mass loss at 480 °C

$W120$ = mass loss at 120 °C

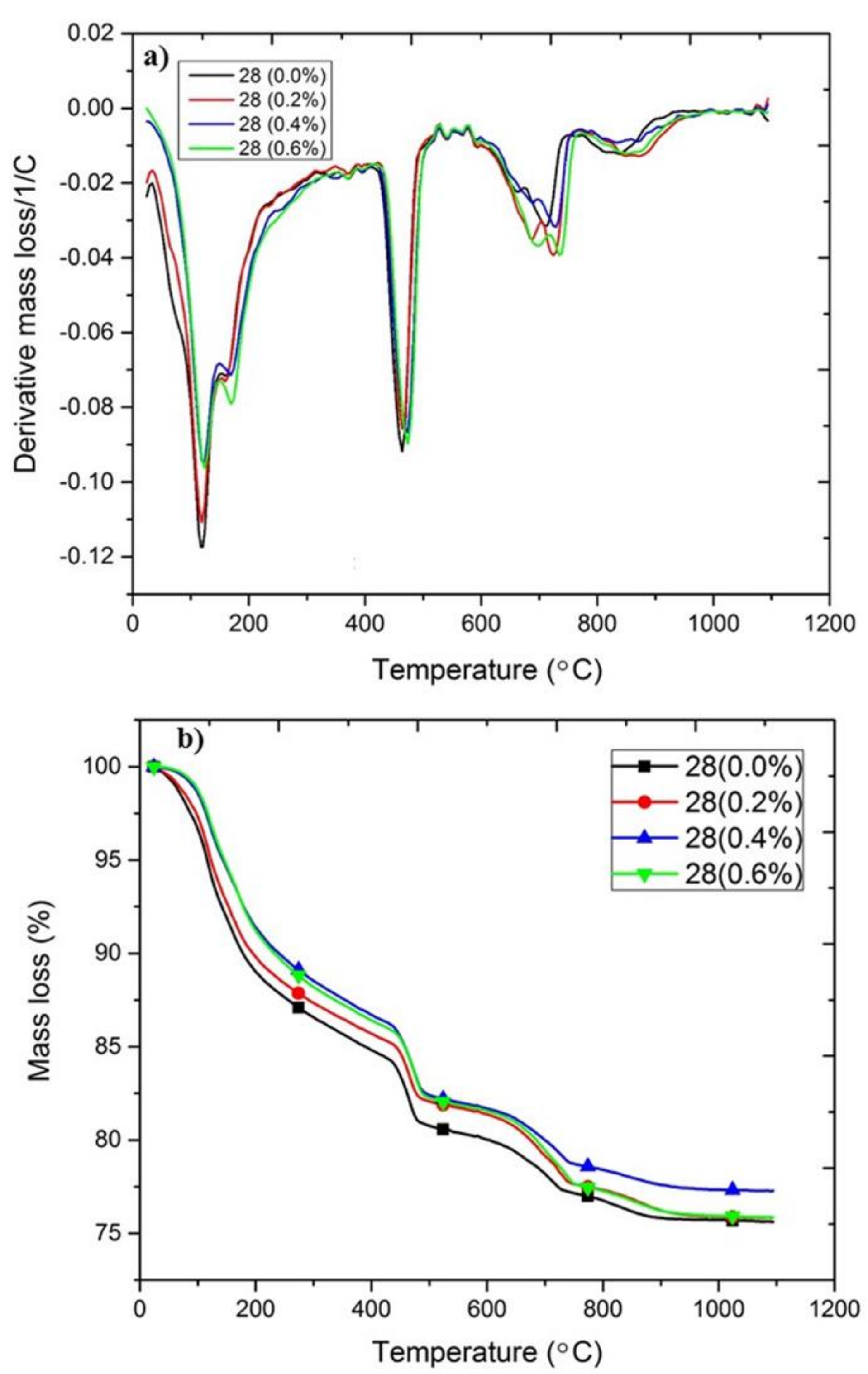

**Figure 4.3:** TGA curves (a) and DTA curves (b) for the cementitious composites at BNP concentrations of 0, 0.2, 0.4 and 0.6-wt% at 28 days

Figure 4.4 presents the $Ca(OH)_2$ content as a function of BNP concentration at 7, 14 and 28 days. At 7 and 28 days, the overall trend observed is that the amount of $Ca(OH)_2$ increases with increasing BNP concentration. However, it is interesting to note that the trend of $Ca(OH)_2$ content increases with increasing BNP concentration, is not evident at 14 days. This needs to be investigated further. The addition of BNP sheets accelerates the hydration of cement resulting in the production of higher $Ca(OH)_2$ content at 7 and 28 days. The highly hydrophilic BNP sheets tend to store water molecules on their surface thus acting like water reservoirs which may release the free water for further hydration. This additional hydration further increases the amount of $Ca(OH)_2$ at 7 and 28 days.

According Cao et al. (2014), the DOH can be obtained by dividing the amount of the chemically bound water (CBW) per unit gram of unhydrated cement by the CBW of fully hydrated cement which is 0.23g. The CBW can be obtained by dividing the mass loss between 140 and 1100 °C by the final mass (Cao et al, 2014). Figure 4.5 shows the DOH as a function of BNP content at 7, 14 and 28 days. As can be seen from this figure, the results clearly show that the DOH increases with increasing BPN content. For example, the DOH of the cement paste with 0.6-wt% of BNP is increased with respect to the plain cement paste by 6%, 7%, and 9% at 7, 14 and 18 days, respectively.

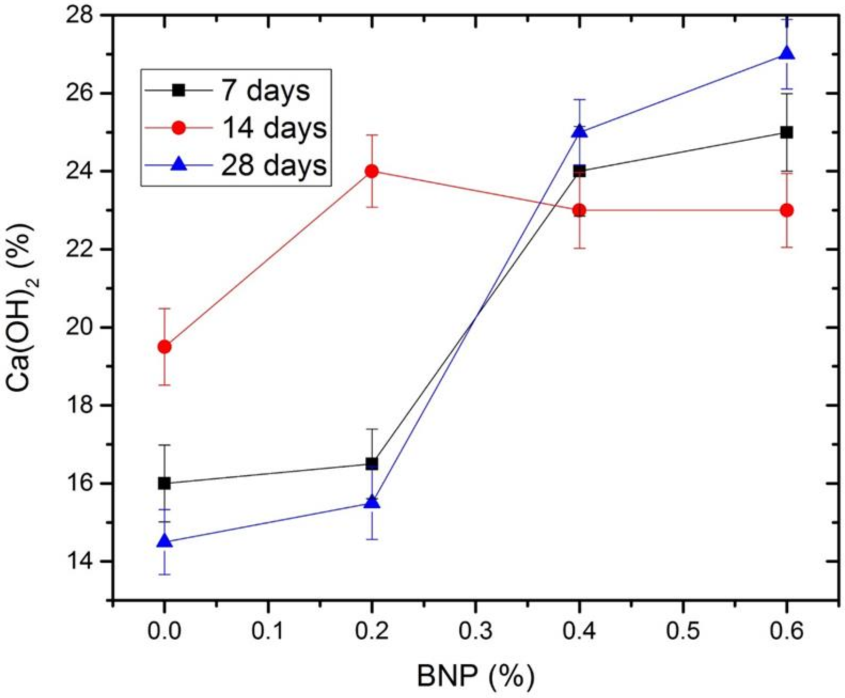

**Figure 4.4:** Content of calcium hydroxide obtained from TGA as a function of BNP concentration at different curing agents.

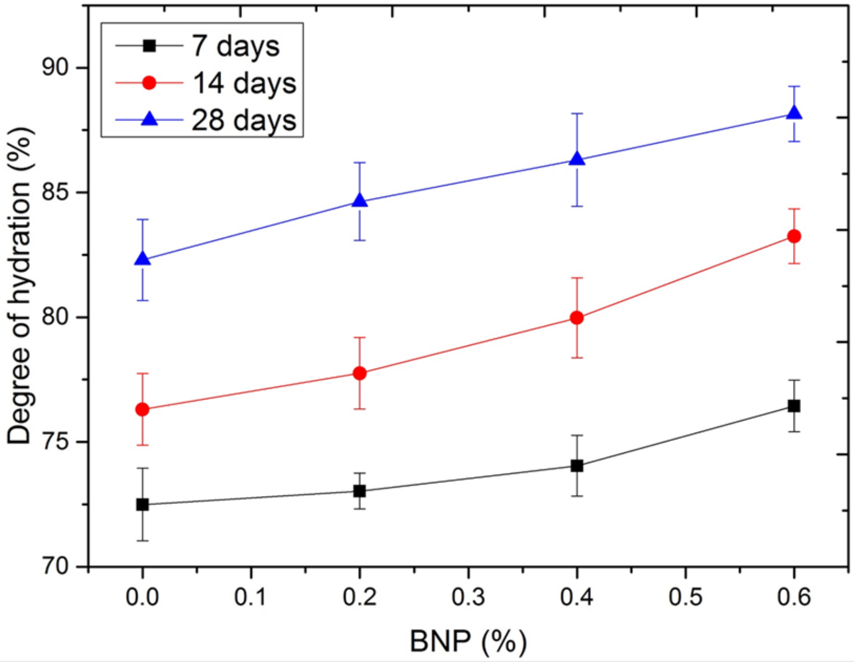

**Figure 4.5:** Degree of hydration (DOH) of the cementitious composites obtained from TGA as a function of BNP concentration at different curing ages.

The improvement in the DOH can be attributed to the effect of the BNP sheets on the reaction of the cement particles with water. Firstly, according to Cao et al. (2014), hydrophilic additives, such as the proposed BNP sheets, disperse the cement particles well during mixing thereby producing uniform distributions of the cement particles which results in higher DOH. Secondly, as discussed above, the BNP sheets act like internal water reservoirs and release free water to amplify the hydration of cement. Thirdly, based on Cao et al.’s (2014) hypothesis, the BNP sheets embedded into the high-density C-S-H could act as water channels to transport water from the pore water solution to the unhydrated cement cores, thus fueling the hydration of the cement particles due to increased amounts of water.

### 4.3.2 Influence of BNP on the hydration phases of cementitious composites: XRD and EDX results

The XRD patterns of the cementitious composites at 7, 14 and 28 days are shown in figure 4.6. As it can be seen from this figure, typical hydration phases such as ettringite, calcium hydroxide $Ca(OH)_2$, tricalcium silicate ($C_3S$) and calcium carbonate ($CaCO_3$) are detected in all cementitious composites at all ages. This indicates that the addition of BNP does not alter the type and structure of the hydration products of the cement pastes. The C-S-H hydration product is difficult to identify by XRD analysis due to both lack of their crystallinity and their indefinite composition. As shown in figure 4.6, the XRD further confirms the TGA findings. The intensity of $Ca(OH)_2$ increases with increasing BNP content at 7, 14 and 28 days. This means the addition of BNP promotes the hydration of cements thereby increasing the amount of the hydration products. Previous research on cementitious composites containing graphene oxide (GO) reported similar findings (Cao et al, 2016; Cao et al, 2016;). Another way to quantify the extent of hydration of cement as a result of BNP is to examine the magnitude of the intensity peaks of the detected $C_3S$ phase. From figure 4.6, it appears that the intensity peaks of $C_3S$ decreases when BNP are present. This could be attributed to the interaction of $C_3S$ with -OH and -R-CH2- functional groups on the surface of the BNP sheets. Phases such as $C_3S$ tend to react with water molecules adsorbed on the surface of the BNP sheets thereby increasing the amount of hydration products. This phenomenon was also observed in cementitious composites reinforced with GO sheets (Wang et al, 2018). Monitoring of $Ca(OH)_2$ crystal size could shed light on the effect of the BNP on the growth of C-S-H phases. The size of $Ca(OH)_2$ obtained from the XRD analysis as a function of BNP concentration at 28 days is shown in figure 4.7. From this figure, it can be observed that the addition of BNP significantly decreases the size of the $Ca(OH)_2$ particles. This is attributed to the fact that BNP promote the growth of C-S-H, thus less space available for $Ca(OH)_2$ to grow in size. Zheng et al. (2017) found that when GO is present in the matrix, the size of $Ca(OH)_2$ becomes smaller and the content of C-S-H increases, resulting in a dense structure. It is noteworthy that the addition of 0.40-wt% BNP and 0.6-wt% BNP leads to a $Ca(OH)_2$ size higher than that at 0.2-wt% BNP. This could be due to the fact that the BNP sheets tend to restack at higher constructions which in return dampers the growth of C-S-H and allows $Ca(OH)_2$ to grow in size. Therefore, based on this observation, it appears that the content of C-S-H reaches a maximum at 0.20-wt% BNP at 28 days.

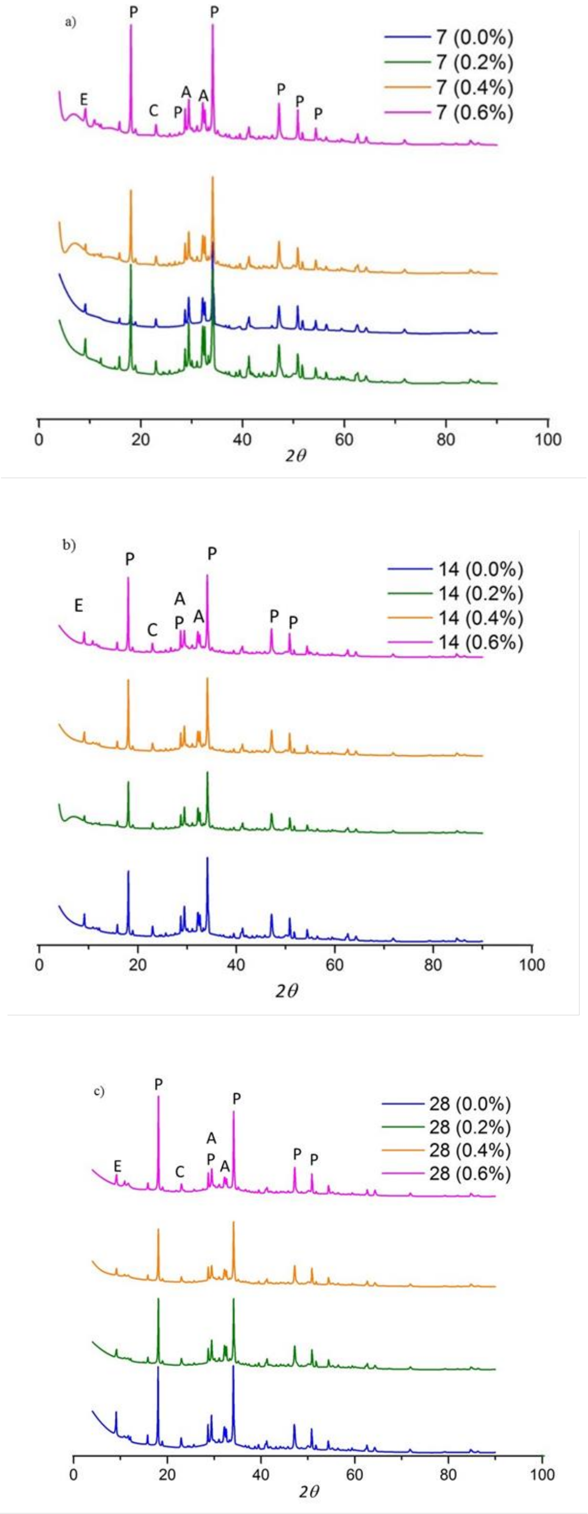

**Figure 4.6:** XRD spectrum of the cementitious composites at different BNP concentrations a) 7 days b) 14 days c) at 28 days. C-S-H: Calcium Silicate hydrate. E: Ettringite, P: Portlandite ($Ca(OH)_2$), A: Alite ($C_3S$), C: Calcite ($CaCO_3$)

The EDX results were employed to further quantify the effect of BNP on the hydration phases and the distribution of the BNP sheets in the hardened cement pastes. Here, the concentration of silica signals are used as indicative of C-S-H growth (Sakalli et al, 2017) whereas the concentration and uniformity of the oxygen signals are used to gain insight into the distribution of BNP in the hardened cement pastes (Cao et al. 2016). Figure 4.8 shows SEM images of the cement paste composites at different BNP concentrations along with their corresponding silica, oxygen and calcium maps. By comparing the silica maps between the cement pastes, it is observed that the cement pastes with 0.20 wt% and 0.4-wt% BNP exhibit higher silica concentration which indicates higher C-S-H content.

On the other hand, silica signals were not overserved in the cement paste with 0.60 wt% BNP, which indicates that $Ca(OH)_2$ is the predominant phase. Furthermore, the comparison of the oxygen signals indicates that the oxygen concentration is higher in the cement pastes with 0.20-wt% BNP and 0.40-wt% BNP and the oxygen signals are uniform throughout the maps, implying better distribution of BNP (Cao et al. 2016).

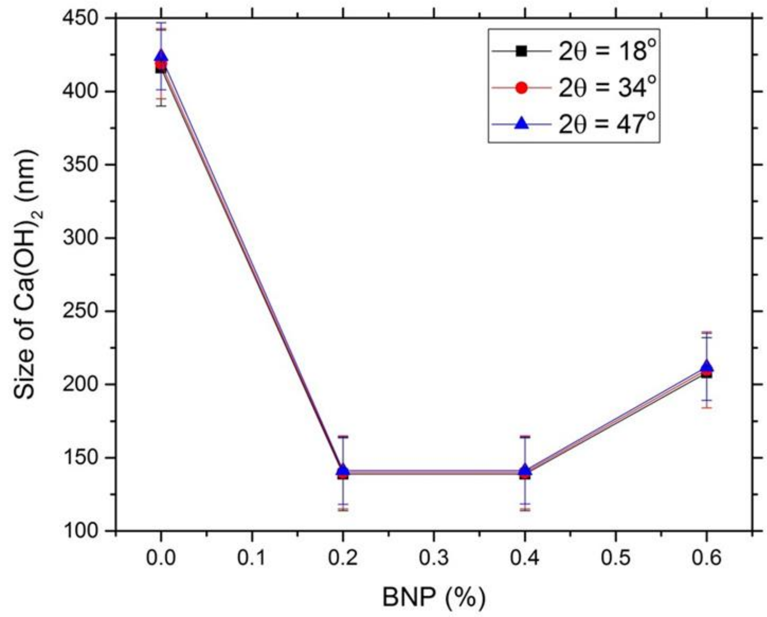

**Figure 4.7:** Size of $Ca(OH)_2$ obtained from XRD as a function of BNP concentration

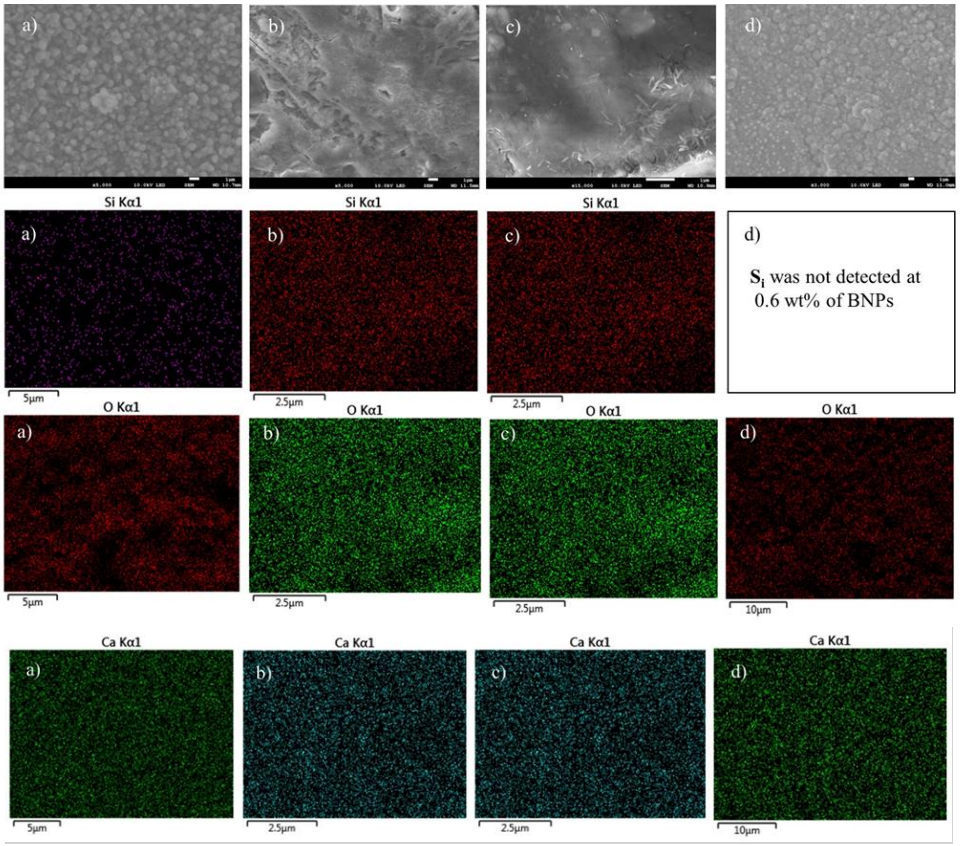

**Figure 4.8:** SEM images with maps of silica, oxygen and calcium elements at 28 days of curing a) plain cement paste b) cement paste with 0.2 wt% of BNP c) cement paste with 0.4 wt% of BNP d) cement paste with 0.6 wt% of BNP

### 4.3.3 Effect of BNP on the microstructure of cementitious composites. SEM and TEM results

The microstructure of the cement paste composites at 7, 14 and 28 days are presented in figures 4.9-4.11. As shown, the microstructure of the plain cement paste at 7 days (figure 4.9a) contains unreacted cement particles and $Ca(OH_2)$ cubes and seeds-like particles, presumably due to a low DOH. The addition of 0.20-wt% of BNP leads to highly dense structure with some $Ca(OH_2)$ particles embedded into the C-S-H gel as shown in figure 4.9b. The hydration phase $Ca(OH_2)$ in the form of cubes and rod-like crystals is observed in the microstructure of the cement paste with 0.40-wt% BNP (figure 4.9c). The cement paste with 0.60-wt% BNP however, is marked by a high content of $Ca(OH)_2$ seed-like crystals (figure 4.9d). It is worth noting that it is challenging to identify the BNP sheets in the SEM images. This is because the hydration products such as ettringite, $Ca(OH)_2$ and C-S-H grow on their surface thus making their morphology undistinguishable.

From figure 4.10a, it can be seen that the microstructure of the plain cement paste at 14 days becomes somewhat porous and contains a relatively high content of $Ca(OH_2)$ seed-like crystals, whereas the cement paste with 0.20-wt% BNP (figure 4.10b) remains dense and its C-S-H content seems to increase which is in agreement with $Ca(OH)_2$ findings. The cement paste with 0.40-Wt% BNP (figure 4.10c) exhibits a morphology different from that of both the plain cement paste and the cement paste with 0.20-wt% BNP. It appears that the $Ca(OH)_2$ seeds transformed into rod-like crystals and began to grow out from the matrix. As can be seen from figure 4.10d, when the BNP concentration increases from 0.4-wt% BNP to 0.6-wt% BNP, the main hydration phase of the cement paste is $Ca(OH)_2$ in the form of agglomerates. At 28 days of curing, the plain cement paste is mainly composed of $Ca(OH)_2$) in the form of regular polyhedral-shaped particles (figure 4.11a). On the other hand, the microstructure of the cement pastes is significantly changed when the BNP sheets are present. The cement paste with 0.20-wt% BNP shows a compact structure with some layers of stacked fabrics-like $Ca(OH)_2$ crystals embedded into a high density C-S-H gel (figure 4.11b-c). Most of these $Ca(OH)_2$ fabrics appear to grow in one-direction. This could be the result of the interaction of the uniformly distributed BNP sheets with the cement particles. When uniformly distributed, the BNP sheets adsorb onto the surface of the cement particles through their -OH and - $CH_2OH$- functional groups. These functional groups then react with $C_3S$ and $C_2S$ to form nucleation and growth sites for the hydration phases. The phase $C_2S$ is less soluble than $C_3S$, thus a slower hydration rate of $C_2S$ at these growth sites. We hypothesize that at lower BNP concentrations, this could allow more time for the hydration phases to self-assemble into fabric-like crystals. At a concentration of 0.4-wt%, the cement contains C-S-H and $Ca(OH)_2$ particles as hydration products. The Ca(OH2) particles are in the form of elliptical needles growing out from the matrix in two directions (figure 4.11d). When the BNP concentration increases to 0.6-wt% BNP, the $Ca(OH)_2$ is the main hydration product and the needle particles become cauliflower-like crystals as shown in figures 4.11 e-f. The SEM investigations suggest that the BNP sheets have the ability to control the crystallization and morphology of the hydration products, which depends on the BNP content in the cement paste. The SEM investigations also suggest that the 0.20-wt% BNP is the optimum concentration for increasing the C-S-H content in the cement paste composite.

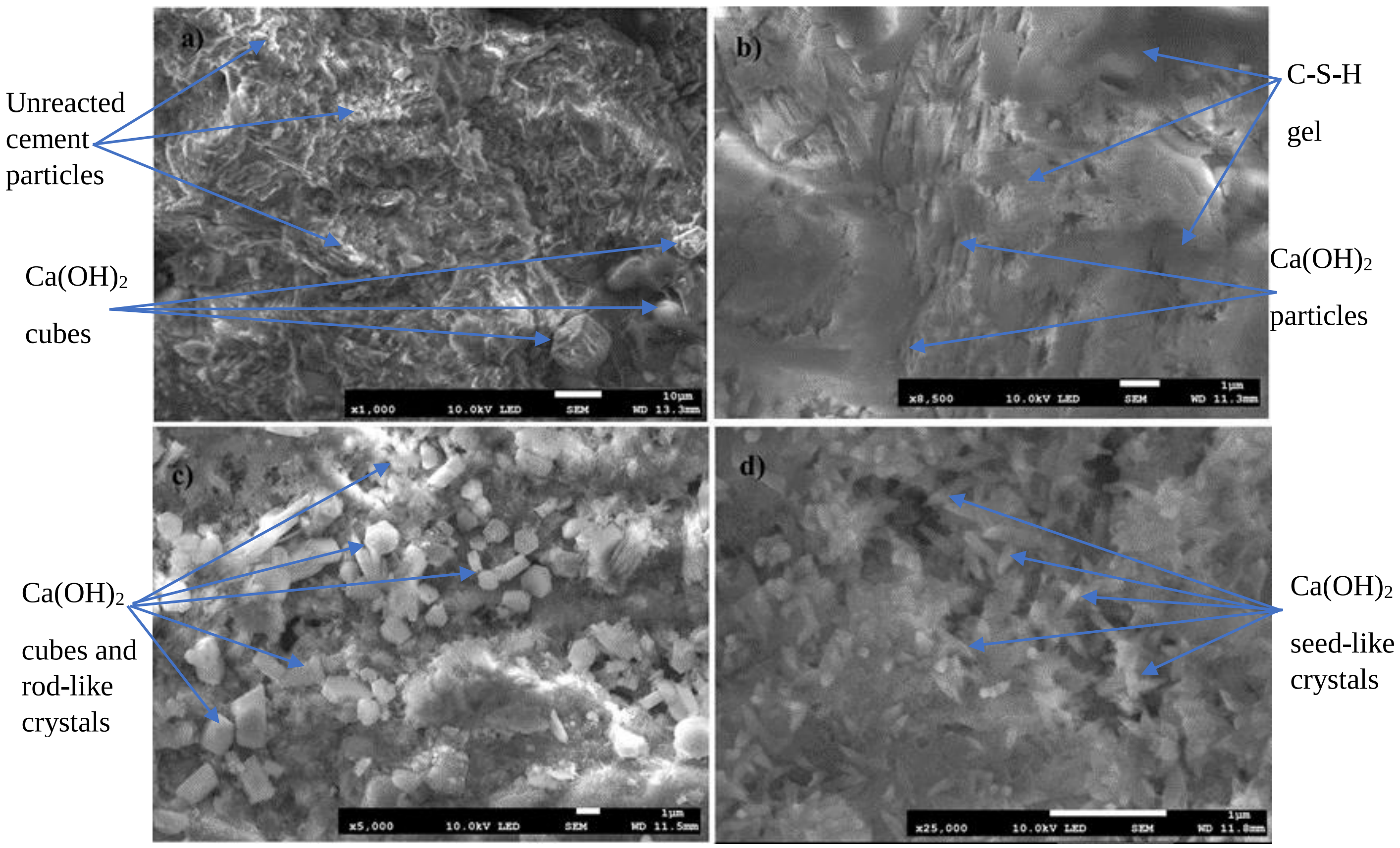

**Figure 4.9:** SEM micro images of the cementitious composites at 7 days (a) plain cement paste, (b) with 0.2 wt% of BNP, (c) with 0.4 wt% of BNP, (d) with 0.6 wt% of BNP

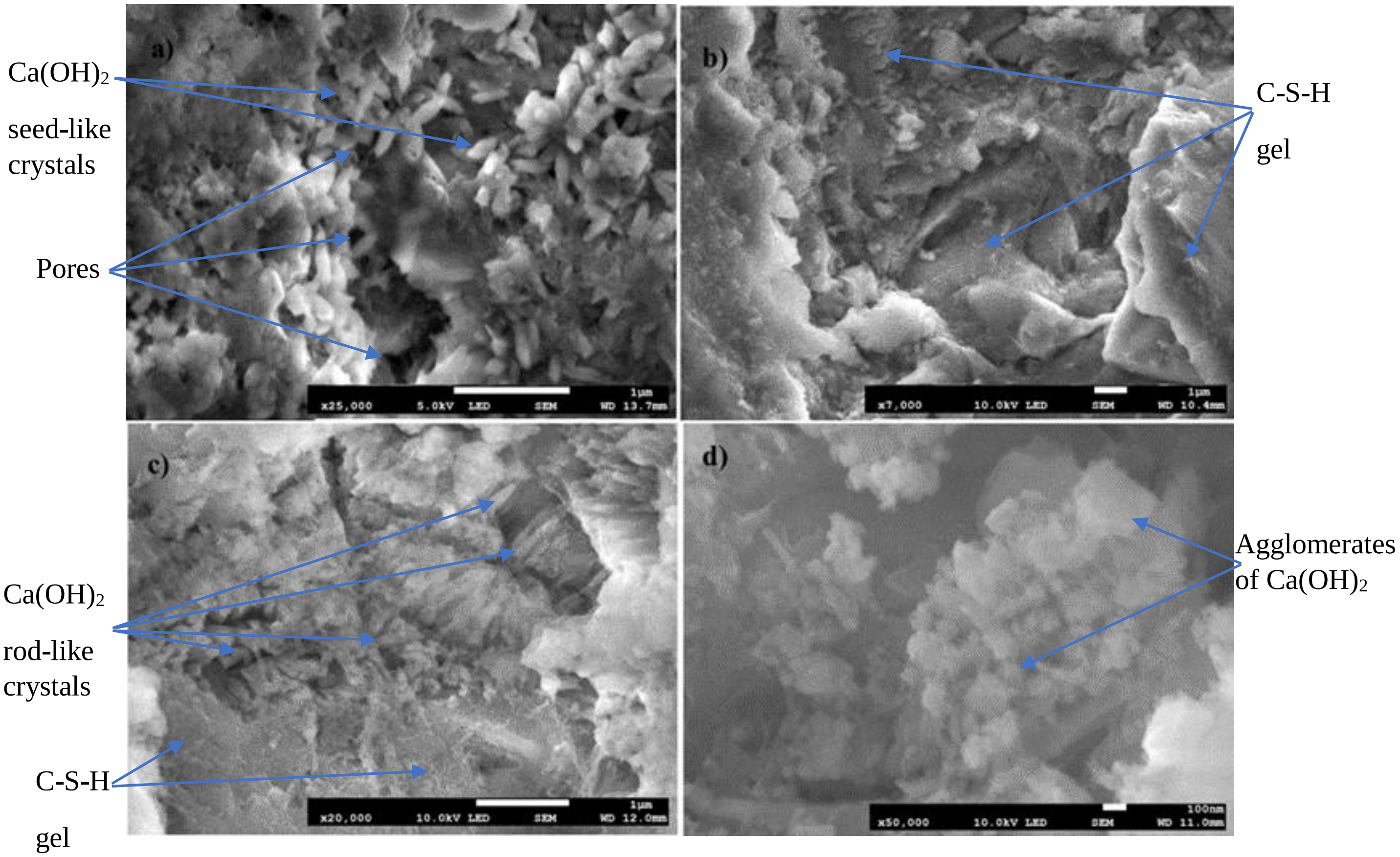

**Figure 4.10:** SEM micro images of the cementitious composites at 14 days (a) plain cement paste (b) with 0.2 wt% of BNP (c) with 0.4 wt% of BNP (d) with 0.6 wt% of BNP

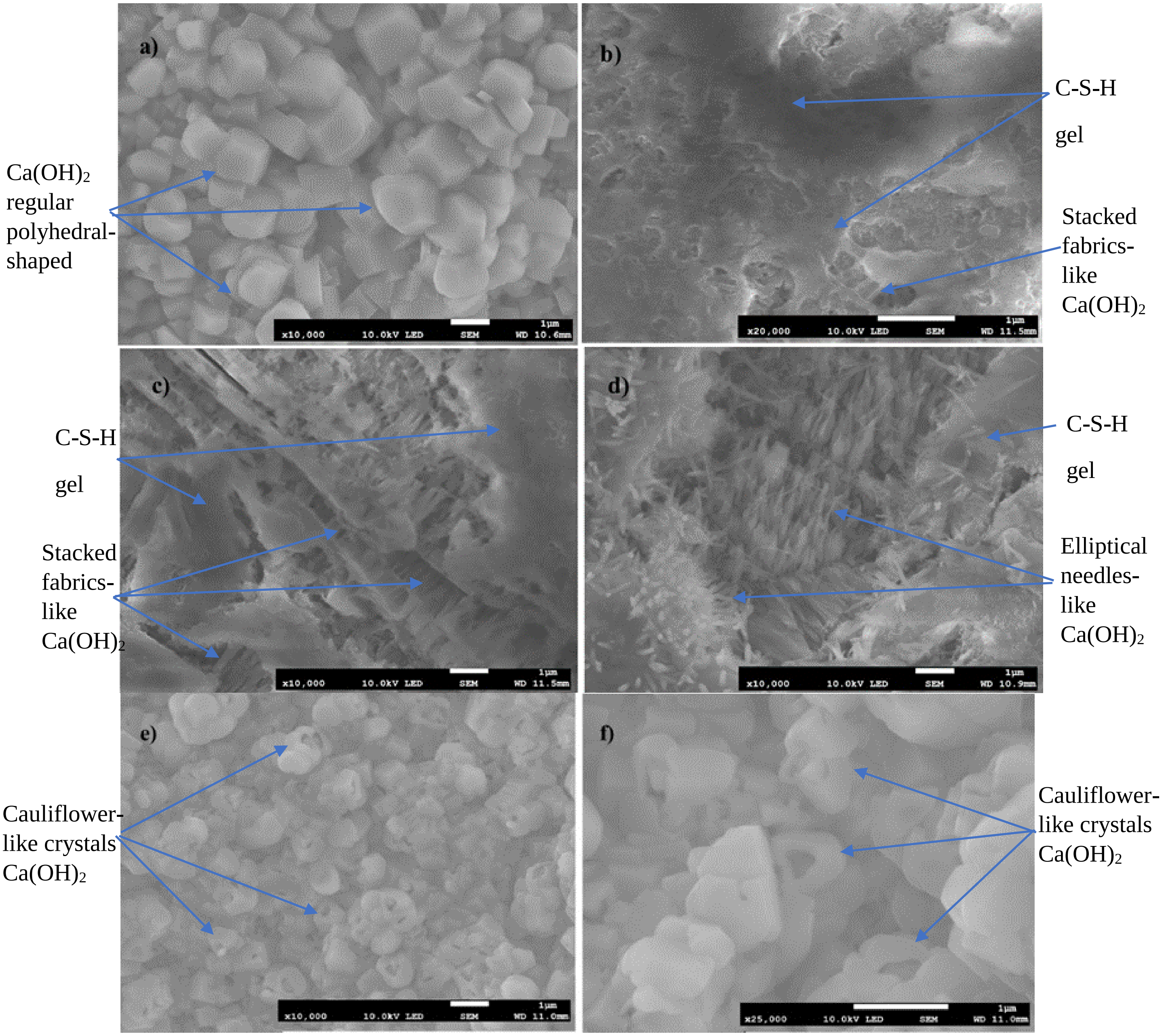

**Figure 4.11:** SEM micro images of the cementitious composites at 28 days (a) plain cement paste (b), (c) with 0.2 wt% of BNP (d) with 0.4 wt% of BNP (e), (f) with 0.6 wt% of BNP

The TEM images in figures 4.12, 4.13, 4.14 and 4.15 show the effect of BNP on the microstructure of the cement pastes at 28 days. As shown, the microstructure of the plain cement paste (figure 4.12) consists mainly of $Ca(OH)_2$ crystals with a low C-S-H content. The addition of 0.2-wt% BNP leads to higher C-S-H content, higher flexural strength, fewer $Ca(OH)_2$ crystals and denser microstructure (figure 4.13). From figure 4.14, the microstructure of the cement paste with 0.4-wt% BNP contains $Ca(OH_2)$ crystals embedded into the C-S-H gel. On the other hand, a significant amount of $Ca(OH_2)$ crystals is observed in the cement paste with 0.6-wt% BNP (figure 4.15). The TEM investigations suggest a good compatibility between the BNP sheets and the hydration products.

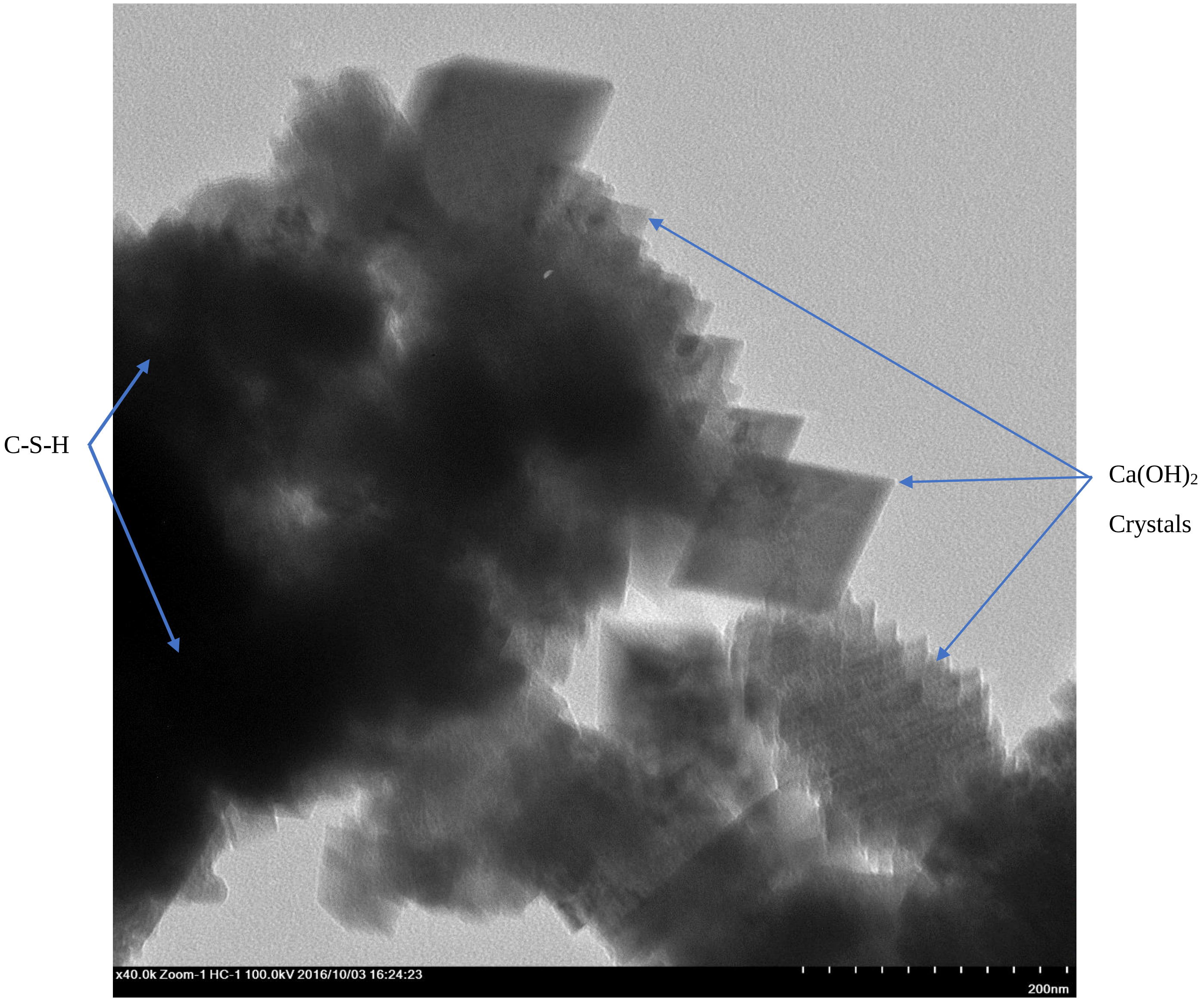

**Figure 4.12:** TEM micro images of plain cement paste at 28 days of curing.

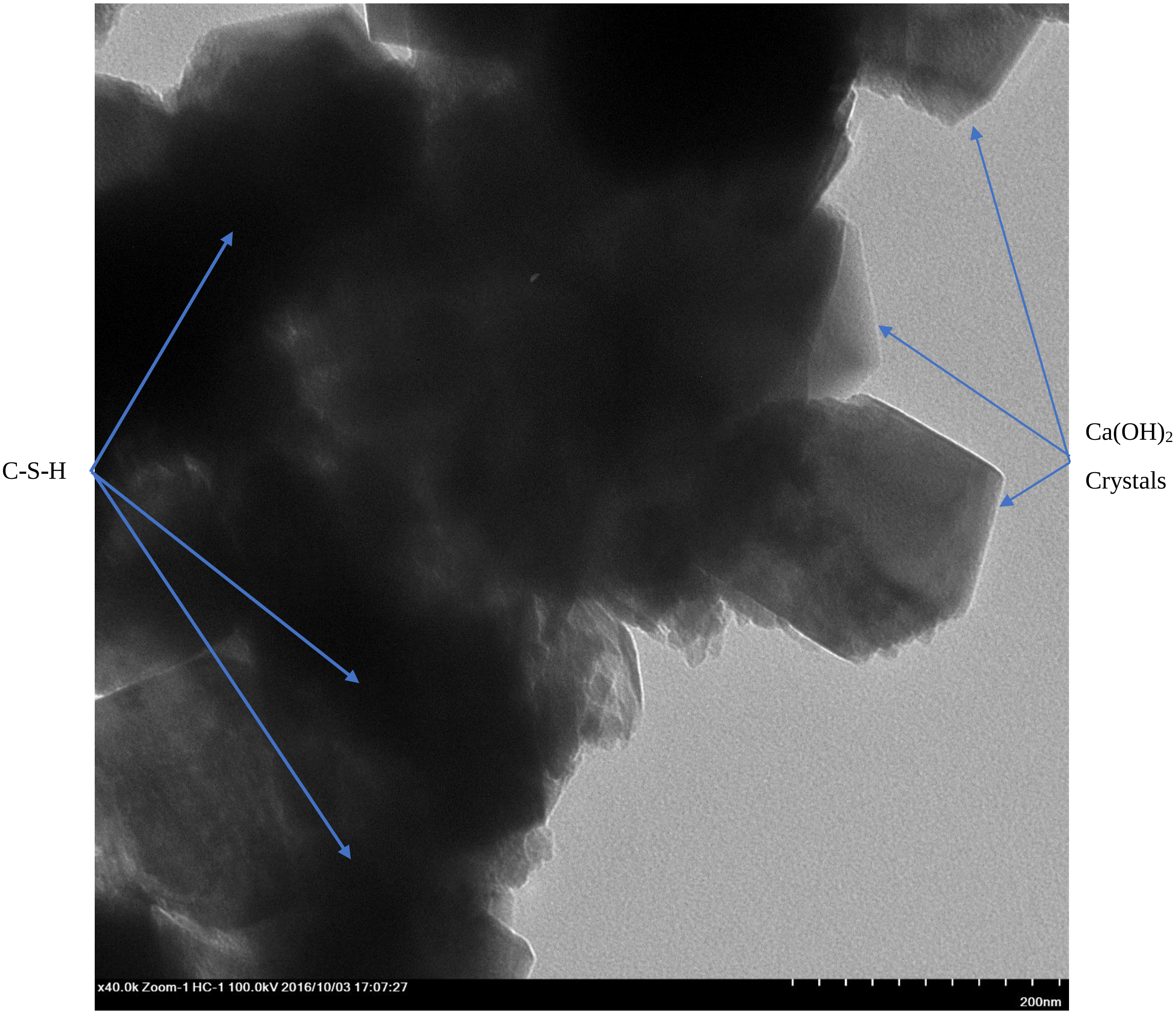

**Figure 4.13:** TEM micro images of cement paste with 0. 2-wt% of BNP at 28 days of curing.

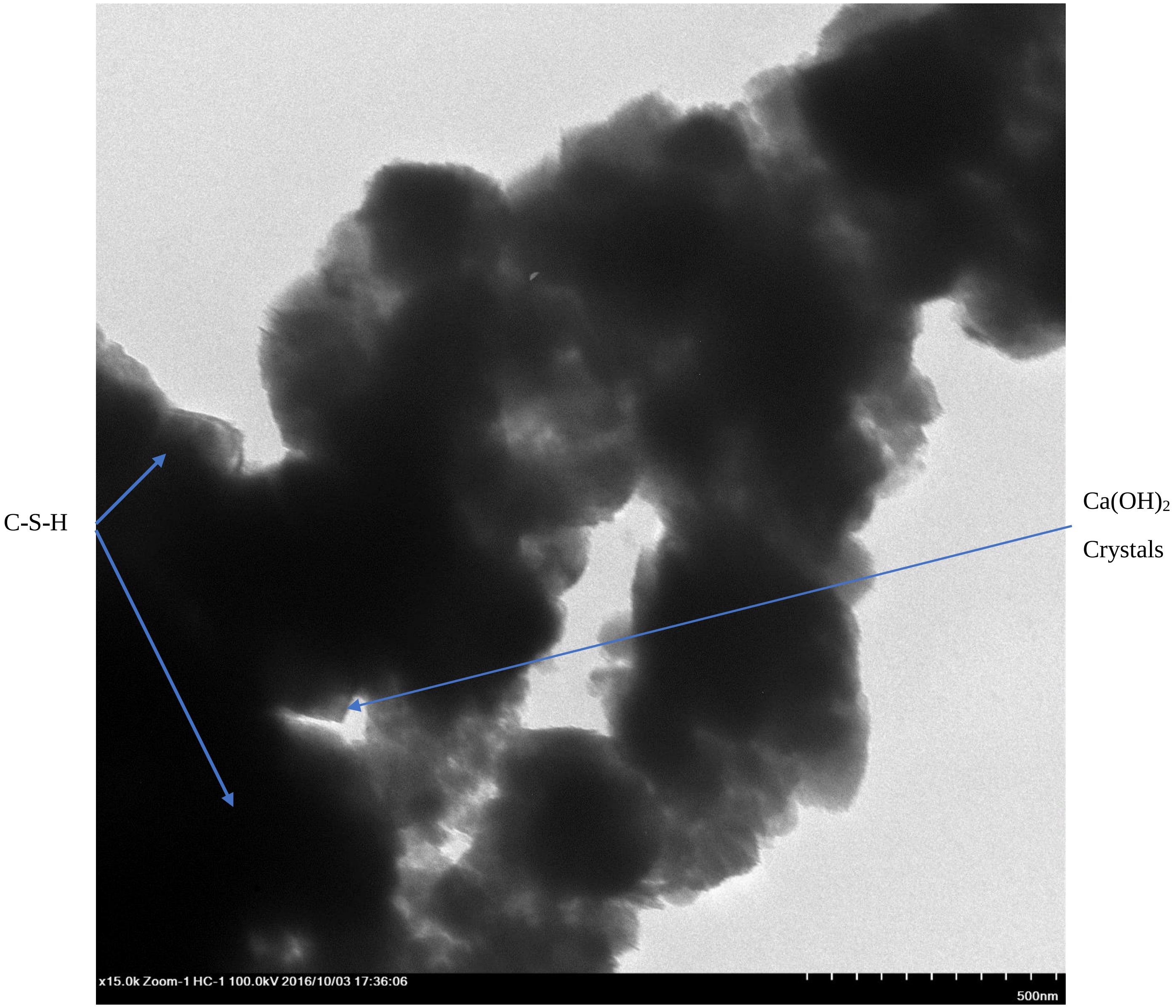

**Figure 4.14:** TEM micro images of cement paste with 0.4-wt% of BNP at 28 days of curing.

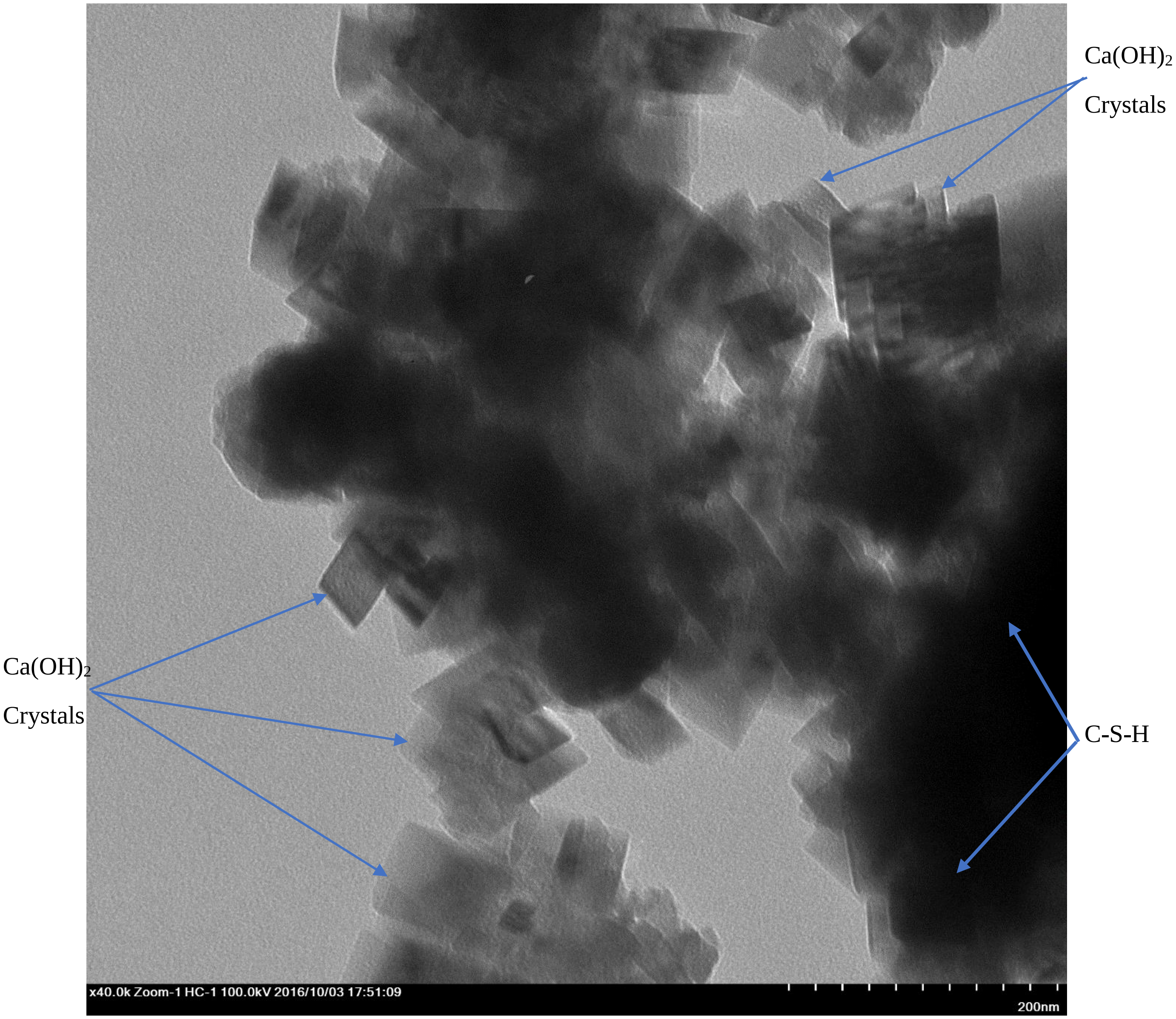

**Figure 4.15:** TEM micro images of cement paste with 0.6-wt% of BNP at 28 days of curing.

### 4.3.4 Mechanical properties of cementitious composites and BNP/matrix interaction

The effect of BNP concentrations on the average flexural strength at 7, 14 and 28 days is given in figure 4.16. The figure shows that at 7 and 14 days, the addition of 0.20-wt% BNP increases the flexural strength of the cement paste by 23% and 20% respectively, whereas no significant increase is observed when 0.4-wt% BNP is present in the cement pastes at 7 days. The flexural strength diminishes at higher BNP concentrations and this is more pronounced at 0.6-wt% BNP. This could be attributed to the synergetic effect of restacking of BNP sheets and high content of $Ca(OH_2)$ crystals. The severe restacking of BNP sheets at high contents in high alkaline cement pastes may causes reduction of the flexural strength of the cement pastes. The high alkaline cement pore solution attenuates the hydroxyl groups on the surface of the BNP sheets and high van-der-Waals forces are created as a result, from where the sheets are stacked on top of each other to form rigid agglomerates. These agglomerates weaken the matrix, causing the cement pastes to fail in a brittle manner with lower mechanical properties (Saafi et al., 2015). The high content of $Ca(OH)_2$ crystals of the cement pastes containing 0.40-wt% BNP and 0.60-wt% BNP could lead flexural strengths lower than that of the cement paste containing 0.20-wt% BNP. Ca(OH)2 crystals are typically weak and brittle in nature thereby weakening the cement matrix by making it highly susceptible to a brittle fracture (Khan et al., 2014).

At 14 days, the flexural strength of the cement pastes is slightly increased at BNP concentrations of 0.4-wt% and 0.6-wt% when compared to plain cement paste samples.

At 28 days, the flexural strength of the cement pastes is increased by about 80%, 50% and 3% at BNP concentrations of 0.2-wt%, 0.4-wt% and 0.6-wt%, respectively. Based on this, 0.20-wt% BNPs is the optimal content for maximum mechanical properties.

The improvement of flexural strength was observed to be time dependent, for plain cement paste, the flexural strength increased slightly at 14 days when compared with its value at 7 days. However, it was almost the same its value at 28 days. The flexural strength of the cement pastes with 0.2-wt% BNP rose slightly at 14 days when compared with its value at 7 days. However, the flexural strength increased sharply at 28 when compared with its value at 7 days. The flexural strength of the cement pastes with 0.4-wt% BNP rose slightly at 14 days when compared to its value at 7 days. However, the flexural strength increased sharply at 28 days when compared with its value at 7 days. The flexural strength of the cement pastes with 0.6-wt% BNP increased dramatically at 14 days when compared with its value at 7 days. However, the flexural strength rose slightly at 28 days when compared with its value at 14 days.

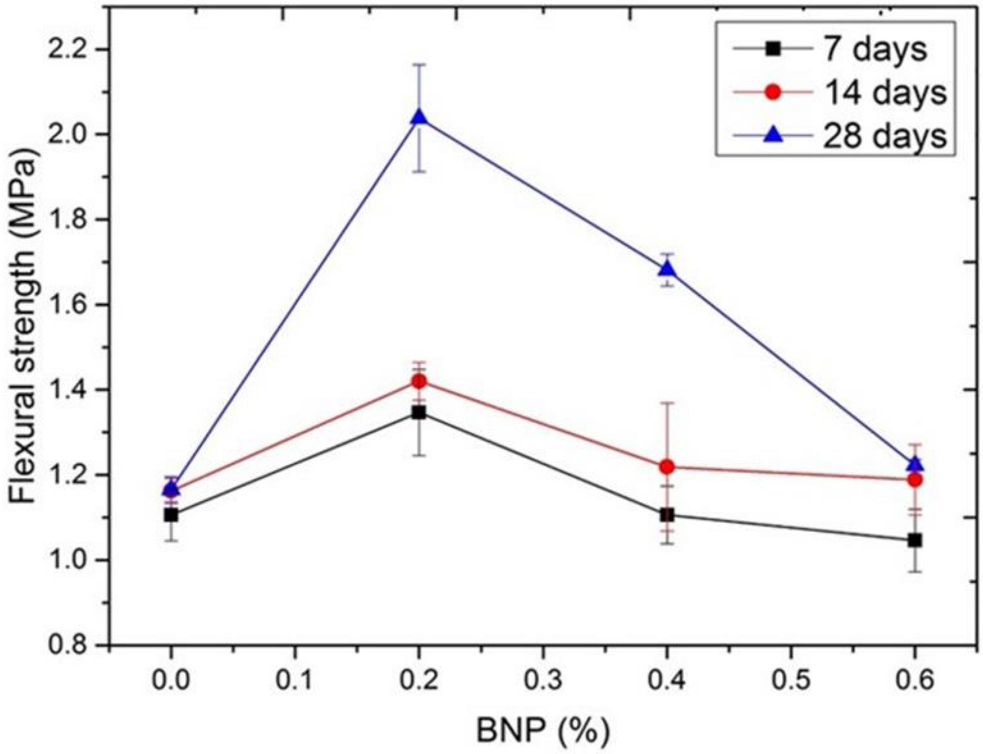

**Figure 4.16:** Variation of the flexural strength as a function of BNP concentration at different curing ages.

The gain in the flexural strength of the cement pastes at 0.2-wt% BNP and 0.40-wt% BNP is partially attributed to improved hydration kinetics of the cement particles which results in denser cement pastes with higher C-S-H content as discussed above. The gain in the flexural strength is also attributed to the reinforcing effect of the BNP sheets. This reinforcing effect is controlled by the mechanical interaction between the BNP sheets and the cementitious matrix coupled with chemical cross-linking type bonding and this chemical cross-linking type bonding was observed to be time dependent and improved with curing age due to depending on developing hydration products. Like GO-cementitious composites, this morphology plays a significant role in the mechanical interaction (i.e. load transfer) between the BNP sheets and the cementitious matrix, because it enhances the mechanical interlocking.

Figure 4.17 and figure 4.18 shows the chemical interaction of the BNP sheet with the hydration phase C-S-H and CH, which is somewhat similar to that of GO with the hydration phase C-S-H. The BNP characterization results indicate that the BNP sheets are fully decorated with oxygen-containing functional groups which are responsible for their high chemical reactivity. These functional groups are believed to adsorb on the surface of the cement particles in the presence of water.

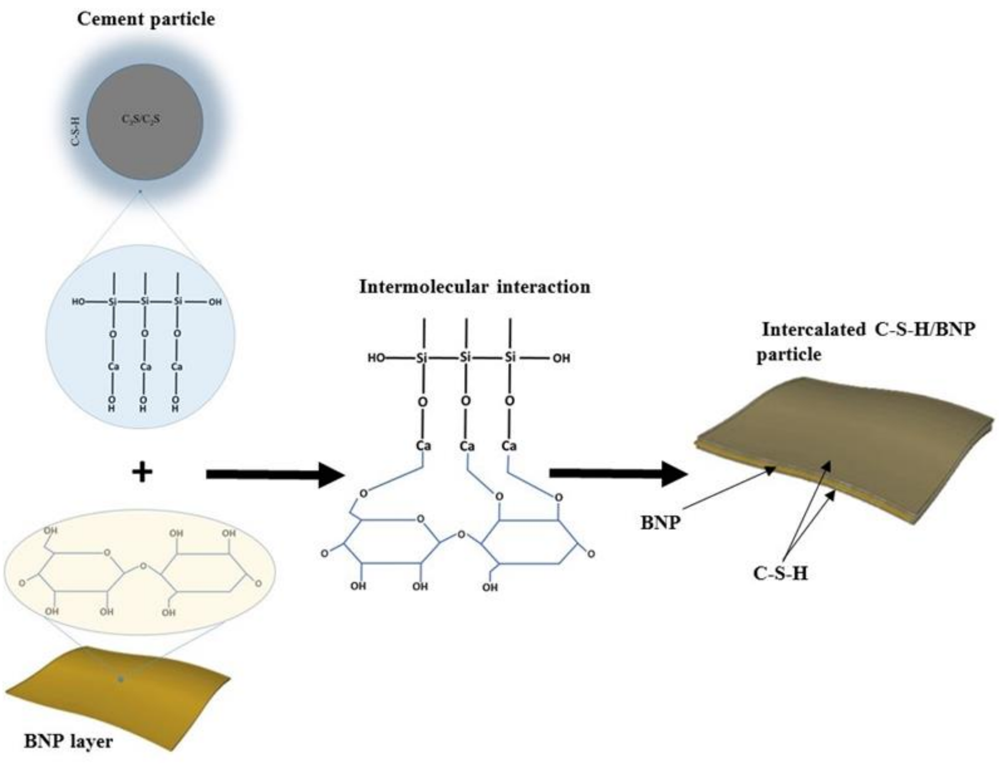

**Figure 4.17:** Intermolecular interaction of BPN with C-S-H phase

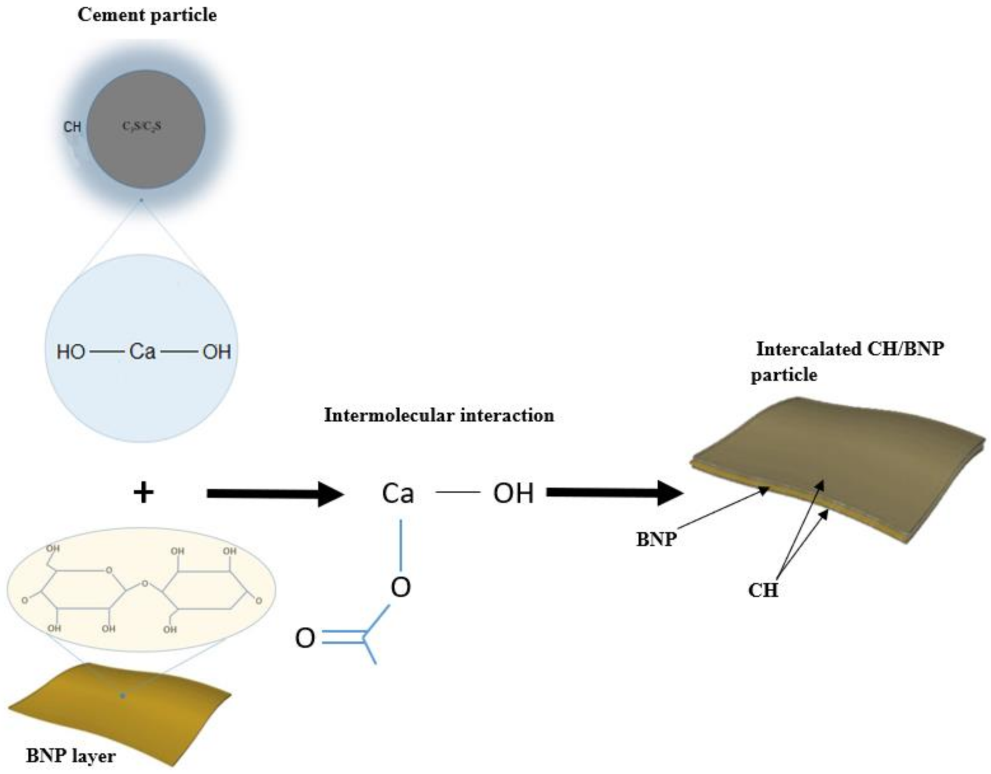

**Figure 4.18:** Intermolecular interaction of BPN with CH phase

In this case, the chemical components of the cement mainly $C_2S$ and $C_3S$ hydrate over the surface of the BNP sheets, leading to intercalated C-S-H/BNP particles (figure 4.17) and intercalated CH/BNP (figure 4.18). The strong interfacial covalent bonding between C-S-H, CH and the functionalized BNP sheets enhances the stress transfer thus improving the overall mechanical properties of the cement pastes at BNP concentrations of 0.20-wt%.

The effect of BNP concentrations on the average compressive strength at 7, 14 and 28 days is given in figure 4.19. The figure shows that after 7 days curing, the compressive strength firstly increased with content of BNP, up to approximately 10% by addition of 0.4wt% BNP, then decreased to be like that of control specimen by addition of 0.6wt% BNP. At 14 days, addition of 0.2-wt% BNP increased the compressive strength by about 10%, further addition of BNP did not alter the compressive strength much, it remained stable at its magnitude at 0.2% wt.% BNP. At 28 days, after 0.2-wt.%, the compressive strength gradually decreased with the increase of content of BNP. Addition of 0.6-wt% BNP decreased the compressive strength by about 8%. It can be concluded that the addition of BNP has no effect on compressive strength at lower concentration of BNP at 28 days. This could be attributed to that, the compressive properties of the cement paste are more likely to be controlled by the cement matrix and not by fibre reinforcement. In contrast, the gain in the compressive strength of cement pastes at 0.20-wt.% and 0.40-wt.% at 7 days age (i.e. early age) and at 0.20-wt.%, 0.40-wt.% and 0.60-wt.% at 14 days (i.e. early age) is attributed to improving hydration process at early ages and the amount of Ca(OH)2 is slightly small and has no effect on compressive strength. Furthermore, at 28 days the compressive strength of cement pastes with BNP loading more than 0.2 wt. % have sight reduction. This could be attributed to high content of Ca(OH)2 crystals. The high content of Ca(OH)2 crystals of the cement pastes containing 0.40-wt% BNP and 0.60-wt% BNP at 28 days could lead to lower compressive strengths than that of the cement paste containing 0.20-wt% BNP.

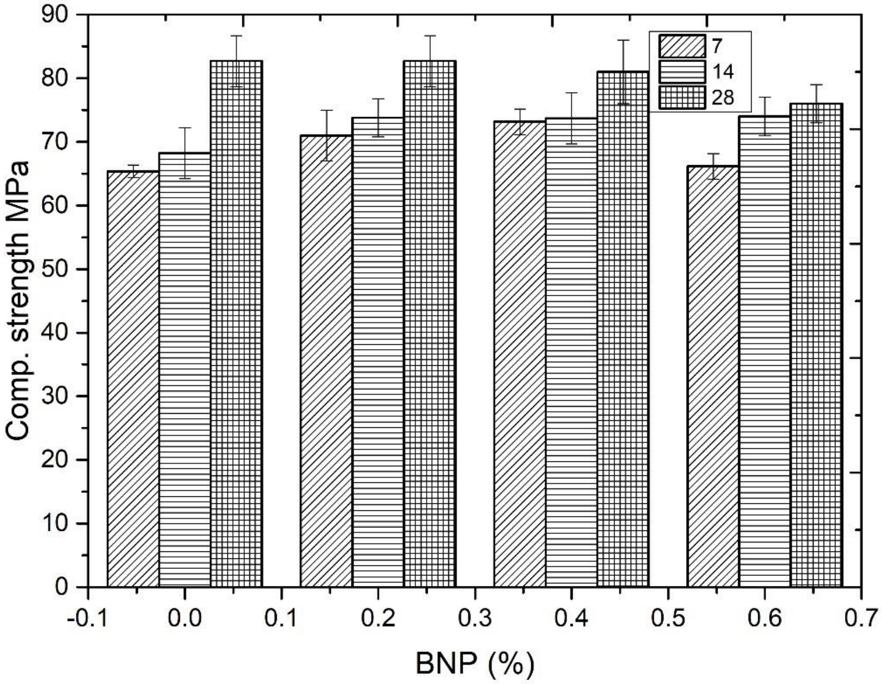

**Figure 4.19:** Compressive strength of hardened cement paste with BNP (%)

### 4.3.5 Comparisons with previous studies

There have been many renowned studies into the enhancement of flexural strength of cementitious composites using a range of additives including CNC, MWCNT and GOs. This study investigated the addition of BNP and the effects of this additive in comparison with traditional materials are outlined below. Figure 4.20 summarises the maximum enhancement of flexural strength of BNP used in this study compared to that of Cellulose Nanocrystals (CNC) by Cao et al. (2015, 2016). As shown, flexural strength was improved in most cases with significant amounts of BNP and CNC. The observed best performance enhancement included a 75% increase of flexural strength with 0.2 wt% of BNP, a 50% increase of flexural strength with 0.5-1.5vol% of CNC (Cao et al., 2016b) and a 30% increase with 0.2vol% CNC (Cao et al., 2015).

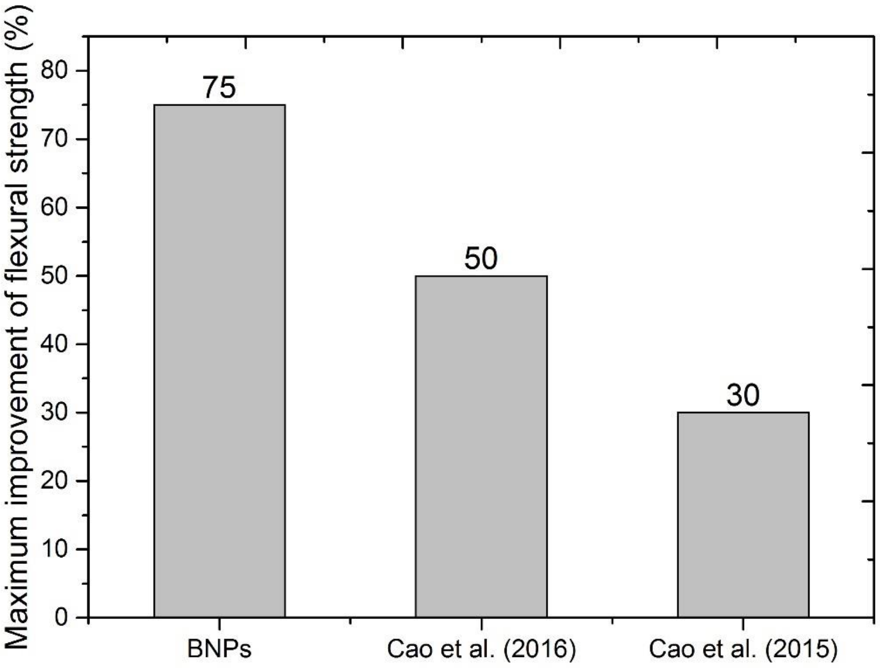

**Figure 4.20:** Maximum enhancement of flexural strength; comparison of BNP and CNC

In addition, the maximum improvement of flexural strength using MWCNT alone compared with BNP in this research are summarised in figure 4.21. In all cases the flexural strength was enhanced with additions of BNP and MWCNT. The best performance enhancement included a 75% increase of flexural strength with 0.2-wt% of BNP; a 50% increase with 0.1wt% of MWCNT (Tyson et al., 2011), a 35.5% increase with 0.2wt% of MWCNT (Luo et al., 2009), a 35% increase with 0.08wt% of MWCNT (Metaxa et al., 2012b), a 38% increase with 0.2wt% of MWCNT (Xu et al., 2015), a 25% increase with 0.5wt% of MWCNT, a 10% increase with 0.042wt% of MWCNT (Li et al., 2005), a 34% increase with 0.5wt% of MWCNT (Musso et al., 2009), a 40% increase with 0.08wt% of long MWCNT (Konsta-Gdoutos et al., 2010), a 25% increase with 0.25wt% of MWCNT (Chan and Andrawes, 2010) and a 50% increase of flexural strength with 0.048wt% of Carbon Nanofibres (CNFs) (Metaxa et al., 2012a).

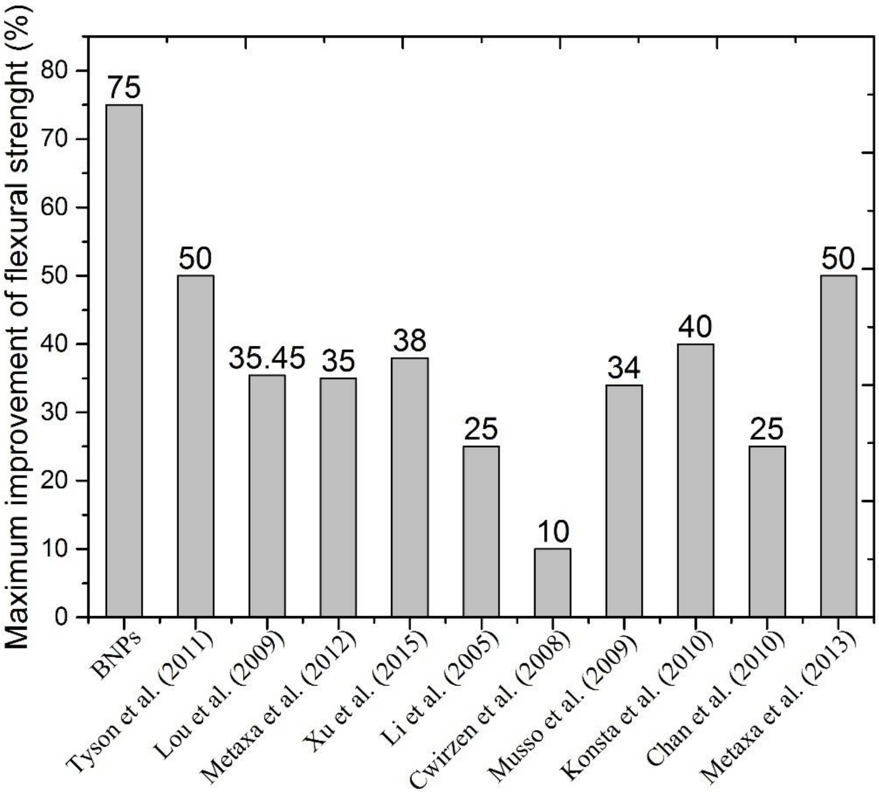

**Figure 4.21:** Maximum enhancement of flexural strength; comparison of BNP and MWCNT

Figure 4.22 summarises the maximum improvement of flexural strength using BNP compared with those studies using GO. Here and as seen previously, the flexural strength was improved with additions of both BNP and GO. The best performance enhancement included a 75% increase of flexural strength with 0.2wt% of BNP, a 67.1% increase with

0.04wt% of GO (Lv et al., 2014b), a 42.1% increase with 0.05wt% of GO (Lv et al., 2014a), a 60.7% increase with 0.03wt% of GO (Lv et al., 2013), a 31.63% increase with 0.01wt% of GO (Zhang H, 2015), a 14.2% increase with 0.04wt% of GO (Li et al., 2017), a 16.7% increase with 0.04wt% of GO (Zhou et al., 2017), a 59% increase with 0.05wt% of GO (Muhit B. 2015), and a 30.37% increase of flexural strength with 0.022wt% of GO (Zhao et al., 2017).

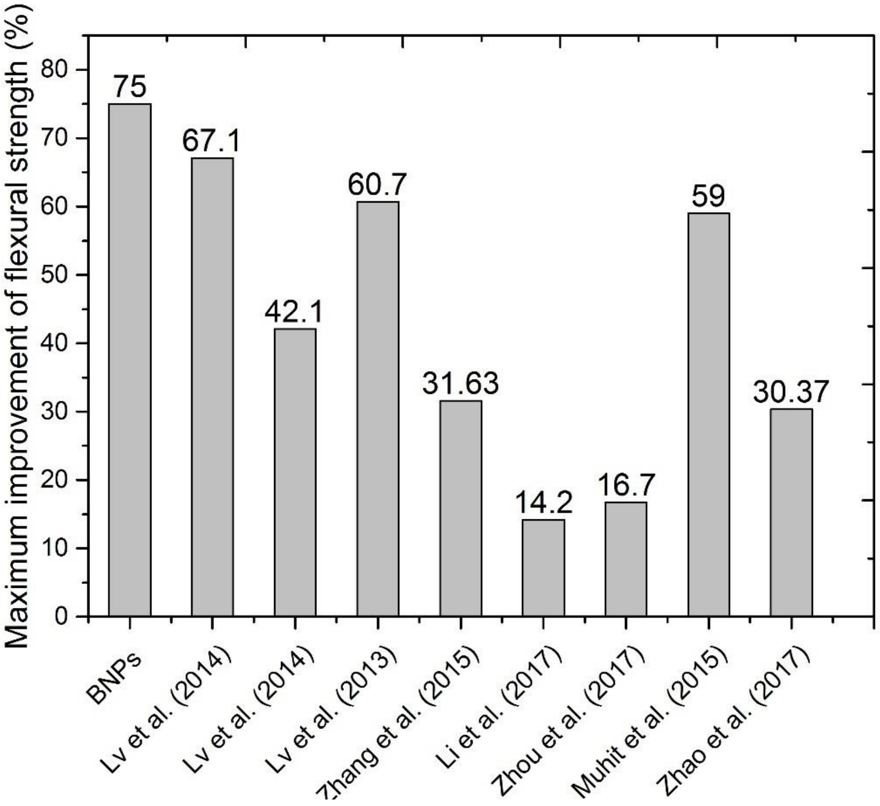

**Figure 4.22:** Maximum enhancement of flexural strength; comparison of BNP and GO

In this study, using BNP greatly enhanced the flexural strength in all cases when compared to previous studies using CNC, MWCNT and GOs. It seems that BNP are very small and adsorbed on the surface of the cement particles and they improve the rate of hydration through two mechanisms: (i) the first mechanism is steric stabilization, which is the same mechanism observed in many water reducing agents (WRA) to disperse cement particles during cement mixing. This results in a finer and more uniform distribution of cement; (ii) the second mechanism is short circuit diffusions which is the mechanism of water molecules diffusing along the BNP networks in the hydration products (Cao, et al., 2015). When the BNP adhere on the surface of hydrated products, the BNP create paths (i.e., channels) for water molecules to more easily diffuse through the hydrated shell and reach the inner unhydrated cement core.

## 4.4 Conclusions

Experimental tests have been carried out to investigate the performance of cementitious composites modified with BNP. The experimental programme has been described and results obtained from experimental tests have been presented and discussed. The TGA/DTA provides insight into the chemical reaction mechanisms in cementitious materials during heating. It can be observed that the mass loss of the cement paste composites decreases with increasing BNP concentration. This is due to the increase of the high density C-S-H content and the creation of new intercalated BNP/C-S-H nanocomposites with higher density. Additionally, the amount of $Ca(OH)_2$ increases with increasing BNP concentration at 7 and 28 days. This could be attributed to the addition of BNP sheets accelerating the hydration of cement resulting in the production of higher $Ca(OH)_2$ content at 7 and 28 days. The XRD further confirms the TGA findings. This means the addition of BNP promotes the hydration of cements thereby increasing the amount of the hydration products. This could be attributed to the highly hydrophilic BNP sheets which tend to store water molecules on their surface thus acting like water reservoirs which may release the free water for further hydration. Additionally, the results clearly show that the DOH increases with increasing BNP content. The microstructure of the plain cement paste consists mainly of $Ca(OH)_2$ crystals with a low C-S-H content. The addition of 0.2-wt% BNP leads to higher C-S-H content, fewer $Ca(OH)_2$ crystals and denser microstructure. The TEM investigations suggest a good compatibility between the BNP sheets and the hydration products. Based on the mechanical properties results, for all three curing ages, the increase in the flexural strength of the cement pastes reaches its maximum at an optimum content of 0.20-wt% BNP. This increase, however, diminishes at higher BNP concentrations and this is more pronounced at 0.6-wt% BNP. This could be attributed to the synergetic effect of restacking of BNP sheets and the high content of $Ca(OH_2)$ crystals.

As the flexural strength is a vital structural property, the maximum increase of flexural strength for our cementitious composites modified with BNP have been compared with previous composites and the results showed that the maximum increase of flexural strength of our composite was significantly greater than the rest of the previous work.

# Chapter five

# 5 Engineering of multifunctional hybrid BNP/MWCNT nanoparticles

## 5.1 Introduction

This chapter presents the development and evaluation of the proposed hybrid BNP/MWCNT nanoparticles as a reinforcing material in cementitious composites. The concept of the hybrid BNP/MWCNT nanoparticles is presented, followed by their synthesis and evaluation. The colloidal properties and stability of the BNP/MWCNT nanoparticles were determined and compared to commercially available MWCNT/GO and MWCNT/MCC particles.

## 5.2 Proposed Multifunctional hybrid BNP/MWCNT Particles

As mentioned earlier in Chapter three, BNP have –OH groups which enables hydrophilicity while -H groups cause hydrophobic faces, thus the appearance of both hydrophilic and hydrophobic faces allows BNP to be used as dispersant. Thereby BNP were used to disperse MWCNT and create a novel hybrid nanomaterial which was created from adsorption of BNP on the MWCNT surfaces (i.e. self-assembly process). That are easy to attribute to the underlying force which comes from hydrophobic interactions that occur between the side wall of the MWCNT and the surface crystalline plane of the amphiphilic BNP (Mougel et al., 2016; Olivier et al., 2012). Figure 5.1 illustrates the mechanism for the creation hybrid BNP/MWCNT, BNP sheets attached to MWCNT through the interaction between its hydrophobic sites and MWCNT hydrophobic plane due to hydrogen bonding between hydrogen groups of BNP sheets and the edges of MWCNT. Additionally, the hybrid BNP/MWCNT was stabilized due to electrostatic repulsion forces between the BNP generated by the charged –OH and $CH_2OH$ groups which come from treatment by dispersant Span 20 that coats the surface of the BNP and prevents the BNP/MWCNT aggregating. This allows them to be more readily re-dispersed in aqueous media.

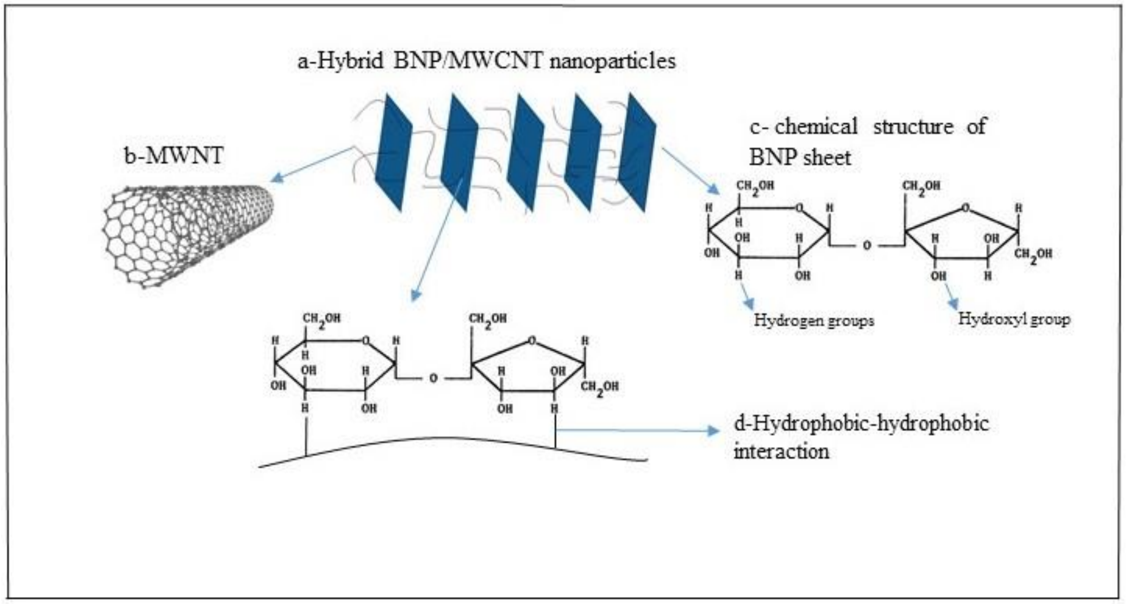

**Figure 5.1:** Schematic of interaction between BNP and MWNCT.

## 5.3 Experimental programme

### 5.3.1 Materials

The BNP were synthesised by our industrial partner, and the BNP properties were investigated in chapter three and used with cementitious composites in chapter four. The Multi wall carbon nanotubes (MWCNT) used in this study were produced by catalytic chemical vapor dispersion (CCVD) by Cheap-tubes (Brattleboro, Vermont, USA). The purity of carbon was 95%. To compare the colloidal properties and stability of the BNP/MWCNT nanoparticles we have used commercially available MWCNT/GO and MWCNT/MCC particles for comparison purpose and we used SP to improve the workability. Cellulose Microcrystalline (MCC) is cellulose derived from high quality wood pulp and was from Blackburn distributions. Graphene oxide (GO) is a solution with 4 mg/ml in aqueous solution and the Superplasticizer (Glenium 51) is a polycarboxylic ether based high range water reducing superplasticizer concrete admixture.

Optical microscopy, UV–vis microscopy, SEM (scanning electron microscope), EDS (energy dispersive X-ray diffraction analysis) and TGA (Thermogravimetry Analysis) were used to investigate dispersion of MWCNT in aqueous solution. Ultraviolet visible spectroscopy was an appropriate technique for estimation of dispersion of MWCNT due to the individual multi wall carbon nanotubes being active under UV-vis spectroscopy. Furthermore, optical microscopy was used to examine dispersion at the microscale level. In addition, SEM and EDS analysis were used to further study the dispersion and the chemical components of materials. Additionally, TGA analysis was used to investigate the thermostability of all materials. Figure 5.2 shows Netzsch thermal analysers which was used to employ thermal analysis for materials.

**Figure 5.2:** Netzsch thermal analyser

Figure 5.3 shows the JEOL JSM-7800F, which is JEOL's industry-leading highest performing Field Emission SEM with ultrahigh resolution at ultra-low kV imaging. It was used to carry out SEM and EDS analysis. It has a magnification range of 25× to 1,000,000×, accelerating voltage of 10 V to 30 kV, probe current range of a few pA to 200 nA and a resolution of 0.8 nm @ 15 kV.

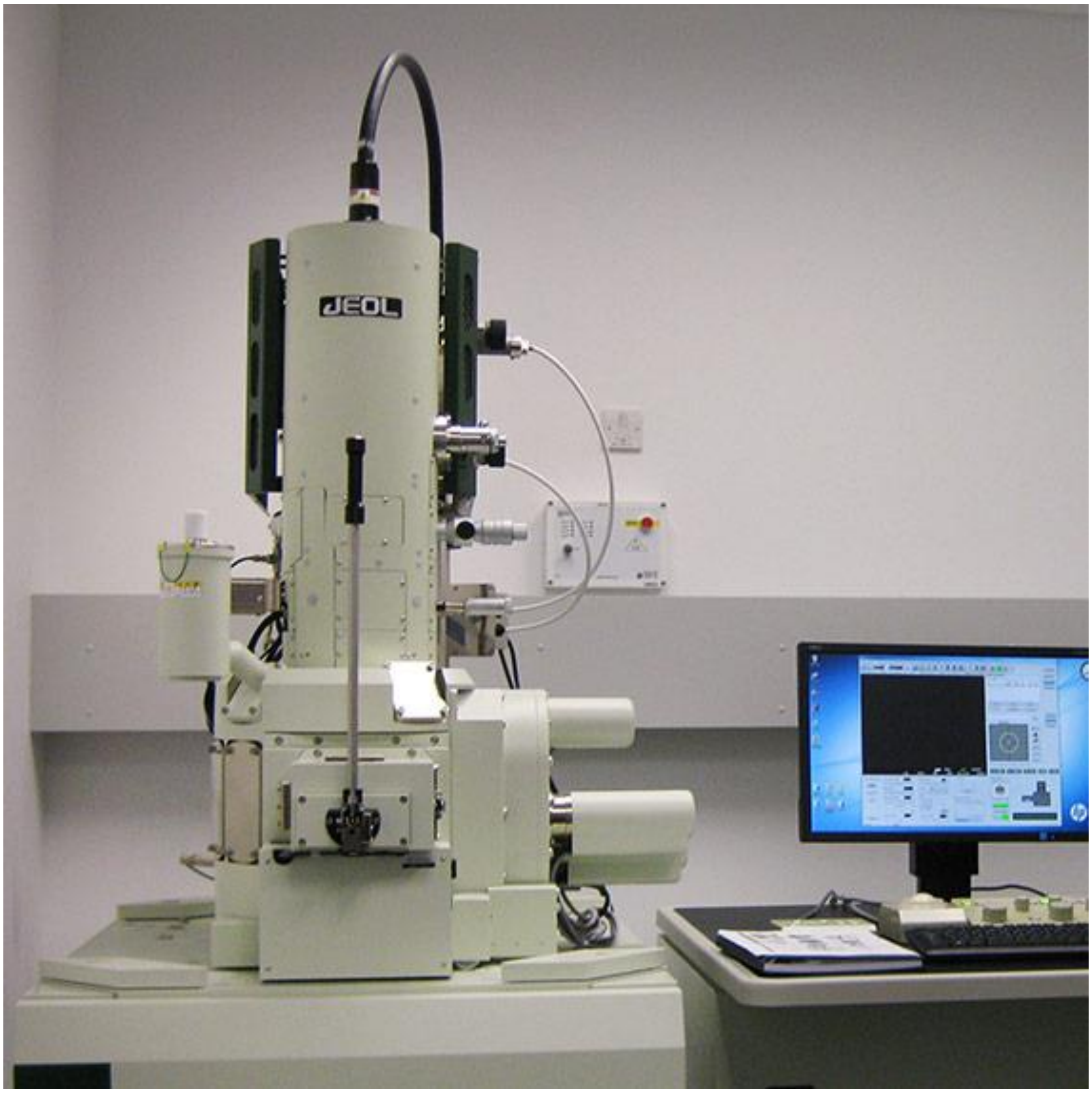

**Figure 5.3:** JEOL JSM-7800F for SEM (scanning electron microscope)

Figure 5.4 shows UV-Visible spectrophotometer device (Evolution 220), which was used to investigate dispersion of materials in aqueous solution.

### 5.3.2 Preparation of BNP/MWCNT solutions

In this study the hybrid BNP/MWCNT nanoparticles were prepared at five concentrations of MWCNT: 0, 2, 4, 6 and 8 g/l of aqueous solution. These were added to 5g/l of BNP (MWCNT/BNP (0.4, 0.8, 1.2 and 1.6)), 20 g/l of MCC (MWCNT/MCC (0.1, 0.2, 0.3 and

0.4)), and 2g/l of GO (MWCNT/GO (1, 2, 3, 4)). Three durations of sonication were used, 30 minutes, 50 minutes and 100 minutes, with rate 40w with 50% duty. To avoid excessive heat, an ice bath was used.

**Table 5.1**: Name of hybrid and the concentrations of MWCNT, BNP, MCC, GO and SP

| Name of hybrid | Concentration of MWCNT g/l | Concentration of BNP g/l | MWCNT/ BNP | Concentration of MCC g/l | MWCNT /MCC | Concentration of GO g/l | MWCNT/ GO | Concentration of SP g/l |
|---|---|---|---|---|---|---|---|---|
| R1 | 0 | 5 | - | 0 | - | 0 | - | 0 |
| R2 | 2 | 5 | 0.4 | 0 | - | 0 | - | 0 |
| R3 | 4 | 5 | 0.8 | 0 | - | 0 | - | 0 |
| R4 | 6 | 5 | 1.2 | 0 | - | 0 | - | 0 |
| R5 | 8 | 5 | 1.6 | 0 | - | 0 | - | 0 |
| R6 | 2 | 5 | 0.4 | 0 | - | 0 | - | 25 |
| R7 | 4 | 5 | 0.8 | 0 | - | 0 | - | 25 |
| R8 | 6 | 5 | 1.2 | 0 | - | 0 | - | 25 |
| R9 | 8 | 5 | 1.6 | 0 | - | 0 | - | 25 |
| R10 | 0 | 5 | - | 0 | - | 0 | - | 25 |
| M1 | 0 | 0 | - | 20 | - | 0 | - | 0 |
| M2 | 2 | 0 | - | 20 | 0.1 | 0 | - | 0 |
| M3 | 4 | 0 | - | 20 | 0.2 | 0 | - | 0 |
| M4 | 6 | 0 | - | 20 | 0.3 | 0 | - | 0 |
| M5 | 8 | 0 | - | 20 | 0.4 | 0 | - | 0 |
| M6 | 2 | 0 | - | 20 | 0.1 | 0 | - | 25 |
| M7 | 4 | 0 | - | 20 | 0.2 | 0 | - | 25 |
| M8 | 6 | 0 | - | 20 | 0.3 | 0 | - | 25 |
| M9 | 8 | 0 | - | 20 | 0.4 | 0 | - | 25 |
| M10 | 0 | 0 | - | 20 | - | 0 | - | 25 |
| G1 | 0 | 0 | - | 0 | - | 2 | - | 0 |
| G2 | 2 | 0 | - | 0 | - | 2 | 1 | 0 |
| G3 | 4 | 0 | - | 0 | - | 2 | 2 | 0 |
| G4 | 6 | 0 | - | 0 | - | 2 | 3 | 0 |
| G5 | 8 | 0 | - | 0 | - | 2 | 4 | 0 |
| G6 | 2 | 0 | - | 0 | - | 2 | 1 | 25 |
| G7 | 4 | 0 | - | 0 | - | 2 | 2 | 25 |
| G8 | 6 | 0 | - | 0 | - | 2 | 3 | 25 |
| G9 | 8 | 0 | - | 0 | - | 2 | 4 | 25 |
| G10 | 0 | 0 | - | 0 | - | 2 | - | 25 |

**Figure 5.4:** UV-Visible spectrophotometer device (Evolution 220)

## 5.4 Results and discussions

### 5.4.1 Colloidal properties of BNP/MWCNT nanoparticles

One ml from each sample prior to mixing was taken, diluted one hundred times with water and then dropped onto glass substrate to investigate the dispersion at the microscale level. Figure 5.5 and figure 5.6 showed a superior dispersion of BNP, MWCNT/BNP and suggests better dispersion for MWCNT- BNP with a lower amount of MWCNT and with SP. In addition, with a higher amount of MWCNT there is still clear dispersion but there is a very slight agglomeration of MWCNT-BNP; this could be because the amount of BNP is not sufficient to achieve good dispersion at high concentrations of MWCNT. R1 also shows some particles of BNP. This could be attributed to some particles of unextracted bio material at the micro-level.

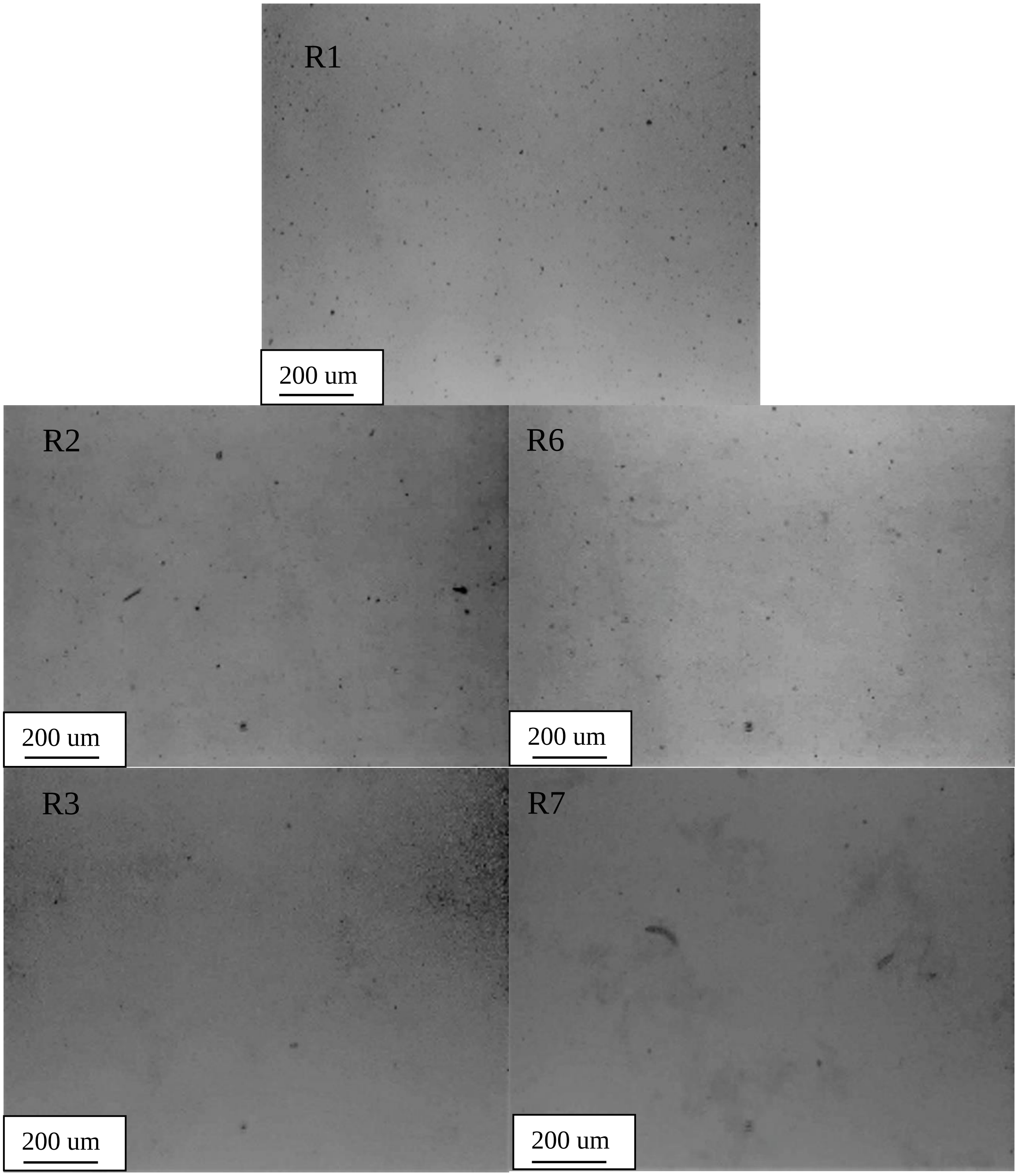

**Figure 5.5:** Optical image of R1, BNP 5g/l without SP, (R2 and R3) MWCNT/BNP (0.4 and 0.8) without (SP) respectively and (R6 and R7) MWCNT/BNP (0.4 and 0.8) with (SP) respectively.

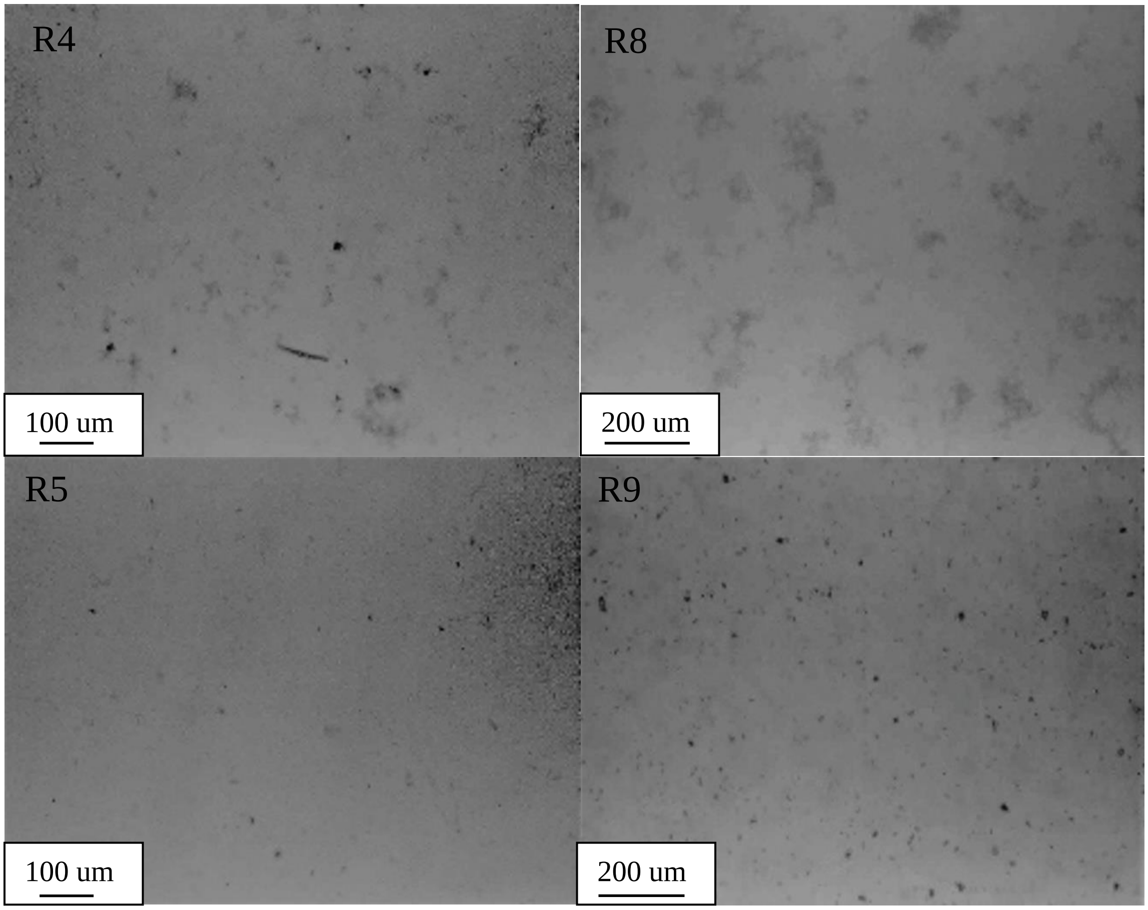

**Figure 5.6:** Optical image (R4 and R5) MWCNT/BNP (1.2 and 1.6) without (SP) respectively and (R8 and R9) MWCNT/BNP (1.2 and 1.6) with (SP) respectively.

Figure 5.7 and figure 5.8 showed histograms of the number of MWCNT/BNP particles of R1, R2, R3, R4, R5, R6, R7, R8 and R9. The histograms results show that, in general by using BNP, there are many smaller particles of MWCNT/BNP than the particles of MWCNT only (figure 5.28), and their solutions were stable. Thus, there is evidence of better dispersion for MWCNT by using BNP.

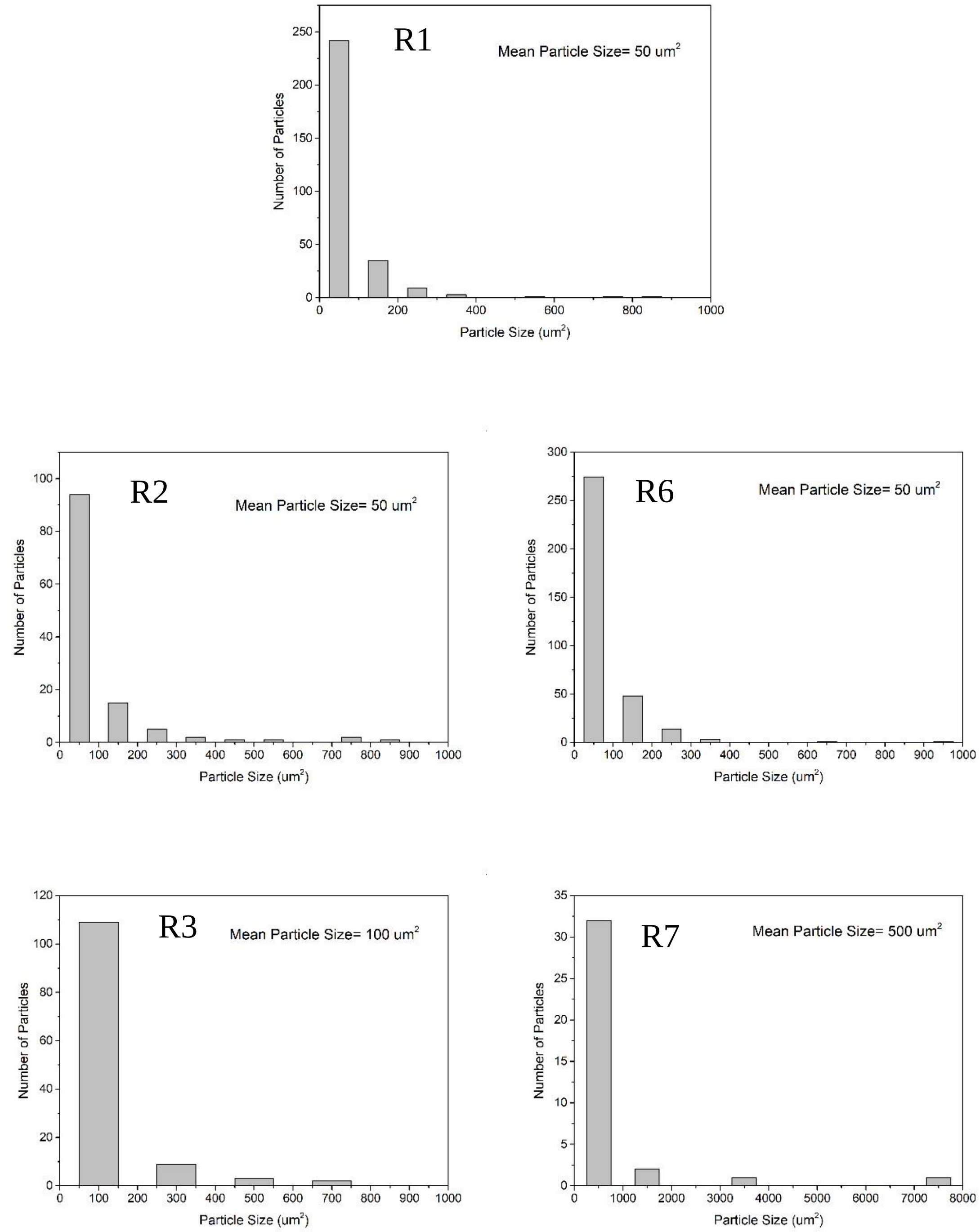

**Figure 5.7:** histograms of the number of MWCNT/BNP particles of R1, R2, R3, R6 and R7.

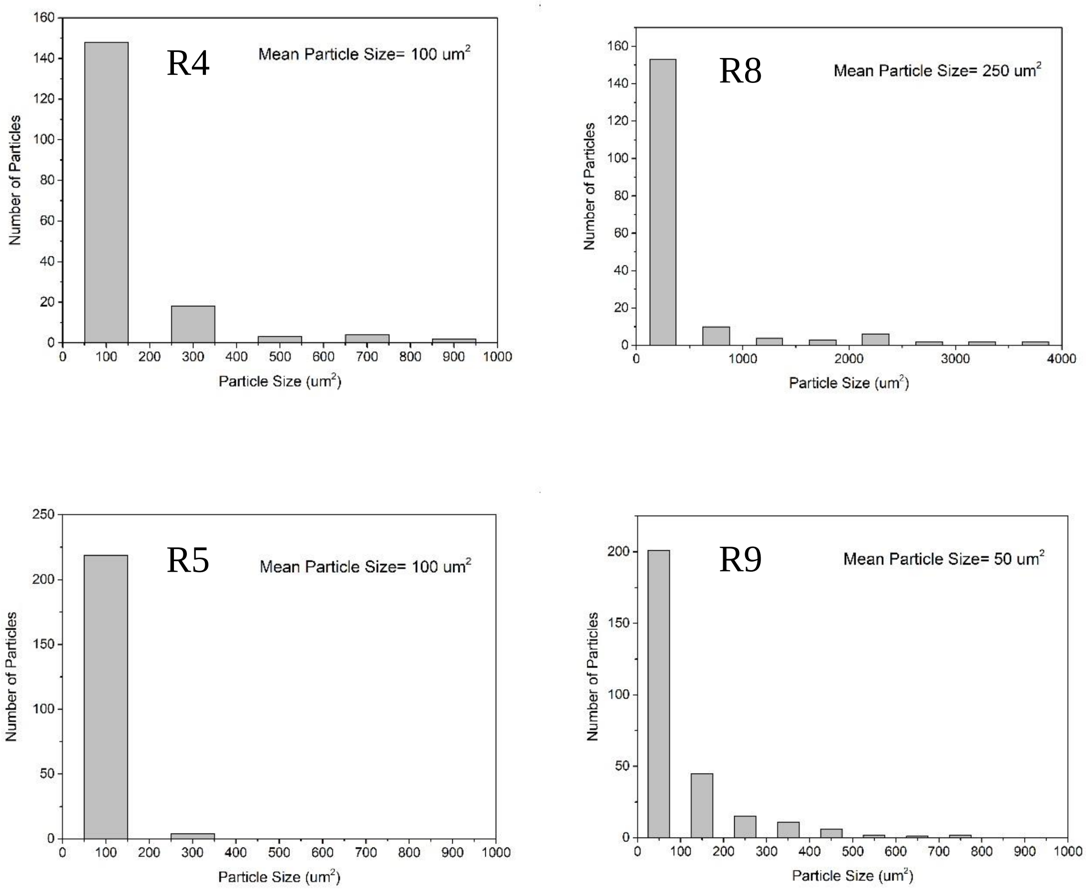

**Figure 5.8:** histograms of the number of MWCNT/BNP particles of R4, R5, R8 and R9.

Ultraviolet visible spectroscopy is a common method for measuring dispersion in a transparent medium. This technique is based on the observation that the more dispersed MWCNT are in a liquid, the darker the liquid will be, and the more light absorbed. Figures 5.9, 5.10, 5.11, 5.12 and 5.13 show that, the absorbance of BNP, and MWCNT/BNP with and without SP. It seems that the absorbance is low for BNP, due to their high transparency (Sabo et al, 2016). On the other hand, the absorbance for MWCNT is high when compared to the absorbance of BNP. In addition, using SP revealed a slight difference in absorbance for all materials. It appears that the absorbance of 0.4 MWCNT/BNP without SP is slightly better than the absorbance of 2 g/l MWCNT only without SP (Figure 5.37 (N1).

Furthermore, the absorbance of MWCNT/BNP without SP for all concentrations is similar except at 0.8 MWCNT/BNP, which is higher than the rest. In contrast, the absorbance has increased with the presence of SP and with an increase in the concentrations of MWCNT/BNP. It seems that, using SP can lead to better dispersion of MWCNT/BNP and the reason for that could be the repulsion force created by (OH) groups of SP is higher the van-der forces of MWCNT and prevents agglomeration of MWCNT. BNP also contribute to stabilize the dispersion of MWCNT through two possible ways. Firstly, through electrostatic repulsion between the BNP, which comes from treatment by dispersant Span 20 that coats the surface of the Bio Nano platelets and prevents the cellulose platelets aggregating This allows them to be more readily re-dispersed in aqueous media. Secondly, from the possible adsorption of the BNP on the nanotubes.

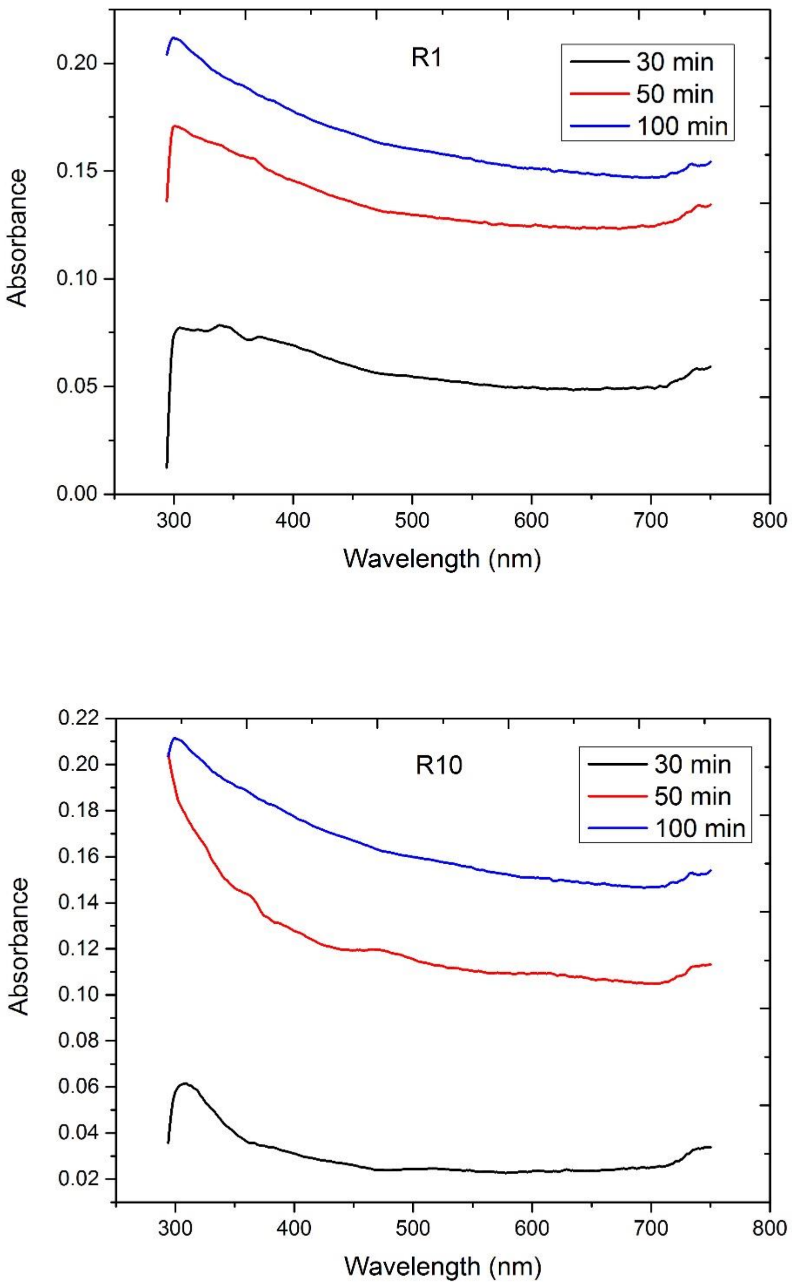

**Figure 5.9:** UV-Vis spectroscopy of (R1) without (SP) and (R10) with (SP)

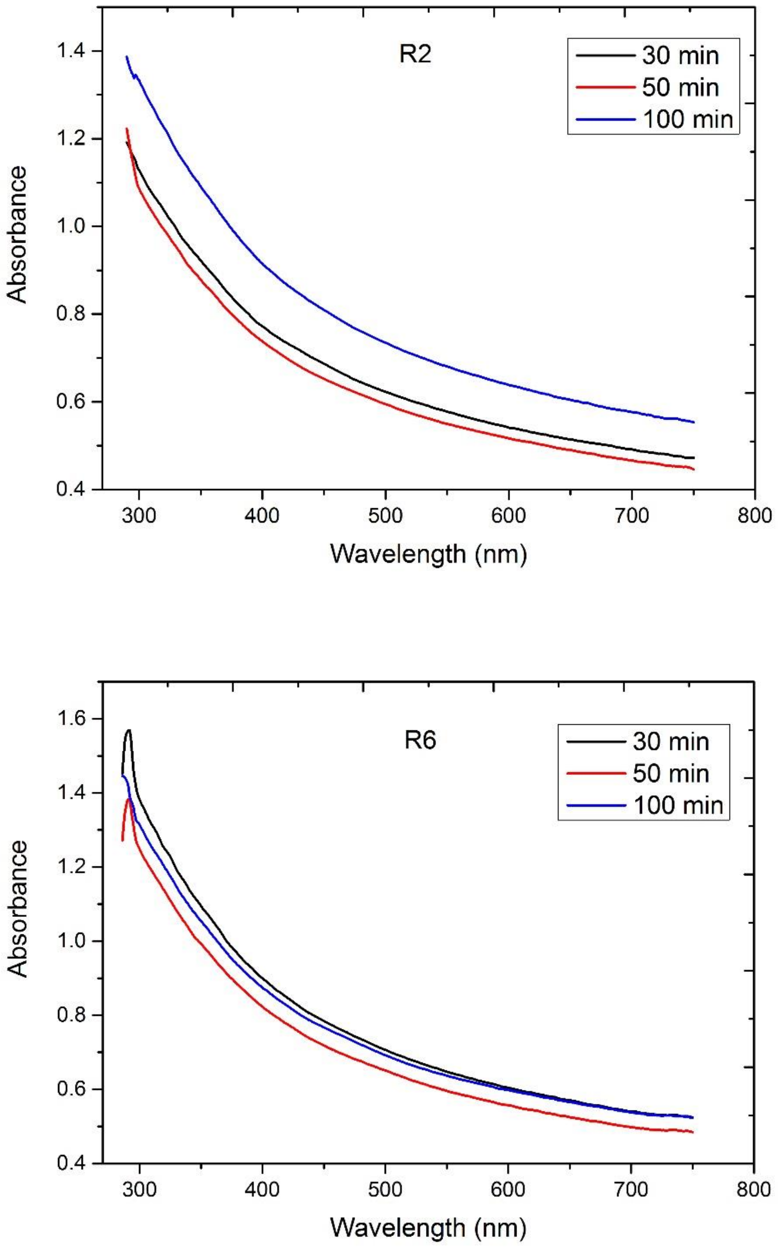

**Figure 5.10:** UV-Vis spectroscopy of R2, MWCNT/BNP (0.4) without (SP) and (R6) MWCNT/BNP (0.4) with (SP).

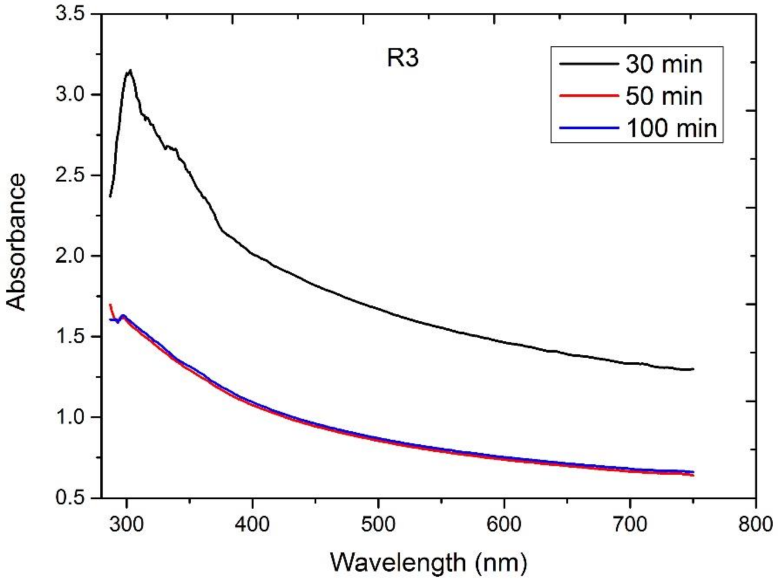

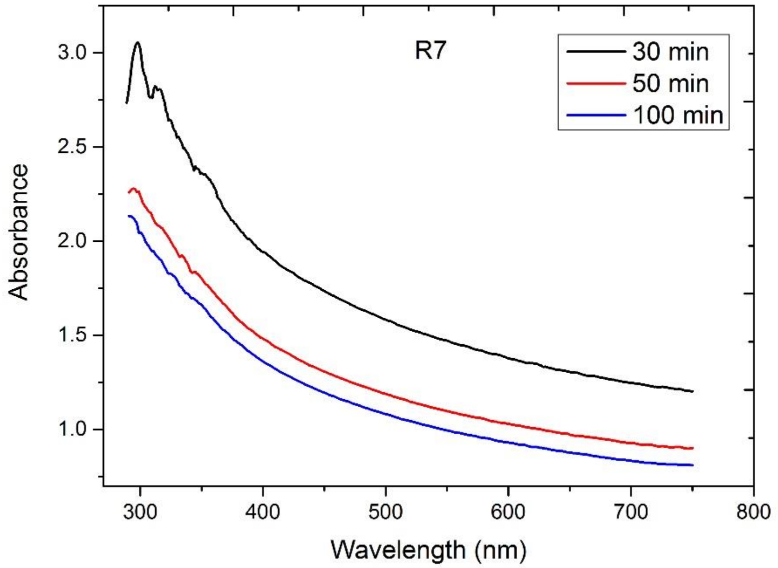

**Figure 5.11:** UV-Vis spectroscopy of (R3) MWCNT/BNP (0.8) without (SP) and (R7) and MWCNT/BNP (0.8) with (SP).

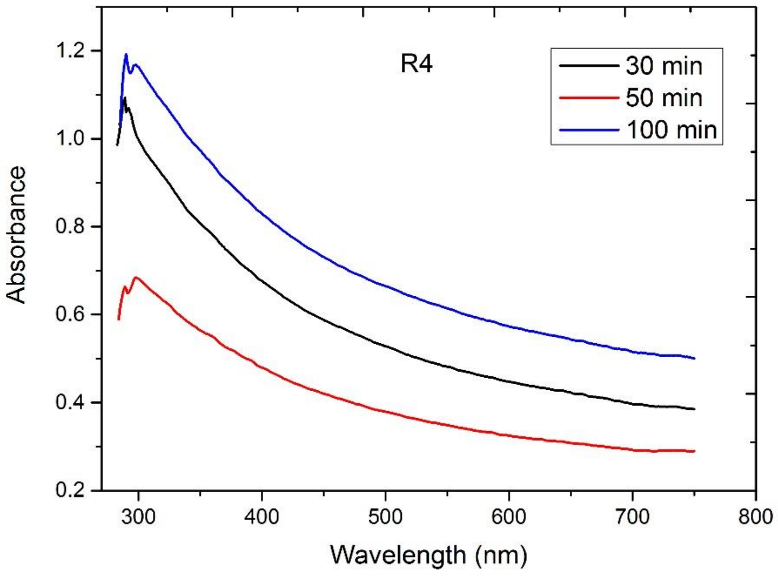

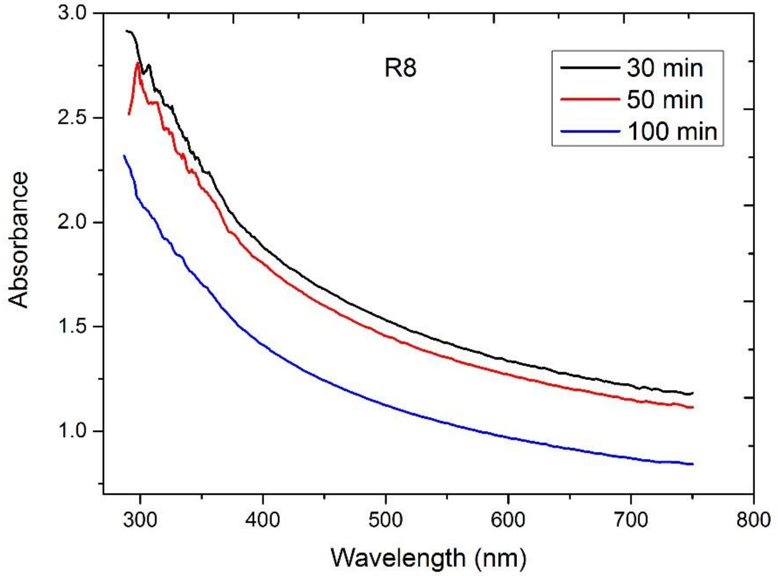

**Figure 5.12:** UV-Vis spectroscopy of (R4) MWCNT/BNP (1.2) without (SP) and (R8) MWCNT/BNP (1.2) with (SP).

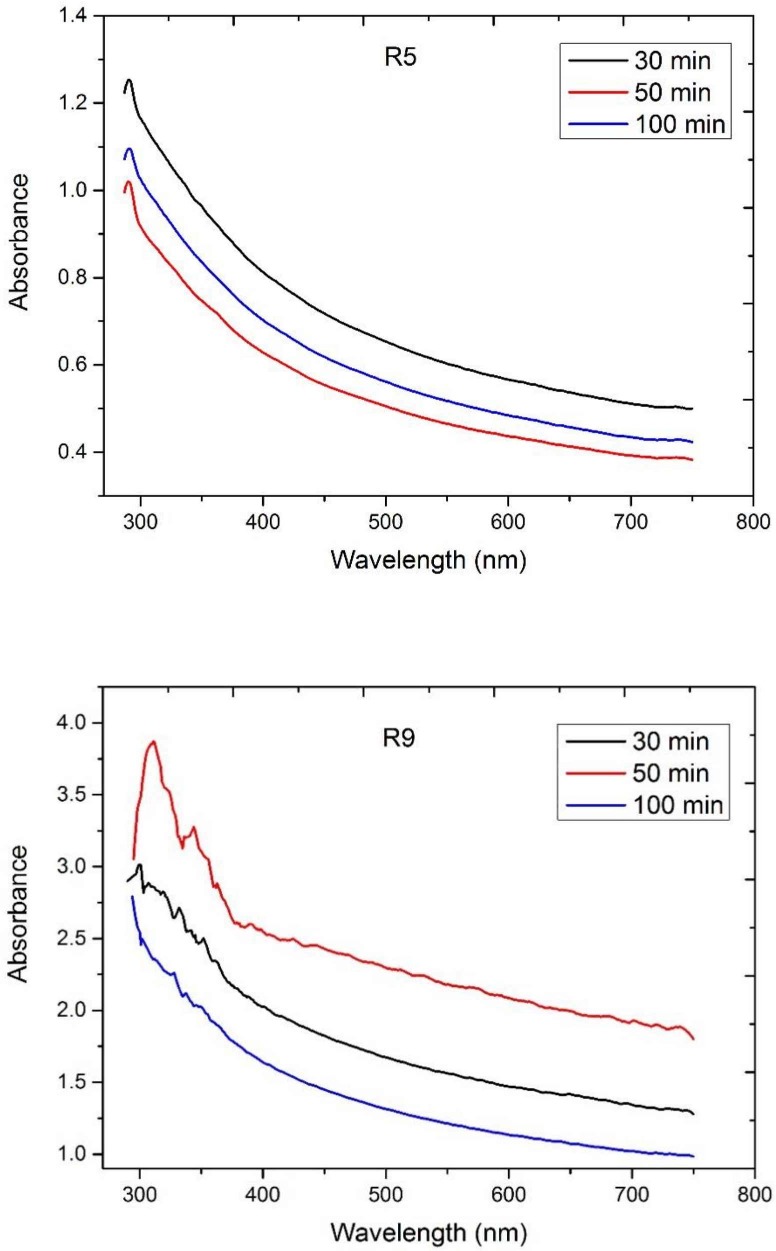

**Figure 5.13:** UV-Vis spectroscopy of (R5) MWCNT/BNP (1.6) without (SP) and (R9) MWCNT/BNP (1.6) with (SP).

It is believed that a novel hybrid nanomaterial was created from adsorption of BNP on the MWCNT surfaces (i.e. self-assembly process), that are easy to attribute to the underlying force which comes from hydrophobic interactions that occur between the side wall of the

MWCNT and the surface crystalline plane of the amphiphilic BNP (Mougel et al., 2016; Olivier et al., 2012).

SEM was used to investigate the dispersion state of MWCNT with different concentrations of MWCNT and BNP, as shown in figure 5.14, SEM image of BNP. Individual fibres of bio nano platelets. Typical SEM's images of MWCNT/BNP (0.4, 0.8, 1.2 and 1.6) (R6, R7, R8 and R9) with SP respectively can be seen in figures 5. 15, 5. 16, 5.17 and 5.18. Interestingly, there was uniform distribution of MWCNT and single tubes could be seen easily. There are individual MWCNT which have a length of 1.5-5 um. What is striking about figure 5.15 is the clear adherence between MWCNT surfaces and the BNP surfaces of their fibres and their platelets surfaces.

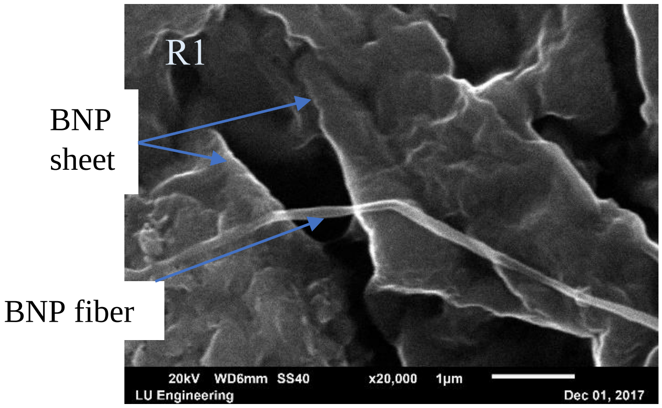

**Figure 5.14:** SEM image of BNP

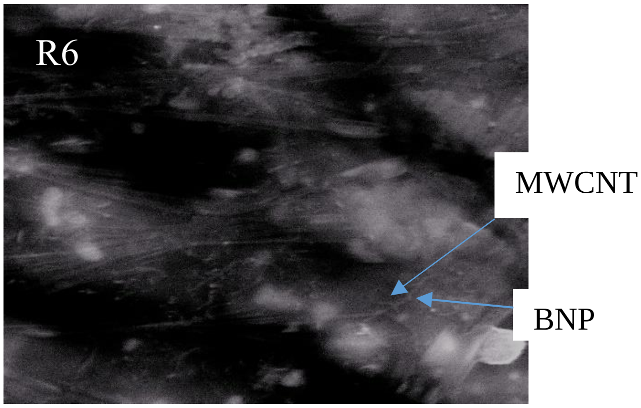

**Figure 5.15:** SEM image of 0.4 MWCNT/BNP

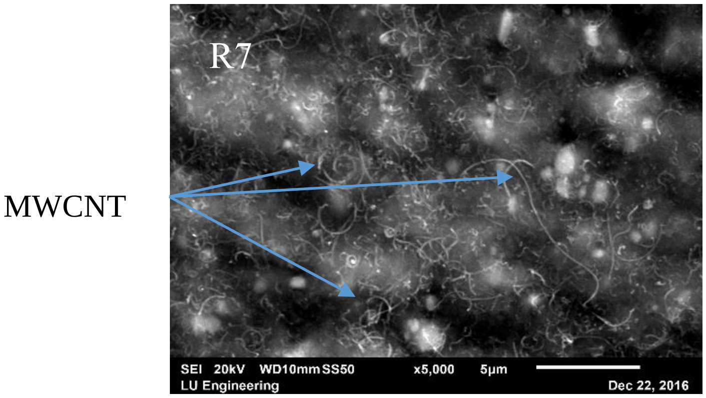

**Figure 5.16:** SEM image of 0.8 MWCNT/BNP

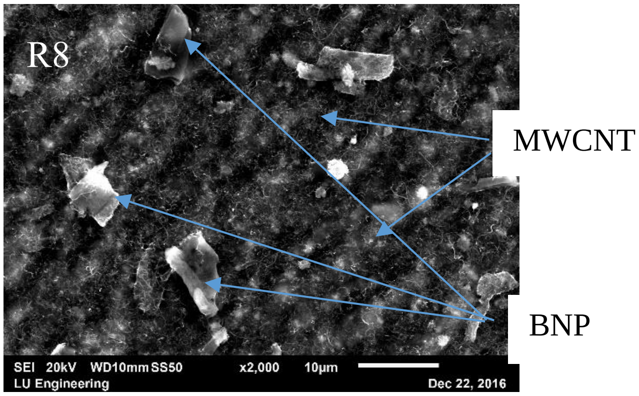

**Figure 5.17:** SEM image of 1.2 MWCNT/BNP

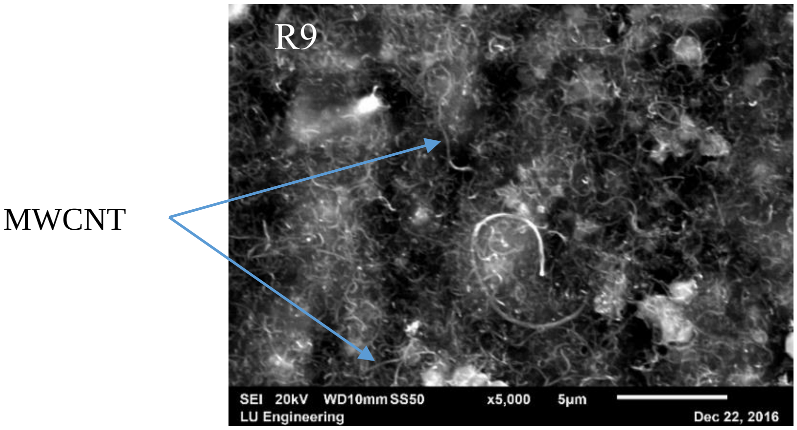

**Figure 5.18:** SEM image of 1.6 MWCNT/BNP

The thermal stability of a material and characterisation of its purity are evaluated by TGA (thermogravimetric analysis). The initiation temperature, oxidation temperature and residual mass are the important parameters measured in the weight loss. The temperature at which material starts to decompose can be named as the initiation temperature. The temperature of maximum weight loss is named as the oxidation temperature and it is often described as the thermal stability of the material. (Lehman et al., 2011; Ling et al., 2013). Figure 5.19 represents the results of thermogravimetric analysis (TGA) for pristine MWCNT, BNP and MWCNT/BNP. The TGA curve of pristine MWCNT shows no significant mass loss up to 500°C due to high temperature decomposition of the main graphitic structures (Amiri et al., 2013). At this point it is worth pointing out that this is attributed to the high oxidizing temperature of a well graphitic structure which starts to oxidize at relatively high temperatures between 600 and 700°C (Datsyuk et al., 2008). The weight loss for BNP occurred in the temperature range from 25 -1100°C. Previous studies have shown that the thermal degradation of sugar beet pulp follows a two-step weight loss process (Yılgın et al., 2010). Hence, the thermal degradation of BNP follows this two-step weight loss process. The first loss, which was observed at 25-200°C, was generally due to the loss of free water absorbed in BNP. The weight loss in the second stage, which corresponds to the elimination of hydroxyl groups and decomposition of the carbon chains, occurred at 200-600°C. The TGA curves of MWCNT/BNP also exhibited mass loss in two steps in the same temperature ranges as for BNP on their own. In the range of 500 to 700°C there was also decomposition of graphitic structure. However, the mass loss decreased with increasing MWCNT in the range of 350 to 700°C due to the attachment of MWCNT on the surfaces of BNP, which increased the thermal stability of MWCNT/BNP. This might be an indication of attachment mechanism and production of a new hybrid material.

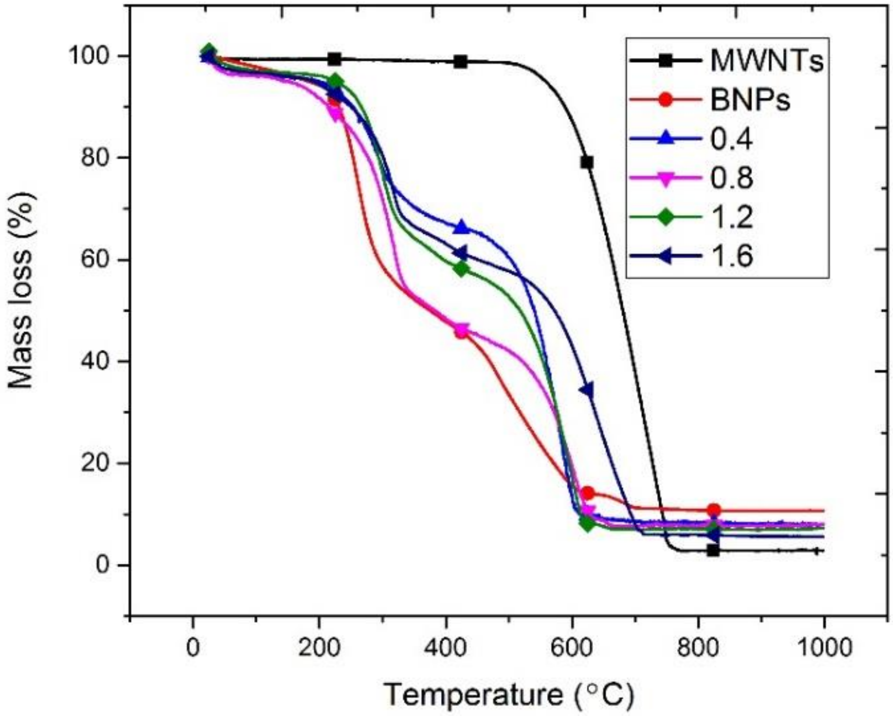

**Figure 5.19:** TGA curves of MWCNT only, BNP only, and MWCNT/BNP (0.4, 0.8, 1.2 and 1.6)

To obtain chemical element compositions of composites, more information about the composites and the component elements was necessary. For this process, an energy dispersive spectrometer (EDS) was employed. EDS measures the energies and intensities of the X-ray spectroscopy. In figure 5.20, the EDS of MWCNT only reveals the presence of C, Fe, Al and FeKesc. Their presence can be attributed as follows: C is related to MWCNT, Fe and FeKesc are impurities and Al belongs to the substrate material. In figure 5.21 the qualitative analysis of EDS shows that BNP only have C, O, Al, Au, and FeKesc and the most obvious finding to emerge from this EDS analysis is that, C and O are related to BNP. In addition, Al, Au and Fekesc are related to the substrate material and gold coating. Figures 5.22, 5.23, 5.24 and 5.25 illustrate EDS analysis for MWCNT/BNP (0.4, 0.8, 1.2 and 1.6) respectively. Although there was expected to be an increase of C intensity with increasing the concentration of MWCNT, no increase was noticed. This may have occurred due to the drying process of the samples, during which the majority of MWCNT/BNP move to the edge of the sample and the rest remain at the centre where the EDS analysis is conducted. Consequently, the EDS analysis in this case cannot reflect the dispersion of MWCNT. In addition, EDS analysis displayed the chemical components of MWCNT/BNP as C, O, Fe, Al, Au and FeKesc. C and O were related to BNP and MWCNT, and the others were related to the Aluminium substrate and gold coating.

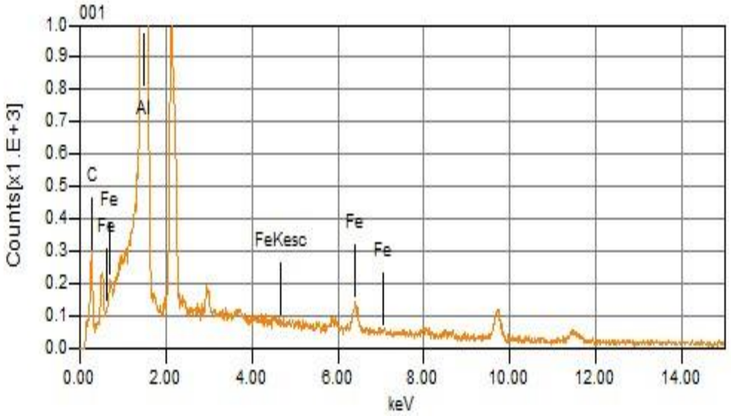

**Figure 5.20:** EDS analysis of MWCNT only

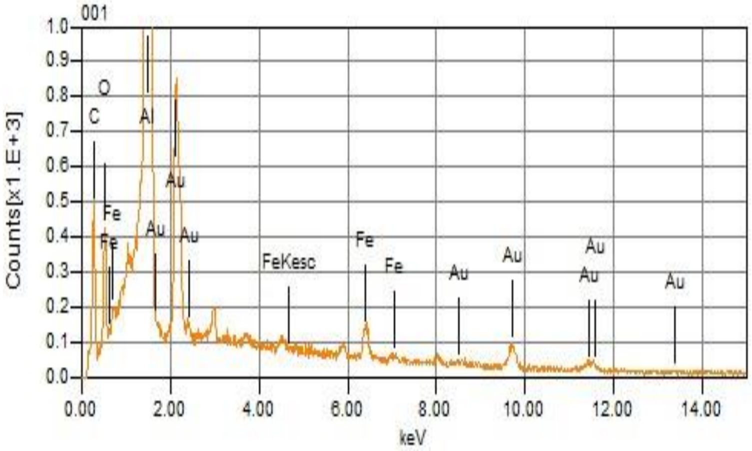

**Figure 5.21:** EDS analysis of BNP only

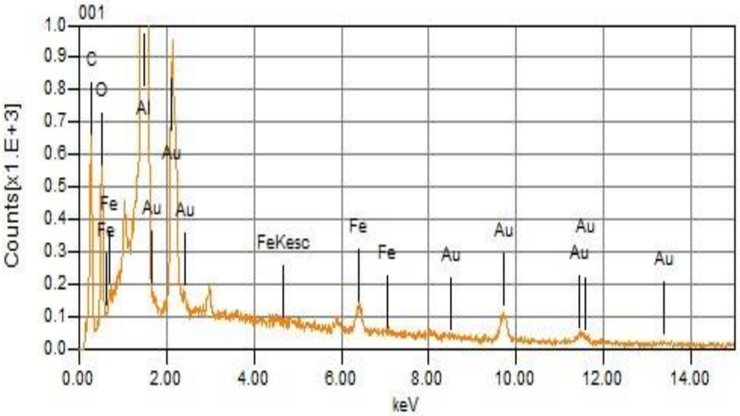

**Figure 5.22:** EDS analysis of 0.4 MWCNT/BNP

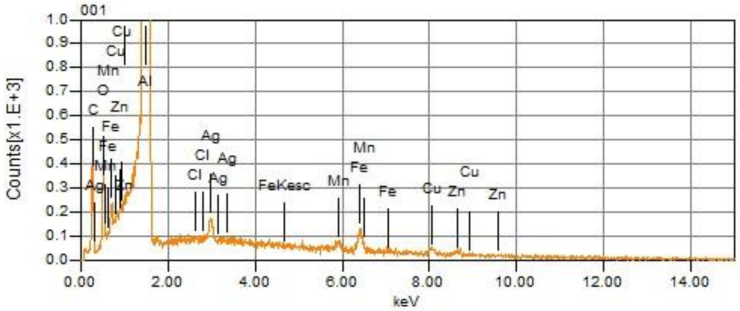

**Figure 5.23:** EDS analysis of 0.8 MWCNT/BNP

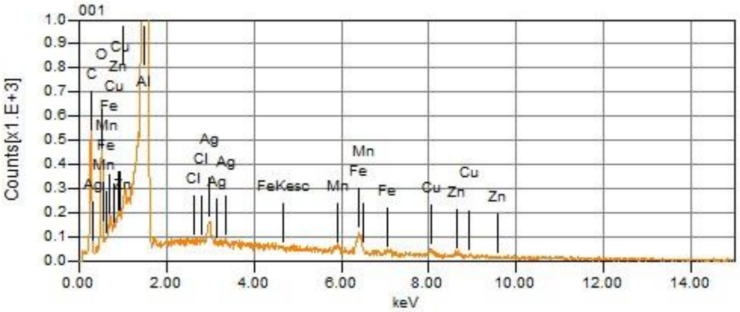

**Figure 5.24:** EDS analysis of 1.2 MWCNT/BNP

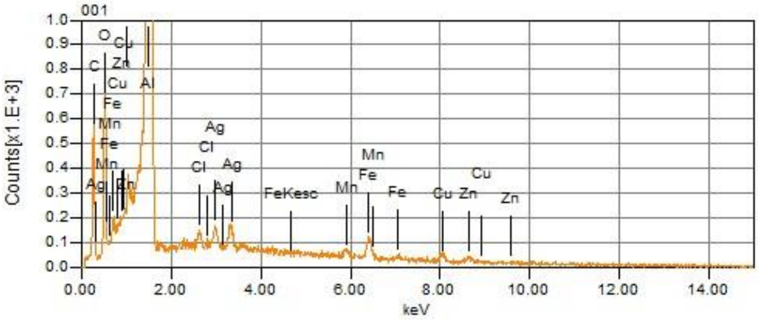

**Figure 5.25:** EDS analysis of 1.6 MWCNT/BNP

### 5.4.2 Colloidal properties of MWCNT/GO and MWCNT/MCC and their comparison to MWCNT/BNP

Figure 5.26 shows the actual solutions of BNP, MCC, GO and pristine MWCNT using the sonication process, which includes using a sonicator and an ice bath to keep the temperature of the solution from overheating during sonication. A stable homogeneous solution for MWCNT in aqueous solution was obtained by sonication of MWCNT in MCC aqueous solution and GO aqueous solution using SP.

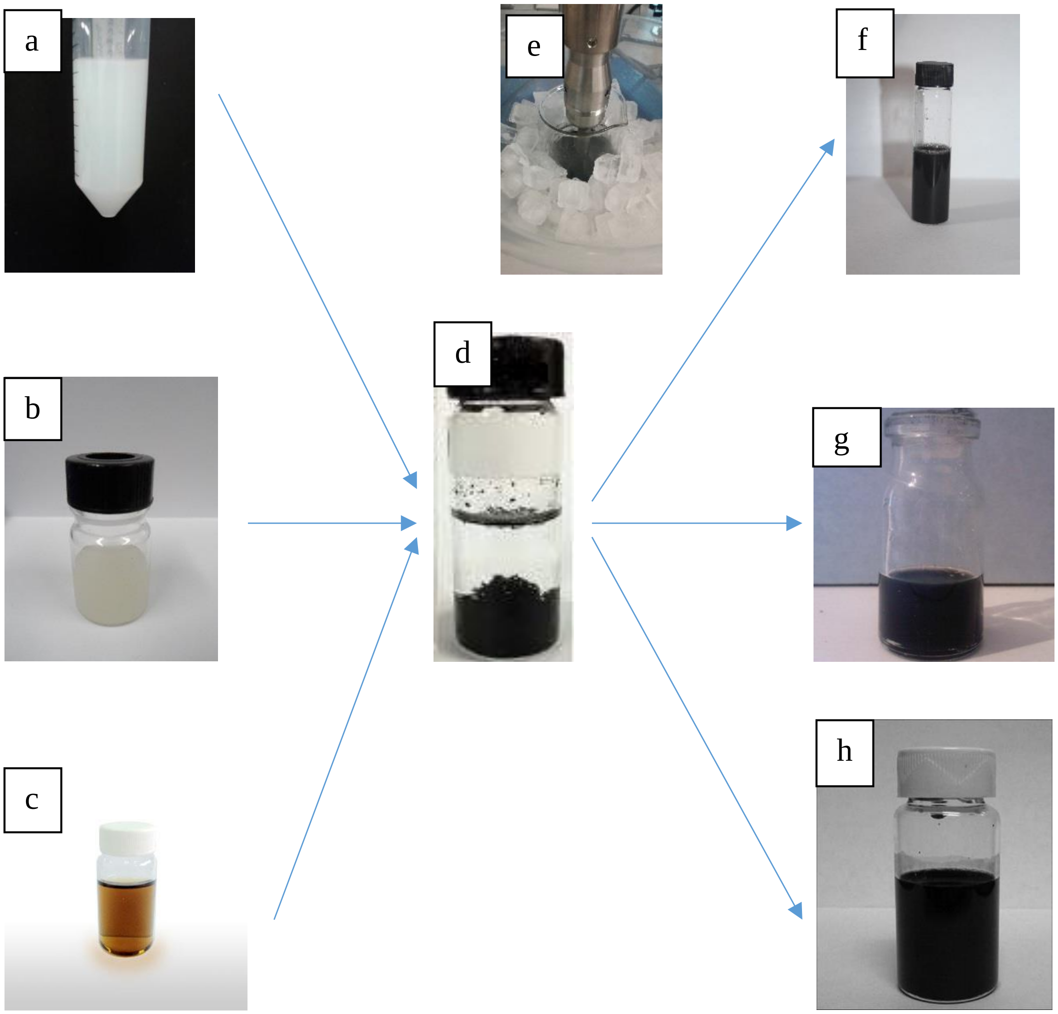

**Figure 5.26**: (a) MCC solution, (b) BNP solution, (c) GO solution, (d) pristine MWCNT solution, (e) sonicator and ice bath, (f) MWCNT/MCC solution, (g) MWCNT/BNP solution (h) MWCNT/GO solution.

However, solutions with a high concentration of MCC (of more than 20mg/ml) with any concentration of MWCNT was found to become thick and difficult to flow. Figure 5.27 shows the initial solutions of MWCNT (N1), which shows agglomerated clumps of MWCNT.

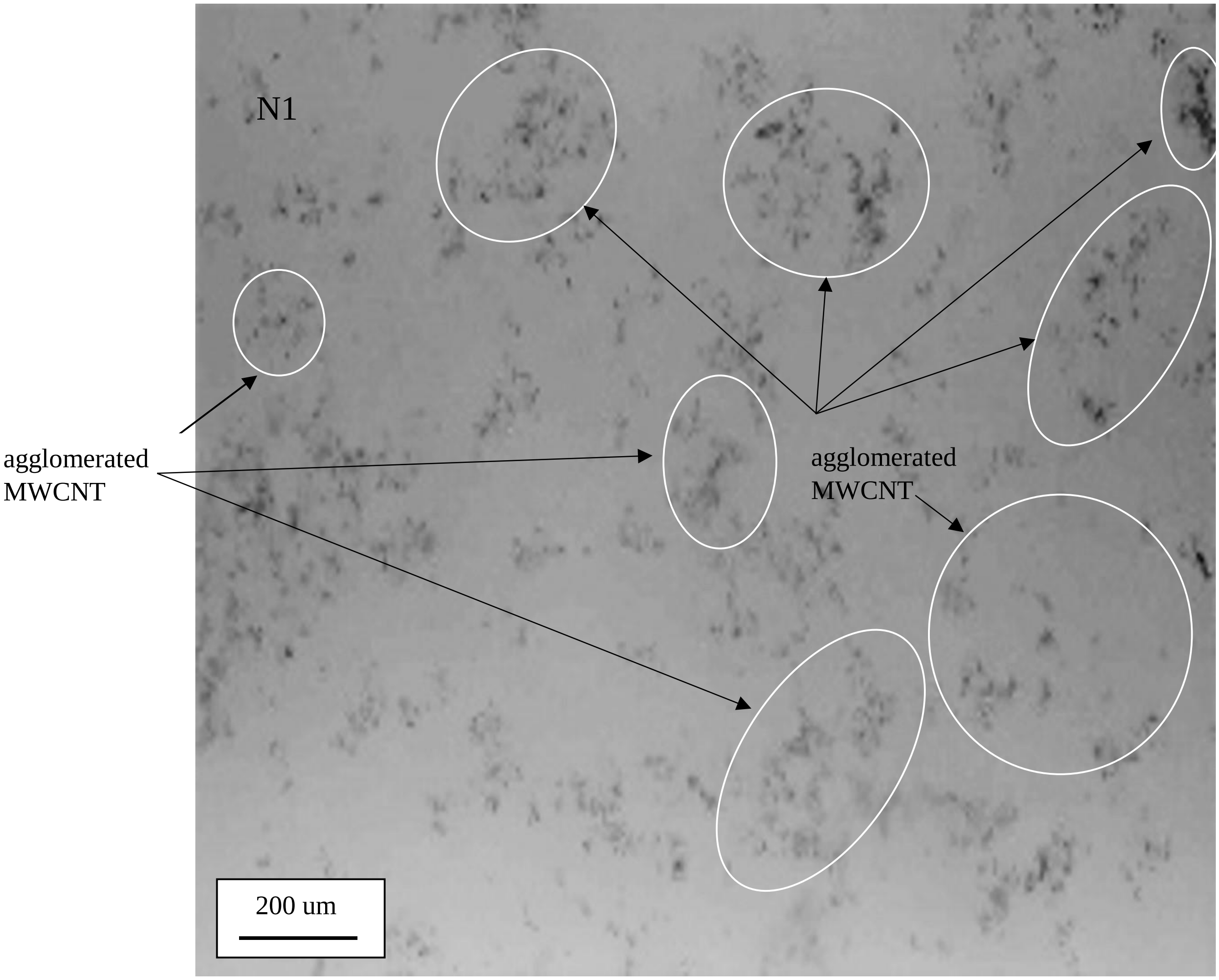

**Figure 5.27:** Optical image of MWCNT only

Figure 5.28 showed histogram of the number of MWCNT particles of MWCNT only. It seems that most of particles are large agglomeration of MWCNT.

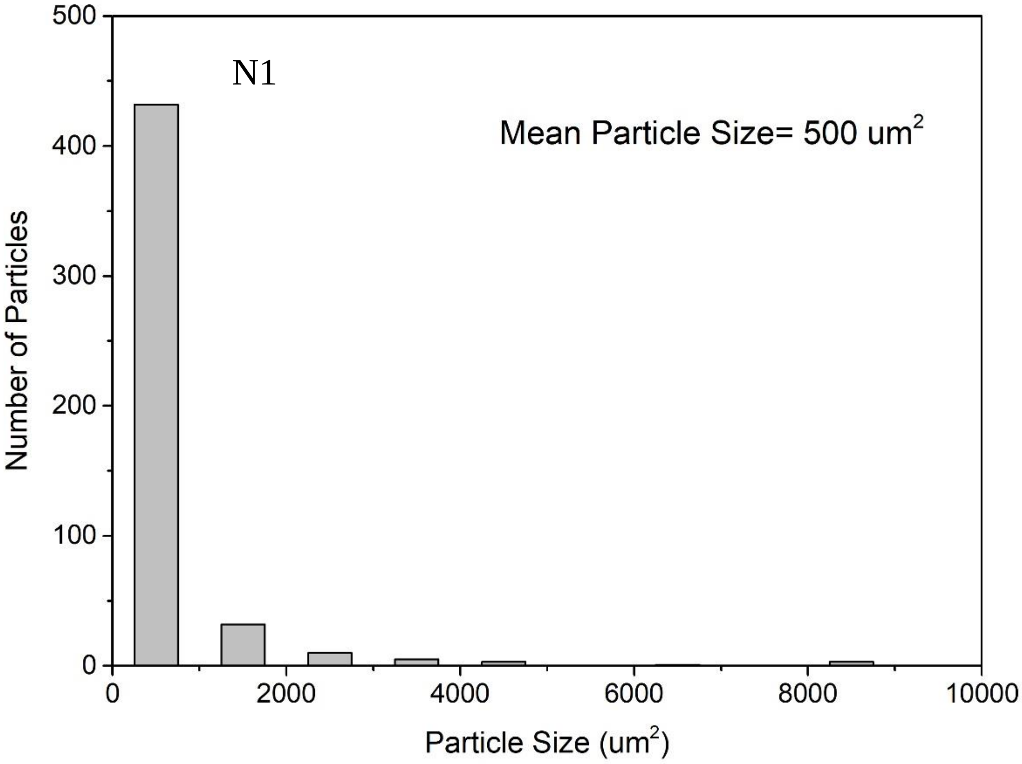

**Figure 5.28:** histogram of the number of MWCNT particles of MWCNT only.

Figures 5.29 and 5.30 show an optical image of MWCNT/MCC and clearly illustrates that dispersion of MWCNT is good without SP. However, with SP it is clear that better dispersion has been achieved.

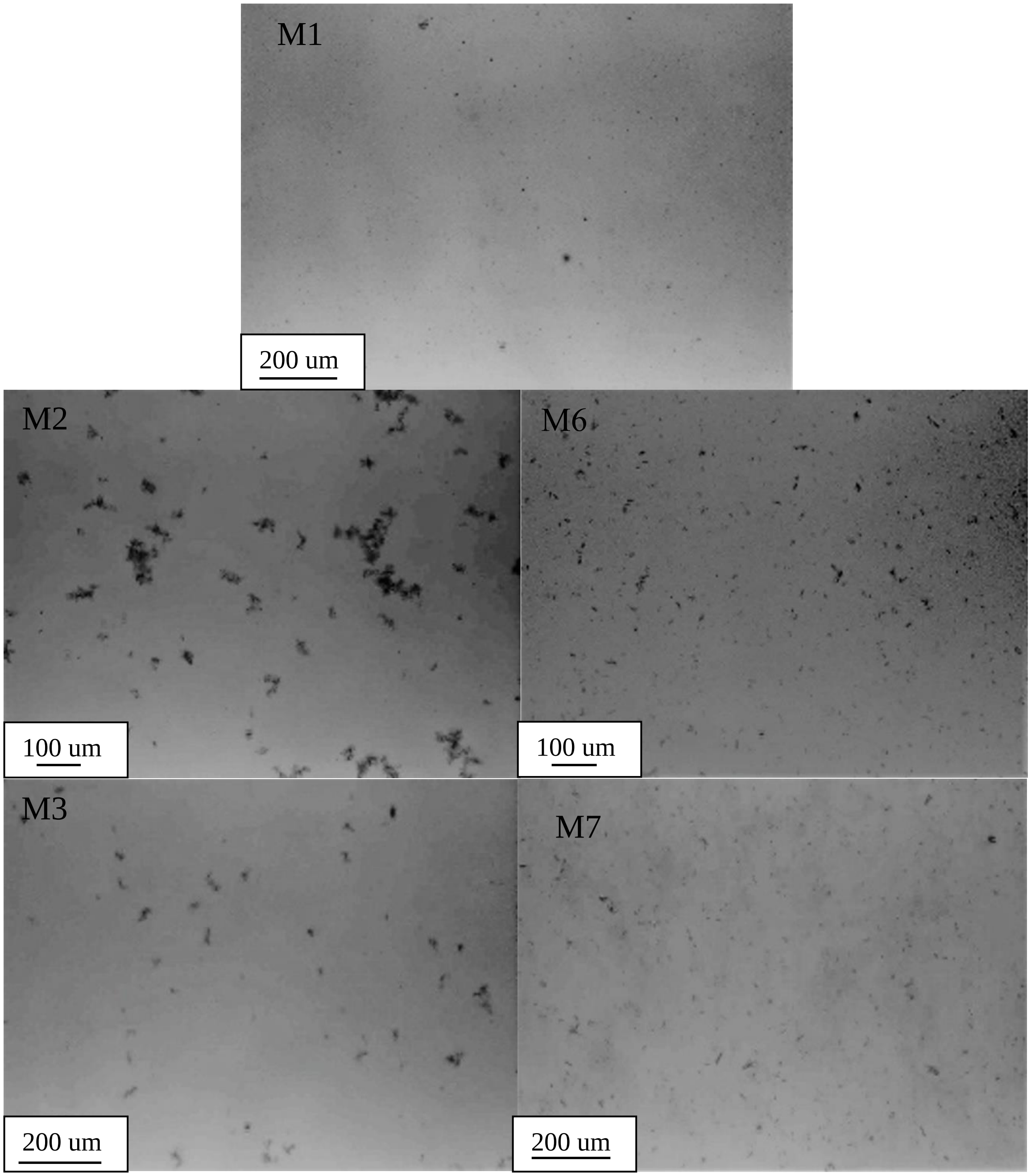

**Figure 5.29:** Optical image of M1, M2, M3 MWCNT/MCC (0.1 and 0.2) without SP respectively and M6 and M7 MWCNT/MCC (0.1 and 0.2) with SP respectively.

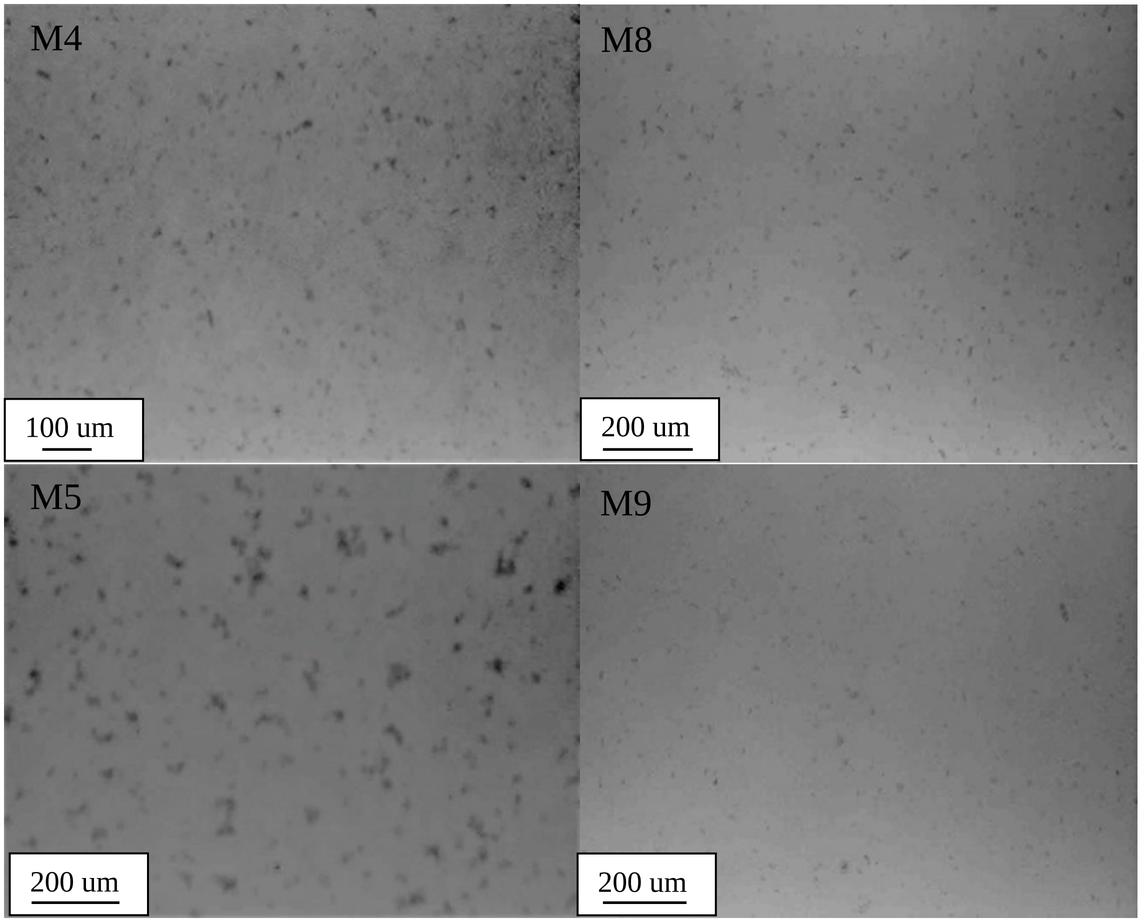

**Figure 5.30:** Optical image of M4 and M5 MWCNT/MCC (0.3 and 0.4) without SP respectively and M8 and M9 MWCNT/MCC (0.3 and 0.4) with SP respectively.

It was clearly observed that the size of agglomerated MWCNT have decreased and the numbers of smaller agglomerated MWCNT have increased. This may be attributed to the effect of SP due to the repulsion force created by OH groups of SP being higher than the van der forces of MWCNT. It was also observed that MCC had micro particles in their solutions (M1). Figure 5.31 and figure 5.32 showed histograms of the number of MWCNT/MCC particles of M1, M2, M3, M4, M5, M6, M7, M8 and M9. The histograms results show that, in general by using MCC, there are many smaller particles of MWCNT/BNP than the particles of MWCNT only (figure 5.28) except M2 which has similar particle size. Thus, there is evidence of better dispersion for MWCNT by using

MCC. In figures 5.33 and 5.34 with MWCNT/GO there appears to be significant differences in the dispersion of MWCNT, depending on the addition of SP. Without SP, there are large agglomerations of MWCNT present when the concentration of MWCNT goes up. Good dispersion of MWCNT using SP could be attributed to the repulsion force created by OH groups of superplasticizers, which is higher than van der forces of MWCNT. It was also observed that GO had micro particles in their solutions (G1), and this was attributed to agglomerated particles of graphene oxides.

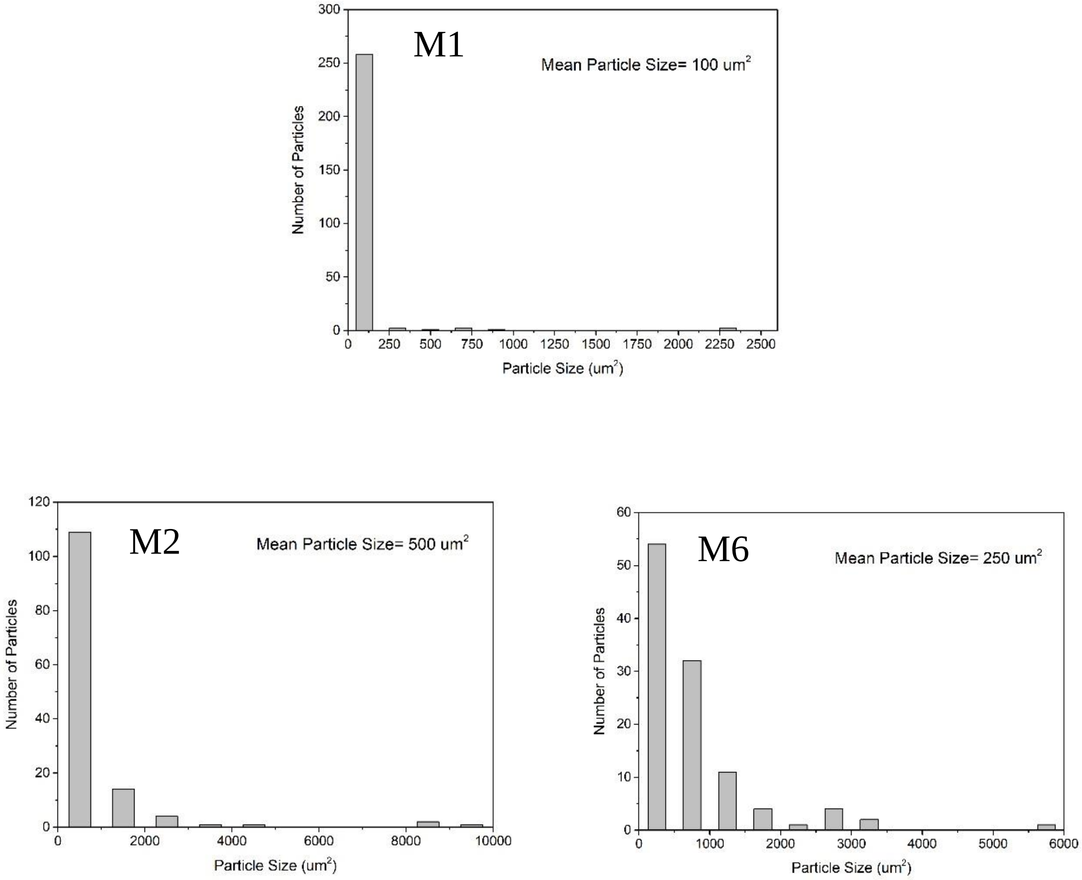

**Figure 5.31:** histograms of the number of MWCNT/MCC particles of M1, M2 and M6.

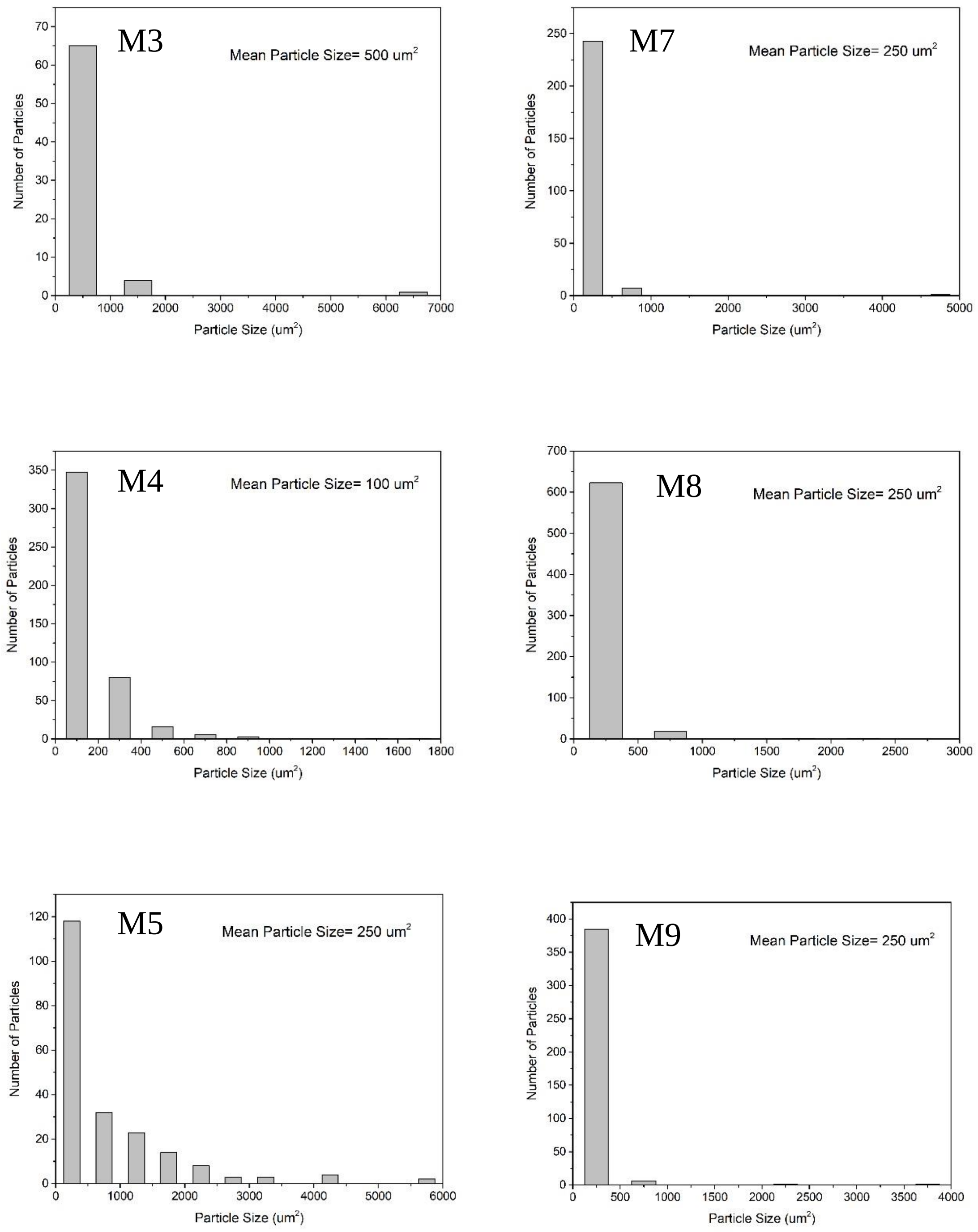

**Figure 5.32:** histograms of the number of MWCNT/MCC particles of M3, M4, M5, M7, M8 and M9.

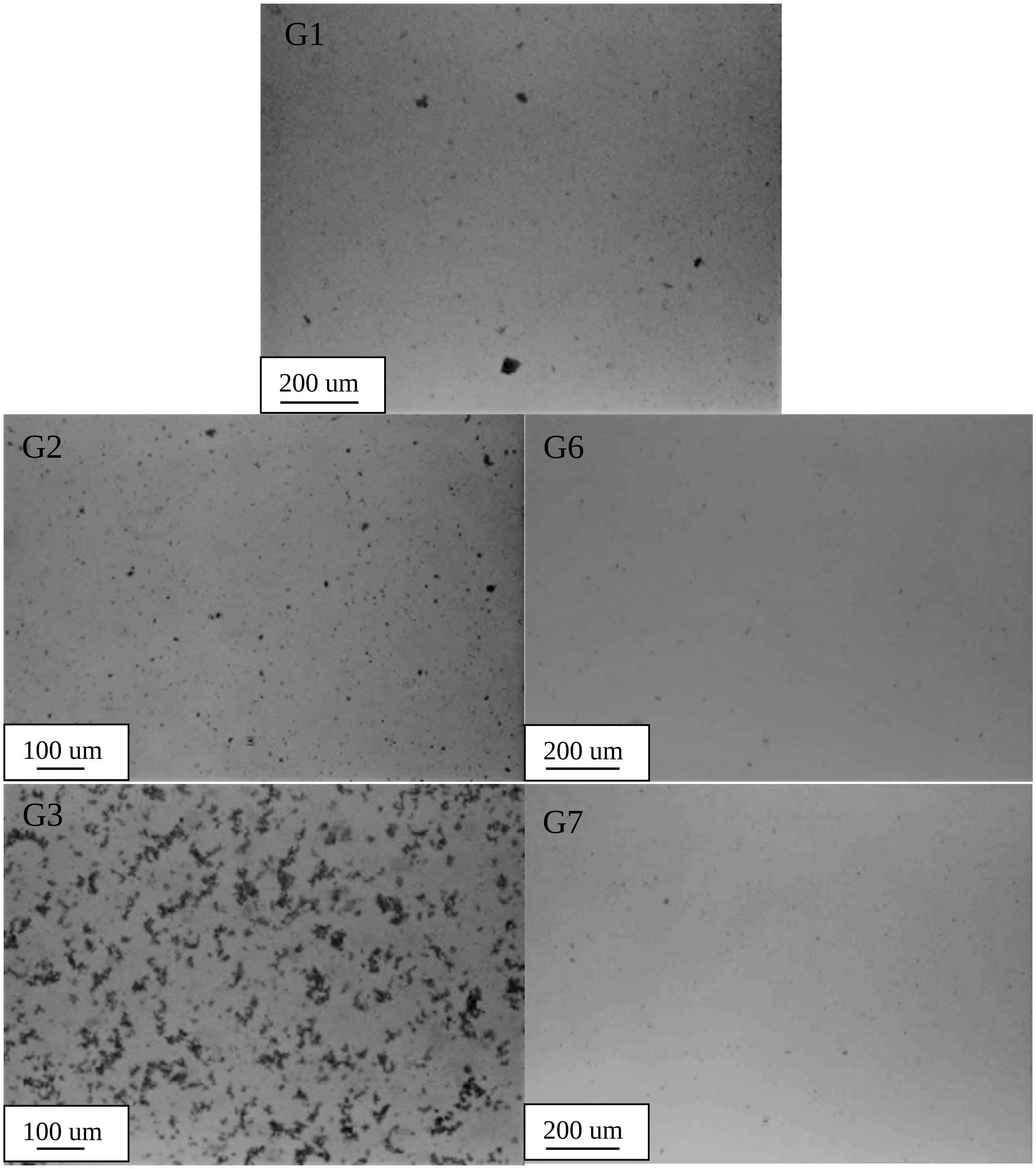

**Figure 5.33:** Optical image of G1; G2 and G3 MWCNT/GO (1 and 2) without SP respectively and G6 and G7 MWCNT/GO (1 and 2) with SP respectively.

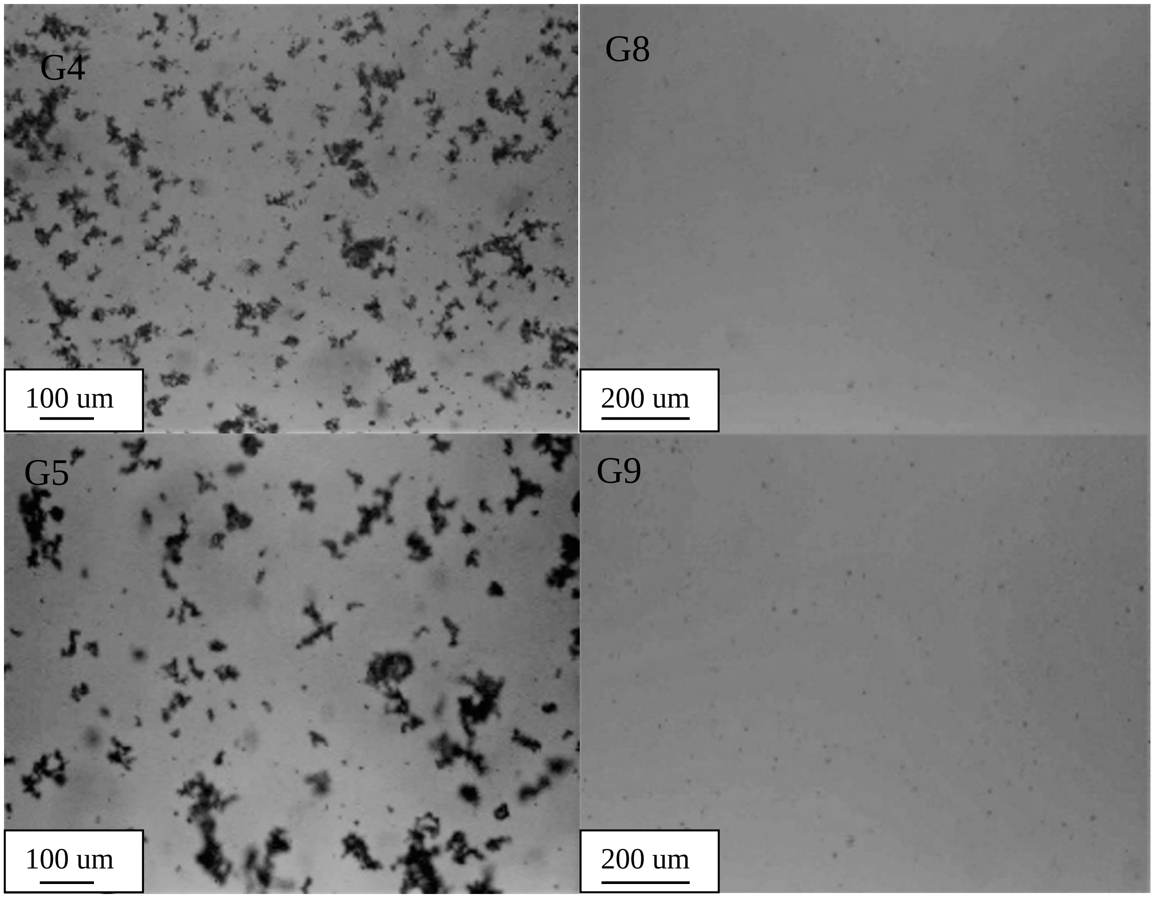

**Figure 5.34:** Optical image of G4 and G5 MWCNT/GO (3 and 4) without SP respectively and G8 and G9 MWCNT/GO (3 and 4) with SP respectively.

Figure 5.35 and figure 5.36 showed histograms of the number of MWCNT/GO particles of G1, G2, G3, G4, G5, G6, G7, G8 and G9. The histograms results show that, in general by using GO with SP, there are many smaller particles of MWCNT/GO than the particles of MWCNT only (figure 5.28). on the other hand, without SP, there are big agglomeration particles of MWNCT/GO and their size increases with increasing the concentration of MWCNT. Thus, this is evidence of poor dispersion of MWCNT/GO without SP.

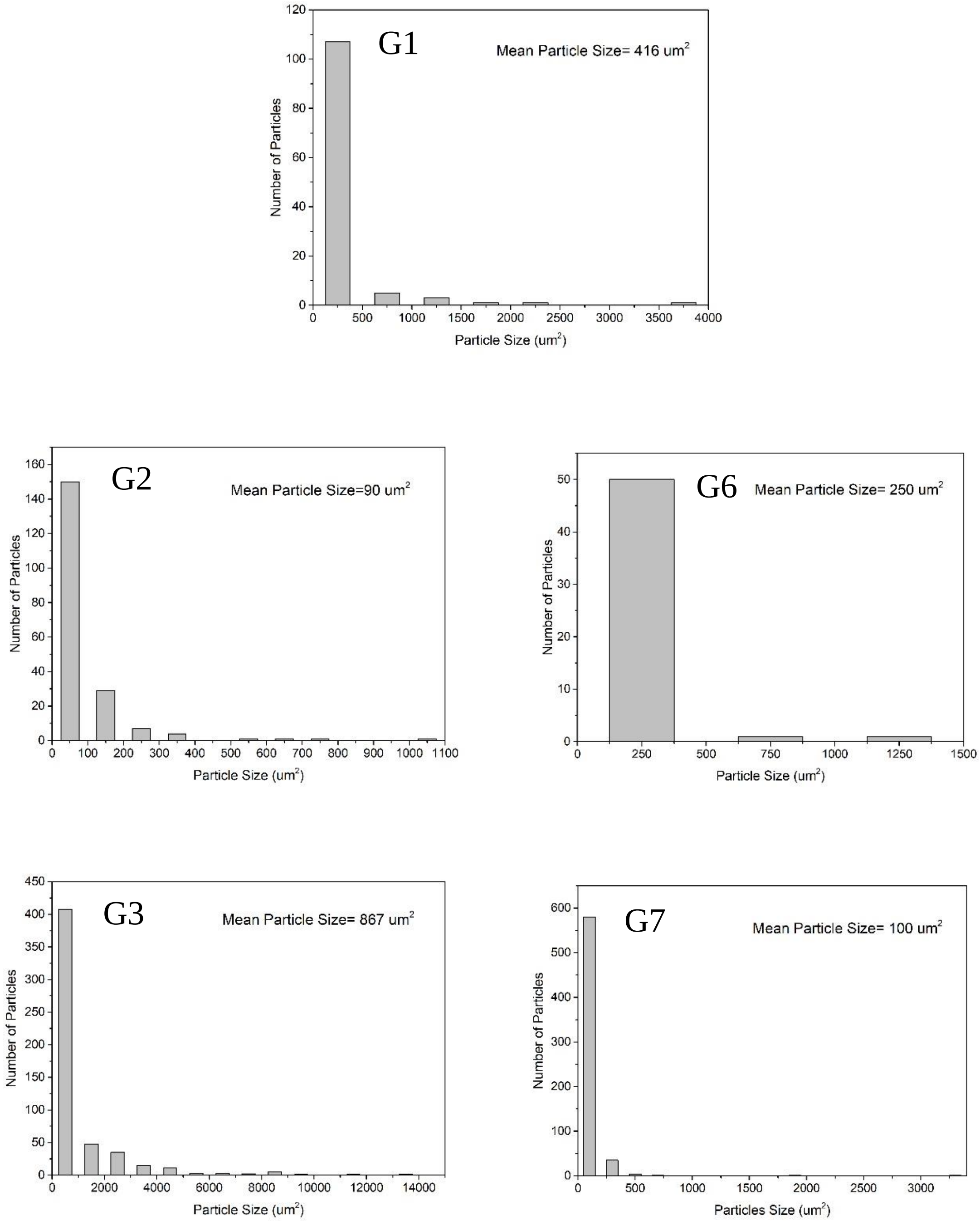

**Figure 5.35:** histograms of the number of MWCNT/GO particles of G1, G2, G3, G6 and G7.

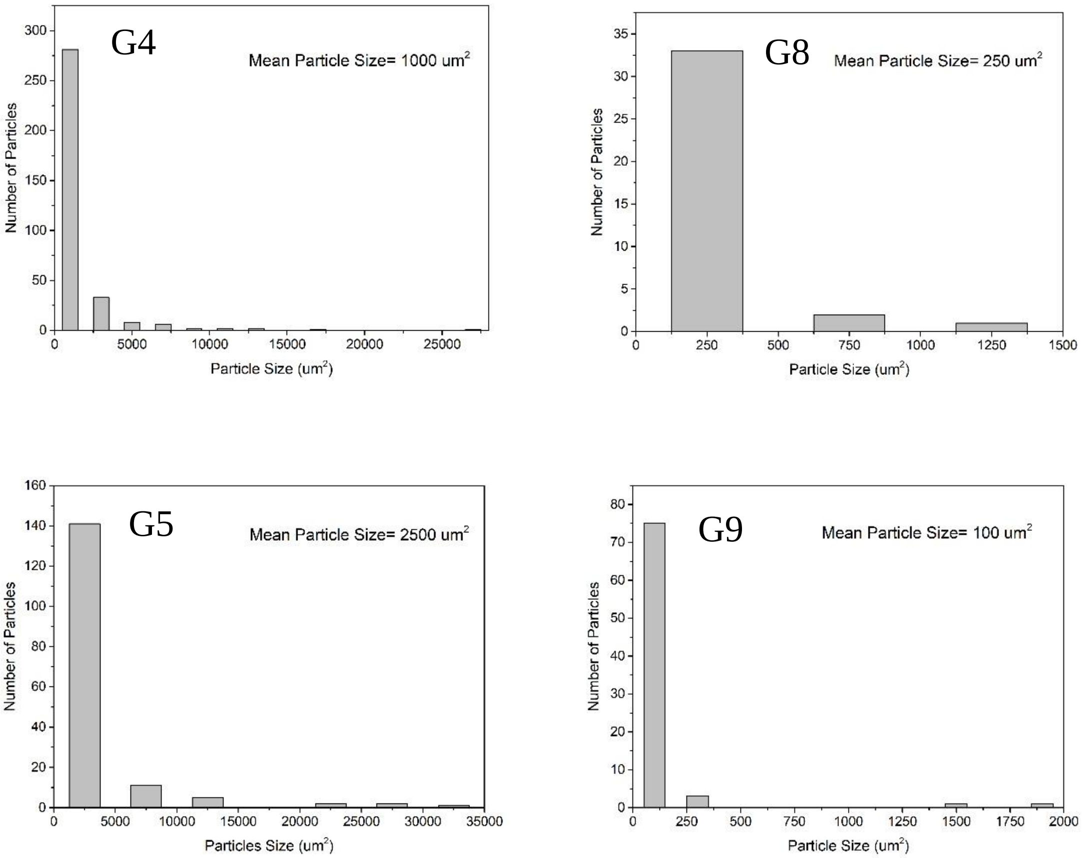

**Figure 5.36:** histograms of the number of MWCNT/GO particles of G4, G5, G8 and G9.

### 5.4.3 Ultraviolet Visible Spectroscopy (UV-Vis) of MWCNT/MCC, MWCNT/GO.

Ultraviolet visible spectroscopy is a common method for measuring dispersion in a transparent medium. This technique is based on the observation that the more dispersed MWCNT are in a liquid, the darker the liquid will be, and the more light will be absorbed. Figure 5.37 demonstrates the absorbance of MWCNT with and without SP. It shows a higher absorbance when compared with the absorbance of BNP, MCC and GO due to the activity of MWCNT. It is also worth mentioning that the absorbance of MWCNT was taken after sonication.

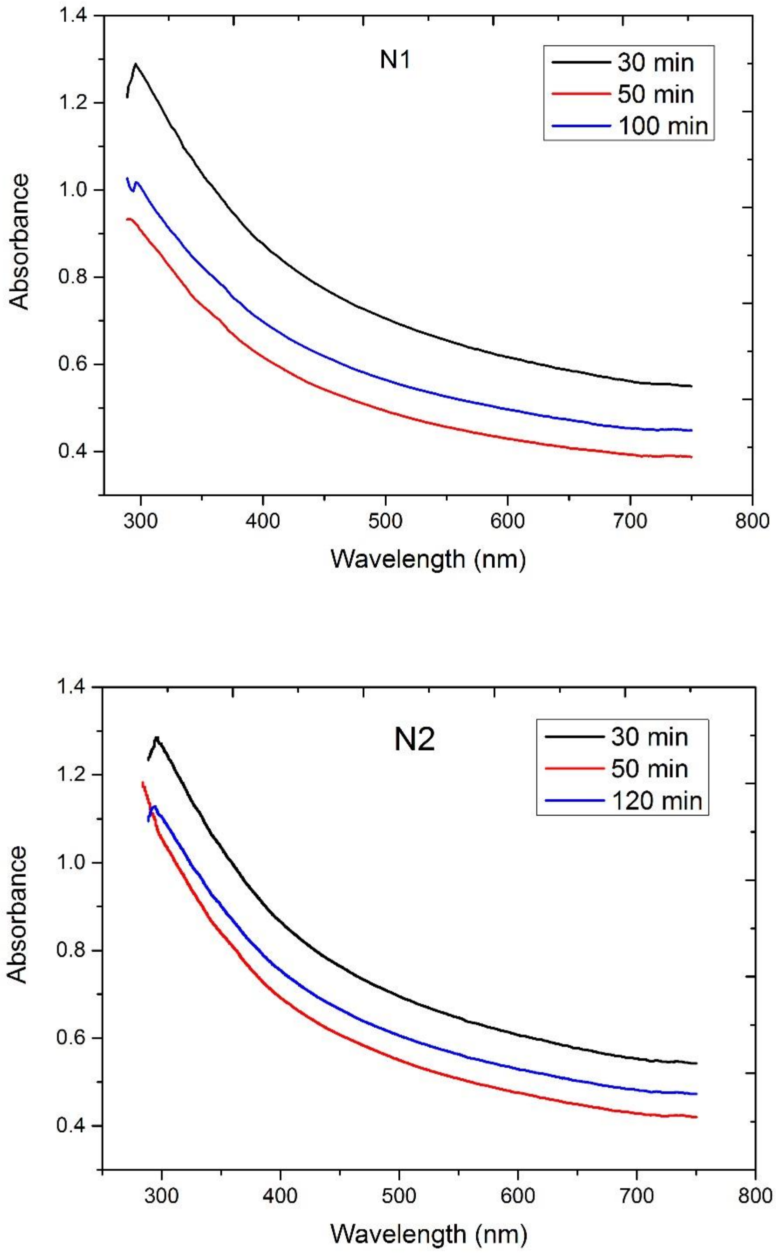

**Figure 5.37:** UV-Vis spectroscopy of MWCNT (N2) with SP and MWCNT (N1) without SP

Figures 5.38, 5.39, 5.40, 5.41 and 5.42 illustrate the absorbance of MWCNT/MCC (0.1, 0.2, 0.3 and 0.4) with and without SP and the absorbance of MCC with and without SP. It seems that the absorbance is low for MCC due to their high transparency (Sabo et al, 2016).

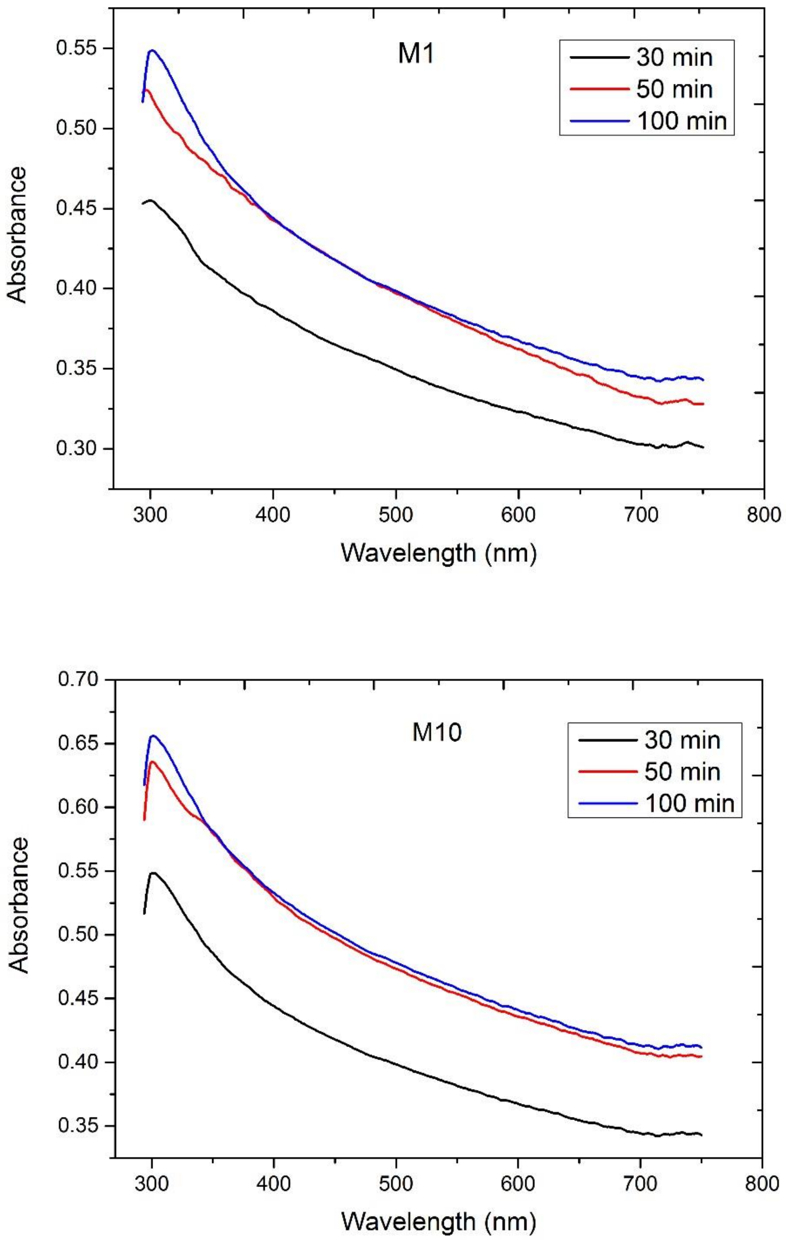

**Figure 5.38:** UV-Vis spectroscopy of M1 without SP and M10 with SP.

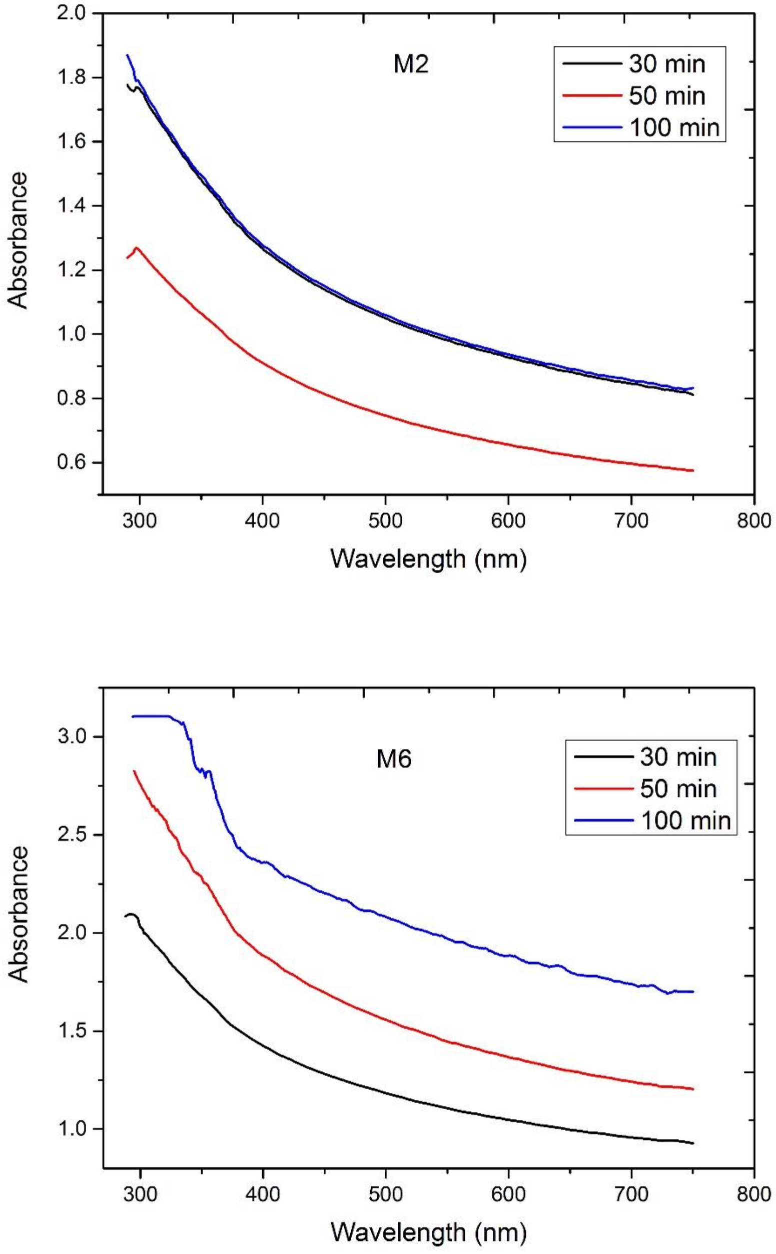

**Figure 5.39:** UV-Vis spectroscopy of M2 MWCNT/MCC (0.1) without SP and M6 MWCNT/MCC (0.1) with SP.

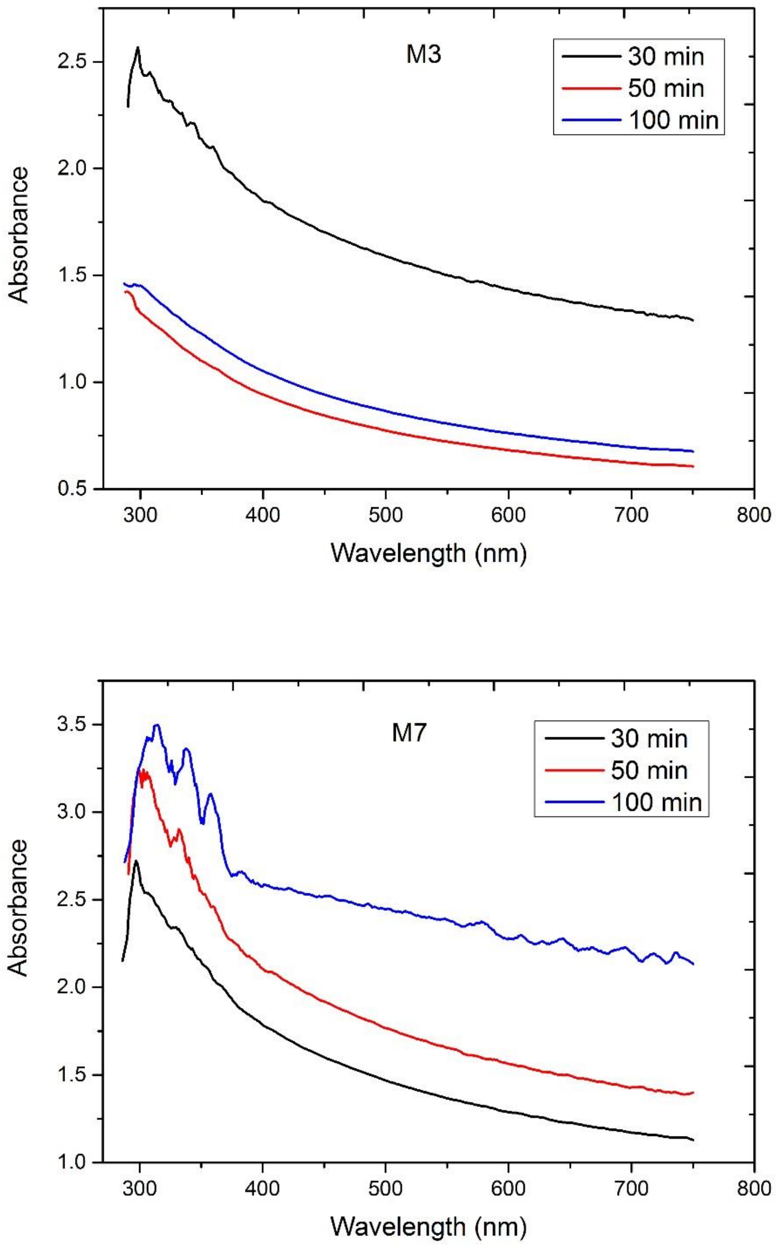

**Figure 5.40:** UV-Vis spectroscopy of M3 MWCNT/MCC (0.2) without SP and M7 MWCNT/MCC (0.2) with SP.

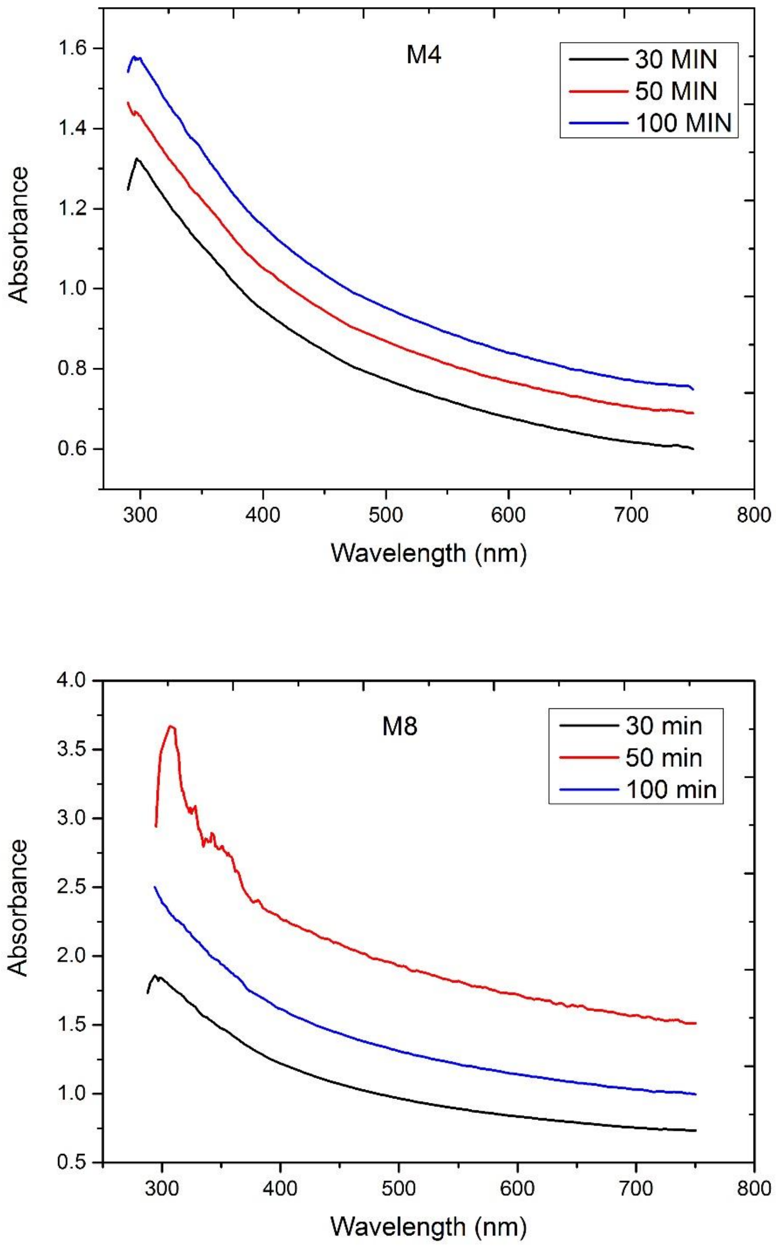

**Figure 5.41:** UV-Vis spectroscopy of M4 MWCNT/MCC (0.3) without SP and M8 MWCNT/MCC (0.3) with SP.

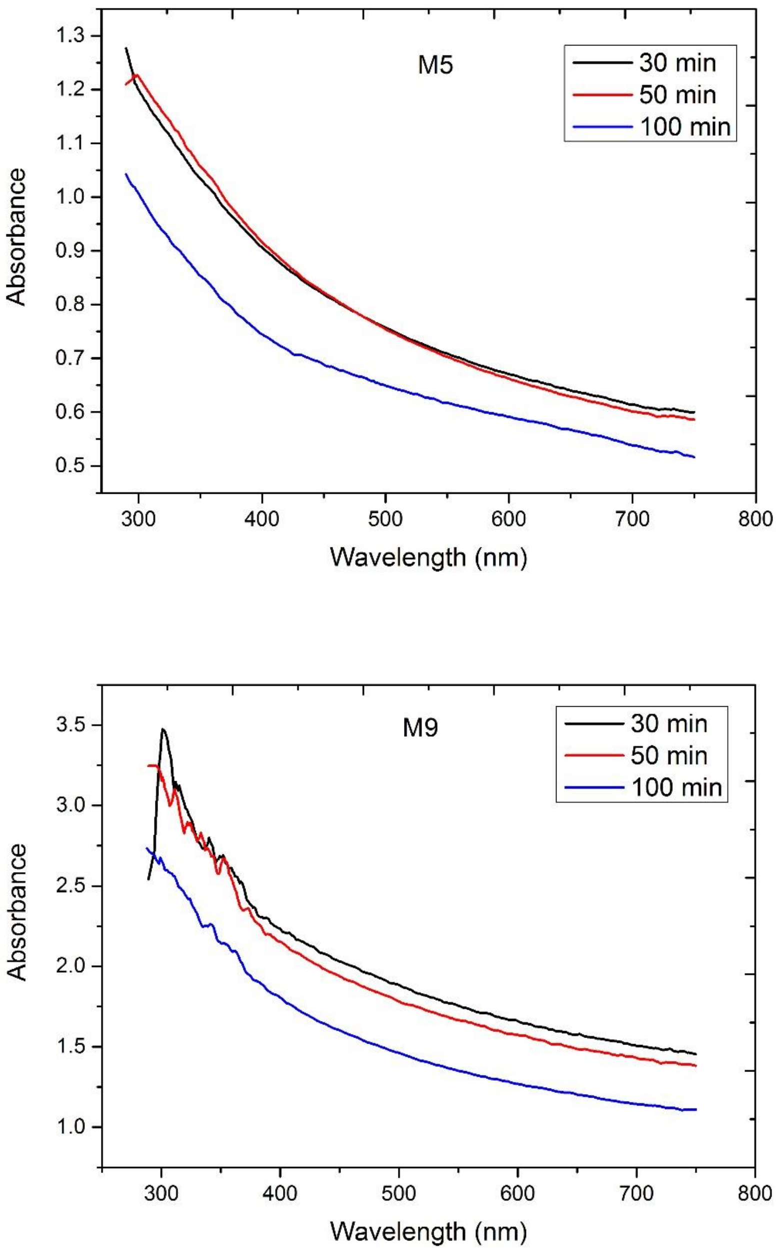

**Figure 5.42:** UV-Vis spectroscopy of M5 MWCNT/MCC (0.4) without SP and M9 MWCNT/MCC (0.4) with SP respectively.

Furthermore, the pattern observed here was that the absorbance of MWCNT/MCC without SP decreased slightly with increasing concentrations of MWCNT.The absorbance of MCC/MWCNT with SP is higher when compared with the absorbance of MWCNT/MCC without SP. The evidence suggests that using SP improves dispersion of MWCNT/MCC. This could be attributed to the repulsion force created by OH groups of superplasticizers, which is higher than the van-der forces of MWCNT, thereby preventing agglomeration.

The absorbance of MWCNT/GO (1, 2, 3, and 4) with and without SP and the absorbance of GO with and without SP are shown in figures 5.43, 5.44, 5.45, 5.46 and 5.47 which indicated that the presence of SP resulted high absorbance at all four concentrations. As previously mentioned, the repulsion force in the SP OH groups may be contributing to MWCNT dispersion. The absorbance of MWCNT/GO without SP was low except for at 1 MWCNT/GO and increasing the concentrations of MWCNT resulted in a decrease in absorbance. This indicated that the dispersion of MWCNT/GO without SP generally decreased with increasing amounts of MWCNT; the GO was insufficient to disperse MWCNT without SP which may be due to the repulsion force of GO being lower than the van-der forces of MWCNT, leading to agglomeration of MWCNT.

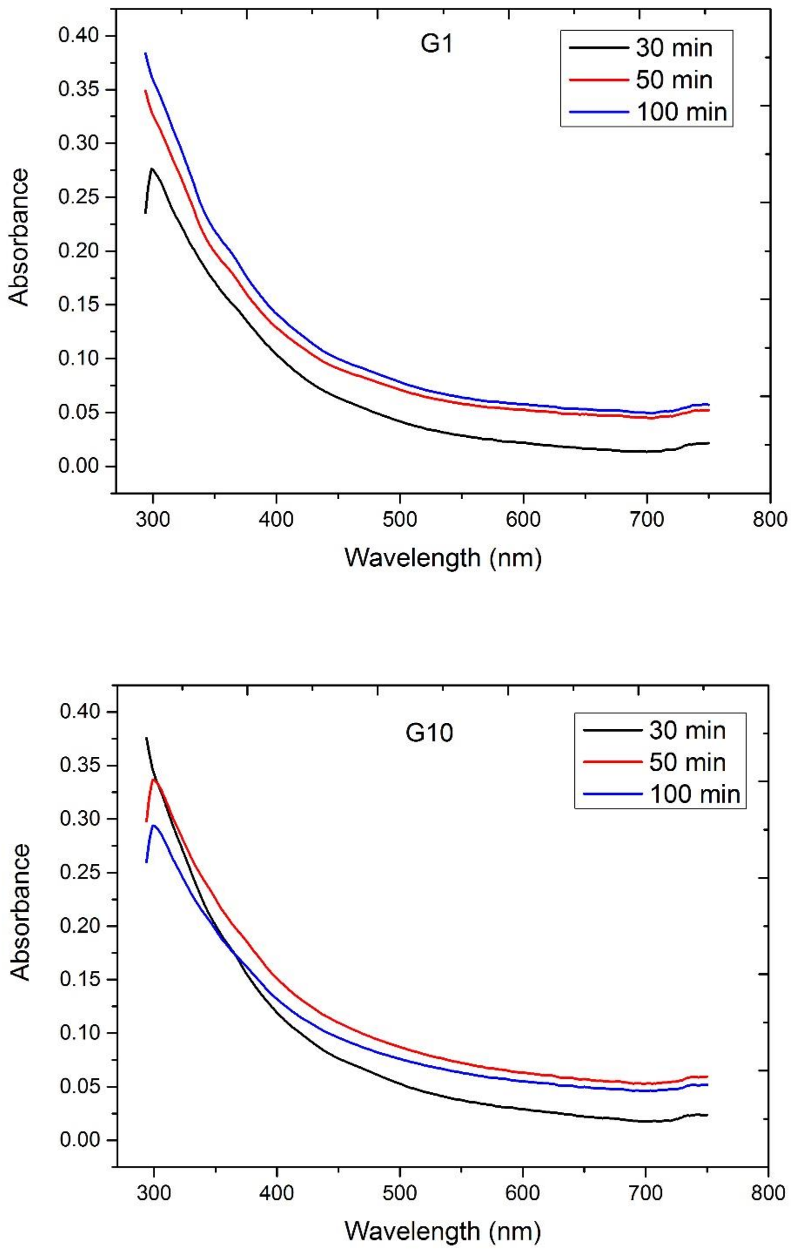

**Figure 5.43:** UV-Vis spectroscopy of G1without SP and G10 with SP.

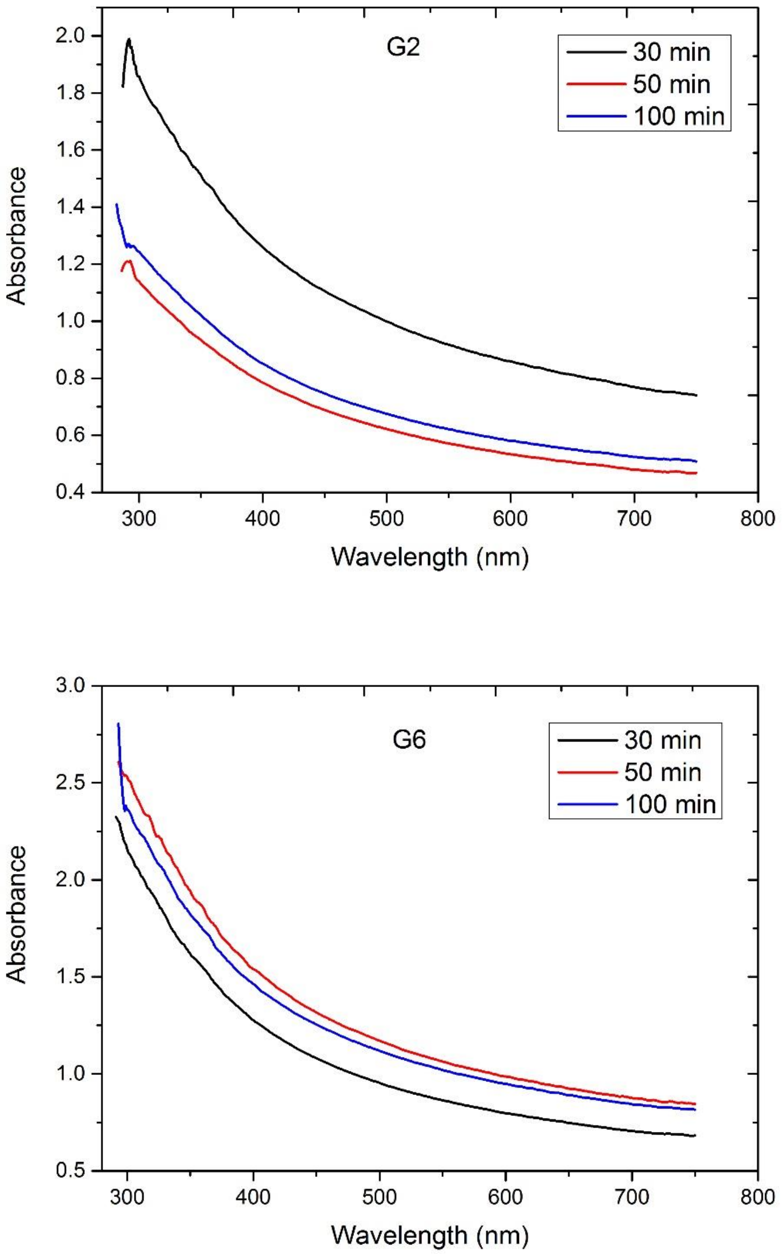

**Figure 5.44:** UV-Vis spectroscopy of G2 MWCNT/GO (1) without SP and G6 MWCNT/GO (1) with SP.

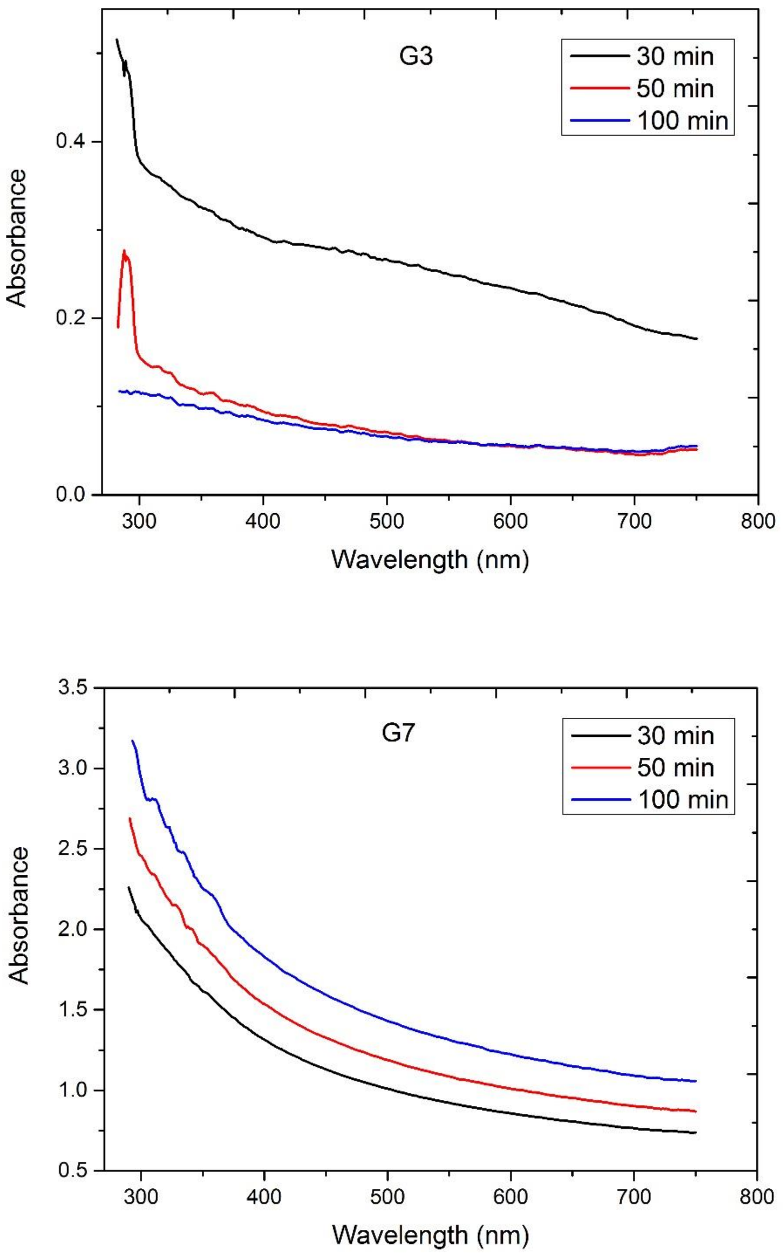

**Figure 5.45:** UV-Vis spectroscopy of G3 MWCNT/GO (2) without SP and G7 MWCNT/GO (2) with SP.

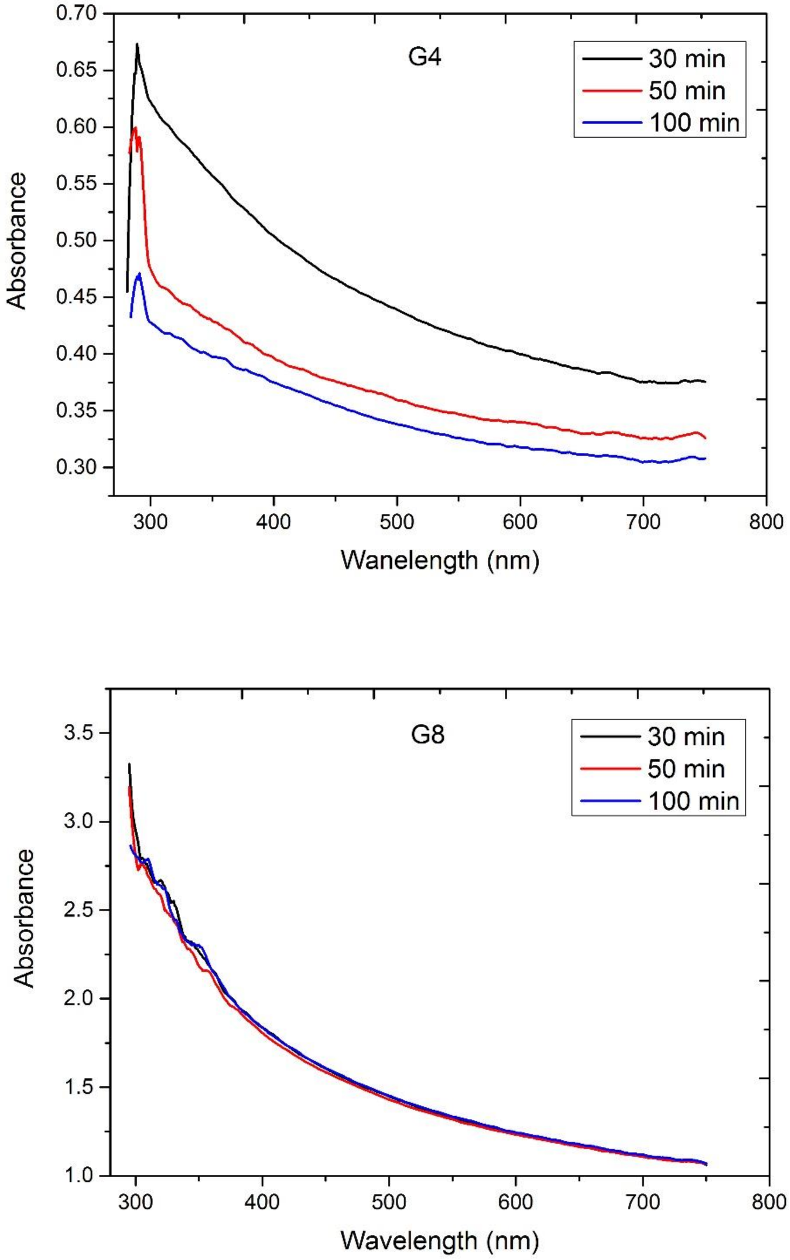

**Figure 5.46:** UV-Vis spectroscopy of G4 MWCNT/GO (3) without SP and G8 MWCNT/GO (3) with SP.

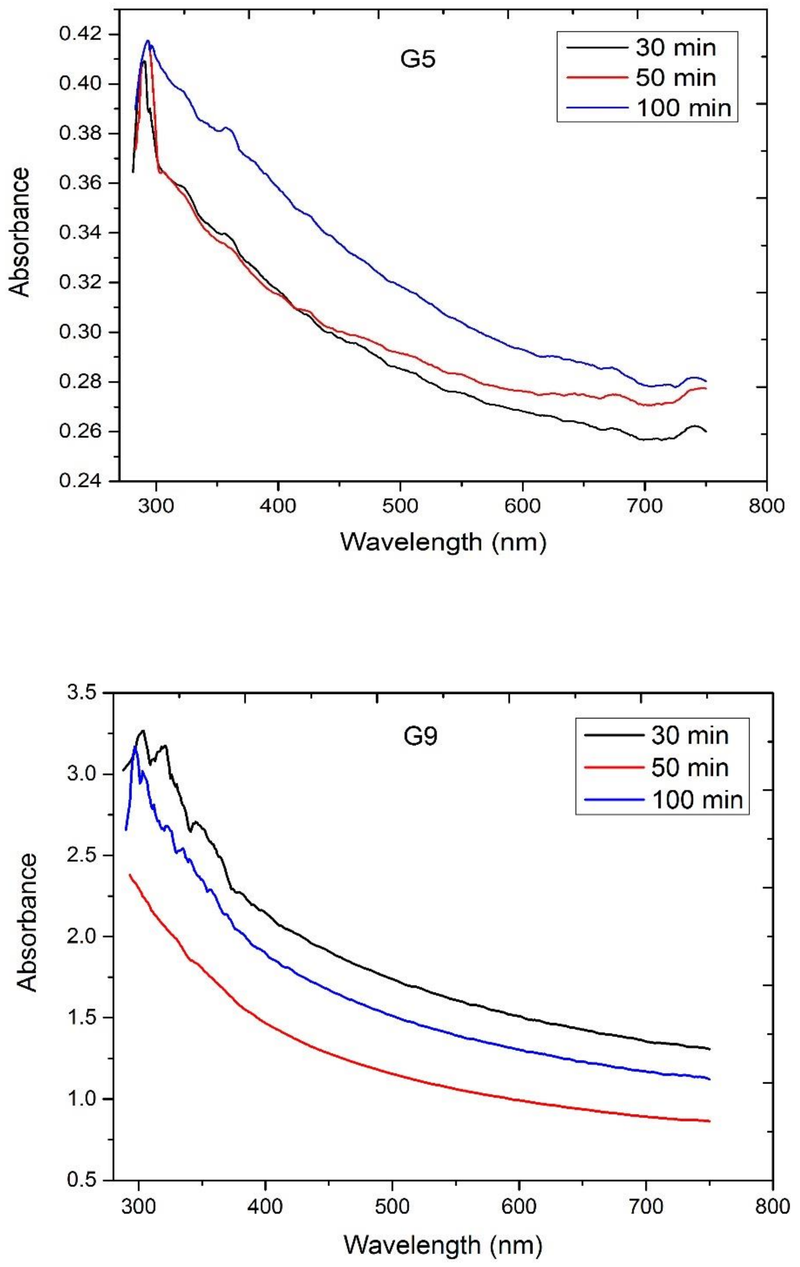

**Figure 5.47:** UV-Vis spectroscopy of G5 MWCNT/GO (4) without SP and G9 MWCNT/GO (4) with SP.

SEM was used to investigate the dispersion state of MWCNT with different concentrations of MWCNT, with several dispersant agents and to investigate the microstructure of GO, MCC and MWCNT. The agglomeration of MWCNT only due to van der forces (which causes adherence of MWCNT) is shown in figure 5.48.

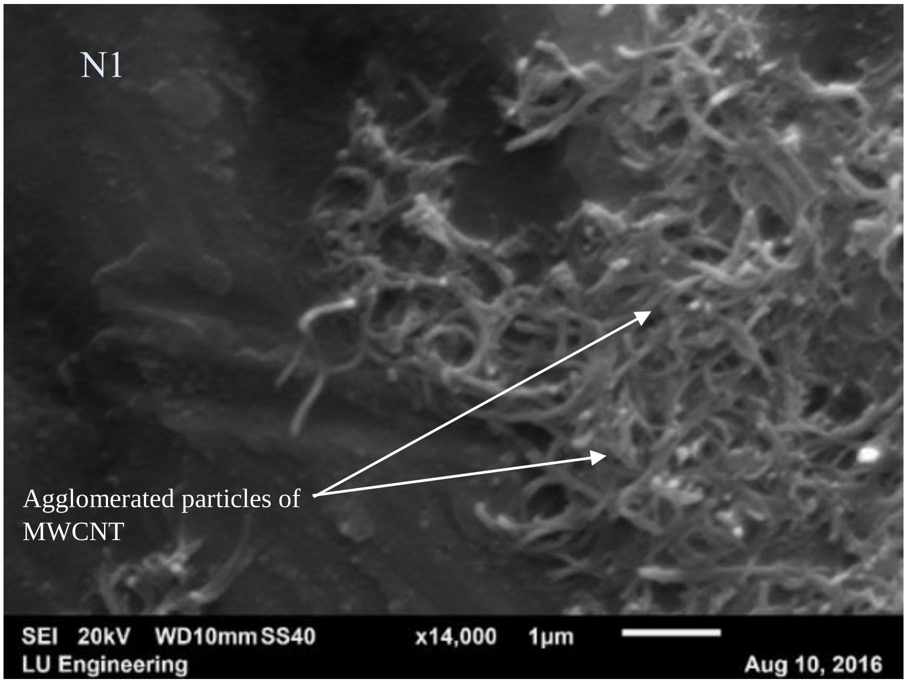

**Figure 5.48:** SEM image of MWCNT only

From figure 5.49 we can see uniformly distributed individual fibres of MCC along with some large clumps of MCC. Looking at figure 5.50, it is apparent that 2D uniformly distributed surfaces of GO.

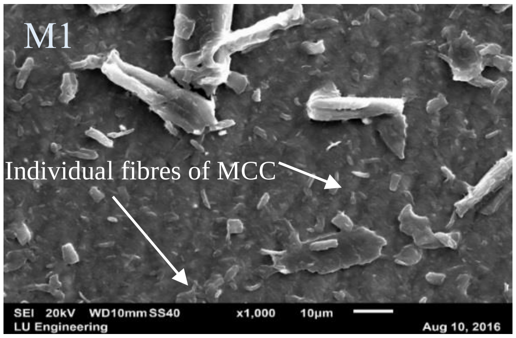

**Figure 5.49:** SEM image of MCC only

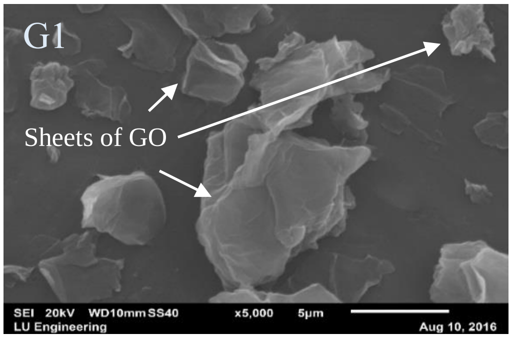

**Figure 5.50:** SEM image of GO only

Typical SEM images of MWCNT/MCC (0.1, 0.2, 0.3 and 0.4) (M6, M7, M8 and M9) with SP respectively are shown in figures 5.51, 5.52, 5.54 and 5.54. These show that there are individual tubes present. What stands out in these figures is the high dispersion state of MWCNT except in Figure 5.54 of M9 which shows some agglomeration of MWCNT. This may be due to a high amount of MWCNT or the lack of sufficient ability of MCC to disperse.

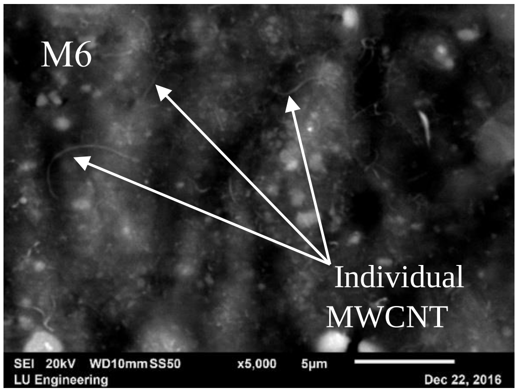

**Figure 5.51:** SEM image of MWCNT/MCC

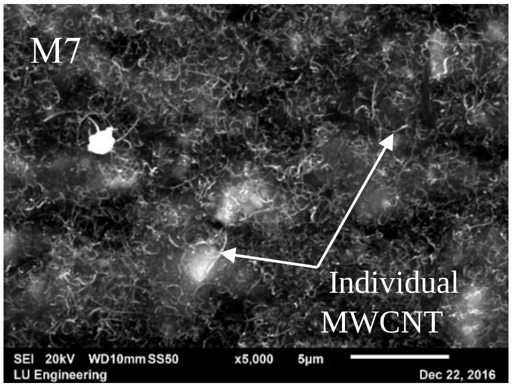

**Figure 5.52:** SEM image of MWCNT/MCC

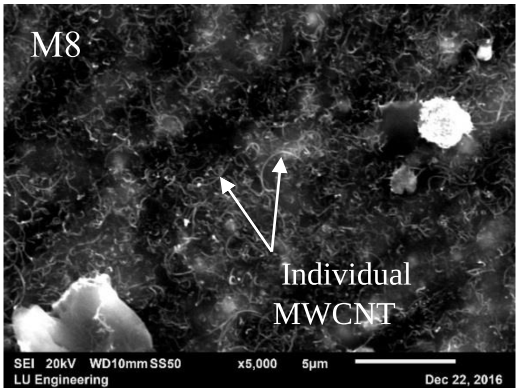

**Figure 5.53:** SEM image of MWCNT/MCC

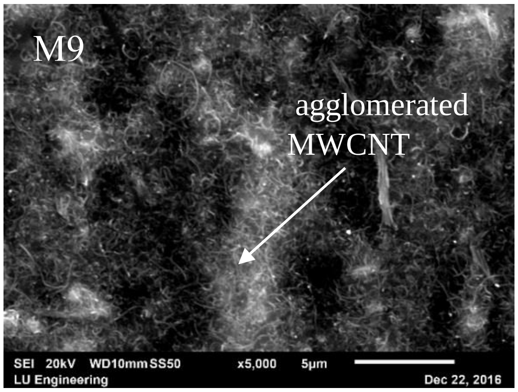

**Figure 5.54:** SEM image of MWCNT/MCC

Typical SEM images of MWCNT/GO (1, 2, 3 and 4) (G6, G7, G8 and G9) with SP respectively are shown in figures 5.55, 5.56, 5.57 and 5.58. Interestingly, using SP resulted in uniform distribution of MWCNT and single tubes can be seen easily. As previously mentioned, the repulsion force in the SP OH groups may be contributing to MWCNT dispersion.

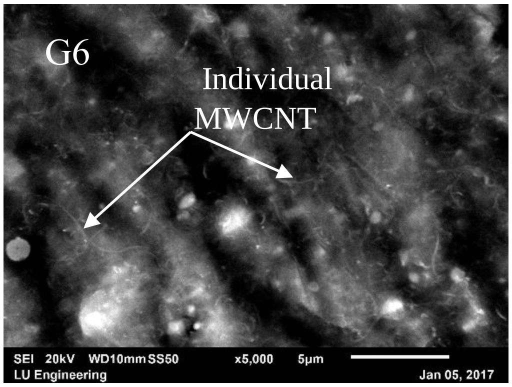

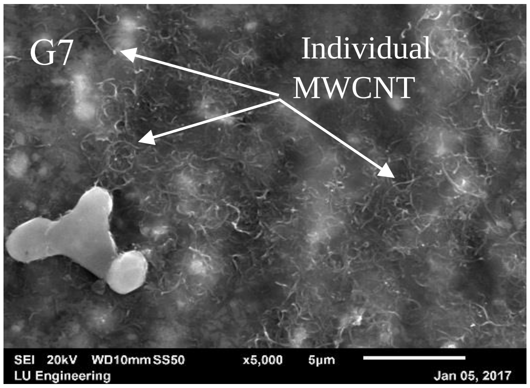

**Figure 5.55:** SEM image of MWCNT/GO

**Figure 5.56:** SEM image of MWCNT/GO

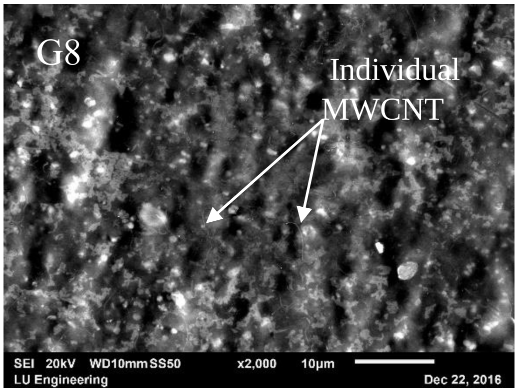

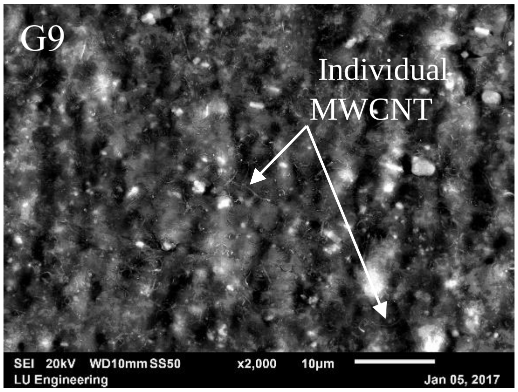

**Figure 5.57:** SEM image of MWCNT/GO

**Figure 5.58:** SEM image of MWCNT/GO

The thermal stability of a material and the characterisation of its purity are evaluated by TGA (thermogravimetric analysis). The initiation temperature, oxidation temperature and residual mass are the important parameters measured in the loss of weight. The temperature at which material starts to decompose can be named as the initiation temperature. The temperature of maximum weight loss is named as the oxidation temperature and it is often described as the thermal stability of the material. (Lehman et al., 2011; Ling et al., 2013). Figure 5.59 represents the results of thermogravimetric analysis (TGA) for pristine MWCNT, MCC and MWCNT/MCC. The TGA curve of pristine MWCNT shows no significant mass loss up to 500 °C due to the high temperature required for the decompostion of main graphitic structures (Amiri et al., 2013). It should be noted that this is attributed to the high oxidizing temperature of a well graphitic structure which starts to oxidize at between 600 and 700°C (Datsyuk et al., 2008). The TGA curve of pristine MCC showed three mass loss steps: an initial mass loss up to 200°C, which is attributed to the gradual evaporation of moisture; the second mass loss from approximately 200-350°C, which is due to the decomposition of cellulose which decomposes thermochemically in the range between 275 to 350°C.; and the third mass loss is attributed to lignin which decomposes thermochemically in the range of 250 to 500°C (Yang et al., 2011; Yang et al., 2005; Sun et al., 2002).

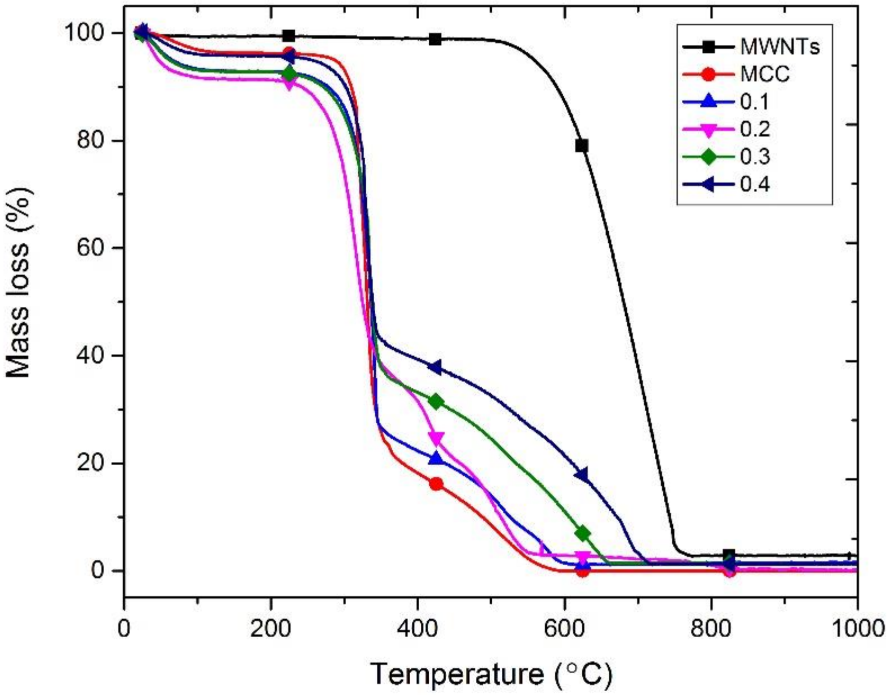

**Figure 5.59:** TGA curves of MWCNT only, MCC only, MWCNT/MCC (0.1, 0.2, 0.3 and 0.4)

The TGA curves of MWCNT/MCC also exhibited mass loss in three steps. An initial mass loss due to gradual evaporation of moisture up to 200°C; the second step from approximately 200 to 350 °C which is due to the decomposition of cellulose; the third step from approximately 250 to 500 °C which is due to the decomposition of lignin; and in the range of 500 to 700 °C there is also decomposition of graphitic structure. However, the mass loss decreased with increasing MWCNT in the range of 350 to 700 °C due to the attachment of MWCNT on the surfaces of MCC which increased the thermal stability of MWCNT/MCC. This might be an indication of an attachment mechanism and the production of a new hybrid material.

Figure 5.60 shows the results of thermogravimetric analysis (TGA) for pristine MWCNT, GO and MWCNT/GO. GO exhibited two mass loss steps, an initial mass loss between 150°C and 300°C which was attributed to the elimination of oxygen-containing functional groups; and the second mass loss was noticed at the temperature range between 450°C and 600°C, which was due to the pyrolysis of carbon skeleton (Wojtoniszak et al., 2012). Clearly, all MWCNT/GO display higher thermostability than the corresponding GO sample. This may be related to the high thermostability of MWCNT. In addition, this might be an indication of an attachment mechanism and the production of a new hybrid material. In order to obtain the chemical element compositions of composites, more information about the composites and to perform component analysis, an energy dispersive spectrometer (EDS) analysis was employed. EDS measures the energies and intensities of the X-ray spectroscopy. The qualitative analysis of EDS of MCC in figure 5.61 showed that MCC have C, O, Al, Au, and FeKesc. As found with the BNP, C and O are related to MCC and Al, Au and FeKesc are related to the substrate material and gold coating. In figure 5.62 the EDS analysis of GO reveals the presence of C, O, Fe, Cu, Mn and FeKesc. It should be noted that GO has C, O and impurities (Cu, Mn), however the Fe and FeKesc are related to the substrate material.

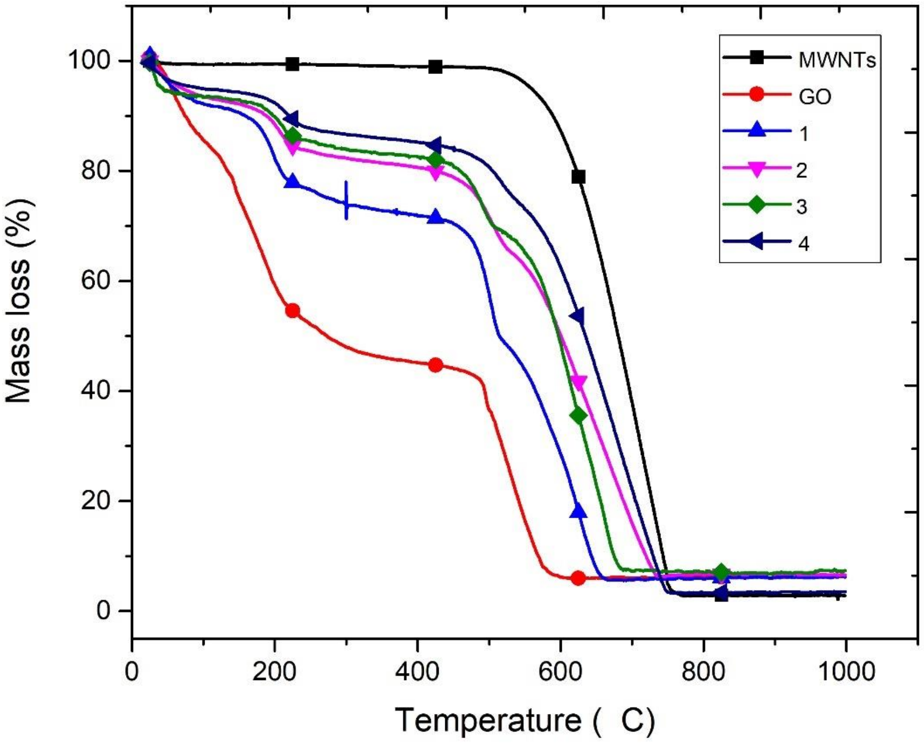

**Figure 5.60:** TGA curves of MWCNT only, GO only, MWCNT/GO (1, 2, 3, and 4)

Figures 5.63, 5.64, 5.65 and 5.66 show the EDS analysis of MWCNT/MCC (0.1, 0.2, 0.3 and 0.4) respectively. Results indicated an increase in the intensity of carbon with increasing concentration of MWCNT. This was expected as more MWCNT attached to surfaces of MCC. Furthermore, EDS analysis showed that the C and O were related to MWCNT/MCC whereas Fe, Al and FeKesc were related to the substrate material.

EDS analysis of MWCNT/GO (1, 2, 3, 4) are shown in figures 5.67, 5.68, 5.69 and 5.70 respectively, which reveals the presence of chemical components C, O, Fe, Al, Au and Fekesc. It is worth pointing out that C and O are related to GO and MWCNT whereas Fe, Al, Au and Fekesc are related to substrate material and gold coating. Although, there was expected to be an increase of C intensity when increasing the concentration of MWCNT, no increase was observed. As with the BNP samples, it is suspected that the drying process is the cause of this result. Consequently, the EDS analysis in this case cannot reflect the dispersion of MWCNT.

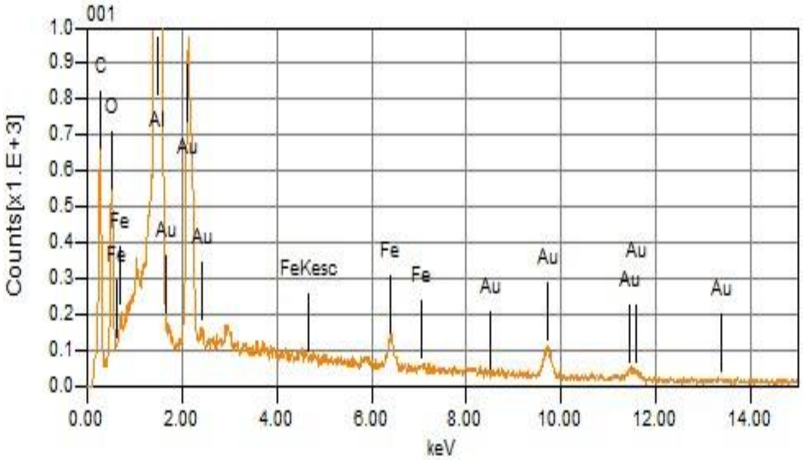

**Figure 5.61:** EDS analysis of MCC only

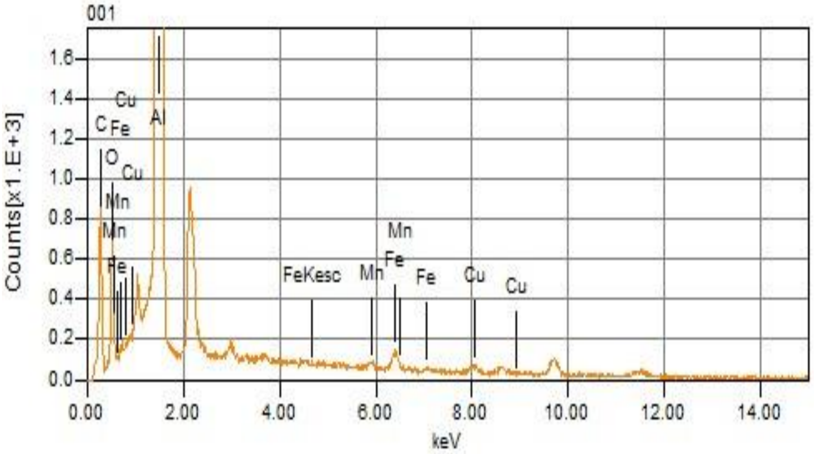

**Figure 5.62:** EDS analysis of GO only

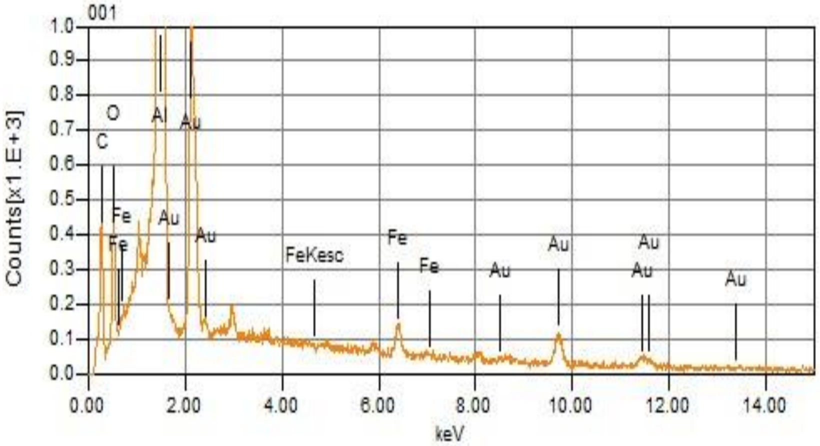

**Figure 5.63:** EDS analysis of 0.1 MWCNT/MCC

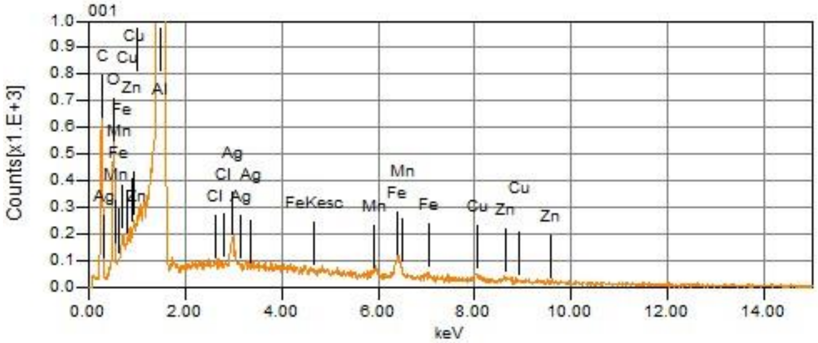

**Figure 5.64:** EDS analysis of 0.2 MWCNT/MCC

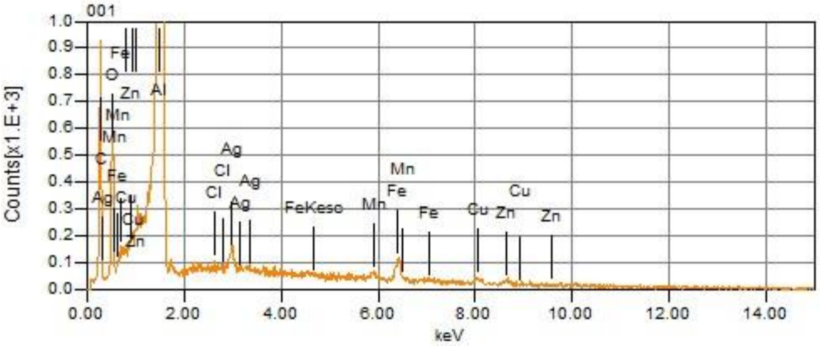

**Figure 5.65:** EDS analysis of 0.3 MWCNT/MCC

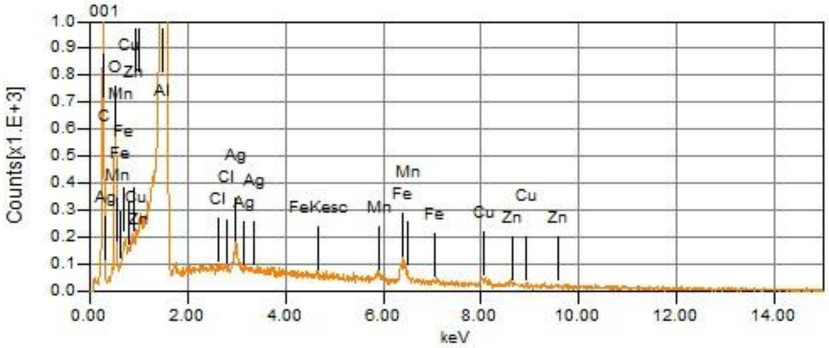

**Figure 5.66:** EDS analysis of 0.4 MWCNT/MCC

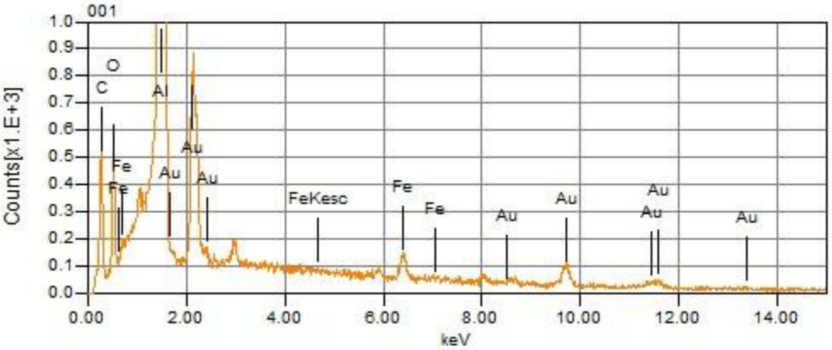

**Figure 5.67:** EDS analysis of 1 MWCNT/GO

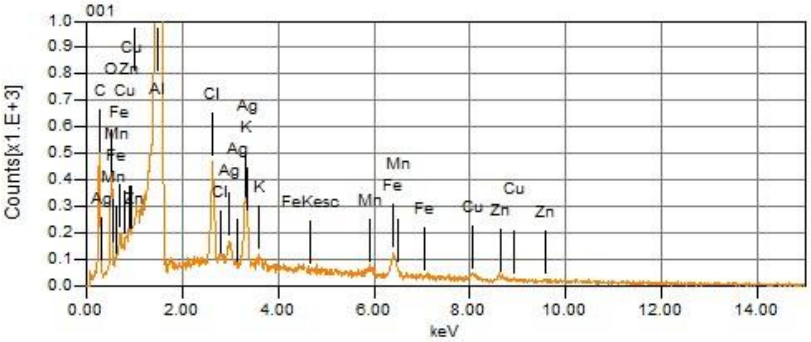

**Figure 5.68:** EDS analysis of 2 MWCNT/GO

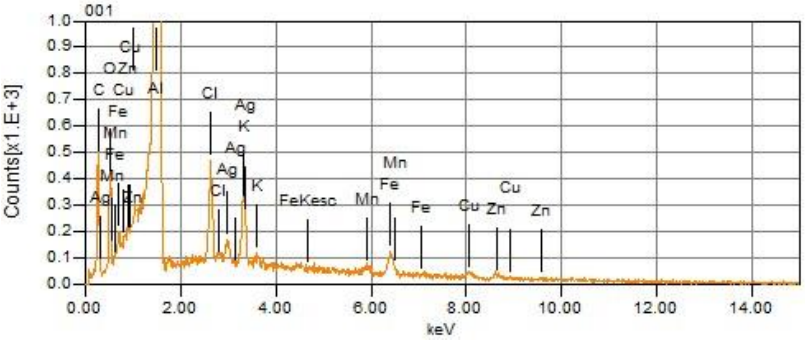

**Figure 5.69:** EDS analysis of 3 MWCNT/GO

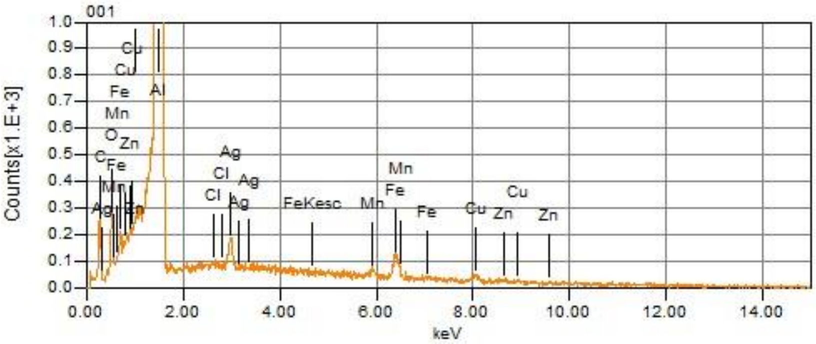

**Figure 5.70:** EDS analysis of 4 MWCNT/GO

## 5.5 Comparison between the colloidal properties and stability of BNP/MWCNT and the colloidal properties and stability of MWCNT/GO and MWCNT/MCC.

The colloidal properties and stability of BNP/MWCNT were compared with the colloidal properties and stability of MWCNT/GO and MWCNT/MCC. The results of analysing the colloidal properties and stability showed that the solution of BNP/MWCNT is more stable than the solution of MWCNT/GO and MWCNT/MCC. Figure 5.71 shows typical images of optical microscopy of BNP only (R1), MCC only (M1) and GO only (G1), BNP have nano sheets which are smaller than some particles of MCC and GO. Furthermore, BNP have more nano particles than MCC and GO.

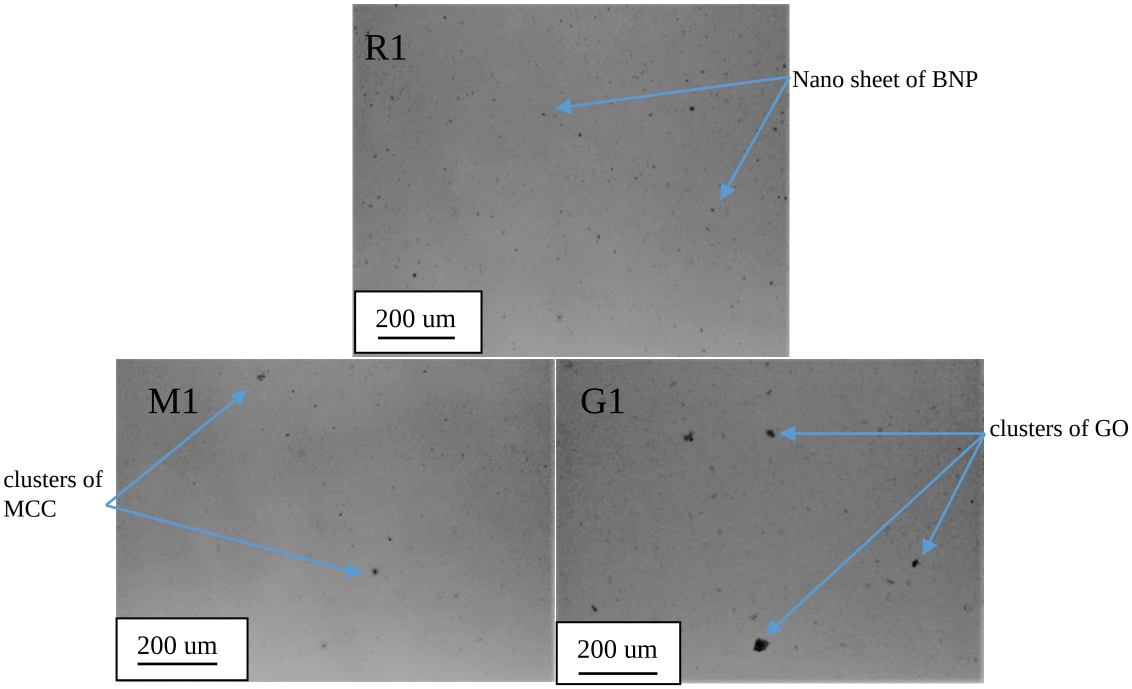

**Figure 5.71:** optical image of BNP only, MCC only and GO only

Figure 5.72 shows 0.4 MWCNT/BNP (R2), 0.1 MWCNT/MCC (M2) and 1 MWCNT/GO (G2). Both R2 and G2 have nano particles and the number of these particles are more for G2. Meanwhile M2 are of lesser number with larger size due to the lack of ability of sufficient dispersal of MWCNT. Thus, the agglomeration of MWCNT occurred and this led to the solution of MWCNT/MCC becoming unstable and the MWCNT settled down at the bottom of their aqueous solution.

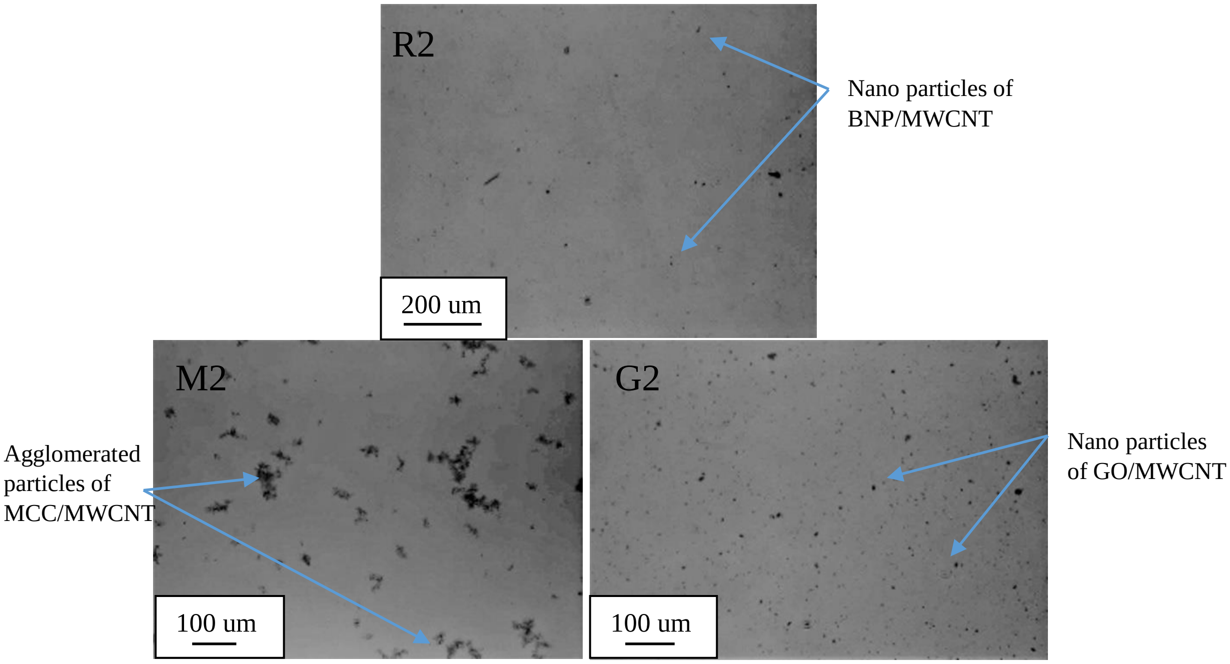

**Figure 5.72:** optical image of R2 (0.4 MWCNT/BNP), M2 (0.1 MWCNT/MCC) and G2 (1 MWCNT/GO)

Figure 5.73 shows 1.6 MWCNT/BNP (R5), 0.4 MWCNT/MCC (M5) and 4 MWCNT/GO (G5). It seems that when increasing the percentages of MWCNT/BNP from (0.4 to 1.6), MWCNT/MCC from (0.1 to 0.4) and MWCNT/GO from (1 to 4), the size of nano particles were not changed in the case of MWCNT/BNP. On the other hand, there is an obvious change in size of particles in case of MWCNT/GO which shows the trend of agglomeration of MWCNT. In addition, there is a noticeably large size of MWCNT/MCC due to agglomeration of MWCNT/MCC which is attributed to instability and the settling down of MWCNT/MCC, which occurred due to the lack of ability of MWCNT to adequately disperse.

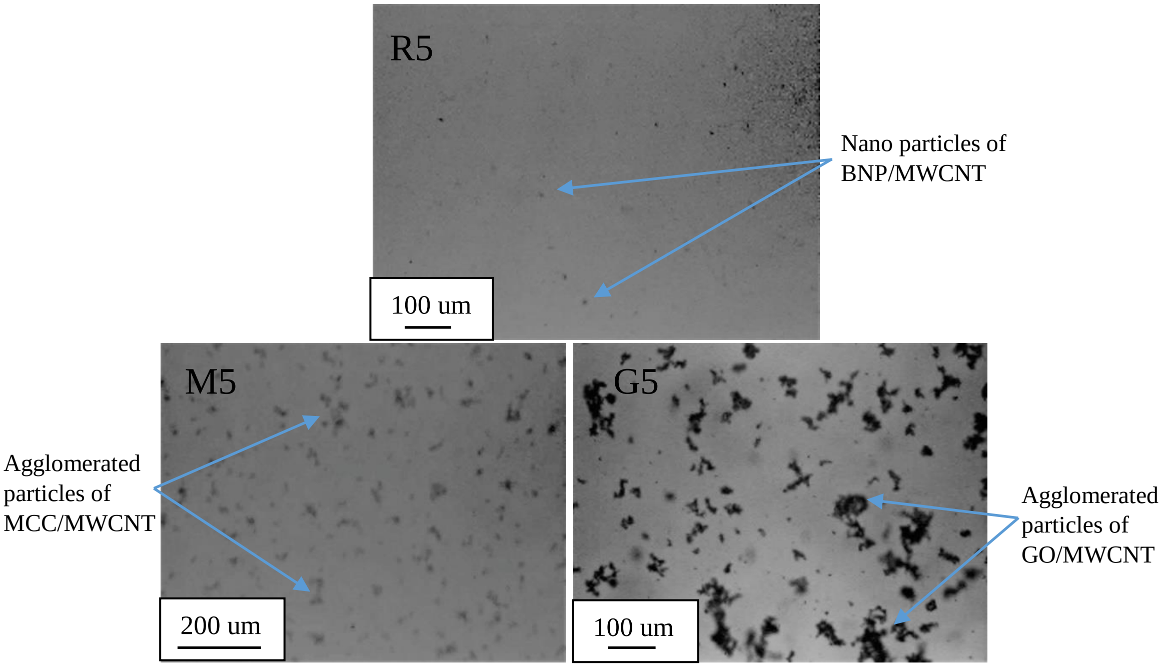

**Figure 5.73:** optical image of R2 (1.6 MWCNT/BNP), M5, (0.4 MWCNT/MCC) and G5, (4 MWCNT/GO)

Figure 5.74 shows typical SEM images of N1, R7 (0.8 MWCNT/BNP), M7 (0.2 MWCNT/MCC) and G7 (2 MWCNT/GO). N1 shows the agglomeration of MWCNT when there is no dispersant agent nor any action like ultra-sonication. This is a clear agglomeration case due to their van der forces which causes a stacking situation between them. The SEM image of R7 shows a clear individual tube of MWCNT (due to the effective repulsion forces of BNP sheets and to the self-assembly between BNP sheets and MWCNT mentioned earlier, which leads to the successful dispersible hybrid MWCNT/BNP). In contrast, the SEM image of M7 shows agglomeration of MWCNT/MCC due to the lack of ability of MWCNT to disperse. Finally, the SEM image of G7 also shows agglomeration of MWCNT/GO with some individual tubes of MWCNT. This occurred due to the insufficient ability of whole tubes of MWCNT to successfully disperse.

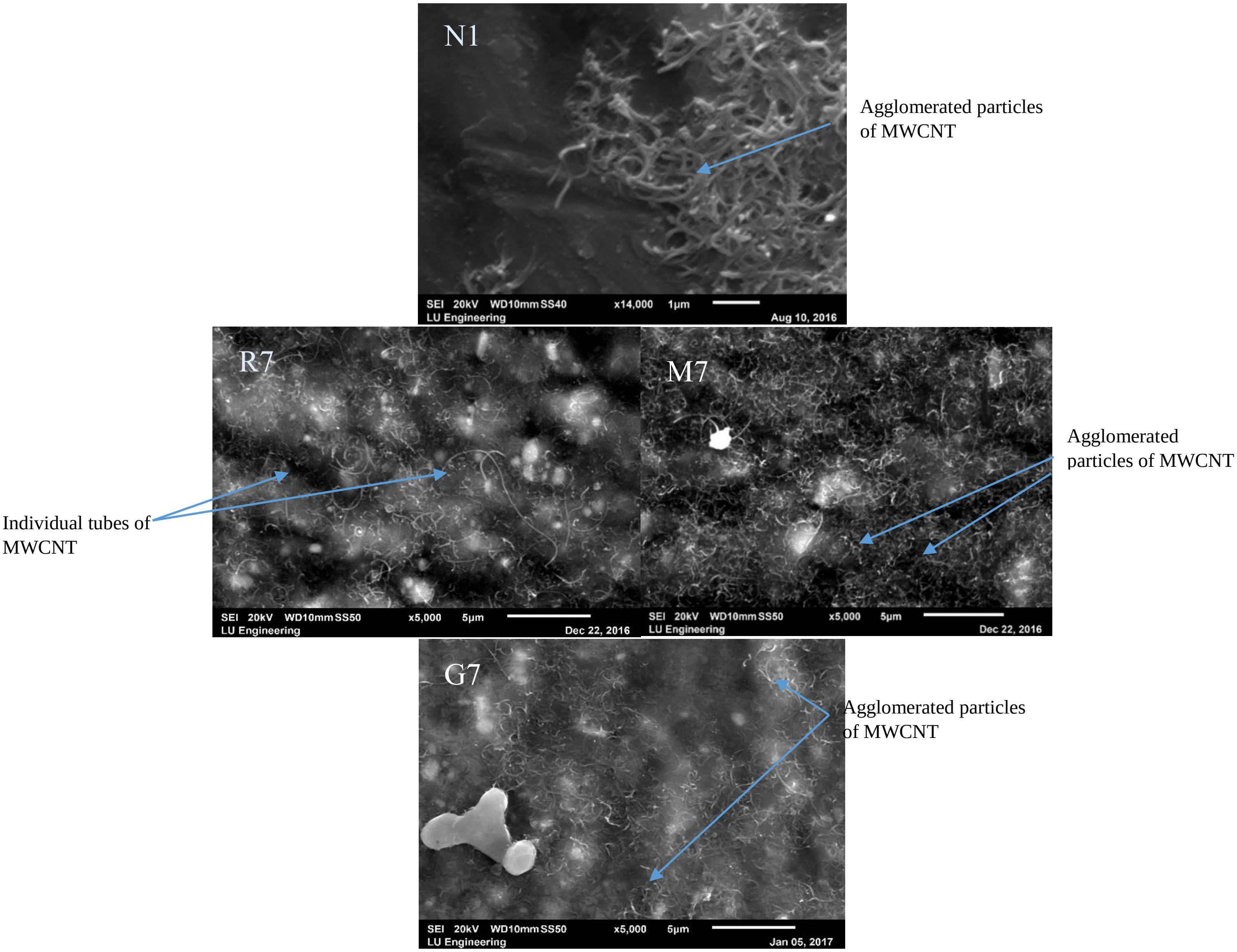

**Figure 5.74:** SEM images of N1 (MWCNT only), R7 (0.8 MWCNT/BNP, M7 (0.2 MWCNT/MCC) and G7 (2 MWCNT/GO)

## 5.6 Conclusions

The aims of this chapter were to create novel hybrid nanoparticles which have supreme characteristics and to tackle the issue of agglomeration of MWCNT. To achieve these aims, we used BNP, which are a green, environmentally friendly, low cost material, are dispersible in aqueous solution, and can be produced on an industrial scale. In addition, this chapter also examined the dispersion of MWCNT in aqueous solution with MCC and

GO for the purposes of comparison since these are both currently used in the construction industry.

UV-Vis spectroscopy results, optical microscopy results, SEM results and TGA results demonstrated that novel hybrid Nano particles were created through a self-assembly mechanism between BNP and MWCNT, furthermore, the BNP helped MWCNT to untangle and disperse uniformly in aqueous solution. It is worth mentioning that the aqueous solution of BNP/MWCNT was very stable for months, although some clumps of MWCNT were observed because it is difficult to achieve complete dispersion for whole MWCNT. It was observed that BNP without SP also exhibited small sized aggregates of MWCNT and high absorption, indicating improved dispersion. Furthermore, the results from SEM results show that well dispersed MWCNT have been achieved by using BNP. This occurred for two reasons. Firstly, owing to electrostatic repulsion between the BNP, which comes from treatment by dispersant Span 20. This coated the surface of the Bio Nano platelets and prevented the cellulose platelets aggregating, allowing them to be more readily re-dispersed in aqueous media. Secondly, the possible adsorption of the BNP on the nanotube's surfaces. It is believed that a novel hybrid nanomaterial was created from adsorption of BNP on the MWCNT surfaces (i.e. a self-assembly process), that is easy to attribute to the underlying force which comes from hydrophobic interactions that occur between the side wall of the MWCNT and the surface crystalline plane of the amphiphilic BNP (Mougel et al., 2016; Olivier et al., 2012).

For the purpose of comparison we have studied the colloidal properties and stability of MWCNT/MCC and MWCNT/GO and the results obtained from optical microscopy showed that aggregates of MWCNT were microscale sized and their size tended to be smaller with the addition of SP, thus the solution of MWCNT/MCC and MWCNT/GO have low stability and improved with the addition of SP.

The SEM results show that, in general by using MCC and GO, there are many clusters of MWCNT, and their solutions were not stable. Thus, there is evidence of poor dispersion for MWCNT. The TGA curves showed a higher thermal stability for pristine MWCNT when compared to BNP, MCC and GO, due to the high decomposition temperature of graphitic structure. The TGA curves for the paired solutions showed higher thermal stabilities than the pristine solutions of BNP, MCC and GO respectively. This may have been due to the attachment of MWCNT to their surfaces and their combined work as a hybrid material. A further increase in MWCNT' concentration gives additional thermal stability to BNP/MWCNT, MWCNT/MCC/ and MWCNT/GO. This may have been through an increase in the number of MWCNT attached onto the surfaces of dispersant agents. Finally, this work produced novel hybrid nanoparticles which is a promising candidate to use with cementitious composites after tackling the big issue of MWCNT agglomeration. This opens the door to use them with the hope of achieving positive impacts on the characteristics of cementitious composites. Leading from this, in the next chapter we will investigate the effects of loading BNP/MWCNT on the characteristics of cementitious composites.

# Chapter Six

# 6 Cementitious composites reinforced by multifunctional hybrid BNP/MWCNT nanoparticles

## 6.1 Introduction

In this chapter, we investigate the performance of cementitious composites modified with hybrid BNP/MWCNT. The hybrid BNP/MWCNT was created in chapter five, and the effect of different concentrations of BNP/MWCNT on the hydration, microstructure, compressive strength and flexural strength of cementitious composites are clarified and the results are reported here.

## 6.2 Experimental programme

### 6.2.1 Materials

The materials utilized in Section 5.3.1 were used in this study.

### 6.2.2 Preparation of BNP/MWCNT/Cementitious Composites

The hybrid BNP/MWCNT solution was prepared first. In this process, BNP at percentage of 0.2 wt.% by weight of cement (the optimal percentage according to investigation in Chapter Four) is added to mixing water. The SP at 1 wt.% by cement weight was then added to the mixing water. The resultant mixing water was sonicated with a horn type sonicator for a duration of 30 minutes. Subsequently, five concentrations of MWCNT (0.0, 0.05, 0.1, 0.2 and 0.4) wt. % (by cement weight) were added to the mixtures. The resultant solutions were then sonicated again for 30 minutes.

The preparation of the cement pastes was begun by adding the BNP/MWCNT solution to the cement powder using a water/cement ratio of 0.4. It is worth mentioning that the internal water of BNP was considered in calculation of water. The materials were then mixed together for 7 minutes using an electrical multi speed planetary blender. Subsequently, the cement pastes were put in the steel moulds and vibrated using a vibrating table for a duration of 30 seconds. The specimens were sealed for 24 hrs, then demoulded and kept in water at a room temperature of 21$^{o}$C until the time of testing to store for 7, 14 and 28 days.

### 6.2.3 Characterisation of BNP/MWCNT cementitious composites

#### 6.2.3.1 Hydration of cementitious composites

Cementitious composite samples with 0.2 wt. % of BNP and five concentrations of MWCNT (0.0, 0.05, 0.1, 0.2 and 0.4) wt. % respectively were collected from the fractured flexural prisms at 7, 14 and 28 days to characterize the effect of BNP/MWCNT on the degree of hydration and microstructure of the composites. Thermogravimetric analysis (TGA) was carried out to elucidate the effect of BNP/MWCNT on the hydration mechanism of the cementitious composites and estimate their degree of hydration (DOH) and the content of $Ca(OH)_2$. In this experiment, the samples were heated from 25 to 1100 $^{o}$C at a rate of 10 $^{o}$C/min under nitrogen (N2). In addition, TGA measurements were performed on BNP, MWCNT and cement particles for correction purposes (Cao et al., 2015). X-ray diffraction (XRD) analysis was also carried out to further investigate the DOH and determine the crystallinity of the cementitious composites.

#### 6.2.3.2 Microstructure and morphology of cementitious composites

Scanning electron microscopy coupled with energy dispersive X-ray spectroscopy (SEM/EDX) were employed to carry out elemental analysis on the chemical composition of the cementitious composites and to investigate the microstructure characteristics such as distribution of BNP/MWCNT and their crack bridging mechanism. The samples were taken from the fractured flexural surfaces. These were then polished to smooth their surfaces prior to analysis.

### 6.2.3.3 Mechanical properties of cementitious composites.

The influence of the hybrid BNP/MWCNT nanoparticles on the mechanical properties of the cementitious composites were investigated at 7, 14 and 28 days. For each BNP/MWCNT loading, twelve beams (40 mm ×40 mm ×160 mm) were prepared and subjected to a four-point bending test, according to ASTM C78 to determine their flexural strength as shown in figures 4.1 and 4.2. The four-point bending tests were carried out under displacement control with a rate of 0.1 mm/min. During testing, load and deflection at the center were recorded continuously. Furthermore, twelve cubes (50 mm ×50 mm ×50 mm) were prepared and subjected to a compressive loading with compressive stress rate 0.5 MPa\min to determine their compressive strength, following to ASTM C 109/C 109M. The modulus of elasticity and flexural strength and compressive strength were calculated according to these equations (Saafi et al., 2015), (C 78),(C 109/C 109M):

$$fm = P/A \ldots\ldots\ldots\ldots\ldots\ldots\ldots\ldots\ldots\ldots\ldots\ldots\ldots\ldots\ldots\ldots\ldots\ldots\ldots\ldots\ldots\ldots(1)$$

$$E = \frac{ma(3l^2-4a^2)}{4b^4} \ldots\ldots\ldots\ldots\ldots\ldots\ldots\ldots\ldots\ldots\ldots\ldots\ldots\ldots\ldots\ldots\ldots(2)$$

$$R = Pl/bh^2 \ldots\ldots\ldots\ldots\ldots\ldots\ldots\ldots\ldots\ldots\ldots\ldots\ldots\ldots\ldots\ldots\ldots\ldots\ldots\ldots(3)$$

Where

$fm$: compressive strength (MPa); P: total maximum load (N); A: area of loaded surface (mm$^2$); E: Modulus of Elasticity (GPa); R: Flexural strength (MPa); b and h are width and height of the specimen (mm); L is the length of support distance (mm); a is the distance between support and loading point (mm); M is the slope of the force- displacement curve.

#### 6.2.3.4 Fracture properties of cementitious composites.

The fracture energy and fracture toughness of the hybrid BNP/MWCNT-cementitious composites were determined using the three-point bending method. Twelve prisms with dimensions of 160 mm × 40 mm × 40 mm were prepared. Each sample contained a notch of 16 mm at the middle of the sample. An Instron testing machine was used for this test with a displacement rate of 0.03 mm/min.

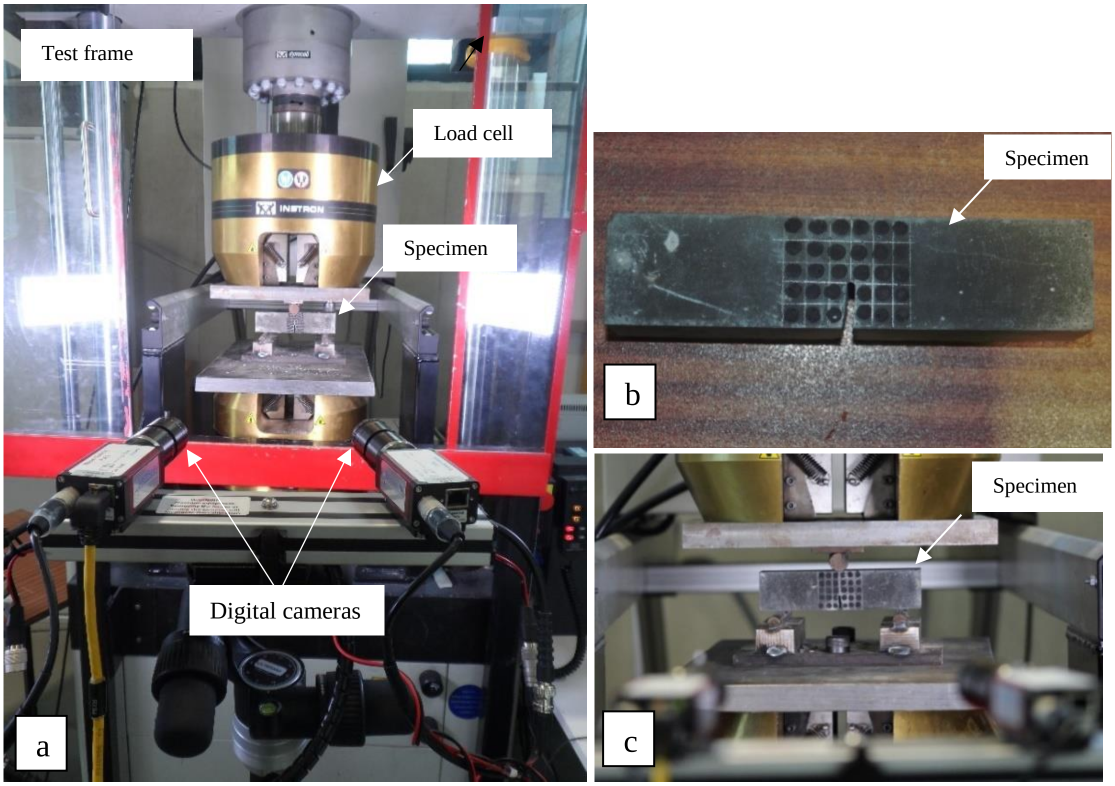

**Figure 6.1:** (a) test set up, (b) close-up photograph of notched beam and (c) close-up photograph of test set up

In addition, the crack mouth opening displacement (CMOD) was measured with a video gauge$^{TM}$ aquired from Imetrum Ltd. The video gauge system consisted of two lenses, an iMetrum system controller and an iMetrum data processing software installed on a computer. As can be seen in figure 6.1(b), five lines of 6 black dots with a dot diameter of 4 mm and a centre-to-centre spacing of 5 mm were printed on the surface of the beams around the notch to define the region where the displacement is measured. The lenses were placed 1.5 m away from the surface of the beams (figure 6.1(c)) and recorded along with the load at a frequency of 15 Hz. The CMOD was obtained by monitoring the horizontal displacement between the two dots adjacent to the mouth of the crack as shown in figure 6.1(b). The load vs CMOD, and the calculated fracture energy and fracture toughness were employed to quantify the contribution of BNP/MWCNT to the fracture resistance of the cementitious composites.

The fracture energy, fracture toughness and modulus of elasticity (Hu et al., 2014) and were calculated according to the following equations:

$$G_f = \frac{mg\delta_\circ + w_\circ}{t(h-a)} = \frac{mg\delta_\circ + \int_0^{\delta_\circ} P(\delta)d\delta}{t(h-a)} \tag{4}$$

$$K_{IC} = \frac{P_{max}S}{th^{3\backslash 2}} f\left(\frac{a}{h}\right) \tag{5}$$

$$f\left(\frac{a}{h}\right) = 2.9\left(\frac{a}{h}\right)^{1/2} - 4.6\left(\frac{a}{h}\right)^{\frac{3}{2}} + 21.8\left(\frac{a}{h}\right)^{\frac{5}{2}} - 37.6\left(\frac{a}{h}\right)^{\frac{7}{2}} + 38.7\left(\frac{a}{h}\right)^{\frac{9}{2}} \tag{6}$$

$$K_{IC} = \sqrt{EG_F} \tag{7}$$

$G_f$ is the fracture energy of the composite; $K_{IC}$ is the fracture toughness of the composite; $w_\circ$ is the area under the load-displacement curve; $m = m_1 + m_2$ where $m_1$ is the mass of the beam between the supports, and $m_2$ is the mass of the fixture not attached to the loading machine that follows the beam during failure; $g$ is the accelaration due to gravity; $\delta_\circ$ is the displacement at final failure of the beam; $P(\delta)$ is the load-displacement curve; $t$ is the width of the specimen; $h$ is the height of the specimen; $a$ is the depth of the slot; $S$ is the span of the beam and $P_{max}$ is the peal load.

## 6.3 Results and Discussion

### 6.3.1 Influence of BNP/MWCNT on hydration mechanism of cementitious composites.

The thermogravimetric analysis (TGA) results in terms of weight loss and the derivative of the weight loss (DTA) are presented in figures 6.2, 6.3, 6.4 and 6.5 for the cementitious composites. In these figures, the percentage of the weight loss gradually decreases as the temperatures increase and the inflections in the DTA represent the decomposition of specific phases of the cement paste composites. The TGA/DTA provides insight into the chemical reaction mechanisms in cementitious materials during heating, illustrating the influence of the addition of hybrid BNP/MWCNT on the degree of hydration. During this test, it was observed that calcium-silicate- hydrate (C-S-H) and carboaluminate phases lose their bound water in the temperature range 180-300 $^{o}$C, the dehydroxylation of calcium hydroxide $Ca(OH)_2$) takes place in the temperature range 430-480$^{o}$C, and the decarbonation of calcium carbonate ($CaCO_3$) occurs in the temperature range 600–780$^{o}$C(Cao et al., 2016a). The initial loss of mass from ~25$^{o}$C to 123.3$^{o}$C was assumed to be due to the loss of physically held water (pore water), the loss of mass from ~123.3 to 427 $^{o}$C was assumed to be due to dehydration of C-S-H, the loss of mass from ~427 to 475 $^{o}$C was assumed to be due to dehydration of CH, and the loss of mass from ~475$^{o}$C to around 797$^{o}$C due to decarbonation of $CaCO_3$ (Calcium Carbonate)(Alessandra Etuko Feuzicana de Souza and Eduvaldo Paulo, 2006).

Some interpretations of these results are presented herein. From figures 6.3, 6.4 and 6.5, it can be observed that the max mass loss of the cement paste composites at 7 days occurred at 0.1% MWCNT due to more water, thereby the hydration being prolonged (Alessandra Etuko Feuzicana de Souza and Eduvaldo Paulo, 2006). At 14 and 28 days the max mass loss of cement paste composites was observed for plain cement paste and cement paste with 0.05% MWCNT which means they have more water content. On the other hand, the water content decreased with increasing MWCNT concentration. This is due to the increase of the high-density C-S-H content and the creation of new intercalated BNP/MWCNT/C-S-H nanocomposites with a higher density. This is consistent with (Sardar Kashif Ur et al., 2018)'s findings where they have shown that decrease in the mass loss of GO reinforced cementitious composites is attributed to both the bonding of C-S-H with the GO sheets and the increase of the C-S-H content. In this case, the GO sheets tend to increase the amount of C-S-H product, thereby filling the pores in the matrix, thus less water is available for evaporation (Sardar Kashif Ur et al., 2018). Furthermore, this is also consistent with (Karim et al., 2016)'s findings which showed that when using Palm oil clinker powder in concrete more C-S-H gel was produced which filled the pores in the matrix, consequently, water in the microstructure of the cementitious composite was reduced. And this is consistent with the results of flexural strength which show higher strength at 14 and 28 days of 0.1%, 0.2% and 0.4% MWCNT than the flexural strength of plain cement and 0.05% MWCNT at the same age.  This is also consistent with Sadiq 2013's findings which showed that the lower-strength cementitious nanocomposites reinforced with acid functionalized MWCNT type E with physisorbed Gum Arabic had more mass loss (i.e. more excess water) than both plain cementitious materials.

Figure 6.2(a) presents the $Ca(OH)_2$ content versus MWCNT concentration at 7, 14 and 28 days.  For 7-day test, the amount of $Ca(OH)_2$ has slightly increased with addition MWCNT and the largest amount of $Ca(OH)_2$ was observed at 0.1% MWCNT. For 14-day test, the amount of $Ca(OH)_2$ has significantly increased with addition MWCNT and the largest amount of $Ca(OH)_2$ was noticed at 0.4% MWCNT. Furthermore, The $Ca(OH)_2$ content has significantly increased with the addition of MWCNT and the largest amount was seen at 0.1% MWCNT at 28 days as shown in figure 6.2(a). The peak in weight loss between 450$^{o}$C and 500$^{o}$C in figure 6.2 was assumed to be due to CH dehydration. This peak was quite strong for 0.1% and 0.2% MWCNT, and weak for plain cement, which indicated the presence of more CH in cement paste with MWCNT than in plain cement paste at 28 days. Overall, figure 6.2(a) suggests that the addition of hybrid BNP/MWCNT accelerates the hydration of cement which results in the production of higher $Ca(OH)_2$ contents at 28 days. The addition of BNP sheets accelerates the hydration of cement and the MWCNT works as nucleation points to promote more hydration products resulting in the production of higher $Ca(OH)_2$ contents at 28 days.

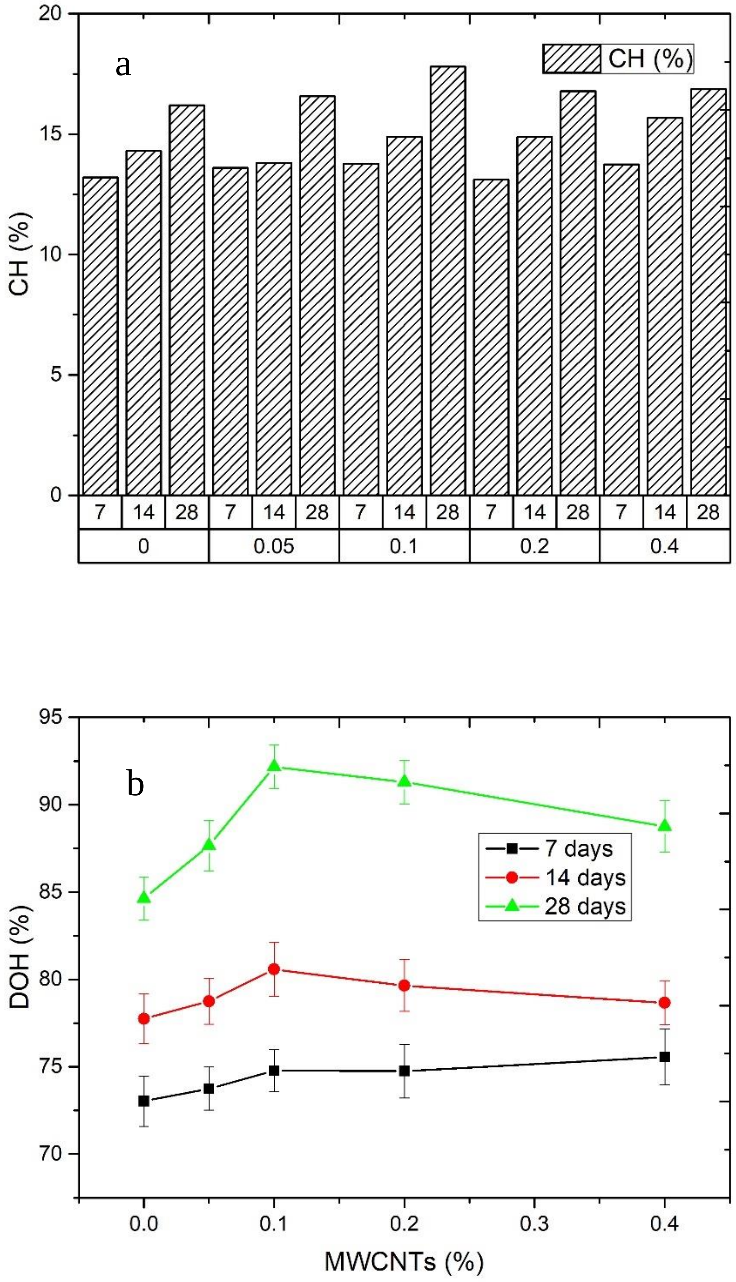

**Figure 6.2: (**a) Percentage of Calcium hydroxide at 7-, 14- and 28-days age and with 0.0%, 0.05%, 0.1%, 0.2% and 0.4% of MWCNT. (b) Degree of hydration at 7-, 14- and 28-days age and with 0.0%, 0.05%, 0.1%, 0.2% and 0.4% of MWCNT

According to (Cao et al., 2015), the DOH can be obtained by dividing the amount of the chemically bound water (CBW) per unit gram of unhydrated cement by the CBW of fully hydrated cement which is 0.23g. The CBW can be obtained by dividing the mass loss between 140 and 1100 $^{o}$C by the final mass. Figure 6.2(b) shows the DOH as a function of MWCNT concentration at 7, 14 and 28 days. As can be seen from this figure, the results clearly show that the improvement of DOH achieved by the presence of MWCNT, for instance, 0.1% MWCNT exhibits an increase of DOH of 4% and 17% with respect to the reference case at 14 days and 28 days respectively. This is likely due to the effects of the hybrid BNP/MWCNT on the hydration mechanism of cement particles, which causing i) uniform distribution of cement particles, ii) releasing further water for further hydration, and iii) providing further nucleation points for further hydration products. According to Cao et al. (2015) hydrophilic additives disperse the cement particles well during mixing thereby producing uniform distributions of the cement particles which results in higher DOH. Furthermore, the hydrophilic BNP sheets tend to store water molecules on their surface thus acting like internal water reservoirs thereby releasing the free water for further hydration. This additional hydration further increases the amount of $Ca(OH)_2$ at 7 and 28 days. In addition, based on Cao et al.'s hypothesis, the BNP sheets embedded into the high-density C-S-H could act as water channels to transport water from the pore water solution to the unhydrated cement cores, thus fuelling the hydration of the cement particles due to the increased amount of water. In addition, MWCNT work as nucleation points to promote more hydration products resulting in the production of higher DOH.

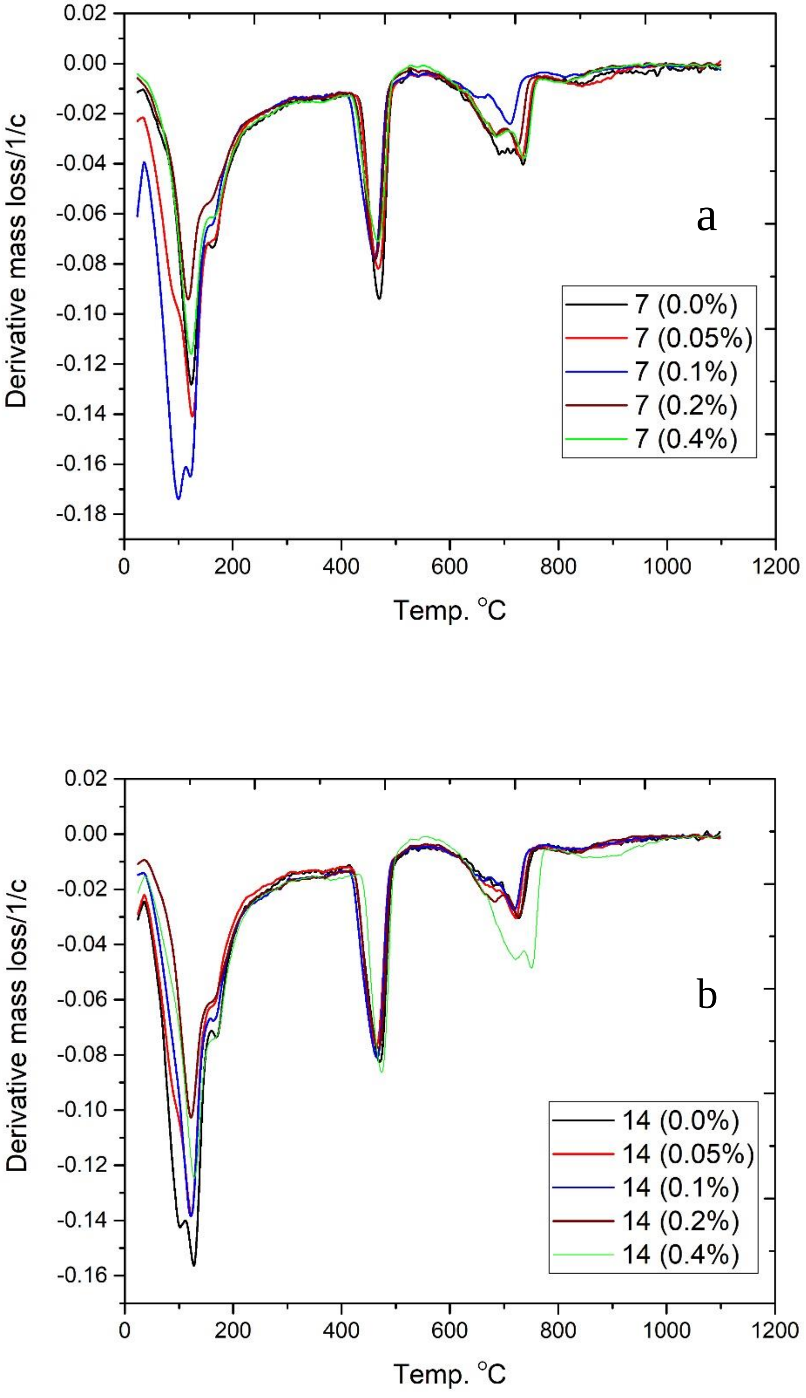

**Figure 6.3:** (a) DTA curves of (0.0%, 0.05%, 0.1%, 0.2% & 0.4%) at 7 days age, (b) DTA curves of (0.0%, 0.05%, 0.1%, 0.2% & 0.4%) at 14 days age.

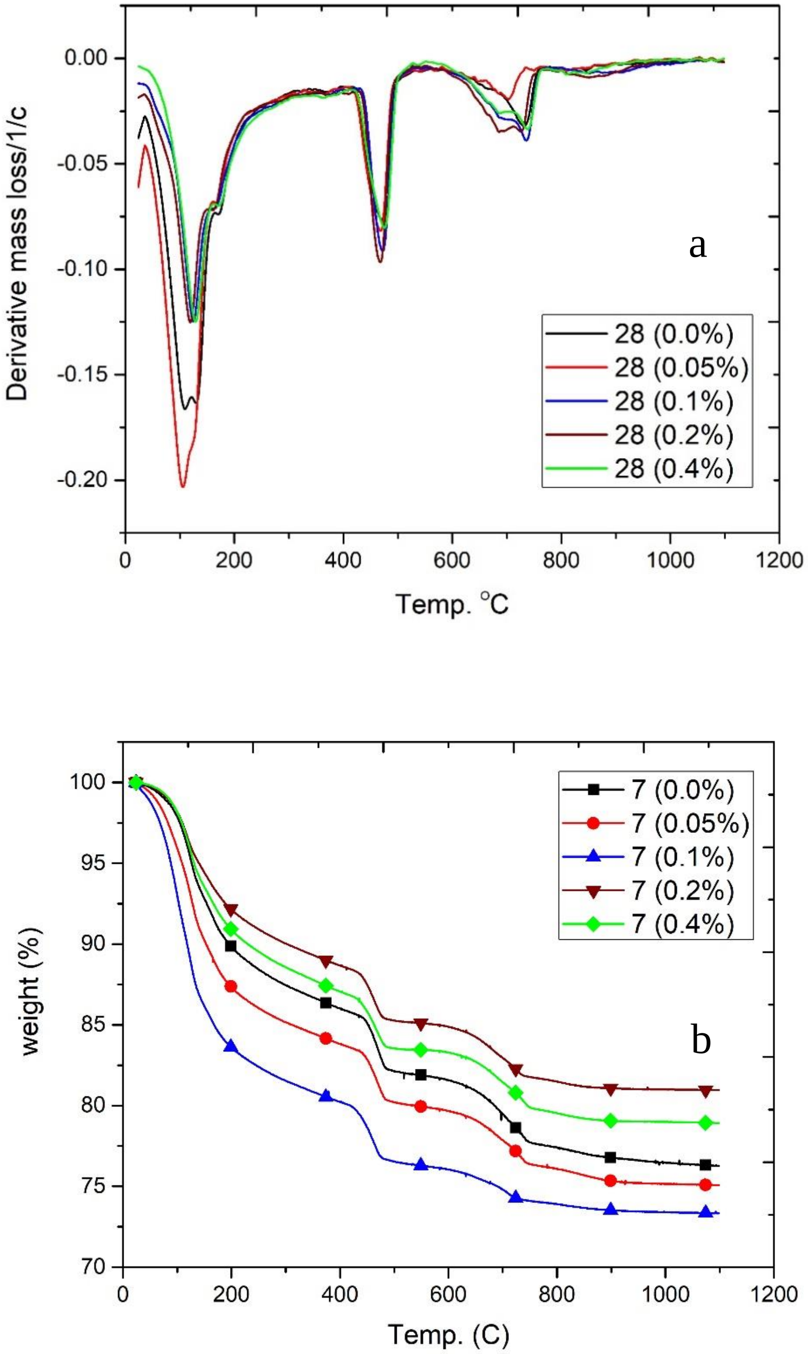

**Figure 6.4:** (a) DTA curves of (0.0%, 0.05%, 0.1%, 0.2% & 0.4%) at 28 days age, (b) TGA curves of (0.0%, 0.05%, 0.1%, 0.2% & 0.4%) at 7 days age.

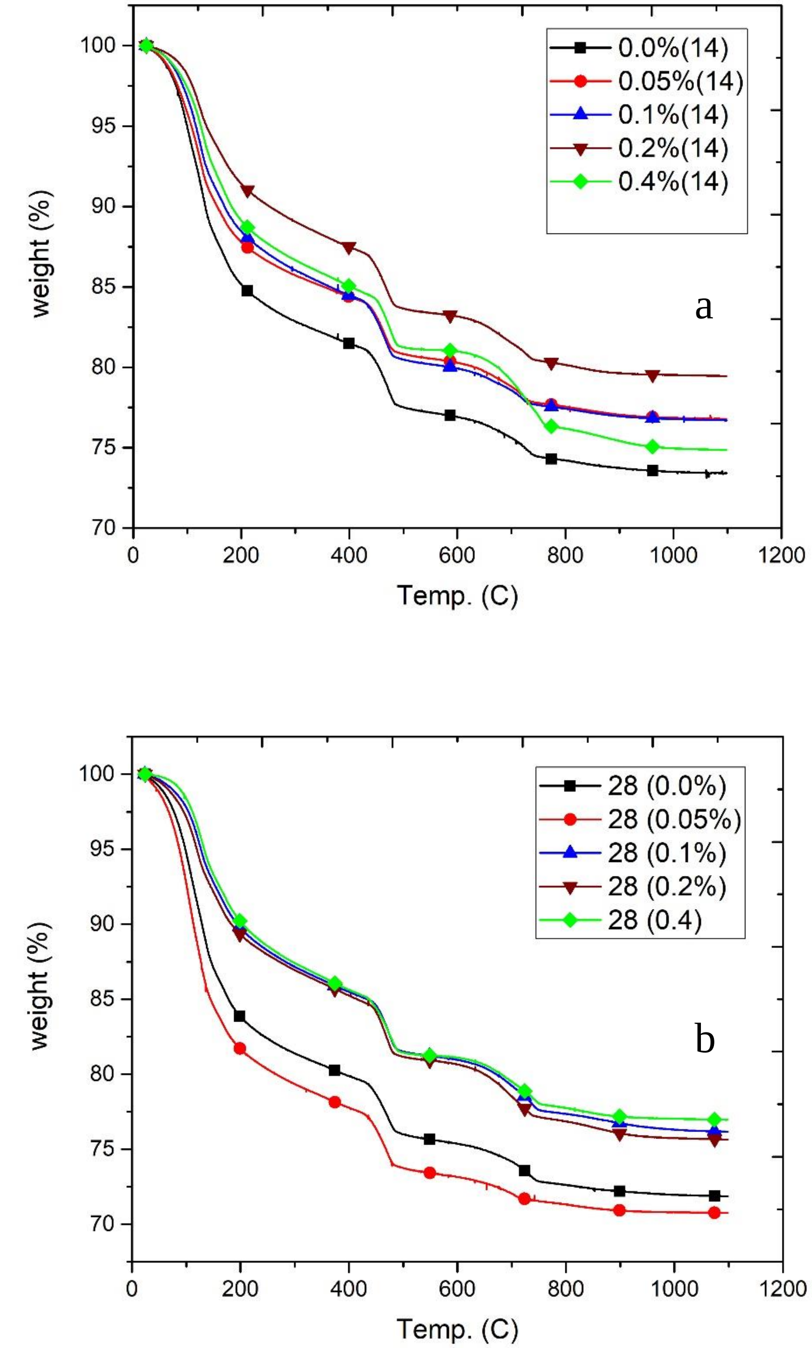

**Figure 6.5:** (a) TGA curves of (0.0%, 0.05%, 0.1%, 0.2% & 0.4%) at 14 days age, and (b) TGA curves of (0.0%, 0.05%, 0.1%, 0.2% & 0.4%) at 28 days age.

XRD analysis was carried out on cementitious pastes with 0%, 0.05%, 0.1%, 0.2% and 0.4% of MWCNT. The spectrum was analysed to identify and pinpoint various crystalline phases for cementitious materials according to their crystalline structure and also to investigate the influence of the addition of hybrid BNP/MWCNT and to monitor the hydration process. The XRD patterns of the cementitious composites at 7, 14 and 28 days are shown in figures 6.6 and 6.7. As can be seen from this figure, typical hydration phases such as ettringite, calcium hydroxide $Ca(OH)_2$, tricalcium silicate ($C_3S$) and calcium carbonate ($CaCO_3$) are detected in all the cementitious composites at all ages. This is consistent with previous studies that show the dissolution of anhydrous cement particles starts with the mixing of water with cement powder which results in the formation of hydration products. The dissolution and precipitation processes continue with curing time and the CH, C-S-H and ettringite precipitate (Lothenbach et al., 2007). Furthermore, this indicates that the addition of hybrid BNP/MWCNT does not alter the type and structure of the hydration products of the cementitious composite. The C-S-H hydration phases are difficult to identify by XRD analysis due to the lack of crystallinity and indefinite composition. The XRD figures of cementitious materials (figures 6.6 and 6.7) exhibited significant differences: overall, the intensities of CH increased with the addition of MWCNT at early age and over time, indicating changes were occurring in the hydration process of the matrix with the introduction of the MWCNT.

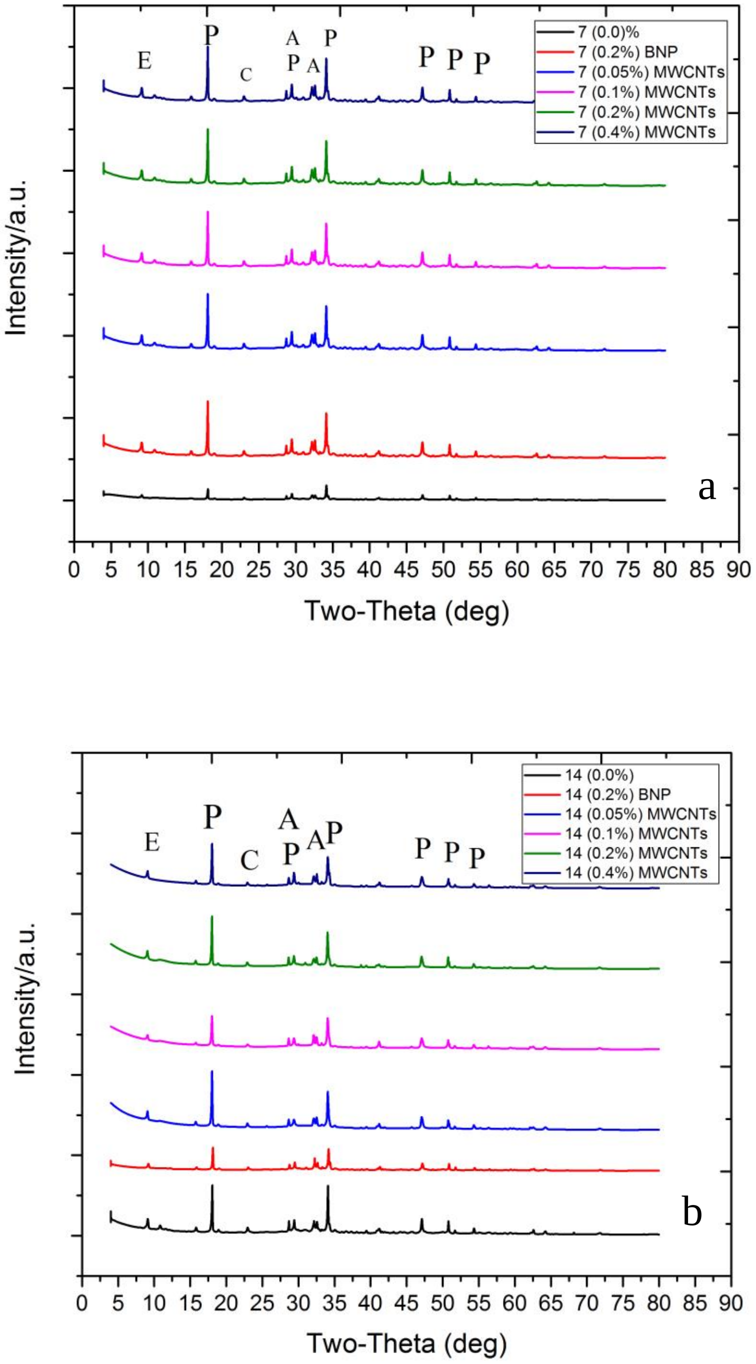

**Figure 6.6: (**a) XRD analysis at 7 days age with all percentages of MWCNT additions, (b) XRD analysis at 14 days age with all percentages of MWCNT additions

Moreover, intensities of CH were higher for cementitious pastes with 0.05%, 0.1%, 0.2% and 0.4% of MWCNT mixtures than intensities of CH for plain cement at 28 days age.

This suggests that a greater amount of anhydrous cement reacts with the addition of hybrid BNP/MWCNT. This means the addition of the hybrid BNP/MWCNT promotes the hydration of cements thereby increasing the amount of the hydration products, thus confirming the TGA findings.

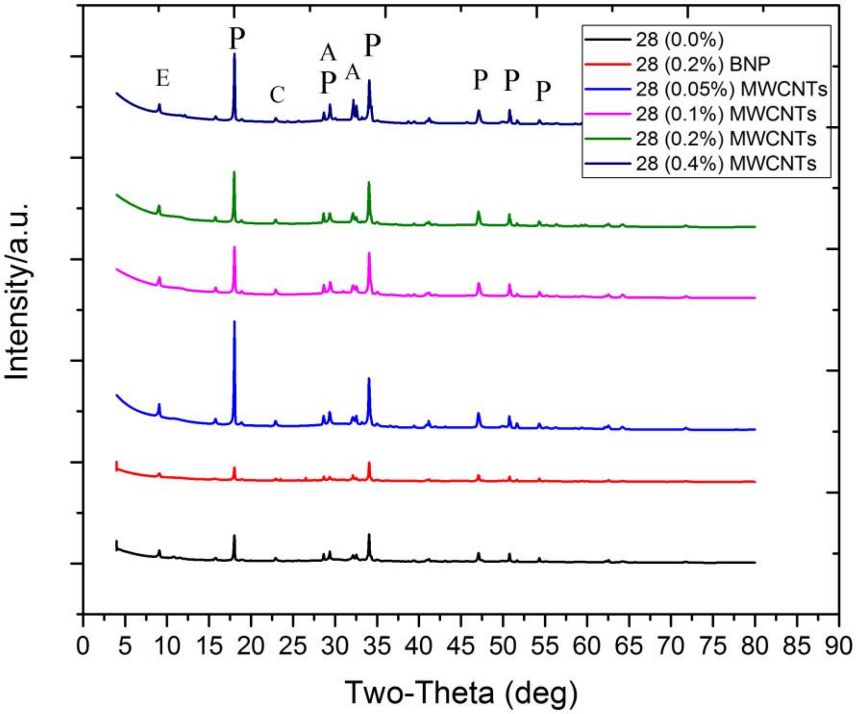

**Figure 6.7:** XRD analysis at 28 days age with all percentages of MWCNT additions. E: Ettringite; P: Portlandite; C-S-H: calcium silicate hydrate; A: Alite and B: Belite.

It is notable that the results did not include C-S-H gel and are more about the relative content between these phases because the main hydration product C-S-H gel is amorphous, which is not detectable under XRD due to the nature of the XRD technique. Moreover, table 6.1 shows that the crystal system of hydration products of cementitious composites and unhydrated components of cementitious composities do not alter. This indicates that the addition of hybrid BNP/MWCNT does not alter the type and structure of the hydration products of the cementitious composites.

Table 6.1 Crystal system of minerals in cementitious composites

| | Crystal system | | | | | | |
|---|---|---|---|---|---|---|---|
| Minerals | Unhydrate cement | 0.0-7 | 0.0-14 | 0.0-28 | 0.05-7 | 0.05-14 | 0.05-28 |
| Alite | triclinic (anorthic) | triclinic (anorthic) | triclinic (anorthic) | triclinic (anorthic) | triclinic (anorthic) | triclinic (anorthic) | triclinic (anorthic) |
| Calcite | trigonal (hexagonal axes) | trigonal (hexagonal axes) | trigonal (hexagonal axes) | trigonal (hexagonal axes) | trigonal (hexagonal axes) | trigonal (hexagonal axes) | trigonal (hexagonal axes) |
| CH | - | trigonal (hexagonal axes) | trigonal (hexagonal axes) | trigonal (hexagonal axes) | trigonal (hexagonal axes) | trigonal (hexagonal axes) | trigonal (hexagonal axes) |
| Ettringite | - | trigonal (hexagonal axes) | trigonal (hexagonal axes) | trigonal (hexagonal axes) | trigonal (hexagonal axes) | trigonal (hexagonal axes) | trigonal (hexagonal axes) |
| | Crystal system | | | | | | |
| Minerals | 0.1-7 | 0.1-14 | 0.1-28 | 0.2-7 | 0.2-14 | 0.2-28 | |
| Alite | triclinic (anorthic) | triclinic (anorthic) | triclinic (anorthic) | triclinic (anorthic) | triclinic (anorthic) | triclinic (anorthic) | |
| Calcite | trigonal (hexagonal axes) | trigonal (hexagonal axes) | trigonal (hexagonal axes) | trigonal (hexagonal axes) | trigonal (hexagonal axes) | trigonal (hexagonal axes) | |
| CH | trigonal (hexagonal axes) | trigonal (hexagonal axes) | trigonal (hexagonal axes) | trigonal (hexagonal axes) | trigonal (hexagonal axes) | trigonal (hexagonal axes) | |
| Ettringite | trigonal (hexagonal axes) | trigonal (hexagonal axes) | trigonal (hexagonal axes) | trigonal (hexagonal axes) | trigonal (hexagonal axes) | trigonal (hexagonal axes) | |
| | Crystal system | | | | | | |
| Minerals | 0.4-7 | 0.4-14 | 0.4-28 | | | | |
| Alite | triclinic (anorthic) | triclinic (anorthic) | triclinic (anorthic) | | | | |
| Calcite | trigonal (hexagonal axes) | trigonal (hexagonal axes) | trigonal (hexagonal axes) | | | | |
| CH | trigonal (hexagonal axes) | trigonal (hexagonal axes) | trigonal (hexagonal axes) | | | | |
| Ettringite | trigonal (hexagonal axes) | trigonal (hexagonal axes) | trigonal (hexagonal axes) | | | | |

### 6.3.2. Influence of BNP/MWCNT on Morphology and microstructure of cementitious composites.

Residual cement, and various hydration products that together have a complex and porous microstructure, are the components of the cement paste. Individual grains of cementitious materials and water that may also contain chemical admixtures are initially mixed to make a cement paste. Over curing time, various hydration products are produced from hydration reactions which consume the cement and some of these hydration products grow on the surface of the cement grains while progressively filling the initial water-filled space. The shape of residual portland cement particles seems to be angular to subangular and dense. The shape of Alite ($C_3S$) normally seems to have at least one crystal face whereas belite ($C_2S$) is normally rounded and sometimes striated. The major hydration product of portland cement is C-S-H which is amorphous or very poorly crystalline. The calcium to silica ratio, water to cementitious materials ratio, curing conditions, degree of cement hydration, and chemical admixtures all effect the morphology of C-H-S. However, at high magnifications of SEM, the morphology of C-S-H differs from very fine fibrous growths, to sheet-like units, to irregular massive grains.

The second major phase of cement hydration is Portlandite ($Ca(OH)_2$) which has variable sizes and shapes including platy hexagonal crystals and sheet-like masses, depending on the orientation. $Ca(OH)_2$ is usually noticed throughout the cement paste. Sometimes secondary deposits in voids and cracks are also noticed. A primary product of the reactions between calcium aluminates and the sulfate phases in cement is Ettringite which has an acicular shape (ASTM standard C1723-10).

As shown in figure 6.8(a), the microstructure of the plain cementitious composite at 7 days contains unreacted residual cement particles which have angular to subangular shape, which could be $C_3S$ or $C_2S$ as well as $Ca(OH_2)$ cubes or seeds-like particles, presumably due to a low DOH as well as that C-S-H is usually amorphous or very poorly crystalline. The addition of 0.20-wt% of BNP leads to some layers of stacked fabric-like $Ca(OH)_2$

crystals embedded into a high-density C-S-H gel as well as some unreacted residual cement particles which have angular to subangular shape, which could be $C_3S$ or $C_2S$ as shown in figure 6.8(b). Most of these $Ca(OH)_2$ fabrics appear to grow in one-direction in pores and cracks, acting as fillers and crack arrestor through cracks bridging thus these stacked fabric-like $Ca(OH)_2$ crystals increase flexural strength of cementitious composite (Lv et al., 2016). This could be the result of the interaction of the uniformly distributed BNP sheets with the cement particles.  When uniformly distributed, the BNP sheets adsorb onto the surface of the cement particles through their -OH and -OH-$CH_2$- functional groups.  These functional groups then react with $C_3S$ and $C_2S$ to form nucleation and growth sites for the hydration phases. Figure 6.8(c) shows that the microstructure of cementitious composite which contains hybrid BNP/MWCNT, with a concentration of 0.05 wt% MWCNT at 7 days. Some residual cement particles, $Ca(OH)_2$ cubes or seed like particles as well as C-S-H and MWCNT were seen in this microstructure. Furthermore, the cracks are presumably full with MWCNT and the growth of hydration products ($Ca(OH)_2$ and C-S-H) on the surfaces of hybrid BNP/MWCNT due to the interaction of $C_3S$ and $C_2S$ with functional groups of BNP which are stuck on the surfaces of MWCNT due to hydrophobic-hydrophobic interaction between them.

Figure 6.8(d) shows that the microstructure of cementitious composite which contains hybrid BNP/MWCNT, with a concentration of 0.1 wt% MWCNT at 7 days, displays $Ca(OH)_2$ cubes and seed-like particles as well as C-S-H and well dispersed MWCNT in cracks, with also a growth of hydration products on their surfaces ($Ca(OH)_2$ and C-S-H) in this microstructure.

Figure 6.8(e) illustrates the microstructure of cementitious composite which contains hybrid BNP/MWCNT with a concentration of 0.2 wt% MWCNT at 7 days. Well dispersed MWCNT, $Ca(OH)_2$ flower like crystals and C-S-H were seen in this microstructure. The formation of $Ca(OH)_2$ flower-like crystals could be attributed to the effect of hybrid BNP/MWCNT with a high dosage of MWCNT, which causes a growth of hydration products ($Ca(OH)_2$ and C-S-H) on the surfaces of hybrid BNP/MWCNT. This is due to the interaction of $C_3S$ and $C_2S$ with functional groups of BNP, which are stuck on the surfaces of MWCNT due to hydrophobic-hydrophobic interaction between them. The results indicate that hybrid BNP/MWCNT have a significant effect on the microstructure of cementitious composites and the results confirm that hybrid BNP/MWCNT can control the shape and the ordered arrays of cement hydration products. This also suggests that hybrid BNP/MWCNT work as templates in the formation of hydration products. $Ca(OH)_2$ and C-S-H especially will grow on their surfaces leading to the acceleration of the hydration products. Like GO-cementitious composites, this morphology plays a significant role in the mechanical interaction (i.e. load transfer) between hybrid BNP/MWCNT and the cementitious matrix as it improves the mechanical interlocking (Lv et al., 2013; Lv et al., 2014b).

Figure 6.8(f) shows the microstructure of cement composite with an addition of hybrid BNP/MWCNT with 0.4% MWCNT at 7 days. The microstructure contains $Ca(OH)_2$ and C-S-H. It is worth mentioning that the number of MWCNT had increased due to a high concentration of MWCNT and also worth noting that growth of C-S-H was seen on the surface of MWCNT, confirming our hypothesis about growing hydration products on the surfaces of MWCNT.

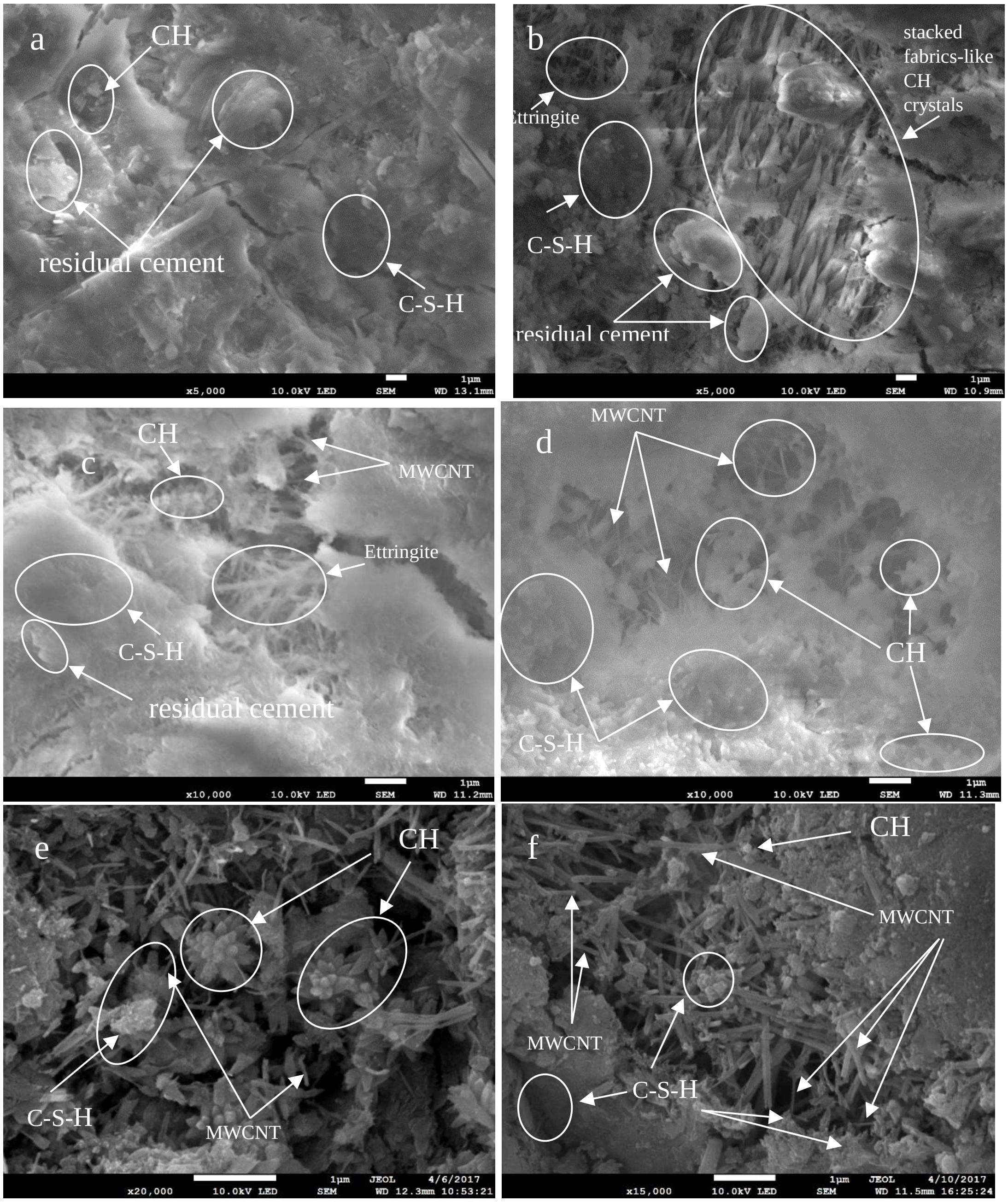

**Figure 6.8:** SEM images of fracture surfaces of the hardened cement pastes with different hybrid BNP/MWCNT contents at 7 days, BNP contents: (a) 0.0%, (b) 0.2%, (c) 0.2%, (d) 0.2%, (e) 0.2%, and (f) 0.2%; MWCNT contents, (a) 0.0%, (b) 0.0%, (c) 0.05%, (d) 0.1%, (e) 0.2% and (f) 0.4%

As shown, the microstructure of the plain cementitious composite at 14 days (figure 6.9 (a)) contains residual cement, few $Ca(OH)_2$ cubes and some C-S-H, which indicates that the hydration process is in progress. On the other hand, denser C-S-H were seen in the microstructure of 0.2% BNP and that supports our hypothesis in chapter four about the effect of BNP on the hydration process. When uniformly distributed, BNP sheets absorb onto the surfaces of the cement particles through their -OH and -OH-$CH_2$ functional groups. These functional groups then react with $C_3S$ and $C_2S$ to form nucleation and growth sites for hydration products.

Figure 6.9(c) shows that the microstructure of cement composite with an addition of hybrid BNP/MWCNT with 0.05% MWCNT at 14 days. Some residual cement grains, $Ca(OH)_2$ cubes and seed-like as well as C-S-H and MWCNT, were seen in this microstructure. Furthermore, the cracks are presumably full of MWCNT and growth of hydration products $Ca(OH)_2$ and C-S-H can be seen on the surfaces of hybrid BNP/MWCNT due to the interaction of $C_3S$ and $C_2S$ with functional groups of BNP which are stuck on the surfaces of MWCNT due to a hydrophobic interaction between them.

Figure 6.9(d) shows the microstructure of cement composite with an addition of hybrid BNP/MWCNT with 0.1% MWCNT at 14 days. MWCNT embedded in dense C-S-H gel were observed in the microstructure. It seems that there is a tremendous difference between this microstructure and the microstructure of plain cement at the same age. The C-S-H gel is more compact due to the effect of hybrid BNP/MWCNT on the hydration process.

Figure 6.9(e) shows the microstructure of cement composite with an addition of hybrid BNP/MWCNT with 0.2% MWCNT at 14 days. C-S-H, $Ca(OH)_2$ flower-like crystals and MWCNT embedded in C-S-H and $Ca(OH)_2$ were seen in this microstructure. It seems that with the increasing the dosage of MWCNT, the flower-like crystals become denser and tend to aggregate. This could have happened due to more MWCNT working as templates in the formation of hydration products, especially $Ca(OH)_2$ and C-S-H, which will grow on their surfaces and lead to the acceleration of the hydration products.

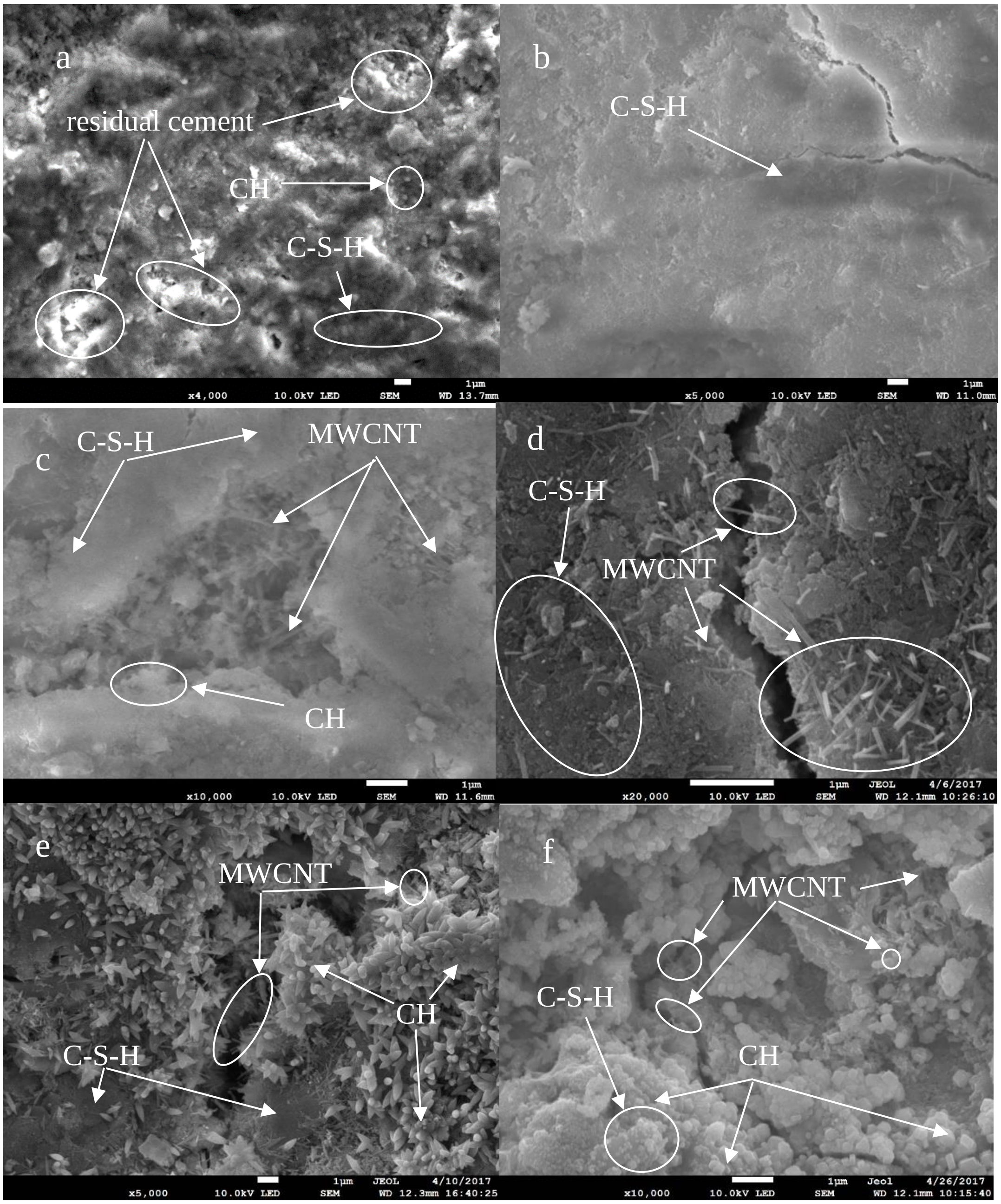

**Figure 6.9:** SEM images of fracture surfaces of the hardened cement pastes with different hybrid BNP/MWCNT contents at 14 days, BNP contents: (a) 0.0%, (b) 0.2%, (c) 0.2%, (d) 0.2%, (e) 0.2%, and (f) 0.2%; MWCNT contents, (a) 0.0%, (b) 0.0%, (c) 0.05%, (d) 0.1%, (e) 0.2% and (f) 0.4%

Figure 6.9(f) shows the microstructure of cement composite with an addition of hybrid BNP/MWCNT with 0.4% MWCNT at 14 days. MWCNT were seen in cracks, $Ca(OH)_2$ crystals transformed from flower-like crystals to cube-like crystals and dense C-S-H were observed. The change in shape of $Ca(OH)_2$ presumably was due to the smaller space available for growing $Ca(OH)_2$ crystals, together with the increase in dosage of MWCNT. Thus more compact, dense and cube-like crystals of $Ca(OH)_2$ were produced.

As shown in figure 6.10(a), the microstructure of the plain cementitious composite at 28 days is mainly composed of $Ca(OH)_2$ in the form of regular polyhedral shaped particles. On the other hand figure 6.10(b) shows that the microstructure of the cement paste is significantly changed with 0.2-wt% BNP. A compact structure can be seen with some $Ca(OH)_2$ crystals embedded into high density C-S-H gel as mentioned earlier and this change in microstructure is due to the effect of BNP.

Figure 6.10(c) shows the microstructure of cement composite with an addition of hybrid BNP/MWCNT with 0.05-wt% MWCNT at 28 days. As shown, there are a few MWCNT embedded in the C-S-H gel and some $Ca(OH)_2$ crystals embedded in the dense C-S-H. It is worth mentioning that there is a significant difference between this microstructure and the microstructure of plain cement due to the effect of hybrid BNP/MWCNT for the reasons mentioned earlier. It is worth noting, however, that there is a slight difference between this microstructure and the microstructure of 0.2-wt% BNP cementitious composite due to the low dosage of MWCNT.

Figure 6.10(d) shows the microstructure of cement composite with an addition of hybrid BNP/MWCNT with 0.1-wt% MWCNT at 28 days. As shown, the intensive growth of $Ca(OH)_2$ flower-like crystals, their change in shape from a polyhedral shape in plain cement, and more dense growth of the C-S-H gel (due to increasing the dosage of MWCNT), has led to the flower-like crystals becoming denser and aggregating. This could be due to more MWCNT working as templates in the formation of hydration products (especially $Ca(OH)_2$ and C-S-H) which grow on the surface and lead to the acceleration of the hydration products. The effect of hybrid BNP/MWCNT on the regulation of hydration products and the formation of flower-like crystals also has a great effect on flexural strength due to these flower-like crystals having a distinct impact on the flextural strength which is caused by the formation of a massive compact cross-linking structure through the flower-like crystals over time. Previous research on cementitious composites containing GO reported similar findings (Lv et al., 2013).

Figure 6.10(e) shows the microstructure of cement composite with the addition of hybrid BNP/MWCNT with 0.2-wt% MWCNT at 28 days. As shown, dense C-S-H gel as well as MWCNT in cracks also promotes growth of hydration products on their MWCNT surfaces. The aggregation of flower-like crystals continued to form a smooth structure and a clear uniform dispersion of MWCNT could easily be observed.

Figure 6.10(f) shows the microstructure of cement composite with an addition of hybrid BNP/MWCNT with 0.4-wt% MWCNT at 28 days. As shown, the microstructure contains $Ca(OH)_2$ flower-like crystals, the growth of hydration products ($Ca(OH)_2$ and C-S-H) on the surfaces of MWCNT and a large number of MWCNT embedded in dense C-S-H gel. These features were due to a high dosage of well dispersed MWCNT and because the surfaces of the MWCNT have BNP, which have a large number of oxygen-containing groups (-OH, -O, and $-CH_2OH$). These functional groups then react with $C_3S$, $C_2S$ to form nucleation and growth sites for hydration phases.

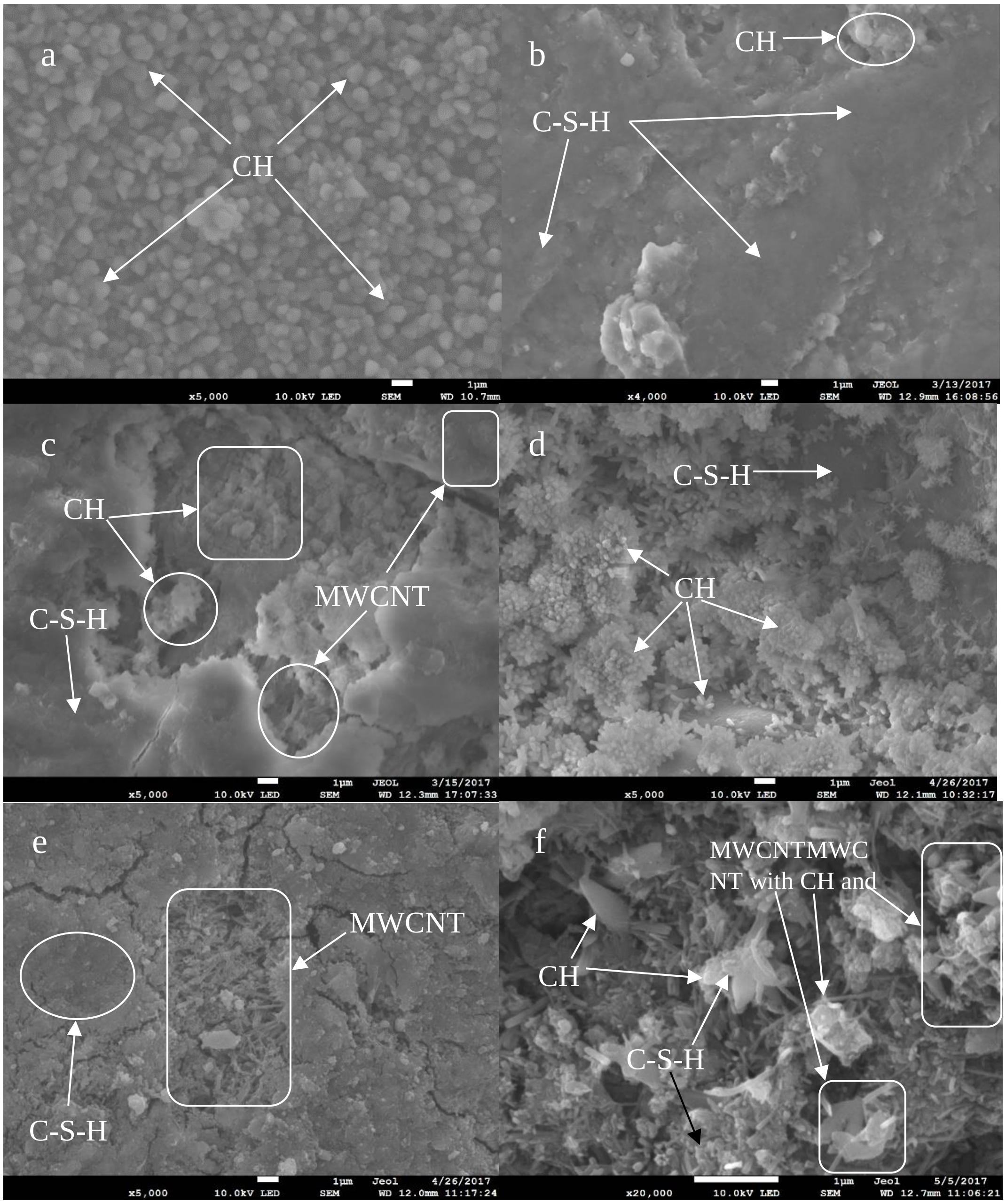

**Figure 6.10:** SEM images of fracture surfaces of the hardened cement pastes with different hybrid BNP/MWCNT contents at 28 days, BNP contents: (a) 0.0%, (b) 0.2%, (c) 0.2%, (d) 0.2%, (e) 0.2%, and (f) 0.2%; MWCNT contents, (a) 0.0%, (b) 0.0%, (c) 0.05%, (d) 0.1%, (e) 0.2% and (f) 0.4%.

The SEM findings confirm that hybrid BNP/MWCNT has three ways of enhancing cementitious composites characteristics. Firstly, through accelerating hydration products.

Secondly, through the regulation of hydration products, as mentioned earlier, the formation of flower-like crystals has a significant effect on flexural strength because a massive compact cross-linking structure through the flower-like crystals is forming over time. Thus flower-like crystals have a distinct impact on the flexural strength. Previous research on cementitious composites containing GO reported similar findings (Lv et al., 2013). Thirdly, through working as reinforcement materials, both BNP and MWCNT have high tensile strength.

### 6.3.2.1 Regulatory effect of hybrid BNP/MWCNT on the microstructure of cementitious composites.

Figure 6.11 shows SEM images of the cement hydration products at 7, 14 and 28 days, which are helpful in understanding their formation process. Figure 6.11(a)-(c) shows a SEM image of cement paste with 0.2% MWCNT and 0.2% BNP. It can be seen from figure 6.11 that the MWCNT fibres are uniformly distributed in the cement matrix and in figure 6.11 (b) that the flower-like products are constructed from thicker rod-like crystals. Over time these flower-like products tend to form a denser structure as can be seen in figure 6.11 (c). In summary, the SEM images in figure 6.11(b) clearly reveal that hybrid BNP/MWCNT can assemble flower-like cement hydration products at different MWCNT dosages ranging from (0.1 -0.4)%.

In accordance with the above results, the following possible regulatory mechanism of hybrid BNP/MWCNT on cement hydration products can be proposed. The surfaces of the MWCNT have BNP which have a large number of oxygen-containing groups (-OH, -O, and -$CH_2OH$). These reactive functional groups react preferentially with $C_3S$, $C_2S$ and $C_3A$ and form growth points for these hydration products, and the hydration reaction continues with the formation of thicker rod-like crystals. These rod-like crystals consist of Aft, AFm, CH and C-S-H and many flower-like crystals result from the effect of BNP/MWCNT on the assembly. The flower-like crystals are usually generated in gaps or holes within cement composites and form a cross-linked structure that can greatly contribute to improving the toughness of the material. Furthermore, at the end of 28 days of hydration, the microstructure becomes denser and compacted due to further growth of hydration products taking place on the hybrid BNP/MWCNT. The presence of MWCNT with a high surface area provide further nucleating sites for hydration products which tend to grow in large numbers.

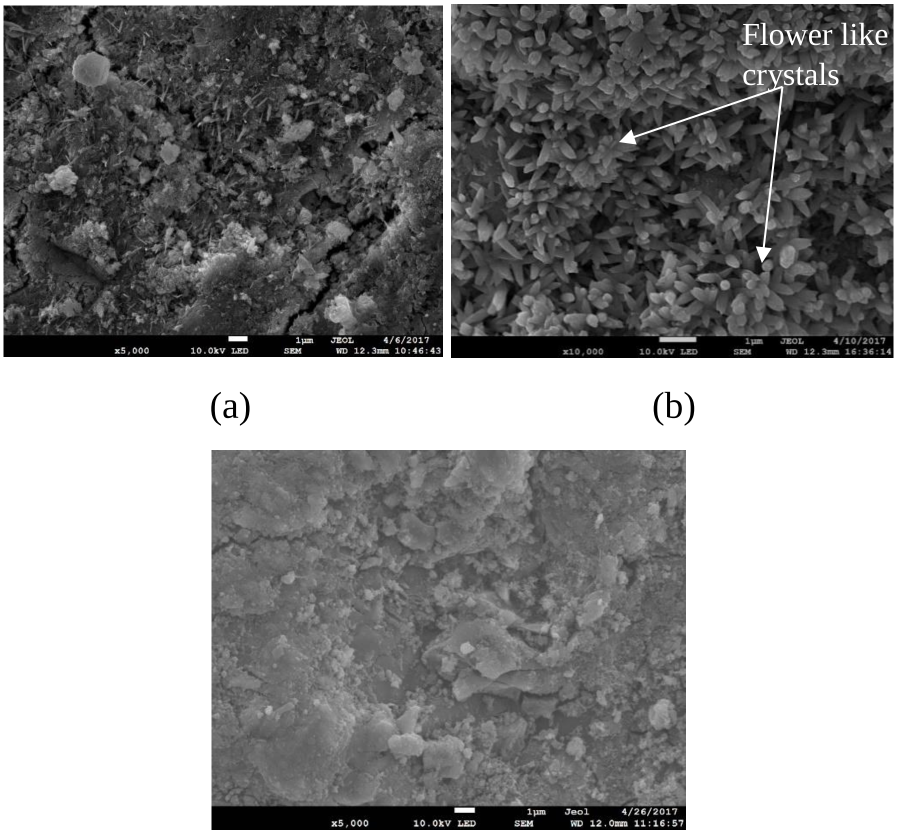

(a) (b)

(c)

**Figure 6.11:** Formation process of cement hydration crystals with 0.2% MWCNT and 0.2% BNP at 7, 14 and 28 days; (a), (b) and (c) respectively.

### 6.3.2.2 Dispersion characteristics of BNP/MWCNT in cementitious composites structure.

The SEM observations of the fractured surface of the hardened cement containing hybrid BNP/MWCNT showed uniform dispersion within the cement matrix. The most important factor in this test was the large areas observed under the SEM which showed uniform dispersion of hybrid BNP/MWCNT. Figure 6.12(a) and (b) show the typical SEM images. In the images below, uniform dispersion of MWCNT can be seen. It has been observed that, the initial uniform dispersion (i.e. formation of individual tubes) observed in aqueous solution for hybrid BNP/MWCNT, emerged in cement matrix. It may be that the electrostatic repulsion forces between the surfaces of BNP disrupt the van der wall forces (i.e. attracting forces between MWCNT) leading to successful reinforcement.

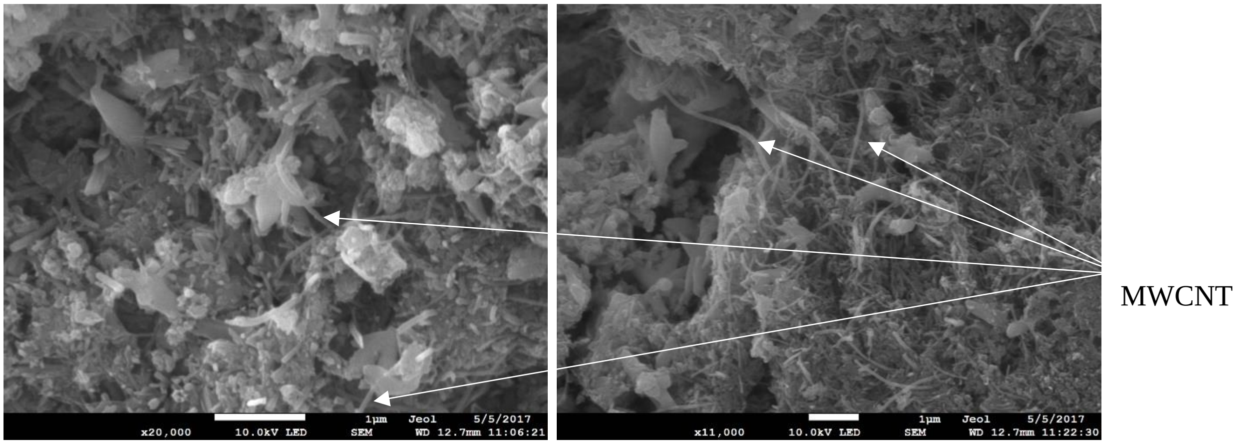

(a) (b)

**Figure 6.12:** (a) and (b) SEM image of the fractured surface with uniform dispersion of MWCNT within the region at 0.2-wt% BNP with 0.4-wt% MWCNT at 28 days

#### 6.3.2.3 Bridging and filling of cracks by BNP/MWCNT in cementitious composite microstructure.

Figure 6.13 (a) shows an SEM image of the plain cement paste with an empty crack (i.e. clear crack with no fibres). Figure 6. 13(b) illustrates MWCNT bridging a micro-crack. Figure 6.13(c) shows MWCNT bridging a crack and filling a hole which offers a different reinforcement mechanism.

These SEM images represent clear evidence that the hybrid BNP/MWCNT particles act as networks and bridge across pores and cracks and consequently this bridging effect of hybrid BNP/MWCNT will lead to higher flexural strength. It is clear that the presence of BNP improves the performance of MWCNT, and possible reasons for this could be that it is improving the chemical bonding between MWCNT and cement products, or that it is due to irreversible adsorption of BNP on the surfaces of MWCNT. It could also be due to the reaction between the active groups of BNP and the chemical phases of cement.

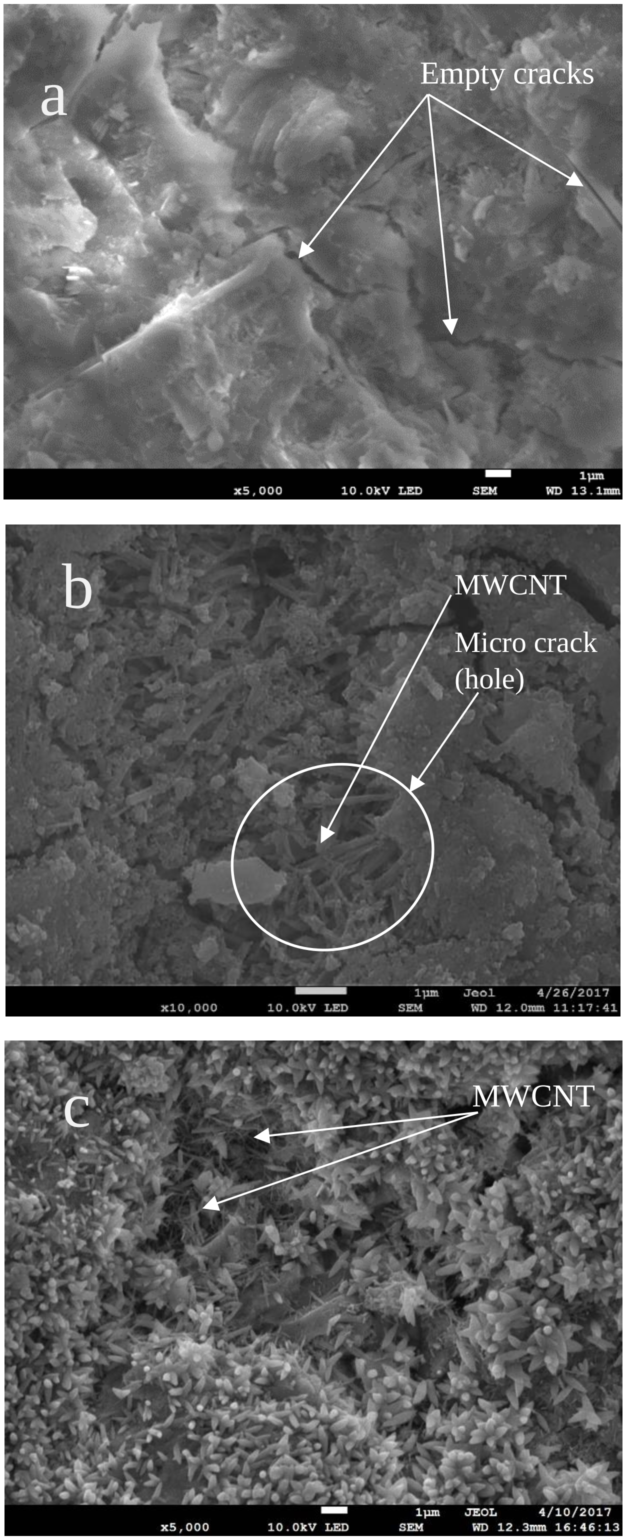

**Figure 6.13:** (a) SEM image of plain cement paste, (b) SEM image of a micro-crack bridged by hybrid BNP/MWCNT and (c) SEM image of hole fill by MWCNT

### 6.3.3 EDS analysis of BNP/MWCNT reinforced cementitious composites

Elemental analyses were performed on samples of cementitious materials to examine the effects of addition of hybrid BNP/MWCNT on the hydration process of cementitious composites. The observations from the results of EDS analyses of cementitious matrices with 0 and 0.4% of MWCNT seemed to indicate that, the incorporation of hybrid BNP/MWCNT into cementitious matrix produced similar elemental compositions to those of the plain cementitious matrix, except for the higher Si content in cementitious composite.

Figures 6.14, 6.15, 6.16, 6.17, 6.18 and 6.19 show the SEM image and EDS results for plain cement paste, cement paste with 0.2% BNP, cement paste with 0.2% BNP and 0.05%, 0.1%, 0.2% and 0.4% MWCNT respectively. It can be seen that the elements for cement paste were Calcium, Oxygen, Silicon, Carbon, Aluminium, Potassium and Magnesium, which are also the main chemical components of cement hydration products.

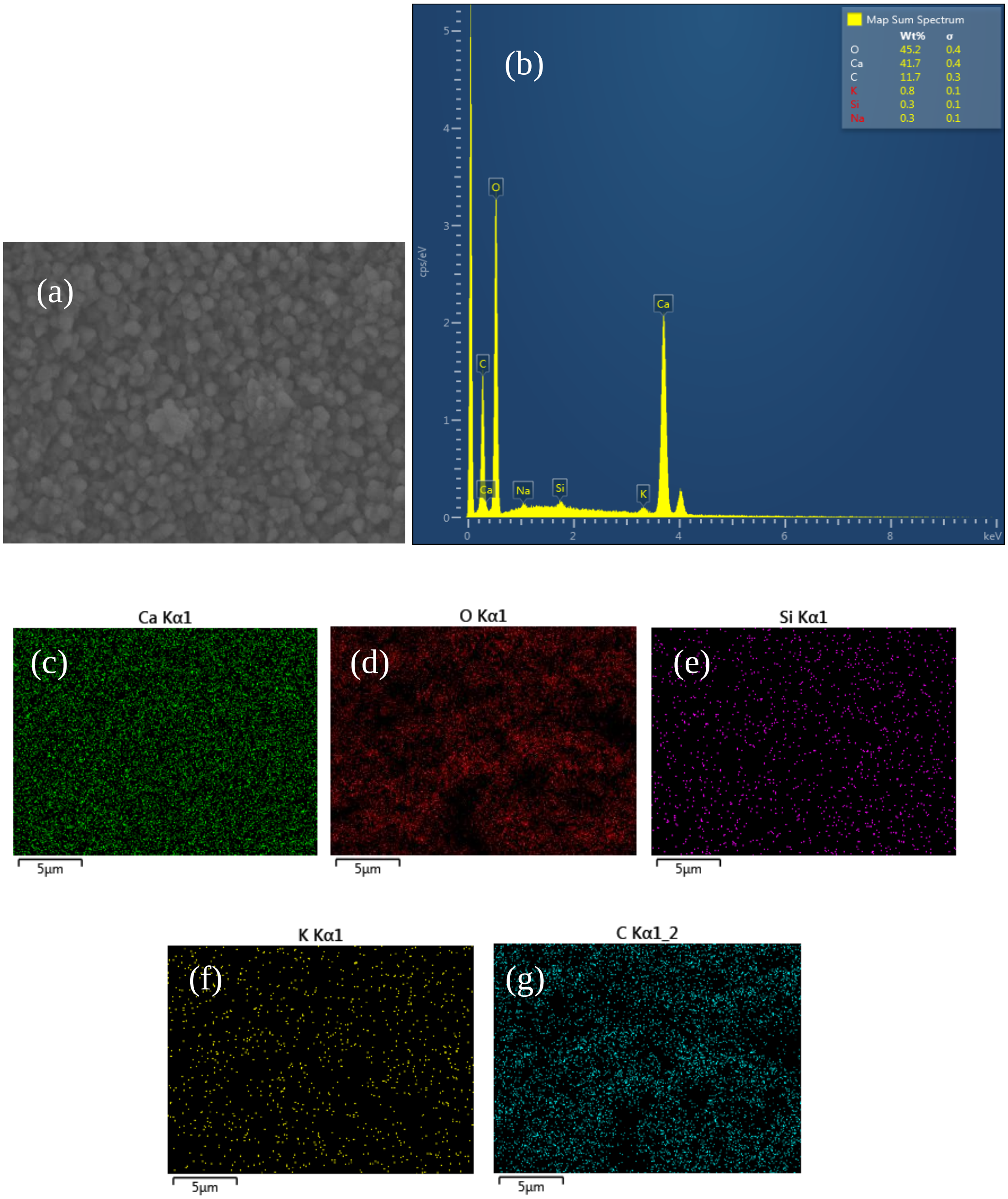

**Figure 6.14:** (a) SEM of plain cement, (b) EDS analysis of plain cement, (c) map content of (Ca), (d) map content of (O), (e) map content of (Si), (f) map content of (K) and (g) map content of (C); all at 28 days age

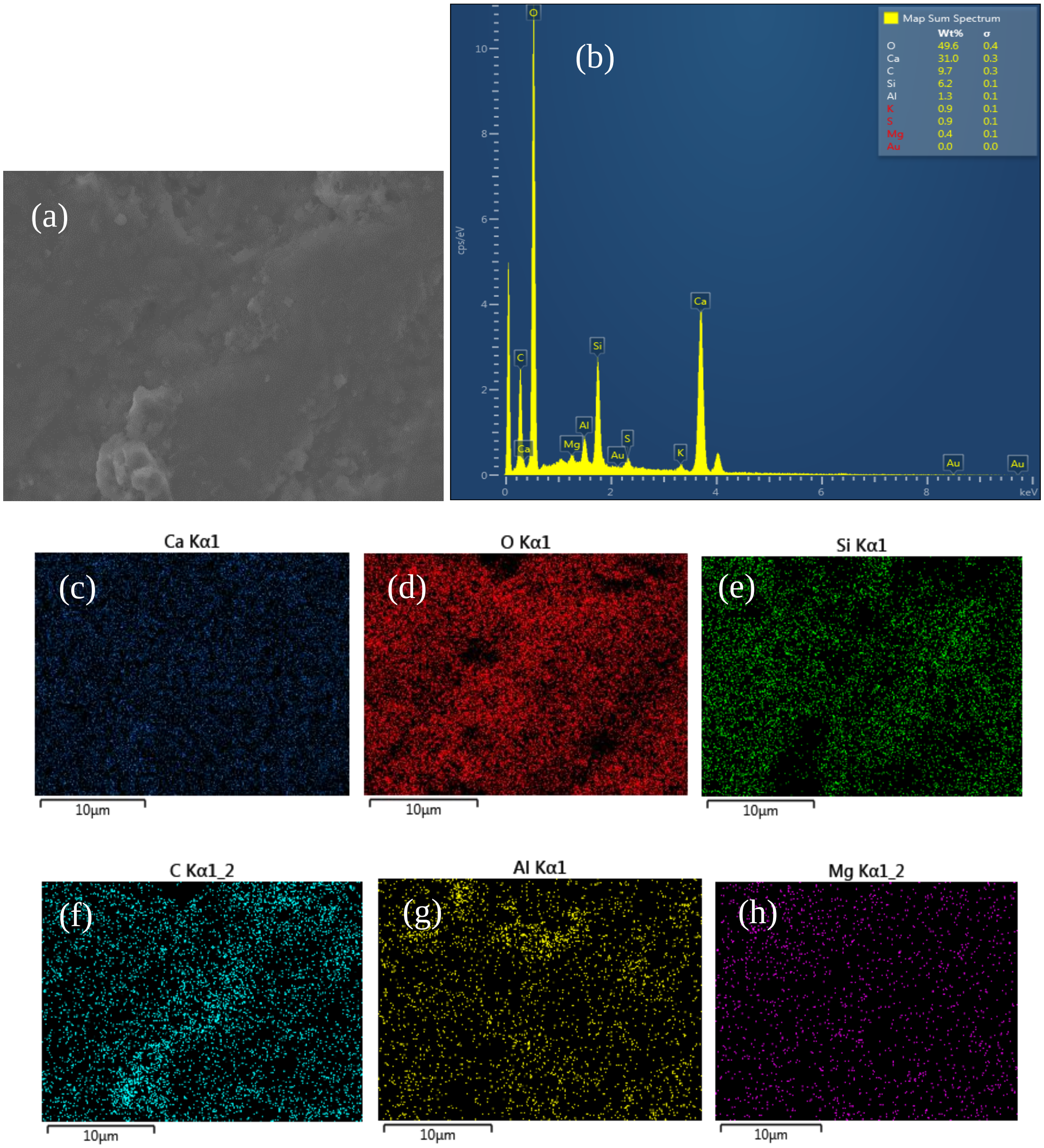

**Figure 6.15:** (a) SEM of cement paste with 0.2 % of BNP, (b) EDS analysis of cement paste with 0.2 % of BNP, (c) map content of (Ca), (d) map content of (O), (e) map content of (Si), (f) map content of (C), (g) map content of (Al) and (h) map content of (Mg); all at 28 days age

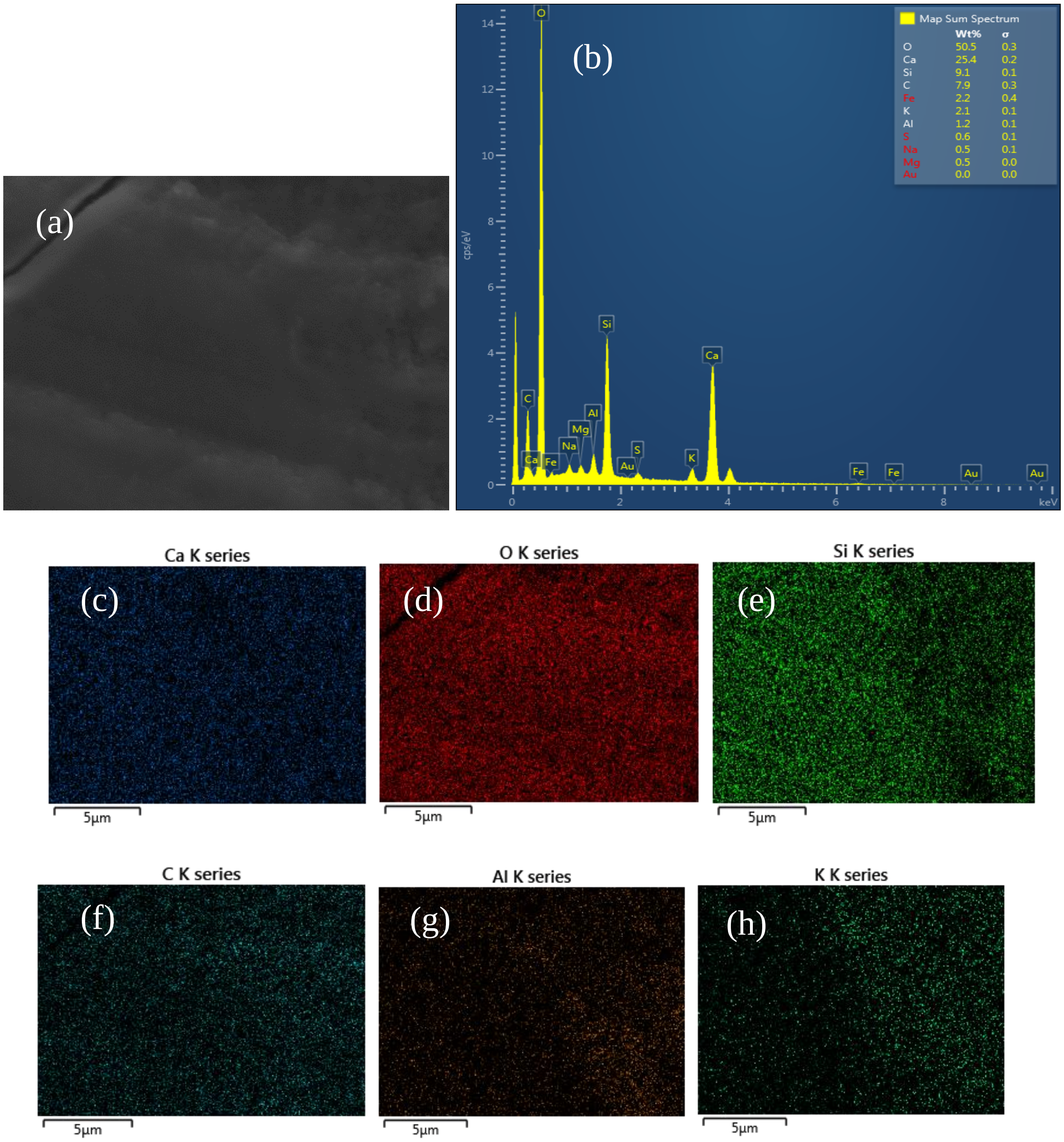

| | Wt% | σ |
|---|---|---|
| O | 50.5 | 0.3 |
| Ca | 25.4 | 0.2 |
| Si | 9.1 | 0.1 |
| C | 7.9 | 0.3 |
| Fe | 2.2 | 0.4 |
| K | 2.1 | 0.1 |
| Al | 1.2 | 0.1 |
| S | 0.6 | 0.1 |
| Na | 0.5 | 0.1 |
| Mg | 0.5 | 0.0 |
| Au | 0.0 | 0.0 |

**Figure 6.16:** (a) SEM of cement paste with 0.2 % of BNP and 0.05% MWCNT, (b) EDS analysis of cement paste with 0.2 % of BNP and 0.05% MWCNT, (c) map content of (Ca), (d) map content of (O), (e) map content of (Si), (f) map content of (C), (g) map content of (Al) and (h) map content of (K); all at 28 days age

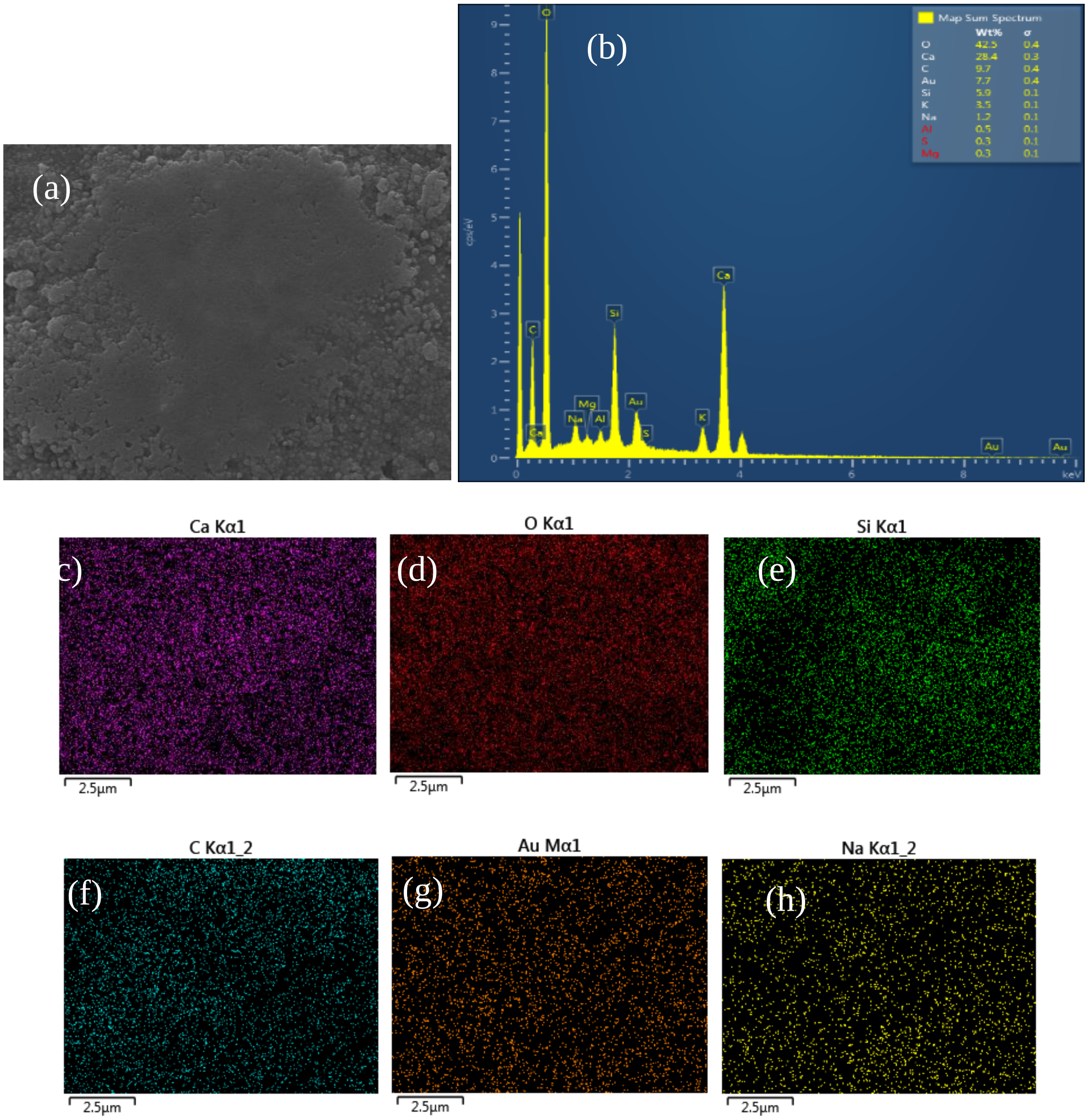

Map Sum Spectrum

| | Wt% | σ |
|---|---|---|
| O | 42.5 | 0.4 |
| Ca | 28.4 | 0.3 |
| C | 9.7 | 0.4 |
| Au | 7.7 | 0.4 |
| Si | 5.9 | 0.1 |
| K | 3.5 | 0.1 |
| Na | 1.2 | 0.1 |
| Al | 0.5 | 0.1 |
| S | 0.3 | 0.1 |
| Mg | 0.3 | 0.1 |

**Figure 6.17:** (a) SEM of cement paste with 0.2 % of BNP and 0.1% MWCNT, (b) EDS analysis of cement paste with 0.2 % of BNP and 0.1% MWCNT, (c) map content of (Ca), (d) map content of (O), (e) map content of (Si), (f) map content of (C), (g) map content of (Au) and (h) map content of (Na); all at 28 days age

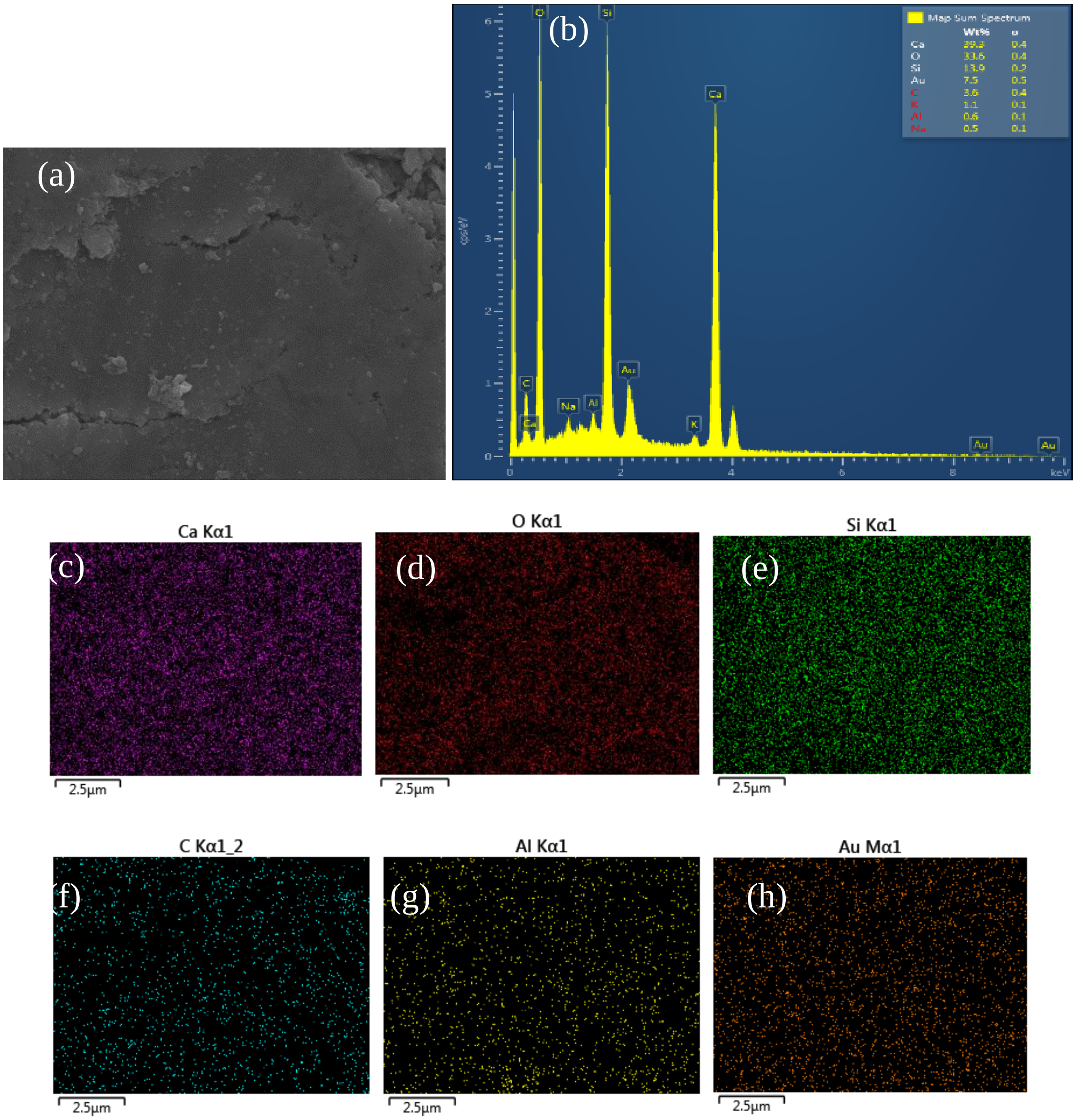

**Figure 6.18:** (a) SEM of cement paste with 0.2 % of BNP and 0.2% MWCNT, (b) EDS analysis of cement paste with 0.2 % of BNP and 0.2% MWCNT, (c) map content of (Ca), (d) map content of (O), (e) map content of (Si), (f) map content of (C), (g) map content of (Al) and (h) map content of (Au); all at 28 days age

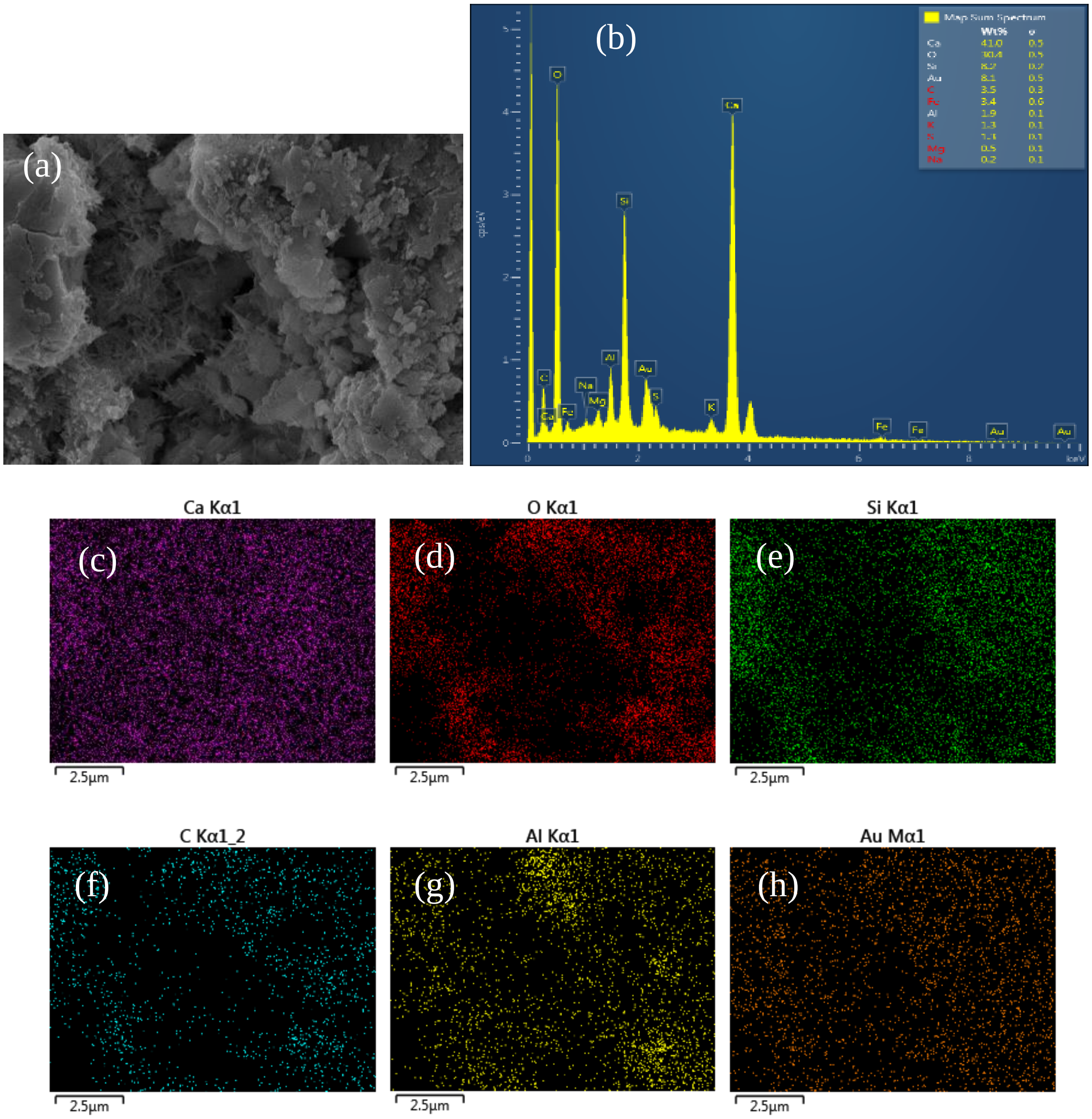

**Figure 6.19:** (a) SEM of cement paste with 0.2 % of BNP and 0.4% MWCNT, (b) EDS analysis of cement paste with 0.2 % of BNP and 0.4% MWCNT, (c) map content of (Ca), (d) map content of (O), (e) map content of (Si), (f) map content of (C), (g) map content of (Al) and (h) map content of (Au); all at 28 days age

### 6.3.4. Interaction between BNP/MWCNT and cement matrix

As mentioned earlier in chapter three, The BNP characterization results indicate that the BNP sheets are fully decorated with hydroxyl functional groups which are responsible for their high chemical reactivity. The hydroxyl functional groups enable hydrophilicity while -H groups cause hydrophobic faces; thus, the appearance of both hydrophilic and hydrophobic faces allow BNP to be used as a dispersant agent to disperse MWCNT. BNP were therefore used to disperse MWCNT, as mentioned in chapter five, and create a novel hybrid nanomaterial which was made from the adsorption of BNP on the MWCNT surfaces (i.e. a self-assembly process) that are easy to attribute to the underlying force which comes from hydrophobic interactions that occur between the side wall of the MWCNT and the surface crystalline plane of the amphiphilic BNP (Mougel et al., 2016; Olivier et al., 2012). The functional groups of the hybrid BNP/MWCNT are believed to adsorb on the surface of the cement particles. In this case, the chemical components of the cement, mainly $C_2S$ and $C_3S$, hydrate over the surface of the BNP sheets, leading to intercalated C-S-H/BNP/MWCNT and $Ca(OH)_2$/BNP/MWCNT particles.

Figure 6.20 shows the chemical interaction of the hybrid BNP/MWCNT with C-S-H. The strong interfacial covalent bonding between C-S-H and the hybrid BNP/MWCNT enhances the stress transfer thus improving the overall mechanical properties of the cementitious composites.

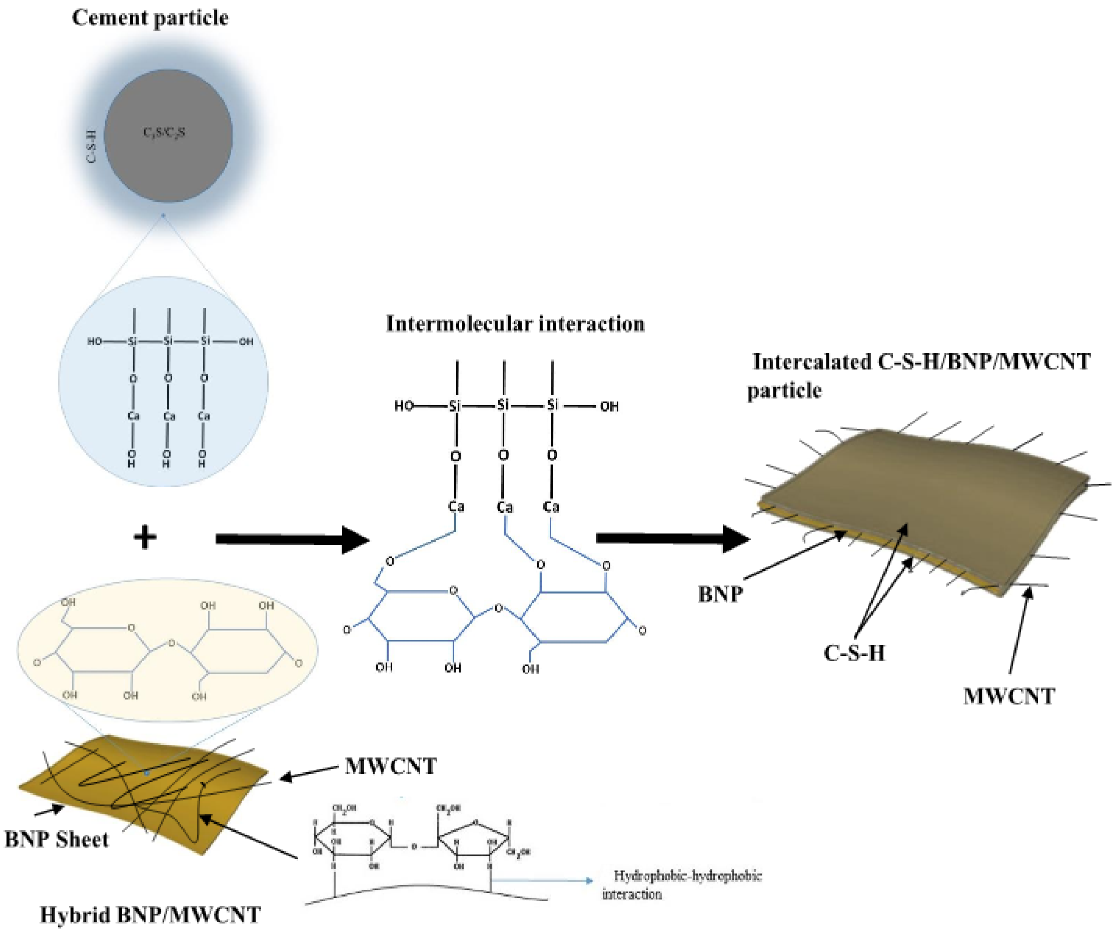

**Figure 6.20:** Intermolecular interaction of BNP/MWCNT with C-S-H phase

Figure 6.21 shows the chemical interaction of the BNP/MWCNT with $Ca(OH)_2$. The strong interfacial covalent bonding between $Ca(OH)_2$ and the hybrid BNP/MWCNT enhances the stress transfer thus improving the overall mechanical properties of the cementitious composites.

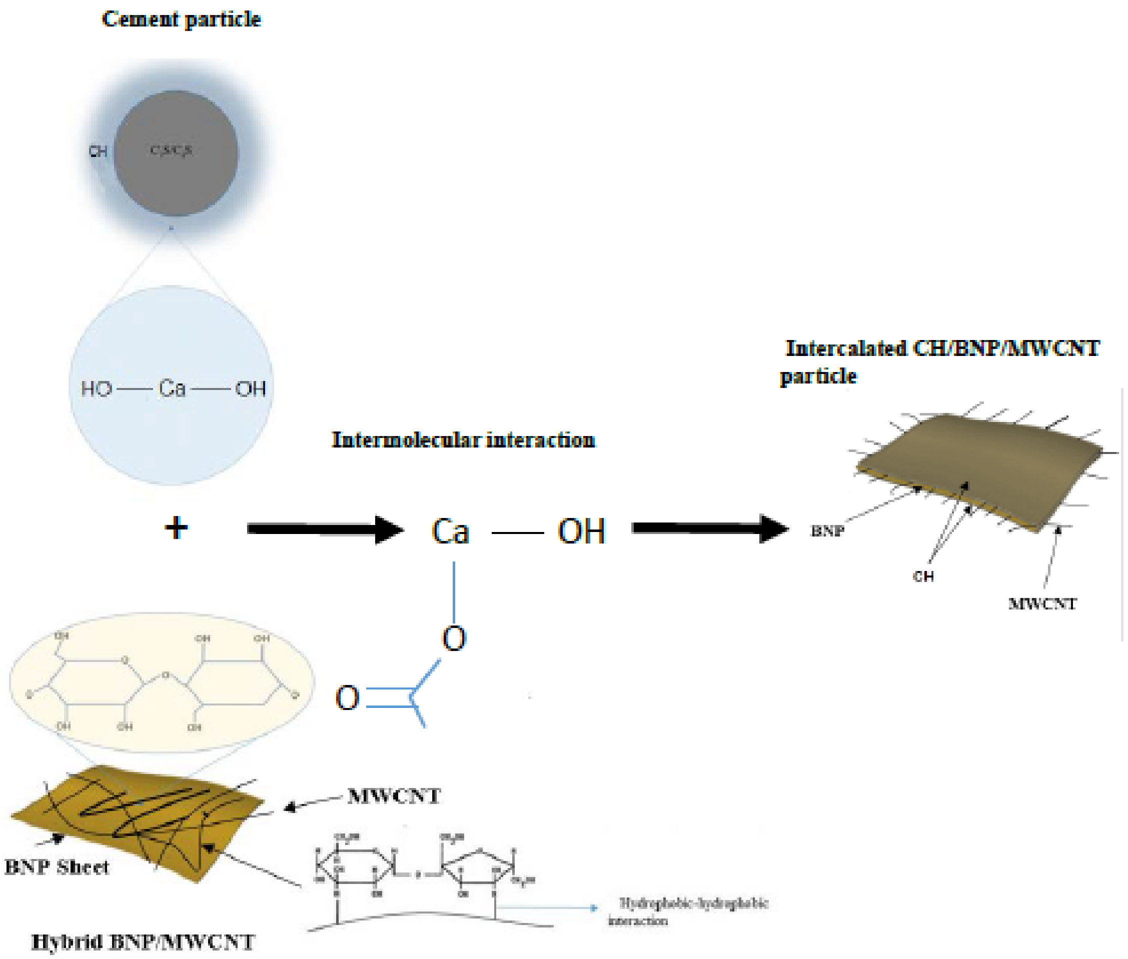

**Figure 6.21:** Intermolecular interaction of BNP/MWCNT with Ca(OH)$_2$ phase

## 6.3.5 Influence of BNP/MWCNT on mechanical properties of cementitious composites.

### 6.3.5.1 Effect of BNP/MWCNT on flexural strength of cementitious composites

The flexural tests were performed at the age of 7, 14 and 28 days and the average peak stress (i.e. the average flexural strength) results are shown in figure 6.22. At 7 days an increase of 67% in flexural strength was observed for 0.4% MWCNT and this rose to 125%

increase at 14 days. For 0.1% MWCNT, an increase of 133% above the plain cement was seen at 28 days. In addition, the results obtained at 28 days for 0.2% and 0.4% MWCNT were similar to those of the 0.1% MWCNT, suggesting concentrations of 0.1% MWCNT and above could result in similar reinforcement effects. The 7 and 14-day test for 0.05% MWCNT showed an increase in flexural strength of 4% and 25% respectively. However, at 28 days, the strength of 0.05% MWCNT showed a 26% increase above the plain cement. At 28 days, 0.2% MWCNT increased 114% and 0.4% MWCNT increased 127% above the reference sample.

The results in figure 6.22 appear to illustrate the trend that flexural strength is age-dependent. The development of flexural performance could be due to improving the bonding between cement and hybrid BNP/MWCNT and the concentration of C-S-H increasing and becoming more influential over time.

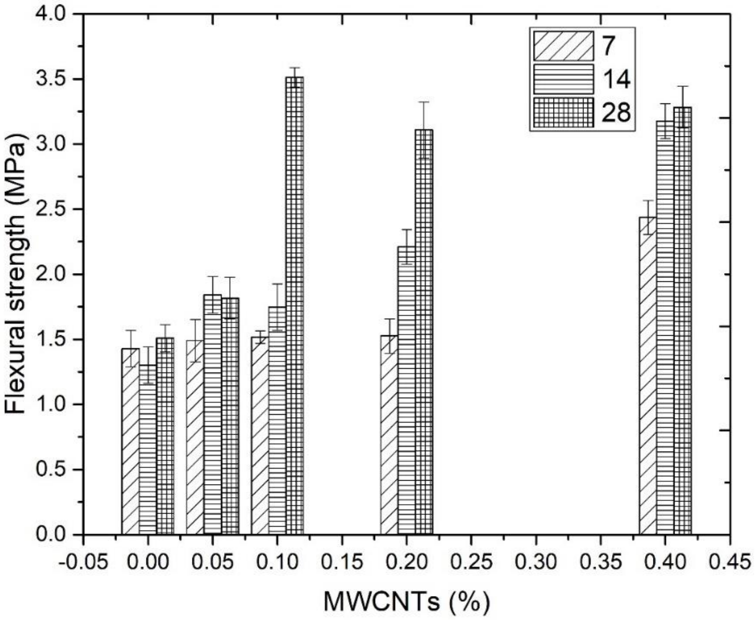

**Figure 6.22:** Flexural strength of hydrated cement paste with MWCNT

Figures 6.23, 6.24 and 6.25 show flexural strength versus displacement at 7 days, 14 days and 28 days respectively, and the curves from all the batches have some common features. They are not linear at the beginning of the loading, a phase known as “seating”. The reason may be that the beam surfaces were not totally flat and some of the initial applied load was consumed to increase the contact area between the load points and the beam.

For 7-day test, the load capacity reached its highest level for 0.4% MWCNT, followed by 0.2% MWCNT. In contrast, the load capacity reached the lowest level for plain cement. In addition, 0.4% MWCNT had the highest stiffness. Plain cement had the lowest level of stiffness. 0.4% MWCNT had the highest toughness (area under flexural strength-disp. curve), in contrast, 0.1% MWCNT had the lowest toughness.

For 14-day test, the load capacity reached its highest level for 0.4% MWCNT, followed by 0.2% MWCNT. In contrast, the load capacity reached its lowest level for plain cement. In addition, 0.1% MWCNT had the highest level of stiffness. In contrast, plain cement had the lowest level of stiffness.

For 28-day test, the load capacity reached its highest level for 0.1% MWCNT followed by 0.4% MWCNT. In contrast, the load capacity reached its lowest level for plain cement. In addition, 0.4% MWCNT had the highest level of stiffness. Plain cement had lowest level of stiffness. 0.2% MWCNT had the highest level of toughness, in contrast plain cement had lowest level of toughness.

the addition of hybrid BNP/MWCNT generally improves load capacity, stiffness and the area under the curve with increase in amount of MWCNT. This is probably due, in part, to the better dispersion of MWCNT with the presence of BNP and the reinforcing effect of

MWCNT. As well as, the tensile strength of MWCNT is more than 10 GPa, which is far higher than that of the cement matrix.

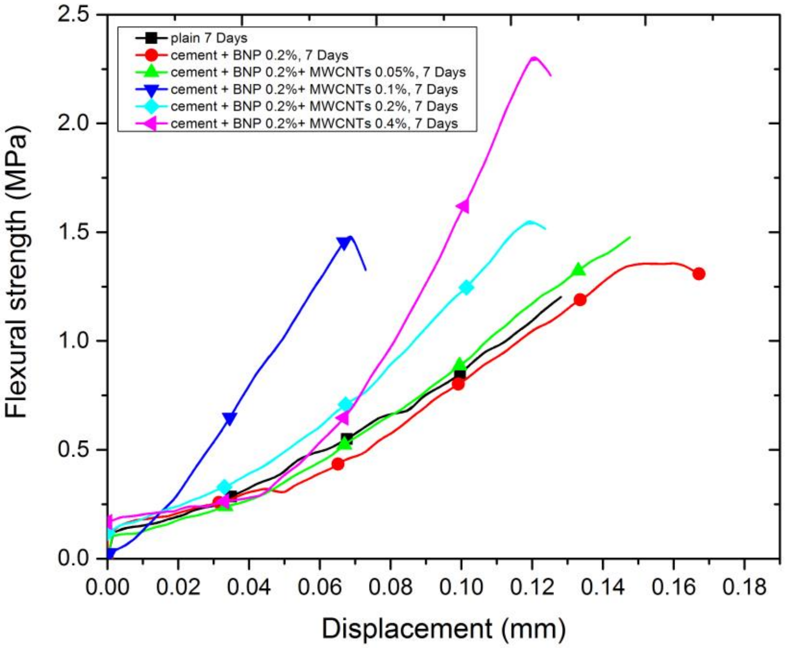

**Figure 6.23:** Flexural strength of hydrated cement paste with MWCNT versus displacement at 7 days

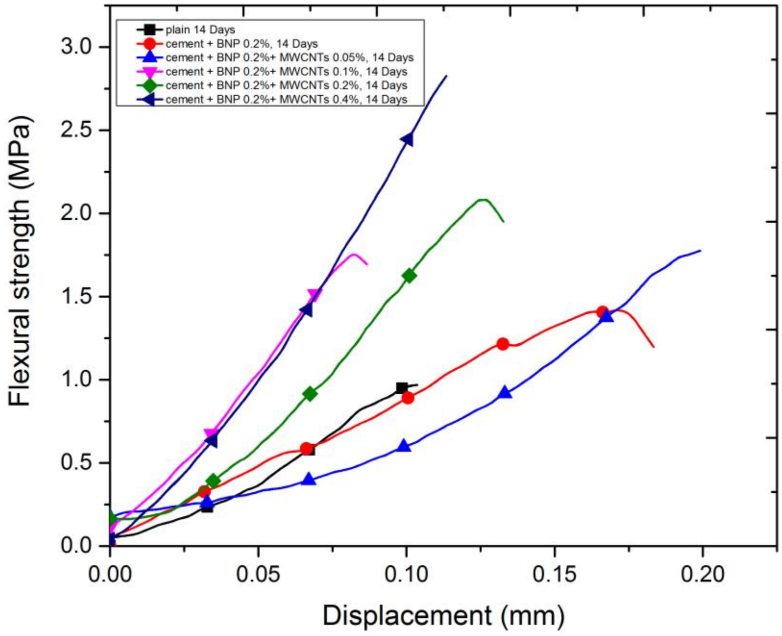

**Figure 6.24:** Flexural strength of hydrated cement paste with MWCNT versus displacement at 14 days

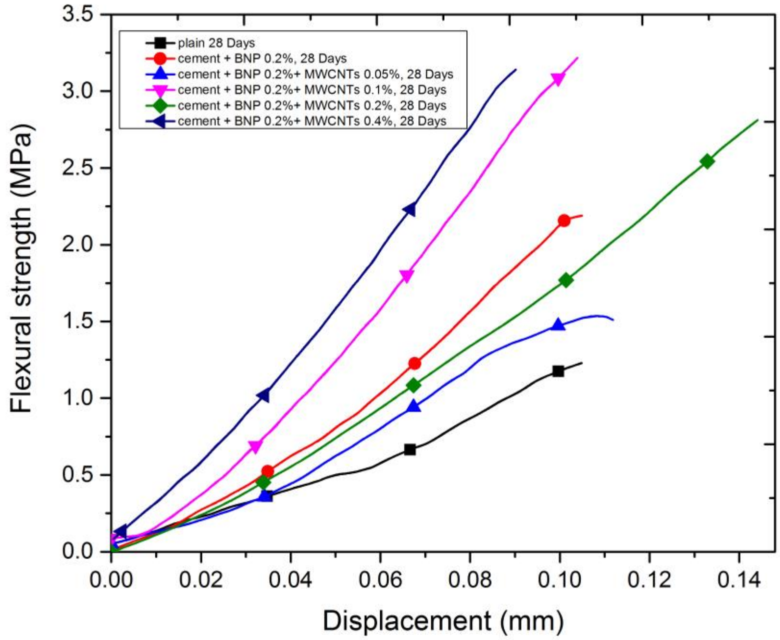

**Figure 6.25:** Flexural strength of hydrated cement paste with MWCNT versus displacement at 28 days

Figure 6.26 shows the modulus of elasticity of cement pastes, as a function of MWCNT content at 7, 14 and 28 days. It clearly illustrates that the modulus of elasticity of cement pastes increased sharply at all ages up to 0.1% MWCNT, then decreased at 0.2% MWCNT. After that, the modulus of elasticity of cement pastes increased clearly at 0.4% MWCNT at all ages. At 28 days age the modulus of elasticity increased slightly from 0.1% to 0.4% MWCNT. This trend is also observed for flexural strength which showed a small difference in flexural strength between 0.1% and 0.4% MWCNT.

As can be seen from this figure 6.26, the results clearly show that the modulus of elasticity of 0.2% MWCNT cement paste is lower when compared with the modulus of elasticity of 0.1% and 0.4% MWCNT cement pastes at all ages. This is likely due to non-uniform dispersion of MWCNT. Although all samples are cast from the same mix and cured under the same conditions with a uniform distribution of MWCNT in aqueous solution, all these processes do not guarantee a uniform distribution of the MWCNT in the composite. This has led to a non-uniform distribution of stress in the composite beam and will cause variability in the modulus of elasticity from one sample to another sample (Abu Al-Rub et al., 2012). The non-uniform distribution of MWCNT in the composite could be caused by the assembly of cement grains once added to the aqueous solution. These grains would hydrate and work as a filter preventing MWCNT to pass among the grains leading to a large area with few MWCNT and other areas with large agglomerations of MWCNT (Tyson et al., 2011).

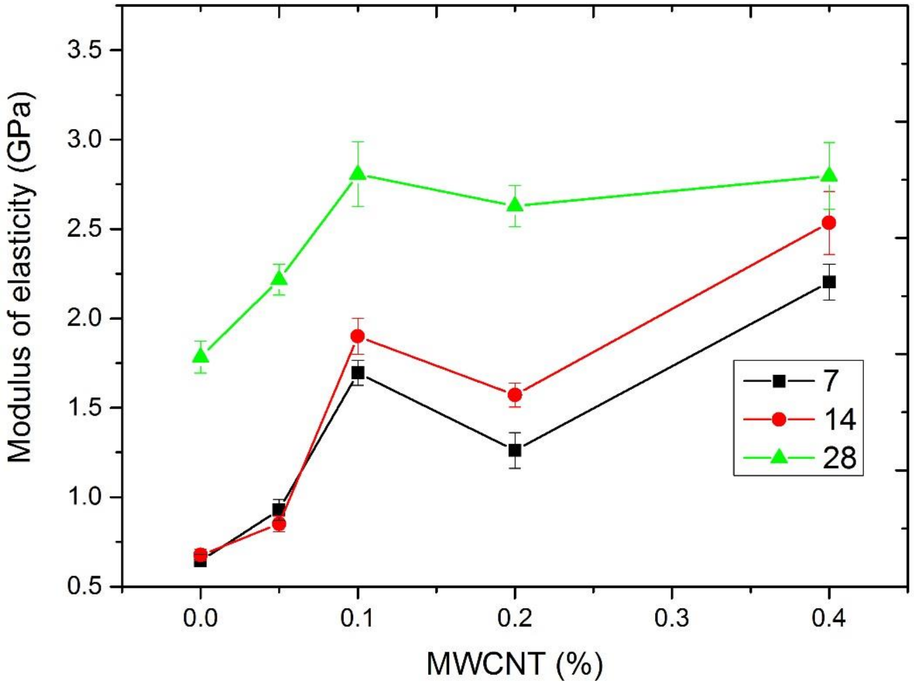

**Figure 6.26:** Modulus of elasticity (GPa) of hydrated cement paste versus MWCNT (%) at 7, 14 and 28 days

### 6.3.5.2 Influence of BNP/MWCNT on the fracture properties of cementitious.

Figure 6.27 shows the measured load versus CMOD responses of the plain prism, the BNP prism and the prisms with BNP and 0.05%, 0.1%, 0.2% and 0.4% MWCNT, that is, the load versus CMOD curves for the cement pastes at 28 days. It is worth mentioning that it was not possible to experimentally capture the post-cracking response of the prisms due to the limitation of the test machine employed in this investigation. As shown, for the BNP prism, the fracture load, stiffness and the amount of absorbed energy are significantly increased, thus there are better fracture properties.

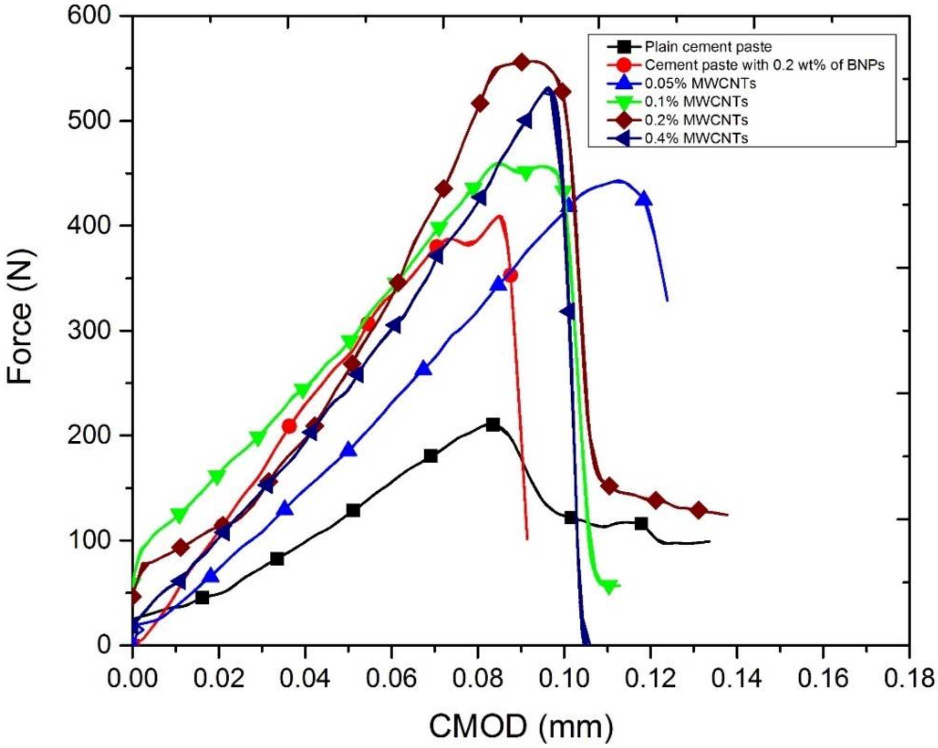

**Figure 6.27:** Fracture force versus CMOD curves

The fracture load, stiffness and the amount of absorbed energy reached their highest level for the prism with BNP and 0.2% MWCNT, followed by the prism with BNP and 0.4% MWCNT. In contrast, the fracture load, stiffness and the amount of absorbed energy reached their lowest level for plain cement. In addition, nearly twice the fracture load, stiffness and the amount of absorbed energy of the plain prism was noticed for the prisms with BNP and 0.05%, 0.1% MWCNT. There is an increase in the fracture properties which has happened as a result of the reinforcing effect of MWCNT and the better dispersion of MWCNT with the presence of BNP (i.e. uniform distribution of stress as a result of uniform distribution of MWCNT). Furthermore, the tensile strength of MWCNT is more than 10 GPa, which is far higher than that of the cement matrix. Thus the fracture properties increased as a result of crack bridging action and the progressive withdrawal of well distributed MWCNT. As can be seen from the results displayed in table 6.2, the incorporation of 0.2% BNP resulted in an increase in fracture energy of 81.8%. The fracture toughness showed an increase of 92.5%; and the modulus of elasticity showed an increase of 95.1% respectively.

Table 6.2 Fracture energy (GF), Fracture toughness (Kic) and Modulus of Elasticity (E) of plain cement and with 0.2% BNP

| | Plain cement | 0.2% BNP |
|---|---|---|
| GF (N/M) | 10.08 | 18.33 (81.8%) |
| Kic (mpa/m^0.5) | 0.1575 | 0.3032 (92.5) |
| E (GPa) | 2.618 | 5.11 (95.1%) |

Figure 6.28 shows fracture energy versus BNP concentration. It is clear that there is an increase in fracture energy with an addition of BNP.

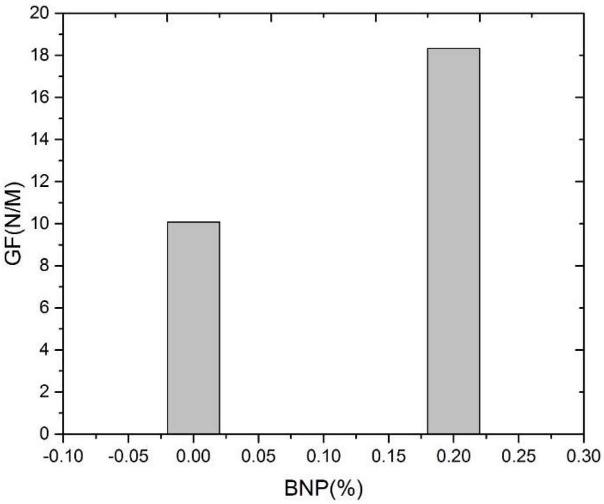

**Figure 6.28:** Fracture energy versus BNP (%) only

Figure 6.29 illustrates that the addition of BNP to cementitious composite leads to an enhancement of fracture toughness. Figure 6.30 shows that the Modulus of elasticity of cementitious composite improved with the addition of BNP.

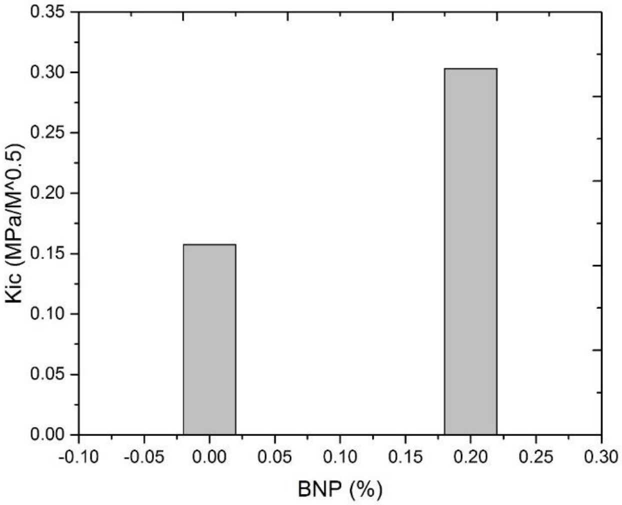

**Figure 6.29:** Fracture toughness versus BNP (%) only

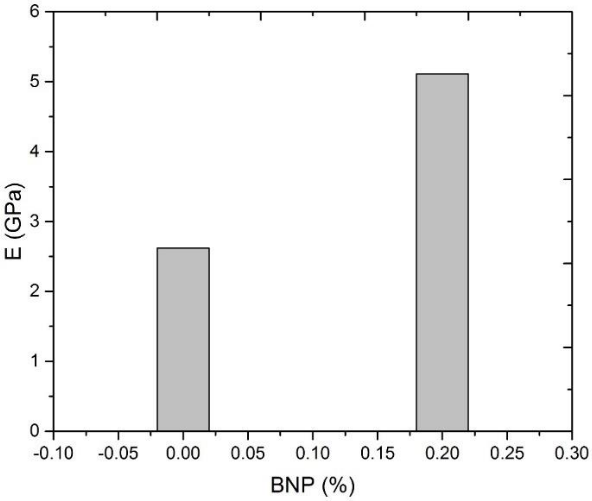

**Figure 6.30:** Modulus of elasticity versus BNP (%) only

The incorporation of the hybrid BNP/MWCNT at 0.05% MWCNT, 0.1% MWCNT, 0.2% MWCNT and 0.4% MWCNT resulted in an increase in fracture energy of 134%, 145%, 183% and 136% respectively as shown in table 6.3 and figure 6.31.

Table 6.3 Fracture energy (GF), Fracture toughness (Kic) and Modules of Elasticity (E) of plain cement and hybrid BNP/MWCNT

| | Plain cement | 0.05% MWCNT | 0.1% MWCNT | 0.2% MWCNT | 0.4% MWCNT |
|---|---|---|---|---|---|
| GF (N/M) | 10.08 | 23.61 (134%) | 24.77 (145%) | 28.6 (183%) | 23.8 (136%) |
| Kic (mpa/m^0.5) | 0.1575 | 0.3289 (109%) | 0.338 (114%) | 0.4128 (162%) | 0.3935 (149%) |
| E (GPa) | 2.618 | 6.23 (138%) | 6.58 (151%) | 9.82 (275%) | 8.92 (240%) |

Figure 6.31 illustrates that there is a dramatic increase of fracture energy with the increase in concentration of MWCNT. The fractue energy reached its highest level at 0.2% MWCNT.

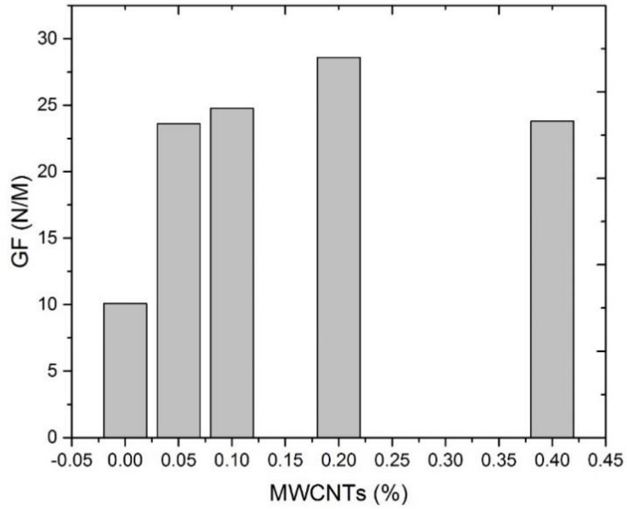

**Figure 6.31:** Fracture energy versus hybrid BNP/MWCNT with different dosages of MWCNT

As shown in figure 6.32, there is a gradual increase of fracture toughness with the increase in concentration of MWCNT.

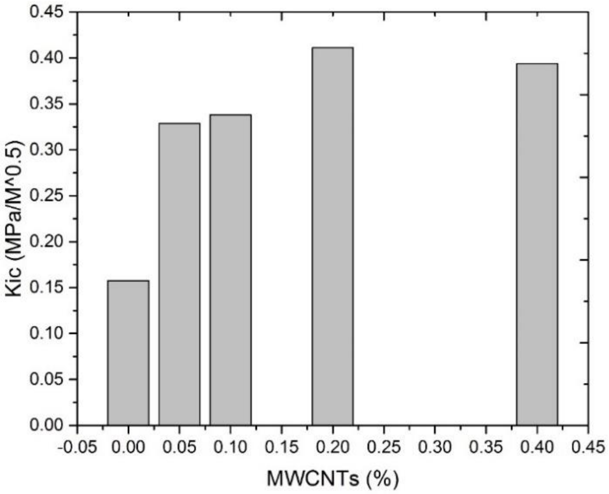

**Figure 6.32:** Fracture toughness versus hybrid BNP/MWCNT with different dosages of MWCNT

The fracture toughness reached its highest level at 0.2% MWCNT. The fracture toughness increased by 109%, 114%, 162% and 149% respectively with the concentrations of MWCNT (0.05%, 0.1%, 0.2% and 0.4%) as shown in table 6.3 and figure 6.32.

As can be seen from figure 6.33, there is a dramatic rise of modulus of elasticity with the increase in concentration of MWCNT. The modulus of elasticity reached its highest level at 0.2% MWCNT.

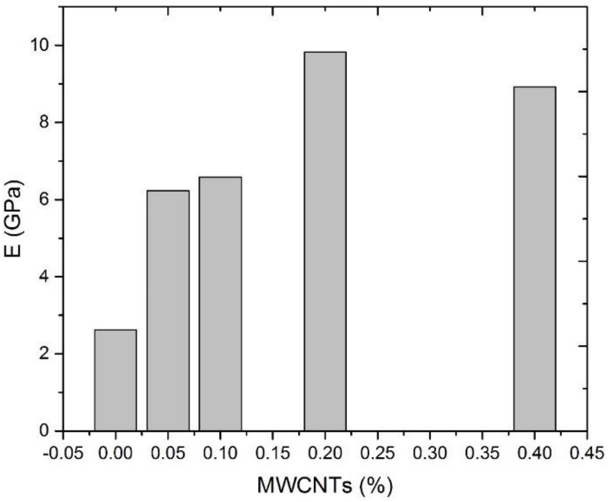

**Figure 6.33:** Modulus of elasticity versus hybrid BNP/MWCNT with different MWCNT dosage

The modulus of elasticity increased by 138%, 151%, 275% and 240% respectively over plain cement mixture in line with the increasing concentration of MWCNT (0.05%, 0.1%, 0.2% and 0.4%) respectively as shown in table 6.3 and figure 6.33.

### 6.3.5.3 Effect of BNP/MWCNT on the compressive strength of cementitious composites.

The compressive properties of the cement paste are more likely to be controlled by the cement matrix and not by fibre reinforcement. Figure 6.34 shows the results of compressive strength according to different levels of MWCNT and clearly illustrates that the addition of MWCNT had no statistically significant effect on the compressive strength of cement paste. Similarly, there were no significant differences between the compressive strength of plain cement and the compressive strength of cement pastes reinforced by all percentages of MWCNT. The effect of hybrid BNP/MWCNT on regulation hydration products and formation flower-like crystals has a great effect on flexural strength and has no effect on compressive strength. These flower-like crystals have a distinct impact on the flextural strength which is caused by the formation of a massive compact cross-linking structure through the flower-like crystals over time. Previous research on cementitious composites contianing GO reported similar findings (Lv et al., 2013).

The presence of MWCNT agglomerates at 0.4% MWCNT did have slightly negative effects on the compressive properties. The MWCNT agglomerates were randomly distributed within the cement matrix and acted as stress concentrators (i.e., defects) within the cement matrix creating zones of weakness in composite materials. When a load was applied, the agglomeration of MWCNT performed as voids, influencing the compressive properties such as porosity (i.e., compressive strength generally decreased with increased size of the porosity). Addition of 0.4% MWCNT resulted in a slight decrease in the compressive strength compared with the control sample; this may have been due to many MWCNT agglomerates being present in the cement matrix.

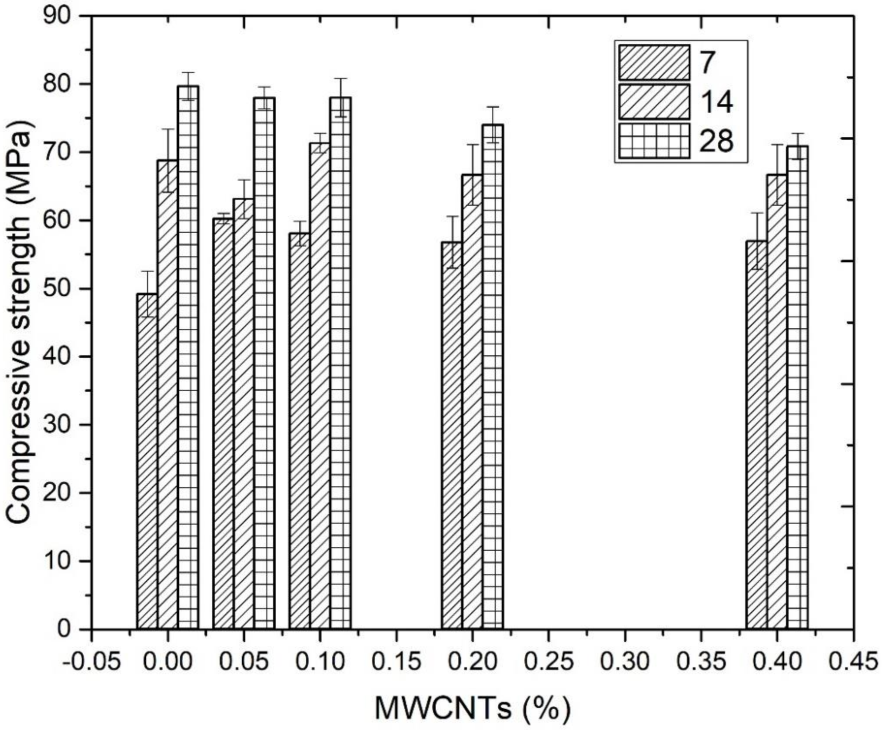

**Figure 6.34:** Compressive strength of hardened cement paste with MWCNT (%)

Although the presence of MWCNT in the cement matrix had limited effects on the composite compressive properties, the addition of MWCNT noticeably enhanced the structural integrity of the composites after compressive testing. This suggests that the propagation of cracks may be controlled by the network created by the MWCNT inside of the agglomerates, creating opportunities for the cement matrix to hold together even after multiple cracking events.

### 6.3.6 Comparisons with previous studies

There have been many renowned studies into the enhancement of the flexural strength of cementitious composites using a range of additives including Cellulose Nanocrystals, MWCNT and GOs. This study investigated the addition of 0.2-wt% of BNP and 0.1-wt%

MWCNT at 28 days and the effects of this additive in comparison with traditional materials as outlined below. Figure 6.35 summarises the maximum enhancement of the flexural strength of BNP/MWCNT used in this study compared to that of Cellulose Nanocrystals (CNC) by Cao et al. (2015, 2016). As shown flexural strength was improved in most cases with significant amounts of BNP/MWCNT and CNC. The observed best performance enhancement included a 133% increase of flexural strength with 0.2-wt% of BNP and 0.1-wt% MWCNT, which is higher than a 50% increase of flexural strength with 0.5-1.5-vol% of CNC (Cao et al., 2016b) and a 30% increase with 0.2-vol% CNC (Cao et al., 2015).

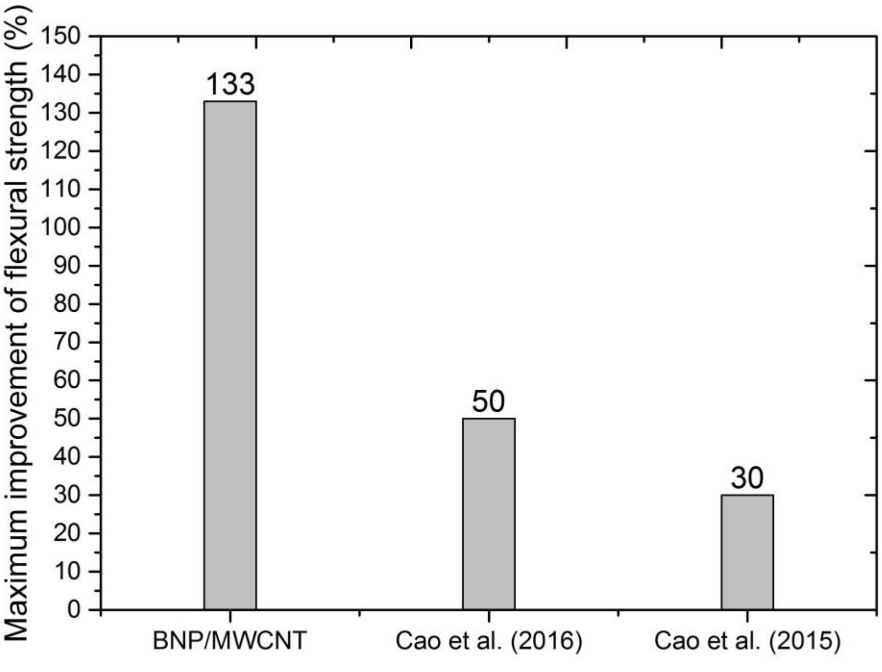

**Figure 6.35:** Maximum enhancement of flexural strength; comparison of BNP/MWCNT and CNC

In addition, the maximum improvement of flexural strength using MWCNT when compared with BNP/MWCNT, as in this research, is summarised in Figure 6.36. In all cases the flexural strength was enhanced with additions of BNP/MWCNT and MWCNT. The best performance enhancement included a 133% increase of flexural strength with 0.2-wt% of BNP and 0.1-wt% MWCNT, which is higher than a 50% increase with 0.1-wt% of MWCNT (Tyson et al., 2011), a 35.5% increase with 0.2wt% of MWCNT (Luo et al., 2009), a 35% increase with 0.08wt% of MWCNT (Metaxa et al., 2012b), a 38% increase with 0.2wt% of MWCNT (Xu et al., 2015), a 25% increase with 0.5wt% of MWCNT, a 10% increase with 0.042wt% of MWCNT (Li et al., 2005), a 34% increase with 0.5wt% of MWCNT (Musso et al., 2009), a 40% increase with 0.08wt% of long MWCNT (Konsta-Gdoutos et al., 2010), a 25% increase with 0.25wt% of MWCNT (Chan and Andrawes, 2010), and a 50% increase of flexural strength with 0.048wt% of Carbon Nanofibres (CNFs)(Metaxa et al., 2012a).

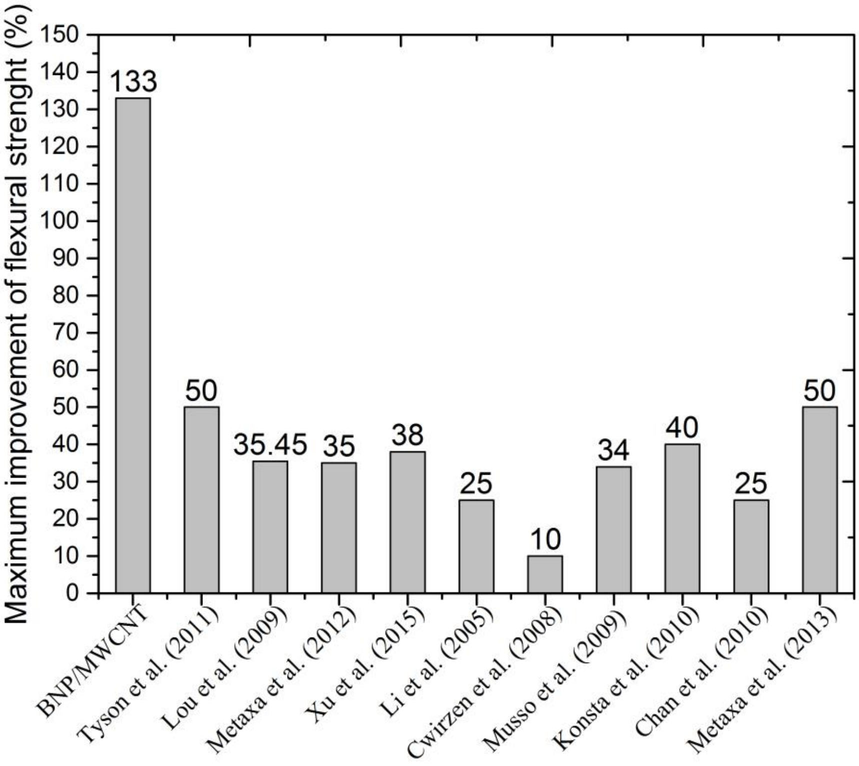

**Figure 6.36:** Maximum enhancement of flexural strength; comparison of BNP/MWCNT and MWCNT

Figure 6.37 summarises the maximum improvement of flexural strength using BNP/MWCNT compared with those studies using GO, and, as seen previously, the flexural strength was improved with the addition of both BNP/MWCNT and GO. The best performance enhancement included a 133% increase of flexural strength with 0.2-wt% of BNP and 0.1-wt% MWCNT, which is higher than a 67.1% increase with 0.04-wt% of GO (Lv et al., 2014b), a 42.1% increase with 0.05-wt% of GO (Lv et al., 2014a), a 60.7% increase with 0.03-wt% of GO (Lv et al., 2013), a 31.63% increase with 0.01-wt% of GO (Zhang H, 2015), a 14.2% increase with 0.04-wt% of GO (Li et al., 2017), a 16.7% increase with 0.04-wt% of GO (Zhou et al., 2017), a 59% increase with 0.05-wt% of GO (Muhit B. 2015), and a 30.37% increase of flexural strength with 0.022-wt% of GO (Zhao et al., 2017). In this study, using BNP/MWCNT greatly enhanced the flexural strength in all cases when compared to previous studies of CNC, MWCNT and GOs.

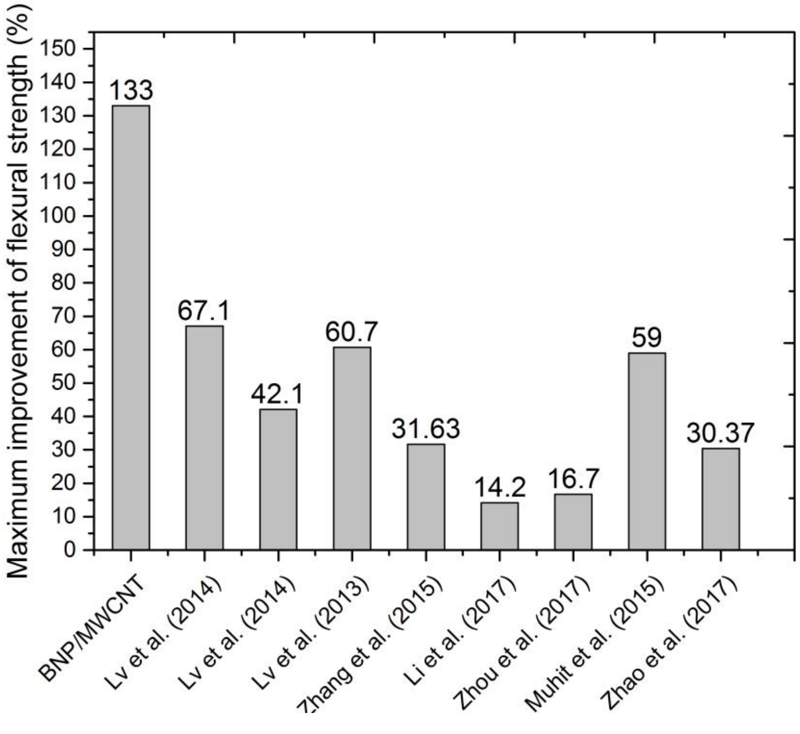

**Figure 6.37:** Maximum enhancement of flexural strength; comparison of BNP/MWCNT and GO

## 6.4 Conclusion

In this chapter, it was demonstrated that, the hybrid BNP/MCWNT can be used as a reinforcing nanomaterial in cementitious composites. The incorporation of the BNP/MWCNT increased the degree of hydration of cement due to the addition of BNP sheets accelerating the hydration of cement and the MWCNT working as nucleation points to promote more hydration products. The microstructure, the type of the hydration phases and the mechanical properties seemed to be highly dependent on the amount of the hybrid BNP/MCWNT. Compared to the plain cementitious composite, the cementitious composite with 0.2% BNP at 0.1%MWCNT at 28 days showed a denser microstructure with C-S-H as the main hydration phase. In addition, flexural strength was improved, and the best percentage of addition was 0.2% BNP at 0.1%MWCNT at 28 days post mixing.

This increase could be attributed to the increase in the DOH of the cement pastes when hybrid BNP/MCWNT are used as well as the regulation of hydration products with the addition of hybrid BNP/MCWNT, and the bridging of cracks by hybrid BNP/MWCNT.

The usage of BNP sheets has an immense potential impact on enhancing the usage of MWCNT in cementitious composites through achieving a good dispersion of MWCNT in the cementitious composite. This dispersion is due to the hydrophobic-hydrophobic interaction between BNP and MWCNT and through the chemical bonding between BNP sheets with $Ca(OH)_2$ and C-S-H due to functional groups, thus the bonding between the hybrid BNP/MWCNT and $Ca(OH)_2$ and C-S-H is obtained.

The flexural strength was also found to be significantly improved with the addition of hybrid BNP/MCWNT. The maximum percentage of the increase of flexural strength at 28 days was 133% at 0.1% MCWNT and the maximum percentage of increase of flexural strength at 14 days was 125% at 0.4% MCWNT. Moreover, the maximum percentage of increase of flexural strength at 7 days was 67% at 0.4% MCWNT. Furthermore, the maximum percentage of increase of the modulus of elasticity at 28 days was 57% at 0.1% MCWNT. This method greatly improves the results obtained with respect to other previous methods, when considering that the dispersant agent (BNP) is a green, low cost dispersant for MWCNT and has achieved better results in terms DOH, microstructure and mechanical properties than previous research. Previous research used expensive chemical dispersants, these chemical dispersants are produced from complex processes, and furthermore these chemical dispersants could negatively affect the properties of MWCNT.

The experimental results seem to indicate that the cementitious pastes reinforced with the hybrid BNP/MWCNT significantly improves the fracture energy, fracture toughness and modulus of elasticity. The optimal MWCNT concentration was 0.20-wt%. The hybrid BNP/MWCNT containing 0.20-wt% increased the fracture energy by 183% the fracture toughness by 162% and the modulus of elasticity by 275% of the cementitious composites. This increase in fracture performance can confidently be attributed to the addition of hybrid BNP/MWCNT. This hybrid BNP/MWCNT causes an increase of DOH of the cementitious composites, better regulation of hydration products and reinforcing effects.

# Chapter Seven

# Conclusions and future work

## 7.1 General

Research on improving the performance of cement-based materials is growing at a rapid pace. This stems from the need for resilient and sustainable civil infrastructure that meets the new performance and sustainability requirements. Because of this, there has been a concerted research effort to reduce the carbon footprint and improve the mechanical properties and durability performance of cementitious composites using a variety of nanomaterials including carbon nanotubes, carbon nanofibres, graphene oxide and graphene. However, the applicability of these nanomaterials in cement-based materials has been hindered by their poor dispersibility in the cement paste as they tend to agglomerate in the matrix, thus little improvement in the performance of cementitious composites is achieved.

The objective of this thesis was to develop new hybrid nanoparticles to enhance the performance of cement-based materials. The hybrid nanoparticles consisted of dispersible self-assembled BNP/MWCNT capable of performing multiple functions when present in the cement matrix including amplification of the cement hydration, steric stabilisation of the cement particles, strengthening and toughening of C-S-H, crack bridging and increasing the conductivity of the cementitious composite which can be exploited for structural health monitoring. BNP sheets were produced from environmentally friendly and sustainable materials such as sugar beet root. BNP sheets exhibit some GO properties such as high specific area, excellent mechanical properties and a large number of hydroxyl groups, thus they have high dispersibility in aqueous solutions.

In this chapter, conclusions deduced from the results of the previous chapters are discussed and future research topics are suggested for further investigation.

## 7.2 Conclusions

A high-throughput experimental approach was employed to characterise the BNP and the BNP/MWCNT nanoparticles and elucidate their effect on the hydration of cement, and hydration phases, microstructure, mechanical properties, fracture and toughness, and crack bridging. The results of this work can be seen in Chapters 2, 3, 4, 5 and 6.

Chapter 2 discusses different nanomaterials and their applications in cementitious composites. This includes MWCNT, G, GO, CNC, and NS. The use of MWCNT, G and GO may be valuable for reinforcing cement hydration at the nano-scale, bridging nano and micro cracks to prevent initial crack propagation and refining the pore structure to densify the cement matrix. However, their benefit extends beyond this to create a self-sensing and self-healing approach, due to MWCNT, GO and G being conductive fillers, and they could easily be used to measure and monitor the electrical properties of concrete structures. The use of CNC in cementitious composites enhances the rate of hydration of this material and this increase in hydration could be explained by two mechanisms. The first mechanism is steric stabilization which disperses cement particles similarly to that of many water reducing agents (WRA). The second mechanism is short circuit diffusion. It seems that this mechanism increases the hydration rate by increasing the transportation of water from outside of the hydration products to the dehydrated cement cores. NS has a positive impact on compressive strength of cementitious composites due to its pozzolanic reactivity, very fine particle size and large surface area.

Despite extensive research efforts over the last decade on cementitious composites modified with nanomaterials, several roadblocks to the widespread application of these nanomaterials in the construction industry still remain. One of the major problems is their agglomeration of nanomaterials in the cement paste, which results in defects that hinder their benefits to cementitious materials. Compared to G and GO, MWCNT are relatively inexpensive and could be very effective reinforcing materials if their agglomeration in cementitious materials is reduced. In addition, good dispersion enables good bonding between MWCNT and the hydrated cement matrix, resulting in excellent mechanical and fracture properties through the effective MWCNT crack bridging mechanism.

Work presented in Chapter 3 revels that:

experimental tests have been carried out to investigate the properties of BNP. Chemical components of BNP obtained from the EDX elemental analysis showed that the BNP is mostly carbon, oxygen and hydrogen. The XRD patterns suggested that the BNP structure can be divided into two regions: the crystalline region and the amorphous region. The (CI) of BNP was 64% which is indicative of high tensile strength and stiffness of BNP. As a result, the proposed BNP is a good candidate for reinforcing composite materials. The FTIR spectrum of BNP showed that there are two main types of absorption. The first absorption is due to hydrogen bonded hydroxyl groups in the structure of BNP, which indicates the hydrophilic nature of the BNP, and the second absorption is due to stretching vibrations of saturated C-H in cellulose.

The TGA/DTA results showed that the BNP displays a good thermal stability in a temperature range of 25 to 100°C, which is the typical range that cementitious composites use. The SEM results showed that the texture of BNP typically consists of crumpled and stacked thin sheets like GO. Clearly there is a high textured morphology in the form of roughness and ribs enabling the BNP sheets to morph around complex shapes and interact mechanically, thus significantly enhancing the mechanical properties of the cementitious composites. Colloidal properties of BNP aqueous solution showed that BNP has a high stability and uniformity distribution without agglomeration due to the hydrophilic nature of BNP, owing to a large number of hydroxyl (OH) groups. According to the results and discussions above, BNP is a good candidate for cementitious composites because of its excellent properties that enable BNP to disperse uniformly within an aqueous solution without agglomeration. In addition, its thermal stability and high textured morphology allow it to morph around complex shapes and interact mechanically.

From the above experimental results, it can be concluded that the proposed BNP is a good candidate for reinforcing composite materials.

Work presented in Chapter 4 reveals that:

experimental tests were carried out to investigate the performance of cementitious composites modified with BNP. The TGA/DTA provides insight into the chemical reaction mechanisms in cementitious materials during heating. It can be observed that the mass loss of the cement paste composites decrease with increasing BNP concentration. This is due to the increase of high-density C-S-H content and the creation of new intercalated BNP/C-S-H nanocomposites with higher density. Additionally, the amount of $Ca(OH)_2$ increases with increasing BNP concentration at 7 and 28 days. This could be attributed to the addition of BNP sheets accelerating the hydration of cement resulting in the production of higher $Ca(OH)_2$ content at 7 and 28 days. The XRD further confirms the TGA findings. This means that the addition of BNP promotes the hydration of cement thereby increasing the amount of the hydration products. This could be attributed to the highly hydrophilic BNP sheets which tend to store water molecules on their surface thus acting like water reservoirs which may release the free water for further hydration. Additionally, the results clearly show that DOH increases with increasing BNP content. The microstructure of the plain cement paste consists mainly of $Ca(OH)_2$ crystals with a low C-S-H content. The addition of 0.2-wt% BNP leads to higher C-S-H content, fewer $Ca(OH)_2$ crystals and denser microstructure. TEM investigations suggest a good compatibility between the BNP sheets and the hydration products. Based on the results of the mechanical properties, for all three curing ages, the increase in the flexural strength of the cement pastes reaches its maximum at an optimum content of 0.20-wt% of BNP. This increase, however, diminishes at higher BNP concentrations and this is more pronounced at 0.6-wt% BNP. This could be attributed to the synergetic effect of stacking of the BNP sheets and the high content of $Ca(OH)_2$ crystals.

Based on the mechanical properties obtained, the application of BNP in cementitious composites significantly increased the flexural strength. Hence these cementitious composites can provide new composites with enhanced flexural strength and dense microstructure.

The aim of chapter 5 was to create novel hybrid nanoparticles which have supreme characteristics and to tackle the agglomeration of MWCNT. To achieve this aim we used BNP, a green environmentally friendly low-cost material, which is dispersible in aqueous solution and can be produced on an industrial scale. In addition, this chapter examined the dispersion of MWCNT in aqueous solution with MCC and GO for the purpose of comparison since these are both currently used in the construction industry.

Experimental results demonstrated that novel hybrid nanoparticles were created through a self-assembly mechanism between BNP and MWCNT. Furthermore, the SEM results show that well dispersed MWCNT have been achieved by using BNP. This occurred for two reasons. Firstly, owing to electrostatic repulsion between the BNP, which comes from treatment by dispersant Span 20. This coated the surface of the BNP and prevented the cellulose platelets aggregating, allowing them to be more readily re-dispersed in aqueous media. Secondly, the possible adsorption of the BNP on the nanotube surfaces. It is believed that a novel hybrid nanomaterial was created from adsorption of BNP on the MWCNT surfaces (i.e. a self-assembly process), that is easy to attribute to the underlying force which comes from hydrophobic interactions that occur between the side wall of the MWCNT and the surface crystalline plane of the amphiphilic BNP (Mougel et al., 2016; Olivier et al., 2012).

The experimental results of the stability and colloidal properties of MCC/MWCNT and GO/MWCNT showed that aggregated MWCNT are microscale in size. Their size tended to be smaller with the addition of SP, thus the solution of MCC/MWCNT and GO/MWCNT had low stability which improved with the addition of SP.

The TGA curves showed a higher thermal stability for pure MWCNTs when compared to the thermal stability of BNP, MCC and GO. This was due to the high decomposition temperature of its graphitic structure. The TGA curves for the paired solutions showed higher thermal stability than the pure solutions of BNP, MCC and GO respectively. This may have been due to the attachment of MWCNTs to their surfaces and their combined work as a hybrid material.  Further increases in the concentration of MWCNTs provides more thermal stability to MWCNT/BNP, MWCNT/MCC and MWCNT/GO. This may have been through an increase in the number of MWCNTs attached onto the surfaces of dispersant agents.

From the experimental results above, it can be concluded that we have created successful novel hybrid multifunctional BNP/MWCNT, which have characteristics that are considerably improved over previous nanomaterials.

Work presented in Chapter 6 reveals that:

The incorporation of BNP/MWCNT increased the degree of hydration of the cement due to the addition of BNP sheets, which accelerate the hydration of cement, and MWCNT, which act as nucleation points to promote further hydration products. The microstructure, the type of hydration phases and the mechanical properties of cementitious composites seemed to be highly dependent on the quantity of hybrid BNP/MCWNT. Compared to the plain cementitious composite, the cementitious composite of 0.2% of BNP at 0.1% of MWCNT in 28 days showed a denser microstructure with C-S-H as the main hydration phase. In addition, the flexural strength was improved. It was concluded therefore that the most effective percentage of addition was 0.2% BNP at 0.1% of MWCNT at 28 days post mixing. From the experimental results, it can be concluded that the fracture energy, fracture toughness and modulus of elasticity of the BNP/MWCNT reinforced cementitious composites were significantly improved. The optimal MWCNT concentration was 0.20-wt%. The hybrid BNP/MWCNT containing 0.20-wt% MWCNT increased the fracture energy of the cementitious composites by 183%, the fracture toughness by 162%, and the modulus of elasticity by 275%. This increase in fracture performance can confidently be attributed to the addition of hybrid BNP/MWCNT. This hybrid BNP/MWCNT causes an increase in the DOH of cementitious composites, better regulation of hydration products and reinforcing effects.

Based on the mechanical properties obtained, the application of BNP/MWCNT in cementitious composites significantly improved the energy needed to initiate nano cracks. Thus, these BNP/MWCNT reinforced cementitious composites can provide novel, crack-free material, with improved fracture energy and strength.

## 7.3 Future work

### 7.3.1 Manufacturing of BNP

It would be interesting to determine the properties of BNP sheets, such as dimensions, mechanical properties, viscosity, internal morphology surface area and functional groups. This will enable a better understanding of the interaction mechanisms between the BNP and the cement matrix and these insights could then be used to optimise the performance of BNP-cementitious composites. Further research is also needed to tune the intrinsic properties of the BNP during the manufacturing process to make them more compatible with the cement matrix.

### 7.3.2. Synthesising of hybrid BNP/MWCNT nanoparticles

Further investigations are required to study the interaction between BNP and MWCNT. There are important questions for future work such as how many MWCNT are attached to BNP sheet surfaces and what are the conditions of the aqueous solution, the concentration of SP and other parameters which could affect this interaction. Finally, how the interaction between BNP and MWCNT affects the reinforcing effect.

### 7.3.3 Workability and dispersion of BNP and MWCNT

Further studies need to be carried out to investigate the workability, viscosity and the location of BNP sheets in aqueous solution. Further improvements and experiments on cementitious composites are required to improve its reinforcement and beneficial effects on the performance of cementitious composites. In addition, quantitative techniques to evaluate the dispersion of BNP and BNP/MWCNT within the aqueous solution are needed to optimise the dispersion of them and optimise their influence on the properties of cementitious materials. Further work should be undertaken to investigate the long-term stability of BNP and BNP/MWCNT solutions to evaluate their potential benefit on cementitious composites when used after long periods of storage. The available methods, such as tests through absorbance (UV-vis absorbance spectrometry), result in semi-qualitative values and the evaluation of the dispersion level through the cement composites via SEM images may not be a completely representative method because it only covered a limited area on the top surface of the investigated area.  The BPN appears to store water, reducing the workability of cementitious composites, and then release it during hydration to amplify the growth of the hydration phases. As such, the water storage and release mechanisms of BNP need to be studied to optimise the workability and the growth of C-S-H.

### 7.3.4. Durability of BNP sheets in cementitious composites

Further experimental investigations are needed to examine the durability of BNP sheets in cementitious composites under severe environmental conditions such as Wet-dry, freeze-thaw, sulphate resistance, chloride penetration and resistance to corrosion. Further research could also be conducted on water absorption of BNP sheets. In addition, further studies are needed to explore the stability of BNP in the pore solution with a high pH level. A high pH environment might have effects on the properties of BNP.

### 7.3.5. The influence of BNP sheets on the microstructure of cementitious composites

More research is required to examine the effect of BNP on the porosity of cementitious composites. Further study is needed on their packing density as the low porosity and dense structure of cementitious composites has positive effects on its performance. Further research is required to provide greater insight into the interaction between C-S-H and BNP. Moreover, further studies on quantifying C-S-H and optimising the amount of C-S-H in BNP reinforced cementitious composites are recommended. To develop the performance of BNP reinforced cementitious composites, the control of $Ca(OH)_2$ growth inside their microstructure is needed due to the size, shape, amount and distribution of $Ca(OH)_2$ effecting the performance of cementitious composites. Further studies are required to better understand the role that BNP and BNP/MWCNT play in hydration of cementitious composites. Furthermore, further investigation is necessary to optimise the water cement ratio and superplasticizer that enhance the characteristics of cementitious composites and maintain better performance of BNP/MWCNT reinforced cementitious composites.

### 7.3.6 Mechanical properties of BNP reinforced cementitious composites

The nanoscale properties of C-S-H phases need to be investigated to elucidate the strengthening effect of BNP. The macro mechanical properties of BNP reinforced cementitious composites such as flexural strength, compressive strength, tensile strength and stress-strain relationships need more investigation to confirm the obtained experimental results and develop guidelines for further research.

### 7.3.7. Fracture properties of reinforced BNP and BNP/MWCNT cementitious composites

Further investigation and experimentation into fracture energy and fracture toughness of BNP and BNP/MWCNT cementitious composites is strongly recommended to confirm these results. The research findings need to be reflected on standard specifications.

### 7.3.8 Reducing cement content in mortars and concretes

Further research should be undertaken to examine the ability of using BNP or BNP/MWCNT to reduce cement content in mortar and concrete. In order to reduce embodied CO2 in concrete by using less cement material, further enhancement of nanoscale properties and its hydration mechanism by using these nanoparticles, is recommended.

### 7.3.9 Modelling the interaction mechanism between BNP and C-S-H.

To develop a full depiction of the interaction mechanism between BNP and C-S-H, additional studies on a molecular model would be required. which could be employed to better understanding the hydration process and uncovering the interaction mechanism between BNP and C-S-H.

# References

Abu Al-Rub, R. K., Ashour, A. I. & Tyson, B. M. 2012. On the Aspect Ratio Effect of Multi-Walled Carbon Nanotube Reinforcements on the Mechanical Properties of Cementitious Nanocomposites. Construction and Building Materials, 35, 647-655.

Alafogianni, P., Dassios, K., Farmaki, S., Antiohos, S. K., Matikas, T. E. & Barkoula, N. M. 2016. On the Efficiency of Uv–Vis Spectroscopy in Assessing the Dispersion Quality in Sonicated Aqueous Suspensions of Carbon Nanotubes. Colloids and Surfaces A: Physicochemical and Engineering Aspects, 495(C), 118-124.

Alessandra Etuko Feuzicana De Souza, A. & Eduvaldo Paulo, S. 2006.Thermogravimetric Analyses and Mineralogical Study of PolymerModified Mortar with Silica Fume. Materials Research, 9(3), 321-326.

Al-Hamadani, Y. A. J., Chu, K. H., Son, A., Heo, J., Her, N., Jang, M., Park, C. M. & Yoon, Y. 2015. Stabilization and Dispersion of Carbon Nanomaterials in Aqueous Solutions: A Review. Separation and Purification Technology, 156(2), 861-874.

Alhelfi, A. and Sunden, B. 2016 Predictions of Temperature and Pressure Fields Due to Collapse of a Bubble in Sulfuric Acid Solution Under Ultrasound. Journal of Thermal Science and Engineering Applicatios 8(4): 041010-041016.

Amiri, A., Memarpoor-Yazdi, M., Shanbedi, M. & Eshghi, H. 2013. Influence of Different Amino Acid Groups on the Free Radical Scavenging Capability of Multi Walled Carbon Nanotubes. Journal of Biomedical Materials Research Part A, 101(8), 2219-2228.

ASTM Standard C 109/C 109M, 1999, Standard Test Method for Compressive strength of Hydraulic Cement Mortars (Using 2-in. or [50-mm] Cube Specimens), ASTM International, West Conshohocken, PA,1999.

ASTM Standard C 78, 1994, Standard Test Method for Flexural Strength of Concrete (Using Simple Beam with Third-Point Loading), ASTM International, West Conshohocken, PA,1994.

Babak, F., Abolfazl, H., Alimorad, R. & Parviz, G. 2014. Preparation and Mechanical Properties of Graphene Oxide: Cement Nanocomposites. The Scientific World Journal, 2014.

Benhelal, E., Zahedi, G., Shamsaei, E. & Bahadori, A. 2013. Global Strategies and Potentials to Curb Co2 Emissions in Cement Industry. Journal of Cleaner Production, 51(C), 142-161.

Brahmayya, M., Dai, S. & Suen, S.-Y. 2017. Sulfonated Reduced Graphene Oxide Catalyzed Cyclization of Hydrazides and Carbon Dioxide to 1,3,4-Oxadiazoles under Sonication. Sci Rep, 7(1), 4675-4675.

Cao, Y., Tian, N., Bahr, D., Zavattieri, P. D., Youngblood, J., Moon, R. J. & Weiss, J. 2016a. The Influence of Cellulose Nanocrystals on the Microstructure of Cement Paste. Cement and Concrete Composites, 74, 164-173.

Cao, Y., Zavaterri, P., Youngblood, J., Moon, R. & Weiss, J. 2015. The Influence of Cellulose Nanocrystal Additions on the Performance of Cement Paste. Cement and Concrete Composites, 56, 73-83.

Cao, Y., Zavattieri, P., Youngblood, J., Moon, R. & Weiss, J. 2016. The Relationship between Cellulose Nanocrystal Dispersion and Strength. Construction and Building Materials, 119, 71-79.

Chan, L. Y. & Andrawes, B. 2010. Finite Element Analysis of Carbon Nanotube/Cement Composite with Degraded Bond Strength. Computational Materials Science, 47(4), 994-

1004.

Collins, F., Lambert, J. & Duan, W. 2012. The influences of admixtures on the dispersion, workability, and strength of carbon nanotube- OPC paste mixtures. Cem. Concr. Compos., 34, 201-207.

Cwirzen. A, Habermehl Cwirzen. K and Penttala. V “Surface decoration of carbon nanotubes and mechanical properties of cement/carbon Nanotube composites” in Advances in Cement Research, 2008, 20, No. 2, April, pp.65–73.

Dassios, K. G., Alafogianni, P., Antiohos, S. K., Leptokaridis, C., Barkoula, N.-M. & Matikas, T. E. 2015. Optimization of Sonication Parameters for Homogeneous Surfactant-Assisted Dispersion of Multiwalled Carbon Nanotubes in Aqueous Solutions. J. Phys. Chem. C, 119(13), 7506-7516.

Datsyuk, V., Kalyva, M., Papagelis, K., Parthenios, J., Tasis, D., Siokou, A., Kallitsis, I. & Galiotis, C. 2008. Chemical Oxidation of Multiwalled Carbon Nanotubes. Carbon, 46(6), 833-840.

Du, H., Du, S. & Liu, X. 2015. Effect of Nano-Silica on the Mechanical and Transport Properties of Lightweight Concrete. Construction and Building Materials, 82(C), 114-122.

Elkady, H., Serag, M., I. & Elfeky, M., S. 2013. Effect of Nano Silica De-agglomeration, and Methods of Adding Super-plasticizer on the Compressive Strength, and Workability of Nano Silica Concrete. Civil and Environmental Research, vol., 3, No.2.

George, J. & Sabapathi, S. N. 2015. Cellulose Nanocrystals: Synthesis, Functional Properties, and Applications.(Report). 8, 45.

Gurunathan, S., Han, J. W., Eppakayala, V. & Kim, J.-H. 2013. Green Synthesis of Graphene and Its Cytotoxic Effects in Human Breast Cancer Cells. International journal of nanomedicine, 8, 1015.

Habibi, Y., Goffin, A.-L., Schiltz, N., Duquesne, E., Dubois, P. & Dufresne, A. 2008. Bionanocomposites Based on Poly(&Epsiv;-Caprolactone)-Grafted Cellulose Nanocrystals by Ring-Opening Polymerization. Journal of Materials Chemistry, 18(41), 5002-5010.

Han, B., Yu, X. & Kwon, E. 2009. Aself-Sensing Carbon Nanotube/Cement Composite for Traffic Monitoring. Nanotechnology, 20(44), 445501.

Horszczaruk, E., Mijowska, E., Kalenczuk, R. J., Aleksandrzak, M. & Mijowska, S. 2015. Nanocomposite of Cement/Graphene Oxide--Impact on Hydration Kinetics and Young's Modulus.(Report). 78, 234.

Hepworth D. and Whale E., 2015. Cellulose Platelet composites, methods of preparing cellulose platelet compositions and products comprising same, United States Patent, US 2015/0059617 A1.

Hou, P., Cheng, X., Qian, J. & Shah, S. P. 2014. Effects and Mechanisms of Surface Treatment of Hardened Cement-Based Materials with Colloidal Nanosio2 and Its Precursor. Construction and Building Materials, 53, 66-73.

Hung, N. T., Anoshkin, I. V., Dementjev, A. P., Katorov, D. V. and Rakov, E. G. 2008.Functionalization and solubilization of thin multiwalled carbon nanotubes. Inorganic Materials, 44, 219-223.

Hu, Y., Luo, D., Li, P., Li, Q. & Sun, G. 2014. Fracture Toughness Enhancement of Cement Paste with Multi-Walled Carbon Nanotubes. Construction and Building Materials, 70, 332-338.

Jang, S., Kawashima, S. & Yin, H. M. 2016. Influence of Carbon Nanotube Clustering on

Mechanical and Electrical Properties of Cement Pastes. Materials, 9(4).

Kang, I., Schulz, M. J., Kim, J. H., Shanov, V. & Shi, D. 2006. Acarbon Nanotube Strain Sensor for Structural Health Monitoring. Smart Materials and Structures, 15(3), 737-748.

Karim, M. R., Hashim, H. & Abdul Razak, H. 2016. Assessment of Pozzolanic Activity of Palm Oil Clinker Powder. Construction and Building Materials, 127, 335-343.

Khan, S. U., Nuruddin, M. F., Ayub, T., & Shafiq N. 2014. Effects of Different Mineral Admixtures on the Properties of Fresh Concrete. The Scientific World Journal, 2014, Article ID 986567, 11.

Kong, D., Corr, D. J., Hou, P., Yang, Y. & Shah, S. P. 2015. Influence of Colloidal Silica Sol on Fresh Properties of Cement Paste as Compared to Nano-Silica Powder with Agglomerates in Micron-Scale. Cement and Concrete Composites, 63, 30-41.

Konsta-Gdoutos, M. S., Metaxa, Z. S. & Shah, S. P. 2010. Highly Dispersed Carbon Nanotube Reinforced Cement Based Materials. Cement and Concrete Research, 40(7), 1052-1059.

Lehman, J. H., Terrones, M., Mansfield, E., Hurst, K. E. & Meunier, V. 2011. Evaluating the Characteristics of Multiwall Carbon Nanotubes. Carbon, 49(8), 2581-2602.

Li, G., Wang, P, Zhao, X. 2005. Mechanical behavior and microstructure of cement composites incorporating surface-treated multi-walled carbon nanotubes. Carbon. 43, 1239-1245.

Li, W., Li, X., Chen, S. J., Liu, Y. M., Duan, W. H. & Shah, S. P. 2017. Effects of Graphene Oxide on Early-Age Hydration and Electrical Resistivity of Portland Cement Paste. Construction and Building Materials, 136, 506-514.

Li, Y., Zhu, H., Shen, F., Wan, J., Lacey, S., Fang, Z., Dai, H. & Hu, L. 2015.

Nanocellulose as Green Dispersant for Two- Dimensional Energy Materials. Nano Energy, 13, 346-354.

Li, X., WEI, W., QIN, H. & HANG HU, Y. 2015. Co-effects of graphene oxide sheets and single wall carbon nanotubes on mechanical properties of cement. Journal of Physics and Chemistry of Solids, 85, 39-43.

Ling, X., Wei, Y., Zou, L. & Xu, S. 2013. The Effect of Different Order of Purification Treatments on the Purity of Multiwalled Carbon Nanotubes. Applied Surface Science, 276, 159.

Lothenbach, B., Winnefeld, F., Alder, C., Wieland, E. & Lunk, P. 2007. Effect of Temperature on the Pore Solution, Microstructure and Hydration Products of Portland Cement Pastes. Cement and Concrete Research, 37(4), 483-491.

Lu, Z., Hou, D., Meng, L., Sun, G., Lu, C. & Li, Z. 2015. Mechanism of Cement Paste Reinforced by Graphene Oxide/ Carbon Nanotubes Composites with Enhanced Mechanical Properties. RSC Advances, 5(122), 100598-100605.

Luo, J., Duan, Z. & Li, H. 2009. The Influence of Surfactants on the Processing of Multi-Walled Carbon Nanotubes in Reinforced Cement Matrix Composites. physica status solidi (a), 206(12), 2783-2790.

Lv, S., Liu, J., Sun, T., Ma, Y. & Zhou, Q. 2014a. Effect of Go Nanosheets on Shapes of Cement Hydration Crystals and Their Formation Process. Construction and Building Materials, 64, 231-239.

Lv, S., Ma, Y., Qiu, C., Sun, T., Liu, J. & Zhou, Q. 2013. Effect of Graphene Oxide Nanosheets of Microstructure and Mechanical Properties of Cement Composites. Construction and Building Materials, 49, 121-127.

Lv, S., Ting, S., Liu, J. & Zhou, Q. 2014b. Use of Graphene Oxide Nanosheets to Regulate the Microstructure of Hardened Cement Paste to Increase Its Strength and Toughness. CrystEngComm, 16(36), 8508-8516.

Lv, S., Zhang, J., Zhu, L. & jia C. 2016. Preparation of Cement Composites with Ordered Microstructures via Doping with Graphene Oxide Nanosheets and an Investigation of their Strength and Durability. Materials, 9(11), 924.

Mejdoub, R., Hammi, H., Suñol, J. J., Khitouni, M., M'Nif, A. & Boufi, S. 2017. Nanofibrillated Cellulose as Nanoreinforcement in Portland Cement: Thermal, Mechanical and Microstructural Properties. Journal of Composite Materials, 51(17), 2491-2503.

Meng Lia, Li-jun Wang, Dong Lia, Yan-Ling Cheng, Benu Adhikari, Preparation and characterization of cellulose nanofibers fromde-pectinated sugar beet pulp, Carbohydrate Polymers 102 (2014) 136– 143, doi:10.1016/j.carbpol.2013.11.021.

Metaxa, Z. S., Konsta-Gdoutos, M. S. & Shah, S. P. 2012. Carbon Nanofiber Cementitious Composites: Effect of Debulking Procedure on Dispersion and Reinforcing Efficiency. Cement and Concrete Composites, 36(1).

Metaxa, Z. S., Seo, J.-W. T., Konsta-Gdoutos, M. S., Hersam, M. C. & Shah, S. P. 2012b.Highly Concentrated Carbon Nanotube Admixture for Nano-Fiber Reinforced Cementitious Materials. Cement and Concrete Composites, 34(5), 612-617.

Mougel, J.-B., Adda, C., Bertoncini, P., Capron, I., Cathala, B. & Chauvet, O. 2016. Highly Efficient and Predictable Noncovalent Dispersion of Single-Walled and Multi-Walled Carbon Nanotubes by Cellulose Nanocrystals. The Journal of Physical Chemistry C, 120(39), 22694-22701.

Mònica, A., Josep, C., Raquel, A., Ferran, P., Elisabetta, A. & Teresa, V. 2012.

Nanofibrillated Cellulose (Nfc) as a Potential Reinforcement for High Performance Cement Mortar Composites. BioResources, 7(3), 3883-3894.

Muhammad Maqbool Sadiq, A., Parviz, S., Arshad, A. & Muhammad Yousaf Saqid, A. 2017. High-Performance Cementitious Matrix Using Carbon Nanofibers. Indonesian Journal of Science and Technology, 2(1), 57-75

Muhit, B. A., 2015 Investigation on the Mechanical, Microstructural, and Electrical Properties of Graphene OxideCement Composite. Master thesis, University of Central Florida.

Musa, N. M., 2014. Thermal Analysis of Cement Paste Partially Replaced with Neem Seed Husk Ash. International Journal of Scientific & Engineering Research. 5, 1, 1101-1105.

Musso, S., Tulliani, J., Ferro, G., Tagliaferro, A. 2009. Influence of carbon nanotubes structure on the mechanical behavior of cement composites. Composites Science and Technology, 69, 1985-1990.

Nasrollahzadeh, M., Babaei, F., Fakhri, P. & Jaleh, B. 2015. Synthesis, Characterization, Structural, Optical Properties and Catalytic Activity of Reduced Graphene Oxide/Copper Nanocomposites. RSC Adv., 5(14), 10782-10789.

Nguyen, H., Carvelli, V., Fujii, T. & Okubo, K. 2016. Cement Mortar Reinforced with Reclaimed Carbon Fibres, Cfrp Waste or Prepreg Carbon Waste. Construction and Building Materials, 126, 321-331.

Njuguna, J., Vanli, O. A. & Liang, R. 2015. A Review of Spectral Methods for Dispersion Characterization of Carbon Nanotubes in Aqueous Suspensions. Journal of Spectroscopy, 2015.

Olivier, C., Moreau, C., Bertoncini, P., Bizot, H., Chauvet, O. & Cathala, B. 2012.

Cellulose Nanocrystal- Assisted Dispersion of Luminescent Single- Walled Carbon Nanotubes for Layer-by- Layer Assembled Hybrid Thin Films. Langmuir: the ACS journal of surfaces and colloids, 28(34), 12463.

Onuaguluchi, O., Panesar, D. K. & Sain, M. 2014. Properties of Nanofibre Reinforced Cement Composites. Construction and Building Materials, 63, 119-124.

Parveen, S., Rana, S. and Fangueiro, R. 2013. A Review on Nanomaterial Dispersion, Microstructure, and Mechanical Properties of Carbon Nanotube and Nanofiber Reinforced Cementitious Composites. Journal of Nanomaterials, 2013, 1-19.

Peng, H., Alemany L. B., Maragrave, J. L. and Khabashesku, V., N. 2003. Sidewall Carboxylic Acid Functionalization of Single-Walled Carbon Nanotubes. Journal of the American Chemical Society, 125, 49, 15174-15182.

Peyvandi, A., Soroushian, P. and Balachandra, A. M. 2014. Reinforcement Efficiency of Modified Carbon Nanofiber in High-Performance Concrete Nanocomposite. Advances in Civil Engineering Materials, 3, 20140019.

Pu, N.-W., Wang, C.-A., Liu, Y.-M., Sung, Y., Wang, D.-S. & Ger, M.-D. 2011. Dispersion of Graphene in Aqueous Solutions with Different Types of Surfactants and the Production of Graphene Films by Spray or Drop Coating. Journal of the Taiwan Institute of Chemical Engineers, 43(1).

Qiaofeng Zheng, Baoguo Han, Xia Cui, Xun Yu, Jinping Ou, Graphene-engineered cementitious composites: Small makes a big impact, Nanomaterials and Nanotechnology, Volume 7 (2017): 1–18, doi: 10.1177/1847980417742304.

S. Alrekabi, A. C., A. Lampropoulos, I. Savina 2016. Experimental Investigation on the Effect of Ultrasonication on Dispersion and Mechanical Performance of Multi-Wall

Carbon Nanotube-Cement Mortar Composites. International Journal of Civil, Enviromental, Structural, Construction and Architectural Engineering, 10, 6.

Saafi M., L. Tang, J. Fung, M. Rahman, J. Liggat, Enhanced properties of graphene/fly ash geopolymeric composite cement, Cem. Concr. Res. 67 (2015) 292–299, doi: 10.1016/j.cemconres.2014.08.011.

Sahranavard, S., Haji-Kazemi, H. and Abbasi, S. 2014. Effect of multi-walled carbon nanotubes on mechanical properties of high-performance mortar. Magazine of Concrete Research, 66, 948-954.

Said A.M., Zeidan M.S., Bassuoni M.T. and Tiian Y. 2012. Properties of concrete incorporating nano- silica. Construction and Building Materials, 36,838-844.

Sardar Kashif Ur, R., Zainah, I., Shazim Ali, M., Md. Toasin Hossain, A., Muhammad Faisal, J., Kashif, M. & Syed Mustafa Ali, S. 2018. Influence of Graphene Nanosheets on Rheology, Microstructure, Strength Development and Self-Sensing Properties of Cement Based Composites. Sustainability, 10(3), 822.

Scheibe, B., Borowiak-Palen, E. & Kalenczuk, R. J. 2010. Oxidation and Reduction of Multiwalled Carbon Nanotubes — Preparation and Characterization. Materials Characterization, 61(2), 185-191.

Shtein, M., Pri-Bar, I. & Regev, O. 2013. A Simple Solution for the Determination of Pristine Carbon Nanotube Concentration. Analyst, 138(5), 1490-1496.

Singh, L. P., Karade, S. R., Bhattacharyya, S. K., Yousuf, M. M. & Ahalawat, S. 2013. Beneficial Role of Nanosilica in Cement Based Materials – a Review. Construction and Building Materials, 47(C), 1069-1077.

Sobolkina, A., Mechtcherine, V., Khavrus, V., Maier, D., Mende, M., Ritschel, M. &

Leonhardt, A. 2012. Dispersion of Carbon Nanotubes and Its Influence on the Mechanical Properties of the Cement Matrix. Cement and Concrete Composites.

Sun, Y., Fu, K., Lin, Y. & Huang, W. 2002. Functionalized Carbon Nanotubes: Properties and Applications. Accounts Chem. Res.

Tyson, B. M., Abu Al-Rub, R. K., Yazdanbakhsh, A. & Grasley, Z. 2011. Carbon Nanotubes and Carbon Nanofibers for Enhancing the Mechanical Properties of Nanocomposite Cementitious Materials.(Author Abstract)(Report). Journal of Materials in Civil Engineering, 23(7), 1028.

USA Patent No: 9,834,664 B2, Cellucomp Limited, Fife, UK.

Wang, L., Zhang, S., Zheng, D., Yang, H., Cui, H., Tang, W., & Li, D. 2017. Effect of Graphene Oxide (Go) on the Morphology and Microstructure of Cement Hydration Products. Nanomaterials, 7(12), 429.

White, C. M., Banks, R., Hamerton, I. & Watts, J. F. 2016. Characterisation of Commercially Cvd Grown Multi-Walled Carbon Nanotubes for Paint Applications. Progress in Organic Coatings, 90(C), 44-53.

Wojtoniszak, M., Zielinska, B., Kalenczuk, R. & Mijowska, E. 2012. Photocatalytic Performance of Titania Nanospheres Deposited on Graphene in Coumarin Oxidation Reaction. Materials Science-Poland, 30(1), 32-38.

Xiuxuan, S., Qinglin, W., Sunyoung, L., Yan, Q. & Yiqiang, W. 2016. Cellulose Nanofibers as a Modifier for Rheology, Curing and Mechanical Performance of Oil Well Cement. Scientific Reports, 6.

Xu, S., Liu, J., Li, Q. 2015. Mechanical properties and microstructure of multi-walled carbon nanotube-reinforced cement paste. Construction and Building Materials, 76, 16-23.

Y.Sakalli, R. Trettin, Investigation of C3S hydration mechanism by transmission electron microscope (TEM) with integrated Super-XTM EDS system, Journal of Microscopy, Vol. 267, Issue 1 2017, pp. 81–88, doi: 10.1111/jmi.12549.

Yang, H.-S., Gardner, D. & Nader, J. 2011. Dispersion Evaluation of Microcrystalline Cellulose/Cellulose Nanofibril-Filled Polypropylene Composites Using Thermogravimetric Analysis. An International Forum for Thermal Studies, 103(3), 1007-1015.

Yang, H. S., Wolcott, M. P., Kim, H. S. & Kim, H. J. 2005. Thermal Properties of Lignocellulosic Filler-Thermoplastic Polymer Bio-Composites. An International Forum for Thermal Studies, 82(1), 157-160.

Yılgın, M., N. Deveci Duranay, and D. Pehlivan, Co-pyrolysis of lignite and sugar beet pulp. Energy Conversion and Management, 2010. **51**(5): p. 1060-1064.

Yizheng Cao, Pablo Zavaterri b, Jeff Youngblood a, Robert Moonc, Jason Weiss, The influence of cellulose nanocrystal additions on the performance of cement paste, Cement & Concrete Composites, 2015 ,56, 73–83, doi:10.1016/j.cemconcomp.2014.11.008.

Yizheng Cao, Nannan Tian, David Bahr, Pablo D. Zavattieri, Jeffrey Youngblood, Robert J. Moon, Jason Weiss, The influence of cellulose nanocrystals on the microstructure of cement paste, Cement and Concrete Composites 74 (2016) 164-173, doi:10.1016/j.cemconcomp.2016.09.008.

Yu, J., Grossiord, N., Koning, C. E. & Loos, J. 2007. Controlling the Dispersion of Multi-Wall Carbon Nanotubes in Aqueous Surfactant Solution. Carbon, 45(3), 618-623.

Yu, M.-F., Lourie, O., Dyer, M. J., Moloni, K., Kelly, T. F. and Ruoff, R. S. 2000. Strength and Breaking Mechanism of Multiwalled Carbon Nanotubes under Tensile Load. Science, 287.

Zannotti, M., Giovannetti, R., Amp, Apos, Amato, C. A. & Rommozzi, E. 2016. Spectroscopic Studies of Porphyrin Functionalized Multiwalled Carbon Nanotubes and Their Interaction with Tio2 Nanoparticles Surface. Spectrochimica Acta Part A: Molecular and Biomolecular Spectroscopy, 153, 22-29.

Zhao, L., Guo, X., Liu, Y., Ge, C., Guo, L., Shu, X. & Liu, J. 2017. Synergistic Effects of Silica Nanoparticles/Polycarboxylate Superplasticizer Modified Graphene Oxide on Mechanical Behavior and Hydration Process of Cement Composites. RSC Adv., 7(27), 16688-16702.

Zhang, J., Liu, G., Chen, B., Song, D., Qi, J. & Liu, X. 2014. Analysis of Co2 Emission for the Cement Manufacturing with Alternative Raw Materials: A Lca-Based Framework. Energy Procedia, 61(C), 2541-2545.

Zhang, M.-H. and Islam, J. 2012. Use of nano-silica to reduce setting time and increase early strength of concretes with high volumes of fly ash or slag. Construction and Building Materials, 29, 573-580.

Zhou, C., Li, F., Hu, J., Ren, M., Wei, J. & Yu, Q. 2017. Enhanced Mechanical Properties of Cement Paste by Hybrid Graphene Oxide/Carbon Nanotubes. Construction and Building Materials, 134, 336-345

Zhou, Z., Lai, C., Zhang, L., Qian, Y., Hou, H. Q., Reneker, D. and Fong, H. 2009. Development of carbon nanofibers from aligned electrospun polyacrylonitrile nanofiber bundles and characterization of their microstructural, electrical, and mechanical properties. Polymer, 50, 2999-3006.

Zhu, Y., Murali, S., Cai, W., Li, X., Suk, J. W., Potts, J. R. and Ruoff, R. S. 2010. Graphene and graphene oxide: synthesis, properties, and applications. Adv Mater, 22, 3906-24